KINETIC SIMULATION OF SELECTED MITOCHONDRIAL PATHWAYS

A thesis submitted for the award of

Doctor of Philosophy

by

Kalyani Korla

11LBPH07

Department of Biochemistry
University of Hyderabad
Hyderabad – 500046
India

2015

Dedicated To Professor Chanchal K Mitra,
The Mentor, The Philosopher and The Inspiration...

Department of Biochemistry
University of Hyderabad
Hyderabad – 500046

CERTIFICATE

This is to certify that this thesis entitled "**Kinetic Simulation of Selected Mitochondrial Pathways**" submitted to University of Hyderabad, Hyderabad by **Ms. Kalyani Korla** for the degree of Doctor of Philosophy, is based on the studies carried out by her under my supervision. I declare to the best of my knowledge that this work has not been submitted earlier for the award of degree or diploma from any other University or Institution.

Chanchal K Mitra	Head
Supervisor	Dept. of Biochemistry

Dean,
School of Life Sciences

Department of Biochemistry
University of Hyderabad
Hyderabad – 500046

DECLARATION

I hereby declare that the work presented in this thesis entitled "**Kinetic Simulation of Selected Mitochondrial Pathways**" is entirely original and has been carried out by me in the Department of Biochemistry, University of Hyderabad, Hyderabad, under the supervision of Prof. Chanchal K Mitra. I further declare that, to the best of my knowledge, this work has not been submitted earlier for the award of degree of diploma from any other University or Institution.

Kalyani Korla	Chanchal K Mitra
11LBPH07	Supervisor

Date:
Place:

ACKNOWLEDGEMENTS

"It is good to have an end to journey toward, but it is the journey that matters, in the end."

A journey of dreams, aspirations, challenges, learning and realizations. In my journey towards the completion of this thesis, I have been quite fortunate to be surrounded by well-wishers at every stage. I am thankful to all those who have made a difference. It is a pleasure to convey my heartfelt gratitude to all of them in my humble acknowledgement.

Well begun is half done, and I started with my registration for Ph.D. under the supervision of Professor Chanchal K Mitra. An exceptional teacher, mentor, supervisor, philosopher and most importantly a wonderful human being. The past three years in his association has been an incredible learning experience ranging from science to philosophy to life. I will always be grateful to him for his patience, encouragement, sincere guidance and valuable critiques.

I would like to express my gratitude to Professor V. Lakshmipathi and Professor M. Durgaprasad for their valuable suggestions. I am thankful to my doctoral committee members, Professor A. K. Kondapi and Dr. S. Rajagopal. I thank the University of Hyderabad for the infrastructural facilities. I am grateful to University Grants Commission, India, for providing financial assistance in the form of the Junior and Senior research fellowship.

I take this opportunity to thank all the members of School of Life Sciences for being a part of this journey and supporting me whenever I needed them.

I express sincere thanks to CICR and UPE2 for the partial travel grant to attend BGRS 2014, Russia.

My lab members in the past three years deserve a special mention for creating a lively atmosphere in the lab. Especially Santosh and Kiran, who were there as friends when I hardly knew anyone in the campus. A special thanks to our beloved lab assistant Mr. Ramesh for all the generous help throughout.

My stay in the University of Hyderabad became a lot more memorable because of my lovely friends. I especially acknowledge Tanvi, Nidhi, Pankaz, Angamba and Prateek for all the beautiful memories. I thank my fellow Ph.D. scholars for all the smiles and the best wishes.

On the personal front, first and foremost, I would like to express my sincerest gratitude to my Mom and Dad, for being my support system. No words would be enough to thank my sister and brother-in-law for always being there for me. I thank my friend, Vigneshwaran, for introducing me to a new lifestyle and transforming me into a better self. My journey would have been incomplete without the presence of my friends outside the campus. I gratefully acknowledge their efforts in cheering me up in my tough times.

Above all, I thank the Almighty for imbibing in me the faith in myself.

TABLE OF CONTENTS

Page

CERTIFICATE....iii
DECLARATION....iv
ACKNOWLEDGEMENTS....v
TABLE OF CONTENTS....vi
LIST OF ABBREVIATIONS....ix
INTRODUCTION....1
Mitochondria....1
Rate equations....2
Concept of activation energy....4
Octave....7
Methodology....8
Assumptions....9
Enzyme kinetics simulation using Octave....10
Single substrate and bi-substrate reactions....10
Cyclic Pathways....14
Cyclic Pathways with five components....18
References....20
SIMULATING THE ENERGY MACHINERY....21
Energy Machinery....21
Krebs Cycle....21
Rate equations....25
Script....26
Result....28
The Electron Transport Chain (ETC)....32
Rate equation....36
Script....39
Result....40
ATP Synthesis....42
Rate equation....43
Script....43
Result....45
Combined Simulation....48
Script....49
Result....51

References....55
MITOCHONDRIAL SHUTTLES....57
Transport system in mitochondria....57
Coupled Transport....58
Simulation....59
Rate equation....62
Script....64
Results and discussion....67
Introduction for shuttles....71
Malate-Aspartate Shuttle....72
Simulation....74
Rate equation....75
Script....76
Result....78
Citrate-Pyruvate shuttle....80
Simulation....82
Rate equation....82
Script....84
Result....86
Associating Krebs cycle with shuttles....88
Rate equation....90
Script....92
Result....96
Comparison with experimental data....101
References....104
REACTIVE OXYGEN SPECIES....106
Reactive Oxygen Species....106
ROS generation by Complex I....107
ROS generation by Complex III....108
Reverse electron transfer (RET)....108
ROS-induced ROS release....108
Superoxide....109
Peroxide....110
Damage caused by ROS....110
mtDNA vs nuclear DNA....110
Defence against ROS....111

Functions of ROS....112
Simulation....112
Rate Equations....113
Script....114
Result....117
Combined Simulation....122
Rate equations....123
Script....123
Result....129
Analysis of all the systems together....133
References....135
MITOCHONDRIAL PROTEIN TRANSLATION....140
Mitochondrial translation....140
Simulation of Protein Translation....142
Initial conditions and concentrations....144
Assumptions....144
Initiation....144
Simulation....147
Rate Equations....147
Script....148
Result....149
Elongation....151
Simulation....154
Rate Equations....156
Script....157
Result....160
Termination....164
Simulation....166
Rate Equations....166
Script....167
Result....168
References....170
SUMMARY....174
References....176
PUBLICATIONS....177

LIST OF ABBREVIATIONS

Abbreviation		**Meaning**
ADP	:	Adenosine diphosphate
ATP	:	Adenosine triphosphate
CoA	:	Coenzyme A
cyt	:	Cytochrome
DHAP	:	Dihydroxyacetone phosphate
DMSO	:	Dimethyl sulfoxide
DNA	:	Deoxyribonucleic acid
ETC	:	Electron transport chain
FAD	:	Flavin adenine dinucleotide
FMN	:	Flavin mononucleotide
G 3-P	:	Glyceraldehyde 3-phosphate
GDP	:	Guanosine diphosphate
GSH	:	Glutathione
GSSG	:	Glutathione disulfide
GTP	:	Guanosine triphosphate
H_2O_2	:	Hydrogen peroxide
IM space	:	Intermembrane space
LHS	:	Left hand side
mRNA	:	Messenger RNA
mtDNA	:	Mitochondrial DNA
mtEF	:	Mitochondrial elongation factor (mtEFTu & mtEFG1)
mtIF	:	Mitochondrial initiation factor (mtIF1& mtIF2)
mtRF1a	:	Mitochondrial release factor 1a
mtRRF	:	Mitochondrial ribosome release factor (mtRRF1 & mtRRF2)
NAD	:	Nicotinamide adenine dinucleotide
NADP	:	Nicotinamide adenine dinucleotide phosphate
$O_2^{\bullet -}$	:	Superoxide anion
ode	:	Ordinary differential equation
pmf	:	Proton motive force

Q	:	Ubiquinone
QH_2	:	Ubiquinol
RET	:	Reverse electron transfer
RHS	:	Right hand side
RNA	:	Ribonucleic acid
ROS	:	Reactive oxygen species
tRNA	:	Transfer RNA
TTFA	:	Thenoyltrifluoroacetone

Chapter 1 Introduction

Mitochondria

Mitochondrion is one of the most vital organelles in the eukaryotic cell and is usually called the powerhouse of the cell. It is known as the powerhouse because it is the primary source of ATP which is the energy currency of the cell. Mitochondria are semi-autonomous organelles. They have their own genome and carry out replication, transcription and translation, along with several essential metabolic pathways as Krebs cycle, oxidative phosphorylation, fatty acid oxidation, etc. Mitochondria depend on the nucleus for a wide variety of proteins, regulatory molecules, metabolites and accessory proteins. These biomolecules are transported by an efficiently managed transport system involving a broad range of exchange channels, shuttles and transport proteins in this process. Mitochondrial genome codes for 13 protein-coding genes, 22 tRNAs and two rRNAs. All the proteins translated from mitochondrial genome form subunits of oxidative phosphorylation complexes.

Modelling a system as mitochondria appears to be a good start point in the process of modelling the whole cell because it has several features similar to a full-fledged cell, with lesser complexities. They can carry out some of the most vital processes present in the cell, and at the same time are comparatively easier and less complicated to simulate.

The current work involves kinetic modelling of selected mitochondrial pathways. A brief outline of the workflow includes:

1. Simulation of Krebs cycle along with oxidative phosphorylation, shuttling mechanism across mitochondrial membrane and establishing the interconnectivity with Krebs cycle.
2. Simulation of mechanism related to generation and scavenging of reactive oxygen species and then combining it with the model of Krebs cycle, the ETC, ATP synthesis and shuttles.
3. Simulation of a molecular mechanism, i.e., mitochondrial translation.

The metabolic pathways inside the cell govern the overall characteristic properties and contribute to the collective property of the system. These metabolic pathways have been studied in great detail by experimental biologists, but the overall collective dynamics of the system is yet to be explored. Several pathways reported in the literature represent a static picture of these processes and lack the dynamic feature

of the live cell. A dynamic model made up by knitting these minute experimental details can open avenues for further exploration beyond the limitations of an experimental setup to know more than what is already known. A dynamic model can predict the system response at any given point in time under a particular set of conditions, which is especially useful to study diseases or stress conditions. It enables us to examine the impact of a single or multiple components on the overall system. Such an approach can be utilised while studying the drug-protein interactions, predicting cell cycle decisions, studying metabolic disorders, etc.

Rate equations

Michaelis-Menten equation was used as the basic model for a single substrate, single intermediate enzyme catalysis. The standard Michaelis-Menten equation is written as

$$v = \frac{V_{max}[S]}{K_M + [S]} \tag{1}$$

this can be rewritten as

$$\frac{v}{V_{max}} = \frac{[S]/K_M}{1 + [S]/K_M} \tag{2}$$

Here, V_{max} is the maximum velocity achieved by the system, when the substrate concentration approaches infinity. K_M is the substrate concentration at which the reaction rate is half of V_{max}. Both v/V_{max} and $[S]/K_M$ are dimensionless and are apt for numerical simulations.

However most of the biological reactions involve more than one substrate, for such a case, a few reasonable assumptions were made, and the basic Michaelis-Menten approach was extended to give the following form:

$$\frac{v}{V_{max}} = \frac{[S_1]/K_{M1}}{1 + [S_1]/K_{M1}} \cdot \frac{[S_2]/K_{M2}}{1 + [S_2]/K_{M2}} \cdot \frac{[S_3]/K_{M3}}{1 + [S_3]/K_{M3}} \tag{3}$$

This formula may be considered as an approximation at least to the first order and thus can be used for simulation purposes. Similar approach was used to derive rate equations for all the metabolites/ components involved in the system.

Regulation plays a critical role in the biological system and therefore forms an integral part of any model. The inhibitors and activators in this case play a significant role. Two most widely seen inhibition mechanisms include competitive

and non-competitive inhibition. Inhibitors of the various reactions simulated in the present work were critically identified from the literature, and their effect was appropriately incorporated in the rate equations.

In competitive inhibition, the inhibitor binds at the substrate site and competes with the substrate for binding, thus increasing the apparent K_M of the substrate and the V_{max} remains unaffected. Here the new K_M can be written as

$$K_M \rightarrow K_M \cdot \left(1 + [I]/K_I\right) \tag{4}$$

where [I] is the concentration of the inhibitor and K_I is the enzyme inhibitor dissociation constant. Substituting this K_M in Equation (1) gives

$$v = \frac{V_{max}[S]}{K_M\left(1 + [I]/K_I\right) + [S]} \tag{5}$$

and this can be further written as

$$\frac{v}{V_{max}} = \frac{[S]/K_M}{1 + [I]/K_I + [S]/K_M} \tag{6}$$

In non-competitive inhibition, the inhibitor binds at an unrelated site and lowers the V_{max} of the enzyme, whereas K_M remains unaffected. V_{max} in this case is reduced by the same factor and can be given as

$$V_{max} \rightarrow V_{max}/\left(1 + [I]/K_I\right) \tag{7}$$

Substituting this value of V_{max} in Equation (1), gives

$$v = \frac{V_{max}[S]/(1 + [I]/K_I)}{K_M + [S]} \tag{8}$$

and can be rewritten a

$$\frac{v}{V_{max}} = \frac{[S]/K_M}{(1 + [I]/K_I).(1 + [S]K_M)} \tag{9}$$

Comparison between equations (6) and (9) indicates that both the equations can be considered same at the first order. This also suggests that as far as kinetics is concerned, both competitive and non-competitive inhibition have similar effects on the rate kinetics, and the exact nature of inhibition is irrelevant.

The reaction between the reactants is governed by several thermodynamic parameters. Most of the enzymatic reactions are reversible in nature, and the direction of the reaction is mainly determined by the energy constraints and concentration of the reactants and the products in the system. An important aspect in this context is the activation energy.

Concept of activation energy

The amount of energy (supplied externally) needed to initiate a chemical reaction is called as the activation energy. Activation energy is required to break the existing bonds and form the new ones. For two molecules to react, they should be close enough in space to interact in a way that the existing bonds are broken, and new bonds are created for the formation of the product. Such an interaction is provided by a collision.

The reaction between reactants is based on the collisions between their molecules. Collisions have to be successful in terms of energy and orientation to result in a chemical reaction. In the case of unimolecular reaction, the collision is with the solvent or background molecules, but in bimolecular or termolecular reactions, the collision has to be with other molecules. A certain amount of energy along with proper orientation of the reactants is required to start a reaction. With the increase in temperature, where heat serves as a source of energy for the reacting molecules, the activation energy is achieved sooner. In other words, a number of molecules attain the energy from the thermal source equivalent or higher than the required activation energy. Thermal energy contributes to the kinetic energy of the reacting molecules. At a given temperature, the reaction with low activation energy will proceed faster than a reaction with high activation energy.

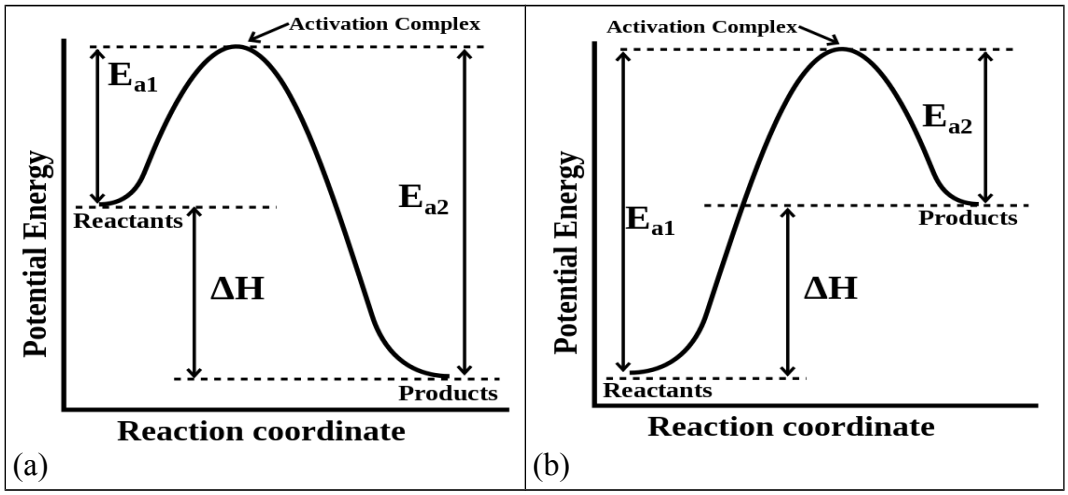

Figure 1.1: Activation energy diagrams for (a) exothermic and (b) endothermic reactions. X-axis indicates the reaction coordinate, which corresponds to the different conformations acquired by the reaction species in its transition from reactant to product. The peak of the curve represents the energy level of the activated complex. ΔH represents the change in enthalpy during formation of products from reactants. E_{a1} and E_{a2} are the activation energies required for the forward and reverse reactions respectively. It is seen that ΔH is negative for the exothermic reaction and is positive for the endothermic reaction.

These energy requirements can be explained by energy diagrams. Activation energy diagrams show the energy profile of the reaction system as it proceeds from reactants to products. Activation energy diagrams (Fig. 1.1) represent both exothermic and endothermic reactions. Here the reaction coordinate plotted along the x-axis corresponds to the different conformations acquired by the reaction species in its transition from reactant to product. E_{a1} and E_{a2} are the activation energies required for the forward and reverse reactions to take place respectively. The peak of the curve represents the energy level of the activated complex, which is also known as the transition state. It represents the conformation attained by the atoms of the reactants for a short time, that may not necessarily be an identifiable intermediate of the reaction. ΔH represents a change in enthalpy during formation of products from reactants (Fig. 1.1). This solely depends on the thermodynamics of the reactions and is independent of the path followed by the reactants to form the products.

Multiple paths can be followed by the reactants to form products, and one such path is via the catalysts. Catalysts are the molecules that speed up a reaction without being consumed in it. In fact, catalyst facilitates a lower activation energy pathway between the reactants and the products. In biochemical processes, there are enzymes made up of proteins that act as biocatalysts. Fig. 1.2 represents graphically the effect of catalysts (enzymes in biochemical systems) on the activation energy. It can be seen that the ΔH for both the reaction pathways remains same. Here E_{a1} and E_{a1c} indicate the activation energies required for uncatalysed and catalysed reactions to take place in the forward direction, respectively. Whereas, E_{a2} and E_{a2c} indicate the activation energies required for uncatalysed and catalysed reactions to take place in the reverse direction, respectively.

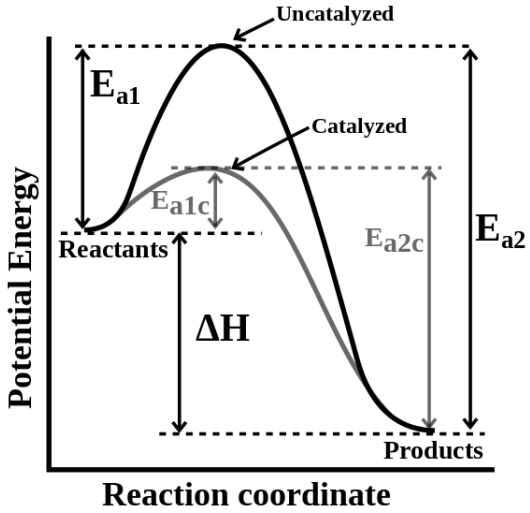

Figure 1.2: Graphical representation of the effect of catalysts (enzymes in biochemical systems) in the activation energy. ΔH for both the reaction pathways remains same.

Here E_{a1} and E_{a1c} indicate the activation energy required for uncatalysed and catalysed reactions in the forward direction, respectively. Whereas, E_{a2} and E_{a2c} indicate the activation energy required for uncatalysed and catalysed reactions in the reverse direction, respectively.

The effect of temperature in speeding up of a chemical reaction can be explained by Fig. 1.3. For two given temperatures, T_1 and T_2, where, $T_2>T_1$, the number of molecules with sufficient kinetic energy to cross the energy barrier is high for a system at a higher temperature.

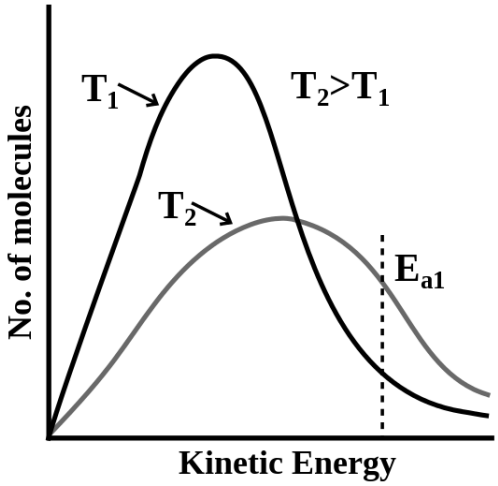

Figure 1.3: Effect of temperature on the energy profile of individual molecules in the reaction system. At higher temperature T_2, a higher number of molecules acquire the threshold energy to lead to the formation of products. E_{a1} represents the activation energy of the system (not drawn to scale).

The collision theory states that when the reactant molecules hit each other, a certain number of collisions result in a chemical change leading to the formation of products. Such collisions are called as successful collisions and are accompanied by the required activation energy. Increasing the concentrations of reactants result in an increased number of collisions and thus increasing the number of successful collisions, ultimately increasing the rate of reaction. The collision theory is closely related to transition state theory.

The transition state theory states that during the conversion of reactants to products an activated complex is formed, which marks the transition from reactants to products. The theory assumes a quasi-equilibrium established between the reactants and the products at this transition state. An activated complex may reform the reactants or may lead to the formation of products. The theory includes three major factors that determine whether the reaction will take place or not:

1. The concentration of the activated complex.
2. The rate at which the activated intermediate complex breaks

3. The final result of the breaking of the activated complex. If it breaks to reform the reactants or if it breaks to form a new complex which will be the products.

On the contrary, the collision theory states that not all the reactants that collide, undergo a reaction.

In case of a bimolecular reaction, the transition state is formed when the old bonds of the molecules are weakened and the new bonds begin to form. Since it takes considerable energy to achieve the transition state, the state is considered a high energy substance. The potential energy of the total system increases at this juncture due to the following reasons:

1. The approaching reactant molecules must surpass the mutual forces between the outer shell electrons of the constituent atoms.
2. Since the bonds are being broken, the atoms must be separated from each other.

The increase in potential energy is proportional to the energy barrier which the reactant molecules require for the reaction to occur; the transition state occurs at the maximum (peak) of this energy barrier.

When complete equilibrium is achieved in the system including activated complex, the concentration of the activated complex can be calculated. The main application of the transition state theory is in reactions catalysed by enzymes. The activation energy of a reaction reduces by the introduction of an enzyme (acts as a catalyst) into a reaction. Transition state theory is helpful in mapping out the course of the reaction by knowing what transition states will be formed and what would be the differing transition energies. Thus it facilitates the calculation of the rate of the reaction and the rate constant.

Octave

> "GNU Octave is a high-level language, primarily intended for numerical computations. It provides a convenient interactive command line interface for solving linear and nonlinear problems numerically, and for performing other numerical experiments. It may also be used as a batch-oriented language for data processing. GNU Octave is freely redistributable software" (Octave).

An ordinary differential equation (ode) is an equation of the general form

$$f(x, y, y', y''...y^n)=0$$

where $y'=dy/dx$ and $y^n = d^n y/dx^n$. n is called the order of the equation. The kinetic equations are first order but non-linear differential equation. First order means

that only the first derivative is involved in any equation. In the present study, there are several variables for y, and therefore they form a system of coupled equations. These values of y and y' are treated as vectors.

A differential equation is called stiff if the conventional numerical methods of solution lead to unstable results. It has been assumed that the systems of equations used in this work are not stiff. However, coupled chemical reaction kinetics in which concentration of different components varies widely can become stiff.

In GNU Octave, there are several methods available to solve ordinary differential equations. In the present work, the *lsode* module has been extensively used. Here, the linear first order differential equations are written in the form:

$$y'(t) = f(t, y)$$

where y and y' are vectors usually supplied as a function. *Lsode* module uses the most common method "Livermore Solver for Ordinary Differential Equations", which is well documented in the literature (Hindmarsh, 1983).

The simulations considered in this work are initial value problems, where initial conditions are supplied, and the solution changes with time depending on these initial conditions.

Methodology

The approach used in simulating metabolic pathways involved four major steps:

1. The set of reactions to be simulated was divided into subsets and information regarding the detailed mechanism of each step in the subsets was compiled. A pictorial representation was constructed for each pathway which clearly represented all the steps which were further used for writing rate equations.
2. Rate equations were written for each component present in the system. These equations were based on the reaction compiled in the previous step. Rate equation for a given component included elements from all the reactions where is it involved. Regulators, inhibitors and activators were also included in the rate equations.
3. An initial concentration has to be provided in the Octave script. The initial concentration was kept in the range of 0-1 depending upon the utilisation and regeneration of the component in the system. Components, that are utilised in the system and have no source of regeneration, were provided a constant input in each subsequent turns. Such an approach keeps the system running and

protects it from degenerating. This leads to a steady-state level in the system. Also, few other reasonable assumptions were made, which are enlisted in the next section, and they were taken into consideration while writing the final script.

4. Script thus written is run on a terminal under Octave. The data can be obtained in the form of a plot, which plots concentration vs time, of the various components. The data can also be saved in a LibreOffice calc format, where the concentrations at all time points are stored in a tabulated form. This data can be further processed to derive the desired set of information. Such data points were used for plotting various phase plots also.

Assumptions

For constructing a generalised kinetic model for mitochondrial metabolic pathways, the following assumptions were made:

1. Rate constants for all the reactions were assumed to be 1. This can be considered equivalent to stating that all rates are expressed in units of V_{max}. This is because the rate constants for a particular component as given in the literature varies in a wide range and moreover is largely affected by the experimental conditions under which enzyme kinetics experiments were conducted. So to maintain the generality of the script, the rate constants were taken as unity. The scripts can be customised by replacing the rate constants with the numerical value for a given organism under a given set of conditions. It can be used to obtain relative concentrations and to study other behavioural and kinetic aspects of the system under study. It is likely to be a good approximation close to the steady-state.
2. The model includes only the reactions shown in the pictorial representation or reaction set and no other reaction which may be otherwise related to the present system. This suggests that the reactants and products of the concerned reactions are restricted to the system under study. All the components, therefore, are shown to be conserved in the given system.
3. To further fine tune the script, the components that are consumed and not regenerated in the system are supplied at a constant rate. The rate of addition matches with the steady-state utilisation rate.

Apart from these general assumptions, few other reasonable assumptions applicable to the respective set of metabolic pathways were made. Those assumptions

will be discussed in the respective sections.

Enzyme kinetics simulation using Octave

Octave has been extensively used in the present work and particularly the ordinary differential equation (ode) solver. The first step in the approach was to simulate basic enzyme reactions such as one substrate and two substrate reactions using Octave. Further, since most of the biological pathways are cyclic in nature, simulation of a basic cyclic pathway was considered a good beginning step.

Single substrate and bi-substrate reactions

A single substrate reaction involves only one substrate. The enzyme (E) binds to the substrate (A) to form an intermediate complex (AE), which then dissociates to release a product (P) and unaltered enzyme (E). This can be schematically represented as

$$S + E \Leftrightarrow ES$$
$$ES \rightarrow E + P$$

Here rate equations were derived for each component. An Octave script was written to simulate this process. The script is presented in Table 1.1.

Table 1.1: Script written for a single substrate, single intermediate enzyme catalysis.

```
1; % plot
ds=zeros(5,1);
s(1) = 1;          % S
s(2) = 1;          % E
s(3) = 0;          % ES
s(4) = 0;          % P
s(5) = 0;          % M-M curve
function ds=plo(s)
k1=1;
k2=1;
k3=1;
ds(1) = -k1*s(1)*s(2)+k2*s(3);
ds(2) = -k1*s(1)*s(2)+k2*s(3)+k3*s(3);
ds(3) =  k1*s(1)*s(2)-k2*s(3)-k3*s(3);
ds(4) =  k3*s(3);
ds(5) =  s(1)/(2+s(1));
return
end

% use lsode to solve this set...
lsode_options("relative tolerance",1e-4);
```

```
lsode_options("absolute tolerance",1e-3);
t=0:0.1:100;
% supply the initial concentrations ...
s0=s;
[s,T,MSG]=lsode(@plo,s0,t);
T
MSG
plot(t,s(:,1),"linewidth",5,t,s(:,2),"linewidth",5,t,s(:,3),"linewid
th",5,t,s(:,4),"linewidth",5,t,s(:,5),"linewidth",5);
grid on;
set (gca,'FontSize', 18);
axis([0,10,0,1.01]);
% title ("Plot");
xlabel ("Time/arbitrary units");
ylabel ("Concentration/arbitrary units");
set (gca,'FontSize', 18)
legend("S","E","ES","P","MM", "location", "east");
```

The data was extracted and saved in a file and then plotted using GNUPLOT.

A bi-substrate reaction involves two substrates which may or may not bind sequentially to give rise to the product. Several mechanisms are known for bisubstrate enzyme reaction.

In the present section, sequential two substrate binding reaction has been simulated. Suppose there are two substrates, A and B, where A first binds to the enzyme (E) giving rise to first intermediate (AE). Subsequent binding of the second substrate (B) to the first intermediate (AE), leads to the formation of the second intermediate (AEB). The second intermediate then dissociates to release the enzyme (E) and the product (P). The scheme can be represented as

$$A + E \Leftrightarrow AE$$
$$AE + B \Leftrightarrow AEB$$
$$AEB \rightarrow E + P$$

Rate equations were derived for each component, an Octave script was written to simulate this process. The script is presented in Table 1.2

Table 1.2: Script written for simulation of two substrates two intermediates enzyme catalysis .

```
1; % plot for two substrate-two intermediate enzyme catalysis

ds=zeros(7,1);
s(1) = 1;          % A
s(2) = 1;          % E
s(3) = 0;          % AE
```

```
s(4) = 1;          % B
s(5) = 0;          % AEB
s(6) = 0;          % P
s(7) = 0;          % M-M curve

function ds=plo(s)
k1=1; k2=1; k3=1; k4=1; k5=1;

ds(1) = -k1*s(1)*s(2)+k2*s(3);
ds(2) = -k1*s(1)*s(2)+k2*s(3)+k5*s(5);
ds(3) =  k1*s(1)*s(2)-k2*s(3)-k3*s(3)*s(4)+k4*s(5);
ds(4) = -k3*s(3)*s(4)+k4*s(5);
ds(5) =  k3*s(3)*s(4)-k4*s(5)-k5*s(5);
ds(6) =  k5*s(5);
ds(7) =  (s(1)/(2+s(1)))*(s(4)/(2+s(4)));
return
end

% use lsode to solve this set...
lsode_options("relative tolerance",1e-4);
lsode_options("absolute tolerance",1e-3);
t=0:0.1:100;
% supply the initial concentrations ...
s0=s;
[s,T,MSG]=lsode(@plo,s0,t);
T
MSG
plot(t,s(:,1),"linewidth",5,t,s(:,4),"linewidth",5,t,s(:,2),"linewid
th",5,t,s(:,3),"linewidth",5,t,s(:,5),"linewidth",5,t,s(:,6),"linewi
dth",5,t,s(:,7),"linewidth",5);
grid on;
set (gca,'FontSize', 18);
axis([0,10,0,1.01]);
% title ("Plot");
xlabel ("Time/arbitrary units");
ylabel ("Concentration/arbitrary units");
set (gca,'FontSize', 18)
legend("A","B","E","AE","AEB","P","MM", "location", "east");
```

The data was extracted and saved in a file and then plotted using GNUPLOT.

The results for the two schemes, single substrate single intermediate enzyme catalysis and two substrates two intermediates enzyme catalysis, are shown in Fig. 1.4 and 1.5 respectively.

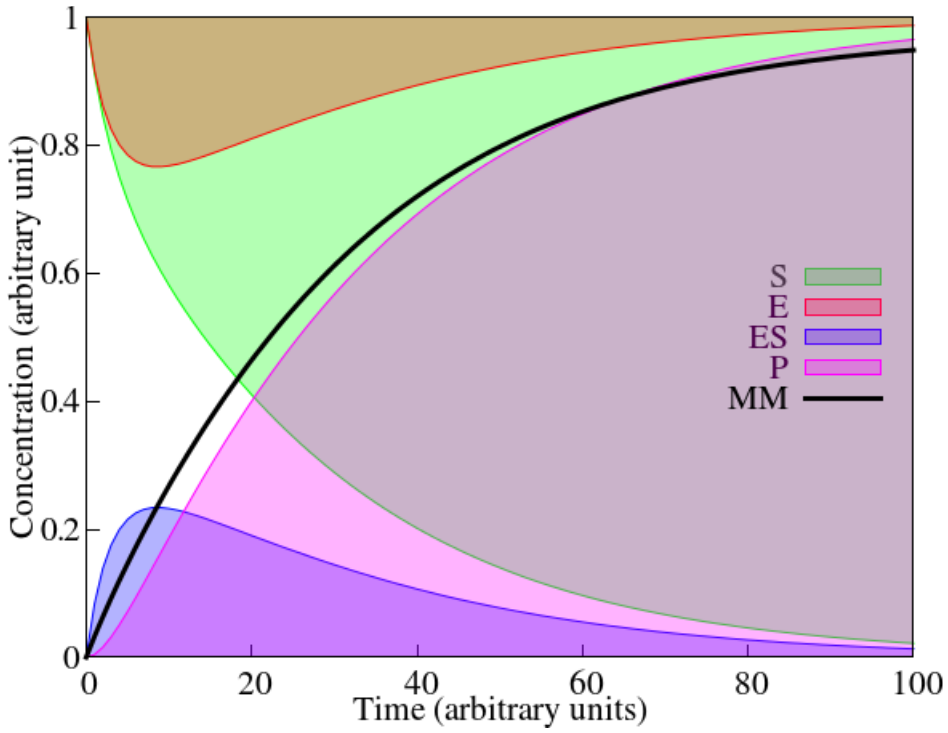

Figure 1.4: Single substrate enzyme kinetics simulation. S=Substrate, E=Enzyme, ES=Enzyme-substrate complex, P=Product, MM=Michaelis-Menten curve.

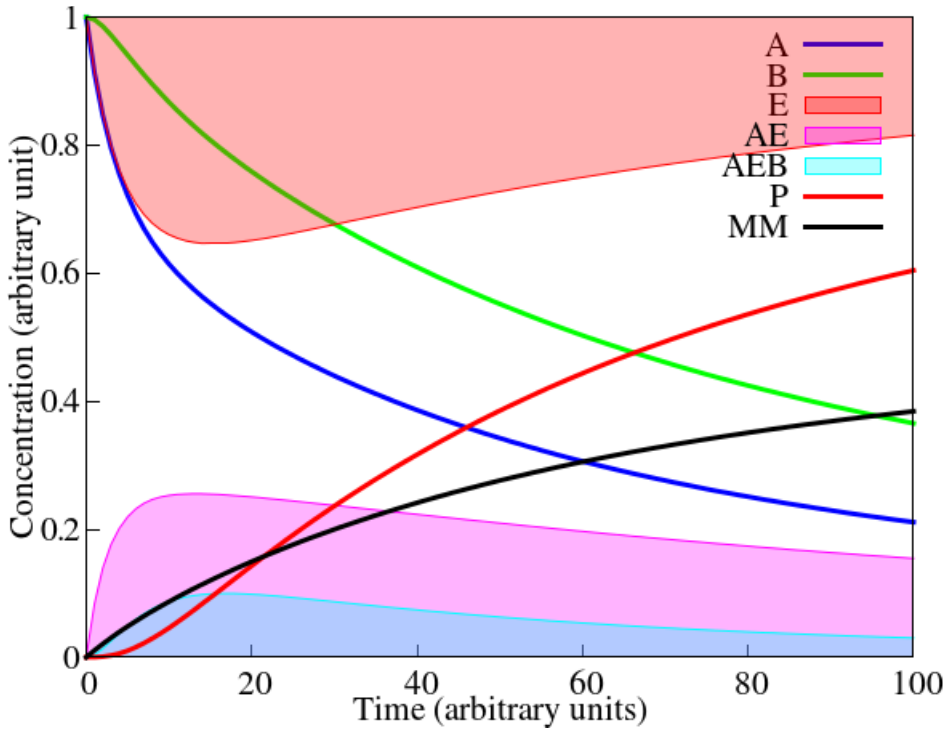

Figure 1.5: Bi-substrate enzyme kinetics simulation. A=First Substrate, B=Second substrate, E=Enzyme, AE=First intermediate, AEB=Second intermediate, P=Product, MM=Michaelis-Menten curve.

In Fig. 1.4, it is seen that the substrate concentration is continuously decreasing as it is being utilised to form a product. The curve for product P rises from zero. The curve for the enzyme falls indicating its utilisation in the system. Subsequent rise in the concentration of enzyme indicates its release after the formation of product. The curve for enzyme-substrate complex (ES) shows the formation of this complex which is then degraded to release the product and the free enzyme.

In Fig. 1.5 concentrations of both the substrates decrease, however the fall is more in the concentration of the first substrate when compared to the second. This is because not all the first intermediate (AE) formed binds to the second substrate, therefore, more of the substrate A is present in the bound form. This also explains the difference in the amount of intermediates formed; the first intermediate is present in higher concentration than the second intermediate.

Cyclic Pathways

A cyclic reaction can be best explained with Fig. 1.6 where there are four species A, B, C and D, which are inter-convertible. For a cyclic pathway, there can be two conditions, (I) when all the components are restricted in a closed system, i.e., none of the components are added or removed once the system is initiated. (II) when at least one of the component is either added or removed, i.e. the system can no more be considered close. Two cases are considered here for simulation using Octave.

Case I: A closed cyclic system: A closed cyclic pathway can be represented as in Fig. 1.6 along with its simulation result: Here, initial concentration of A=1 and B=C=D=0, since it is a closed system, as time passes all the concentrations become equal. Script for such a simulation is given in Table 1.3. The result obtained in this case is shown in Fig. 1.6.

Table 1.3: Script written for simulation of a closed cyclic system with four species.

```
1; % plot for closed cyclic system
ds=zeros(4,1);

s(1) = 1;          % A
s(2) = 0;          % B
s(3) = 0;          % C
s(4) = 0;          % D

function ds=plo(s)
```

```
ds(1) = -s(1)+s(2)-s(1)+s(4);
ds(2) = -s(2)+s(3)-s(2)+s(1);
ds(3) = -s(3)+s(4)+s(2)-s(3);
ds(4) = -s(4)+s(1)+s(3)-s(4);

return
end
% use lsode to solve this set...
lsode_options("relative tolerance",1e-4);
lsode_options("absolute tolerance",1e-3);
t=0:0.1:100;

% supply the initial concentrations ...
s0=s;
[s,T,MSG]=lsode(@plo,s0,t);
T
MSG

plot(t,s(:,1),"linewidth",5,t,s(:,2),"linewidth",5,t,s(:,3),"linewid
th",5,t,s(:,4),"linewidth",5);
grid on;

set (gca,'FontSize', 18);
axis([0,2,0,1.01]);
% title ("Plot");
xlabel ("Time/arbitrary units");
ylabel ("Concentration/arbitrary units");
set (gca,'FontSize', 18)
legend("A","B","C","D", "location", "east");
```

Case II: An open cyclic system: Here the initial concentrations were kept the same as the previous case, only difference was constant addition and removal of 0.5 in A and B respectively. In such a case, the script used is given in Table 1.4. The result obtained in this case is shown in Fig. 1.7.

Table 1.4: Script written for simulation of an open cyclic system with four species, where one of the species is continuously fed into the system, and another species is continuously withdrawn from the system

```
1; % plot for open cyclic system
ds=zeros(4,1);

s(1) = 1;          % A
s(2) = 0;          % B
s(3) = 0;          % C
s(4) = 0;          % D

function ds=plo(s)
```

```
ds(1) = -s(1)+s(2)-s(1)+s(4)+0.5;
ds(2) = -s(2)+s(3)-s(2)+s(1)-0.5;
ds(3) = -s(3)+s(4)+s(2)-s(3);
ds(4) = -s(4)+s(1)+s(3)-s(4);

return
end

% use lsode to solve this set...
lsode_options("relative tolerance",1e-4);
lsode_options("absolute tolerance",1e-3);
t=0:0.1:100;

% supply the initial concentrations ...
s0=s;
[s,T,MSG]=lsode(@plo,s0,t);
T
MSG

plot(t,s(:,1),"linewidth",5,t,s(:,2),"linewidth",5,t,s(:,3),"linewid
th",5,t,s(:,4),"linewidth",5);
grid on;

set (gca,'FontSize', 18);
axis([0,2,0,1.01]);
% title ("Plot");
xlabel ("Time/arbitrary units");
ylabel ("Concentration/arbitrary units");
set (gca,'FontSize', 18)
legend("A","B","C","D", "location", "east");
```

The result obtained for a closed cyclic system with four species is shown in Fig. 1.6. The components of a closed cyclic system reach a steady-state where the concentration of all the components is same.

The result obtained for an open cyclic system with four species is shown in Fig. 1.7. The components reach a steady-state where the concentration of the components becomes steady, but not equal.

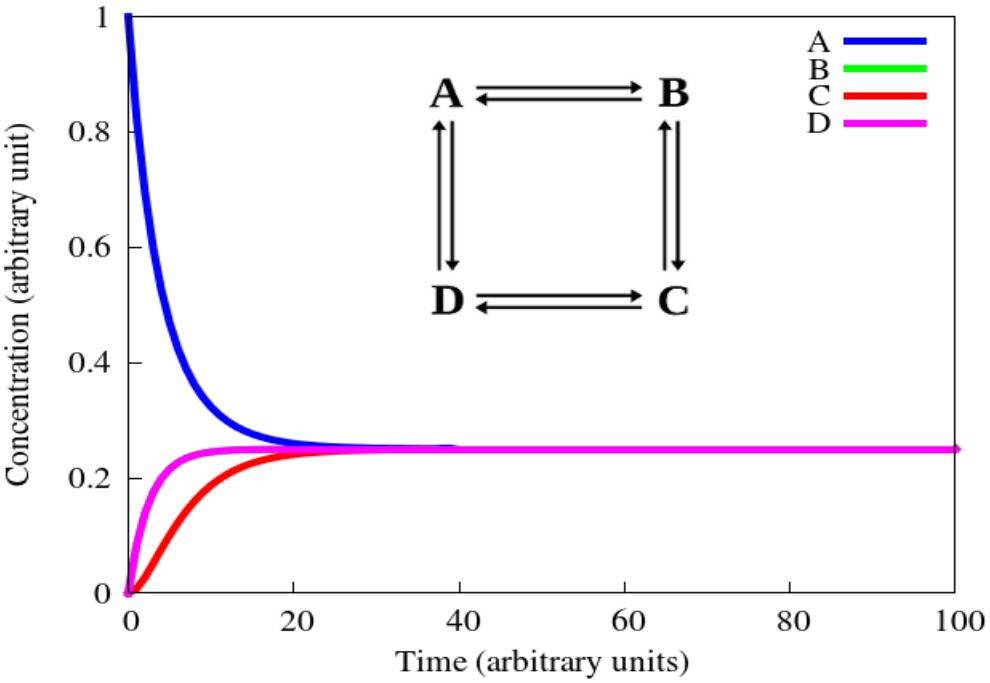

Figure 1.6: A closed cyclic system, where A was given an initial concentration of 1 and all the other species were kept at zero. As time passes, the system attains a steady-state where all the species have the same concentration.

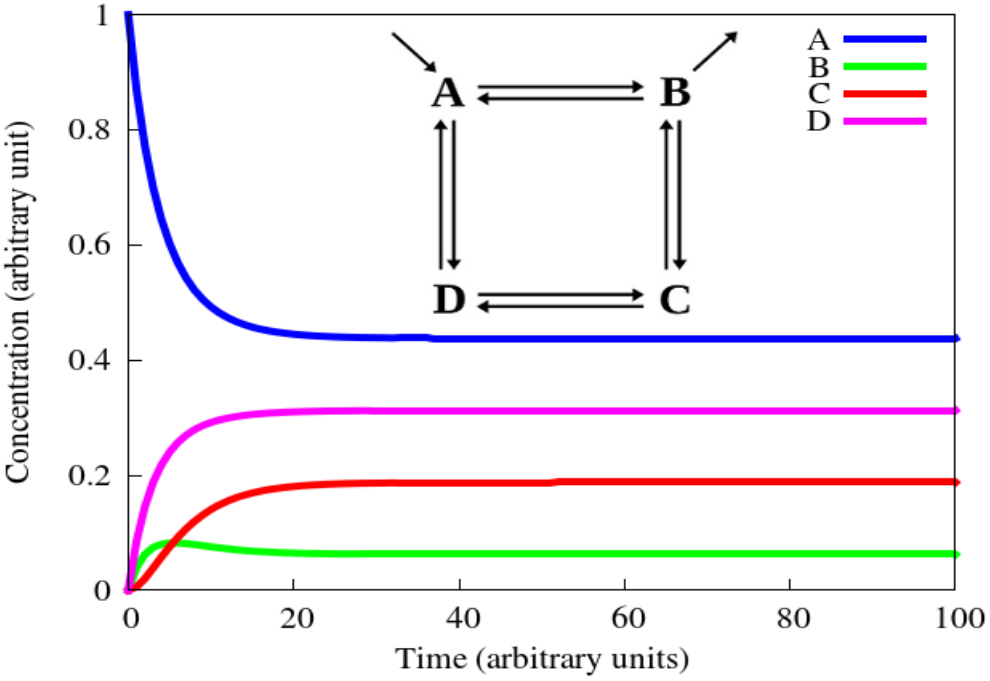

Figure 1.7: An open cyclic system, where a constant input of 0.5 is given to A in each turn and 0.5 units are constantly removed from the concentration of B. The concentrations of all the components reach a steady-state, but unlike a closed cyclic system, all the concentrations are not equal. Equilibrium is never reached in such a system.

Cyclic Pathways with five components

Simulation for cyclic pathways with five components was done to understand the biological cyclic pathways as Krebs cycle. Several combinations of scripts were studied for better visual understanding.

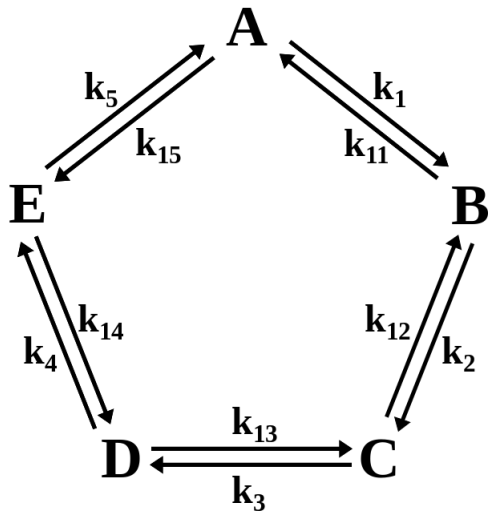

Figure 1.8: A model of cyclic pathway with five metabolites, A, B, C, D and E, used for simulation in this section. The reactions in forward direction A→B→C→D→E→A, have rate constants k_1, k_2, k_3, k_4, k_5, respectively. The backward reactions A→E→D→C→B→A, have rate constants k_{15}, k_{14}, k_{13}, k_{12}, k_{11}, respectively.

Fig. 1.8 shows the schematic diagram of a cyclic pathway with five components. The rate constants for the respective forward and backward reactions are also shown symbolically. A set of simulations using different values for rate constants can provide a better insight to the effect of rate constants on the steady-state values. These simulations were carried out for three set of rate constant values: (I) when all the forward and backward reaction rates are equal to 1 (Fig. 1.9a and 1.10a), (II) when the rate constants for each couple of forward and backward reaction were equal, but different reaction couples (forward and backward) had a different rate constant (Fig. 1.9b and 1.10b), and (III) when the backward reaction rate for every reaction was 0.5 point lower its respective forward reaction rate constant (Fig. 1.9c and 1.10c). Here the initial concentration of A was 1, and all the other metabolites were kept at 0.

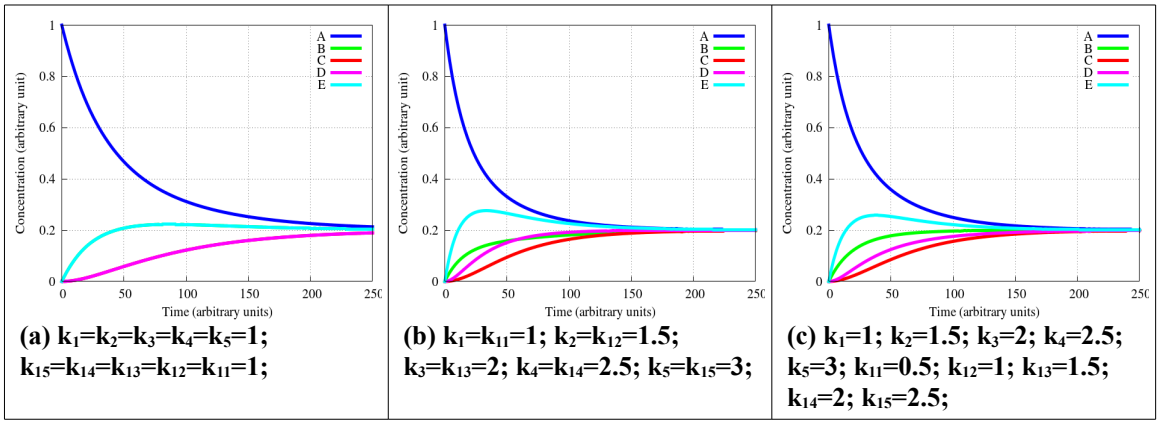

(a) $k_1=k_2=k_3=k_4=k_5=1$; $k_{15}=k_{14}=k_{13}=k_{12}=k_{11}=1$;

(b) $k_1=k_{11}=1$; $k_2=k_{12}=1.5$; $k_3=k_{13}=2$; $k_4=k_{14}=2.5$; $k_5=k_{15}=3$;

(c) $k_1=1$; $k_2=1.5$; $k_3=2$; $k_4=2.5$; $k_5=3$; $k_{11}=0.5$; $k_{12}=1$; $k_{13}=1.5$; $k_{14}=2$; $k_{15}=2.5$;

Figure 1.9: Simulation result of a five-membered cyclic pathway in a closed system.

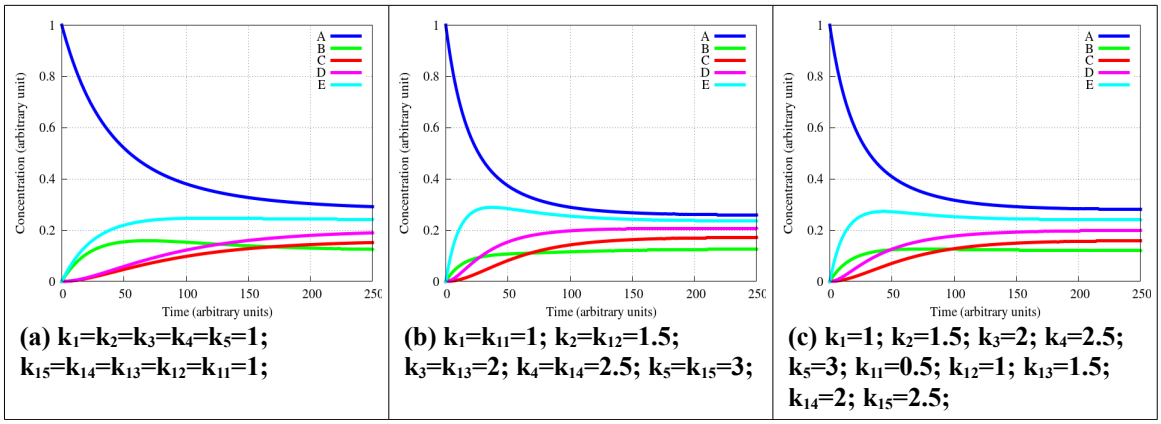

(a) $k_1=k_2=k_3=k_4=k_5=1$; $k_{15}=k_{14}=k_{13}=k_{12}=k_{11}=1$;

(b) $k_1=k_{11}=1$; $k_2=k_{12}=1.5$; $k_3=k_{13}=2$; $k_4=k_{14}=2.5$; $k_5=k_{15}=3$;

(c) $k_1=1$; $k_2=1.5$; $k_3=2$; $k_4=2.5$; $k_5=3$; $k_{11}=0.5$; $k_{12}=1$; $k_{13}=1.5$; $k_{14}=2$; $k_{15}=2.5$;

Figure 1.10: Simulation result of a five-membered cyclic pathway in an open system, with a constant addition of A (0.2 units) and removal of B (0.2 units).

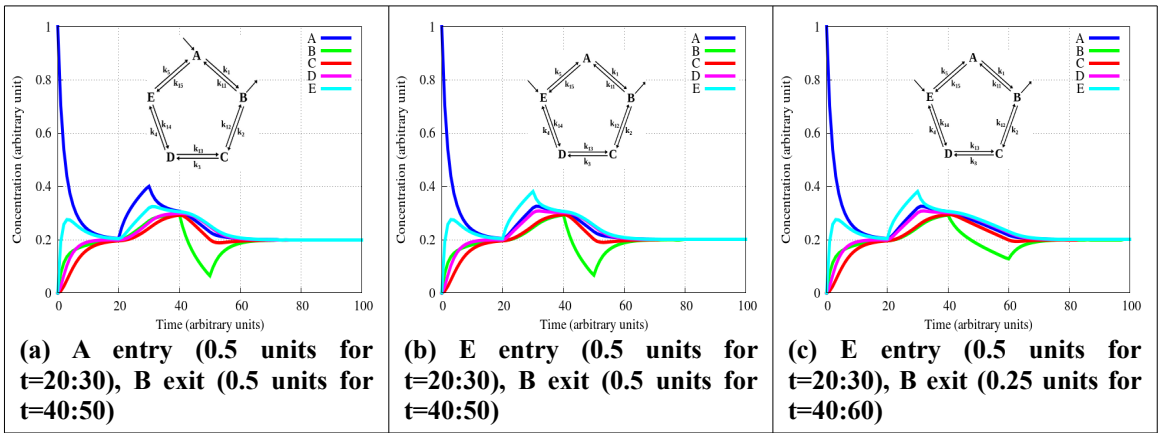

(a) A entry (0.5 units for t=20:30), B exit (0.5 units for t=40:50)

(b) E entry (0.5 units for t=20:30), B exit (0.5 units for t=40:50)

(c) E entry (0.5 units for t=20:30), B exit (0.25 units for t=40:60)

Figure 1.11: Simulation of a five-membered cyclic pathway, where the metabolite were added and removed separately for a short interval of time. $k_1=k_{11}=1$; $k_2=k_{12}=1.5$; $k_3=k_{13}=2$; $k_4=k_{14}=2.5$; $k_5=k_{15}=3$;

The results presented in Fig. 1.9 are obtained from a closed cyclic system, where metabolite A was given an initial concentration of 1 and all the other metabolites were kept at 0. Since it is a closed system, at steady-state, the concentration of all the metabolites become equal. In Fig. 1.9a, only three curves pertaining to A, E and D are seen, this because the curves of B and E are overlapped being equidistant from A, which is the source in this case. Similarly, curves of C and D are overlapped illustrating the symmetry. However due to the difference in rate constants in Fig. 1.9b and 1.9c, all the metabolites behave differently.

Fig. 1.10 presents the simulation results of a five-membered cyclic pathway in an open system. A constant input of 0.2 units was given to A in each cycle and a constant amount of metabolite B, 0.2 units, was removed in each cycle. Since the net addition and removal in the system is zero, the metabolites tend to attain a steady-state. It can be seen that at steady-state, the concentration of A is the highest and B is the lowest, and other components follow the sequence: A>E>D>C>B.

Fig. 1.11 represents the simulation of a five-membered cyclic pathway, where the metabolite were added and removed separately for a short interval of time. The net addition and removal of metabolites in terms of total concentration (in the system) was kept at zero. In Fig. 1.11a, metabolite A was added for a duration of 10 time units at the rate of 0.5 units per cycle, followed by removal of metabolite B for 10 time units at the rate of 0.5 units per cycle. In Fig. 1.11b, similar addition and removal were performed with metabolites E and B. In both these cases the corresponding behaviour of metabolites are similar. In Fig. 1.11c, metabolite E was added 0.5 units for 10 time units and metabolite B was removed at half that rate, i.e., 0.25 units for double the time, i.e., 20 time units. It is interesting to note that the steady-state values for all the three cases are same. This is because the net change in total concentration of the metabolite is same (i.e., zero) in all the cases.

References

Hindmarsh, A. C. (1983). ODEPACK, A Systematized Collection of ODE Solvers, RS Stepleman et al.(eds.), North-Holland, Amsterdam,(vol. 1 of), pp. 55-64. *IMACS transactions on scientific computation*, *1*, 55-64.

Chapter 2 Simulating the energy machinery

Energy Machinery

Pyruvate formed in glycolysis is transported to mitochondria where it is further oxidised to acetyl CoA, which enters Krebs cycle. Krebs cycle is an almost universal metabolic pathway, where acetyl-CoA combines with oxaloacetate to give citrate, and therefore is also called as citric acid cycle. Citrate undergoes a series of reactions in a cyclic manner to regenerate oxaloacetate, which further reacts with another molecule of acetyl-CoA to continue the cycle. Each cycle produces three molecules of NADH (from NAD^+), one molecule of $FADH_2$ (from FAD) and one molecule of GTP or ATP (from GDP or ADP). The NADH and $FADH_2$ produced here are further oxidised in the electron transport chain (ETC) leading to the formation of protonmotive force across inner mitochondrial membrane, and this energy is then used for ATP synthesis. The process of ETC and ATP synthesis is together called as oxidative phosphorylation. The overall process can be divided into three reaction sets (I) Krebs cycle (II) the ETC and (III) ATP synthesis. These processes are simulated individually first and then combined to give an overall dynamic metabolic pathway.

Krebs Cycle

Krebs cycle is also known as tricarboxylic acid cycle, or citric acid cycle, as the first stable product formed in the cycle is citrate, formed by citrate synthase when acetyl-CoA and oxaloacetate reacts. Acetyl-CoA is derived by oxidative decarboxylation of pyruvate. Pyruvate can also enter Krebs cycle through a side reaction catalysed by pyruvate carboxylase where it enters as oxaloacetate (Kornberg, 1966). Breakdown products of many amino acids which give rise to four or five carbon intermediates of the Krebs cycle that can also enter Krebs cycle and are oxidised in the process.

Krebs cycle is amphibolic in the sense that it serves for both catabolism and anabolism in the cell. The intermediates of the Krebs cycle can be drawn off from the cycle and can be used as input for other biosynthesis pathways. In such a condition, where intermediates are taken away from the cycle, they are replenished by other anaplerotic reactions catering to the requirements of the cell (Fig. 2.1).

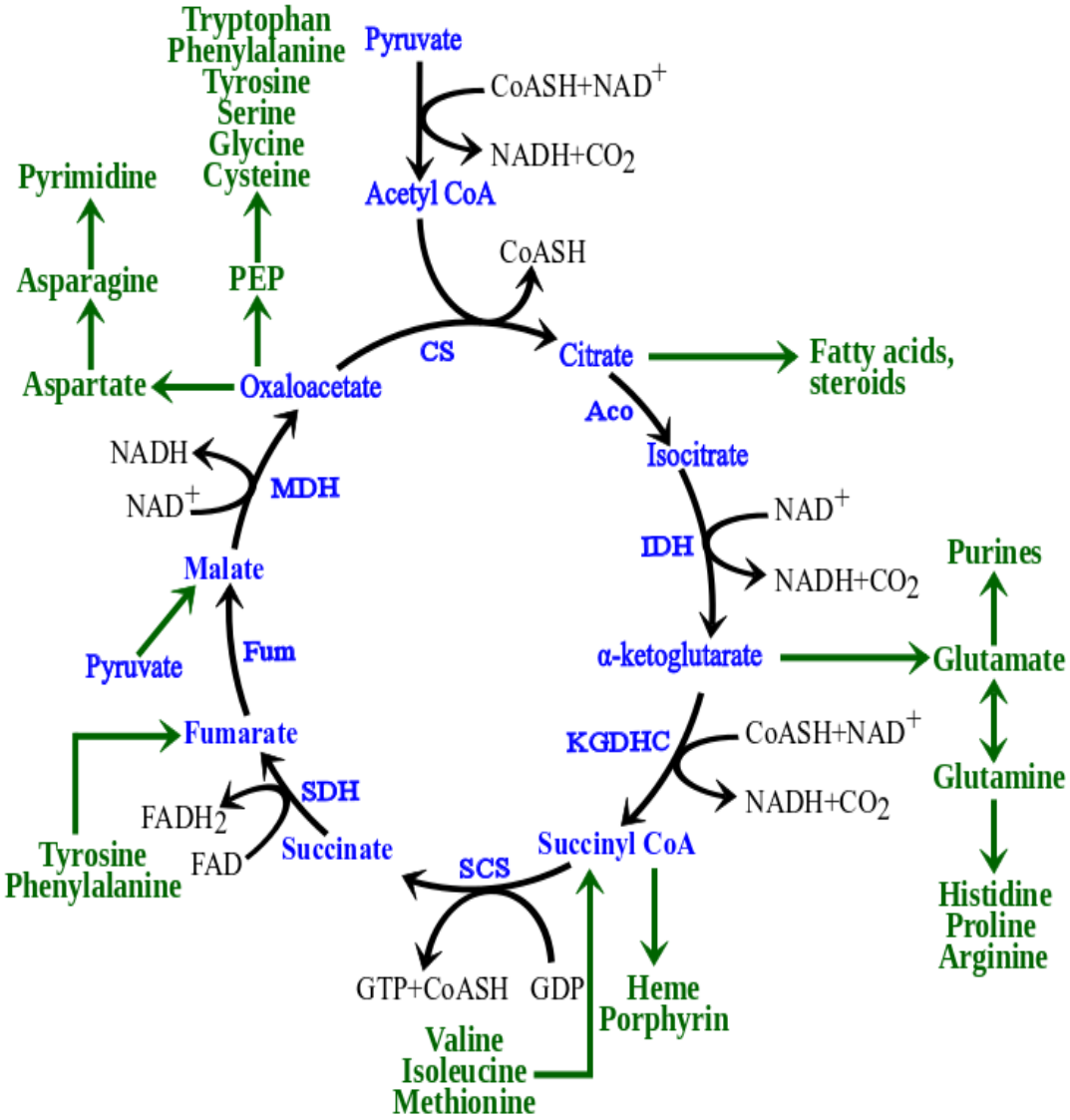

Figure 2.1: Overview of Krebs cycle. (CS= Citrate synthase, Aco=Aconitase, IDH=Isocitrate dehydrogenase, KGDHC=α-ketoglutarate dehydrogenase complex, SCS=Succinyl CoA synthetase, SDH=Succinate dehydrogenase, Fum=Fumarase, MDH=Malate dehydrogenase (Rellán-Álvarez, El-Jendoubi, Wohlgemuth, Abadía, Fiehn, Abadía & Álvarez-Fernández, 2011; Nelson & Cox, 2005).

The cycle consists of eight reactions starting with the formation of citrate, which is followed by seven sequential reactions to form oxaloacetate that again reacts with a new molecule of acetyl-CoA to form citrate. In the whole process, it is acetyl-CoA that is oxidised to form two molecules of carbon dioxide to release energy. The energy, thus released, is used to reduce three molecules of NAD^+, one molecule of FAD and one molecule of nucleoside triphosphate (GTP/ATP). Mitochondria in animals (including humans) have two succinyl-CoA synthetases: one that produces ATP from ADP, and another that produces GTP from GDP (Johnson, Mehus, Tews, Milavetz & Lambeth, 1988).

The reactions involved in this process are enlisted in Table 2.1.

Table 2.1: Reactions involved in the Krebs cycle. The last line indicates the overall reaction.

$Acetyl-CoA + Oxaloacetate + H_2O \rightarrow Citrate + CoA-SH$	(1)
$Citrate \rightarrow Isocitrate$	(2)
$Isocitrate + NAD^+ \rightarrow \alpha-Ketoglutarate + NADH + H^+ + CO_2$	(3)
$\alpha-Ketoglutarate + CoA-SH + NAD^+ \rightarrow Succinyl-CoA + NADH + H^+ + CO_2$	(4)
$Succinyl-CoA + GDP + P_i \rightarrow Succinate + GTP + CoA-SH$	(5)
$Succinate + FAD \rightarrow Fumarate + FADH_2$	(6)
$Fumarate + H_2O \rightarrow Malate$	(7)
$Malate + NAD^+ \rightarrow Oxaloacetate + NADH + H^+$	(8)
$\mathbf{Acetyl-CoA + 2H_2O + 3NAD^+ + GDP + P_i + FAD \rightarrow 3NADH + 3H^+ + FADH_2 + GTP + CoA-SH + 2CO_2}$	

It is seen that the final overall reaction shown in bold in the end does not include several intermediates of the pathway and indicates that this pathway catalyses oxidation of acetyl-CoA to carbon dioxide. The energy released is used in the formation of NADH, $FADH_2$ and GTP (or ATP). A close look on the broad features of the final reaction also suggests that that the cycle acts as a giant catalyst which ultimately catalyses oxidation of acetyl-CoA. The overall rate thus depends on the concentration of catalyst present and is thus controlled by the availability of acetyl-CoA, NAD^+, etc. The concentrations of NAD^+ and NADH play a crucial role, as they belong to the common mitochondrial matrix pool and are shared among several processes inside mitochondria. On the contrary, FAD is tightly bound to the transmembrane enzyme, succinate dehydrogenase, which is also a part of the ETC (complex II). Therefore, the electrons used for reduction of FAD are directly

channelled to the ETC (Stryer, Berg & Tymoczko., 2002). In fact, this enzyme acts as a direct link between the ETC and Krebs cycle.

Table 2.2: The list of enzymes of the Krebs cycle with their reactants, products, activators, inhibitors and EC number (Brenda database).

Reaction Step	Enzyme (EC number)	Input	Output	Inhibitor	Activator
Citrate formation	citrate synthase (EC2.3.3.1)	Oxaloacetate, Acetyl CoA, H_2O	Citrate, CoA-SH	NADH, succinyl-CoA, citrate, ATP	ADP
Isocitrate formation	Aconitase (EC4.2.1.3)	Citrate	Isocitrate		
α-Ketoglutarate formation	Isocitrate dehydrogenase (EC1.1.1.41)	Isocitrate, NAD^+	α-Ketoglutarate, NADH $+H^+$, CO_2	ATP	Ca^{2+}, ADP
Succinyl-CoA formation	α-Ketoglutarate dehydrogenase (EC1.2.4.2)	α-Ketoglutarate CoA-SH, NAD^+	Succinyl-CoA, NADH $+H^+$, CO_2	Succinyl-CoA, NADH	Ca^{2+}
Succinate formation	Succinyl-CoA synthetase (EC6.2.1.4)	Succinyl-CoA, GDP+P_i	Succinate, GTP, CoA-SH		
Fumarate formation	Succinate dehydrogenase (EC1.3.99.1)	Succinate, FAD	Fumarate, $FADH_2$		
Malate formation	Fumarase (EC4.2.1.2)	Fumarate, H_2O	Malate		
Oxaloacetate formation	Malate dehydrogenase (EC1.1.1.37)	Malate	Oxaloacetate, NADH $+H^+$		

Krebs cycle is under tight regulation by virtue of the anaplerotic reactions taking place inside the cell. Several components of Krebs cycle are involved in other processes inside mitochondria in particular and cell in general. They are being transported by means of transporters and shuttles systems across the mitochondrial membrane and form a regulatory link between the cytoplasmic and mitochondrial processes. Besides, the rate of conversion of pyruvate to acetyl-CoA and oxaloacetate also takes care of the side channelling of the other intermediates (as alpha-ketoglutarate, malate, succinate) of the cycle and thus maintaining the turnover. The flux through the cycle is thus also controlled through citrate synthase, isocitrate dehydrogenase, and α-ketoglutarate dehydrogenase, which form the internal regulatory sites. The fluxes through these enzymes are regulated by the end products

and substrates which act as inhibitors and stimulators respectively. A list of various reaction components (input and output) along with their enzymes, activators and inhibitors are compiled and presented in Table 2.2.

Rate equations

The rate equations were derived for all the components of the system, based on the reactions they are involved in, and the inhibitors were also taken into account. Similar approach, as presented in the Introduction (rate equations) section, was used to write rate equations. The rate equations for the 17 components of the Krebs cycle are given in Table 2.3.

Table 2.3: Rate equations of various components of Krebs cycle.

$\frac{d}{dt}[OxAc] = \frac{[OxAc]}{1+[OxAc]}.\frac{[AcCoA]}{1+[AcCoA]}.\frac{1}{1+[Cit]}.\frac{1}{1+[SucCoA]}+\frac{[Mal]}{1+[Mal]}.\frac{[NAD]}{1+[NAD]}$
$\frac{d}{dt}[AcCoA] = \frac{[OxAc]}{1+[OxAc]}.\frac{[AcCoA]}{1+[AcCoA]}.\frac{1}{1+[Cit]}.\frac{1}{1+[SucCoA]}$
$\frac{d}{dt}[Cit] = \frac{[OxAc]}{1+[OxAc]}.\frac{[AcCoA]}{1+[AcCoA]}.\frac{1}{1+[Cit]}.\frac{1}{1+[SucCoA]}-\frac{[Cit]}{1+[Cit]}$
$\frac{d}{dt}[IsoCit] = \frac{[Cit]}{1+[Cit]}-\frac{[IsoCit]}{1+[IsoCit]}.\frac{[NAD]}{1+[NAD]}$
$\frac{d}{dt}[KeGlu] = \frac{[IsoCit]}{1+[IsoCit]}.\frac{[NAD]}{1+[NAD]}-\frac{[KeGlu]}{1+[KeGlu]}.\frac{[CoASH]}{1+[CoASH]}.\frac{[NAD]}{1+[NAD]}.\frac{1}{1+[SucCoA]}$
$\frac{d}{dt}[SucCoA] = \frac{[KeGlu]}{1+[KeGlu]}.\frac{[CoASH]}{1+[CoASH]}.\frac{[NAD]}{1+[NAD]}.\frac{1}{1+[SucCoA]}-\frac{[SucCoA]}{1+[SucCoA]}.\frac{[GDP]}{1+[GDP]}$
$\frac{d}{dt}[Suc] = \frac{[SucCoA]}{1+[SucCoA]}.\frac{[GDP]}{1+[GDP]}-\frac{[Suc]}{1+[Suc]}.\frac{[FAD]}{1+[FAD]}$
$\frac{d}{dt}[Fum] = \frac{[Suc]}{1+[Suc]}.\frac{[FAD]}{1+[FAD]}-\frac{[Fum]}{1+[Fum]}$
$\frac{d}{dt}[Mal] = \frac{[Fum]}{1+[Fum]}-\frac{[Mal]}{1+[Mal]}.\frac{[NAD]}{1+[NAD]}$
$\frac{d}{dt}[CoASH] = \frac{[OxAc]}{1+[OxAc]}.\frac{[AcCoA]}{1+[AcCoA]}.\frac{1}{1+[Cit]}.\frac{1}{1+[SucCoA]}+\frac{[SucCoA]}{1+[SucCoA]}.\frac{[GDP]}{1+[GDP]}-\frac{[KeGlu]}{1+[KeGlu]}.\frac{[CoASH]}{1+[CoASH]}.\frac{[NAD]}{1+[NAD]}.\frac{1}{1+[SucCoA]}$
$\frac{d}{dt}[NAD] = -\frac{[IsoCit]}{1+[IsoCit]}.\frac{[NAD]}{1+[NAD]}-\frac{[KeGlu]}{1+[KeGlu]}.\frac{[CoASH]}{1+[CoASH]}.\frac{[NAD]}{1+[NAD]}.\frac{1}{1+[SucCoA]}-\frac{[Mal]}{1+[Mal]}.\frac{[NAD]}{1+[NAD]}$

$\frac{d}{dt}[NADH] = \frac{[IsoCit]}{1+[IsoCit]} \cdot \frac{[NAD]}{1+[NAD]} + \frac{[KeGlu]}{1+[KeGlu]} \cdot \frac{[CoASH]}{1+[CoASH]} \cdot \frac{[NAD]}{1+[NAD]} \cdot \frac{1}{1+[SucCoA]} + \frac{[Mal]}{1+[Mal]} \cdot \frac{[NAD]}{1+[NAD]}$
$\frac{d}{dt}[CO_2] = \frac{[IsoCit]}{1+[IsoCit]} \cdot \frac{[NAD]}{1+[NAD]} + \frac{[KeGlu]}{1+[KeGlu]} \cdot \frac{[CoASH]}{1+[CoASH]} \cdot \frac{[NAD]}{1+[NAD]} \cdot \frac{1}{1+[SucCoA]}$
$\frac{d}{dt}[GDP] = -\frac{[SucCoA]}{1+[SucCoA]} \cdot \frac{[GDP]}{1+[GDP]}$
$\frac{d}{dt}[GTP] = \frac{[SucCoA]}{1+[SucCoA]} \cdot \frac{[GDP]}{1+[GDP]}$
$\frac{d}{dt}[FAD] = -\frac{[Suc]}{1+[Suc]} \cdot \frac{[FAD]}{1+[FAD]}$
$\frac{d}{dt}[FADH_2] = \frac{[Suc]}{1+[Suc]} \cdot \frac{[FAD]}{1+[FAD]}$

All the components were given a unique identifier (element of an array), and these elements replaced the components' name from the rate equations stated above and were placed in the script.

Script

The script used for simulation of Krebs cycle is given in Table 2.4. The rate of change in concentration of substrates, 11-12, 14-17 have been kept at zero, i.e. throughout the process, their concentrations would remain same as their initial concentrations. These components include NAD^+, NADH, GTP, GDP, FAD and $FADH_2$. Since in the present system they are being utilised or generated only in one reaction and therefore can be kept as constant for the time being considering that they have a constant source and sink. However, while extending this script when these components will be involved in multiple reactions, the equations can be updated to have non-zero rate of change. S13, i.e. CO_2 is continuously produced in the reaction system and is not utilised in the system. Therefore, a constant amount of 0.05 units is removed in each cycle to avoid its sequestration. This value for constant removal has been optimally obtained so as to match its formation rate.

Table 2.4: Script for simulation of the Krebs cycle.

```
1;
% solve the Krebs cycle
function ds=krebs(s)
%
% S1...S10 are, respectively,       Oxaloacetate, Acetyl-CoA
```

```
%           Citrate, Isocitrate, alpha-keto-glutarate, succinyl-CoA
%           Succinate, fumarate, Malate, CoA-SH
% S11 is NAD , S12 is NADH, S13 is CO2 ,S14 is GDP
% S15 is GTP , S16 is FAD ,S17 is FADH2
% KM and VM follow the equation numbers...
% We consider all KM values as 1.

ds=zeros(17,1);
LHS1=(s(1)/(1+s(1)))*(s(2)/(1+s(2)))*(1/(1+s(3)))*(1/(1+s(6)));
% this is inhibited by s3; s6; s12; ATP
LHS2=(s(3)/(1+s(3)));
LHS3=(s(4)/(1+s(4)))*(s(11)/(1+s(11)));
% this is inhibited by ATP
LHS4=(s(5)/(1+s(5)))*(s(10)/(1+s(10)))*(s(11)/(1+s(11)))*(1/(1+s(6)));
% this is inhibited by s6; s12
LHS5=(s(6)/(1+s(6)))*(s(14)/(1+s(14)));
LHS6=(s(7)/(1+s(7)))*(s(16)/(1+s(16)));
LHS7=(s(8)/(1+s(8)));
LHS8=(s(9)/(1+s(9)))*(s(11)/(1+s(11)));
% the rate equations follow:
ds(1) =-LHS1+LHS8;
ds(2) =-LHS1+0.020;
% ds(2) is added continuously from external sources...
ds(3) = LHS1-LHS2;
ds(4) = LHS2-LHS3;
ds(5) = LHS3-LHS4;
ds(6) = LHS4-LHS5;
ds(7) = LHS5-LHS6;
ds(8) = LHS6-LHS7;
ds(9) = LHS7-LHS8;
ds(10)= LHS1-LHS4+LHS5;
% NAD and NADH must be maintained const externally
% ds(11)=-LHS3-LHS4-LHS8;
% ds(12)= LHS3+LHS4+LHS8;
ds(11)=0; ds(12)=0;
ds(13)= LHS3+LHS4-0.040;
% ds(13) is continuously being lost...
%if (ds(13)<0) ds(13)=0;
%end
% GDP,GTP, FAD and FADH2 must be externally maintained
% ds(14)=-LHS5;
% ds(15)= LHS5;
% ds(16)=-LHS6;
% ds(17)= LHS6;
ds(14)=0; ds(15)=0; ds(16)=0; ds(17)=0;
return
end
% use lsode to solve this set...
lsode_options("relative tolerance",1e-4);
lsode_options("absolute tolerance",1e-3);
t=0:0.2:1000;
```

```
% supply the initial concentrations ...
s0=[0.5,0.5,0,0,0,0,0,0,0,0,0.5,0,0,0.5,0,0.5,0];
[s,T,MSG]=lsode(@krebs,s0,t);
T
MSG
plot(t,s(:,1),"linewidth",5,t,s(:,2),"linewidth",5,t,s(:,3),"linewidth",
5,t,s(:,4),"linewidth",5,t,s(:,5),"linewidth",5,t,s(:,6),"linewidth",5);
grid on;
axis([0,100,-0.001,.55]);
set (gca,'FontName','Times, Bold');
set (gca,'FontSize',24);
xlabel ("Time/arbitrary units");
ylabel ("Concentration/arbitrary units");
legend("Ox-Ac","Ac-CoA","Citrate","Iso-Cit","Ke-Glu","Suc-
CoA","location","east");
```

The initial concentrations of the components that are required to initiate the cycle, as acetyl-CoA and oxaloacetate are kept at 0.5. Other intermediates of the cycle that are eventually formed in the cycle, are kept at zero. These intermediates are expected to be formed and utilised as the cycle proceeds.

Result

The script in the previous section when run in Octave terminal yields a plot as shown in Fig. 2.2. Concentrations of selected components of Krebs cycle are plotted here. It is seen in the figure that the concentration of acetyl-CoA and oxaloacetate goes down and all the other intermediates, rise to form a peak and then decline. This essentially suggests that as the cycle proceeds, oxaloacetate and acetyl-CoA are consumed to form the intermediates. Also, the intermediates are formed and then are converted to the succeeding member in the cycle, and therefore the curves show a peak and then a decline in case of citrate, isocitrate, α-ketoglutarate and succinyl-CoA. Another important feature, to be noted, is the sequence of occurrence of peaks for each intermediate. The peak for citrate is followed by peak for isocitrate, α-ketoglutarate and succinyl CoA, which follows the sequence in which they occur in the cycle. It is seen that the system attains a steady-state around 50 time units. In the absence of any external perturbation, the system continues to be in steady-state.

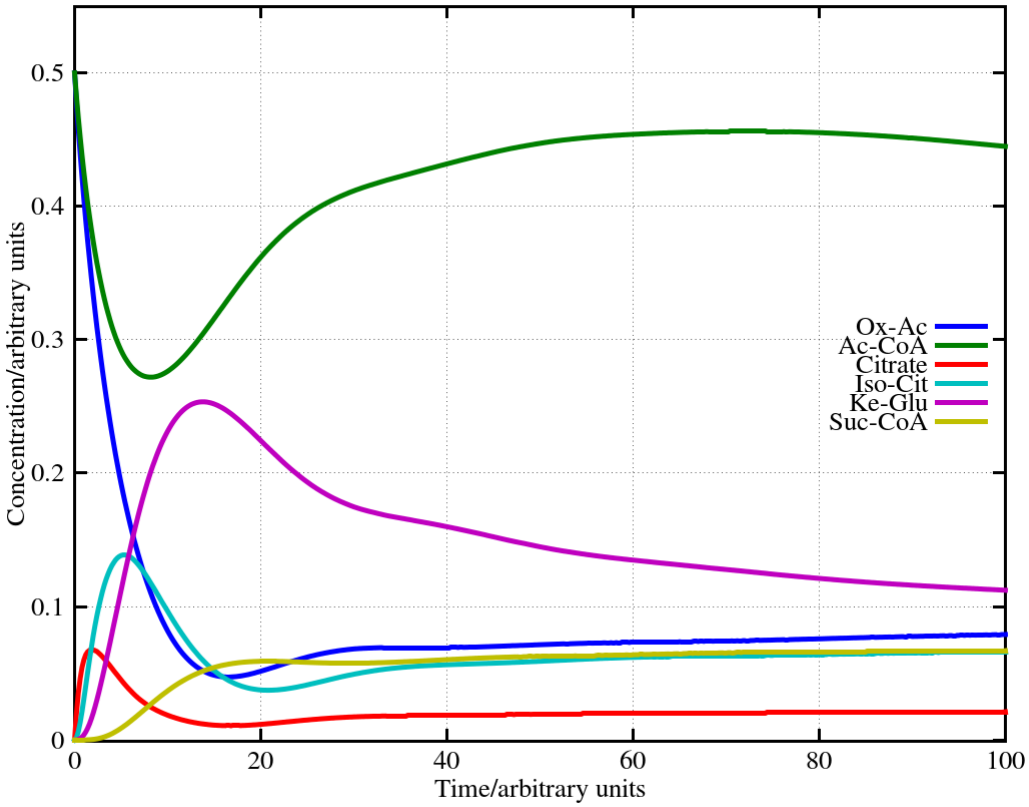

Figure 2.2: Simulation curve for selected components of Krebs cycle. Ox-Ac=oxaloacetate, Ac-CoA= acetyl-CoA, Iso-Cit=Isocitrate, Ke-Glu= α-ketoglutarate and Suc-CoA=succinyl CoA

An analysis of the effect of anaplerotic reactions was carried out by addition and removal of intermediates from the system. In Fig. 2.3 the first figure (2.3a) shows the simulation results in normal simulation environment for visual comparison. In Fig. 2.3b, fumarate was added for the duration of nine time points ranging from 31-39 time points and shortly after this α-ketoglutarate was removed for the same duration of time, i.e., nine time points ranging from 41-49. Similar study was conducted incorporating addition of Succinyl-CoA and removal of oxaloacetate (Fig. 2.3c) and with an addition of oxaloacetate and removal of citrate (Fig. 2.3d). The behaviours of the metabolites in the first 30 time units are similar for all of them, as expected. Variations are seen in the mid region of the curves, where all the concentrations of metabolites change corresponding to the additions and removals made. It is interesting to note that despite the removal and addition of metabolites the system tends to return to the same steady-state. Also, the final concentrations at 100 time point for a given metabolite settle around the same region and not far from the concentrations seen in normal simulation (Fig. 2.3a). This behaviour suggests stability of the reaction system (and the equations derived therefrom) under regular perturbations.

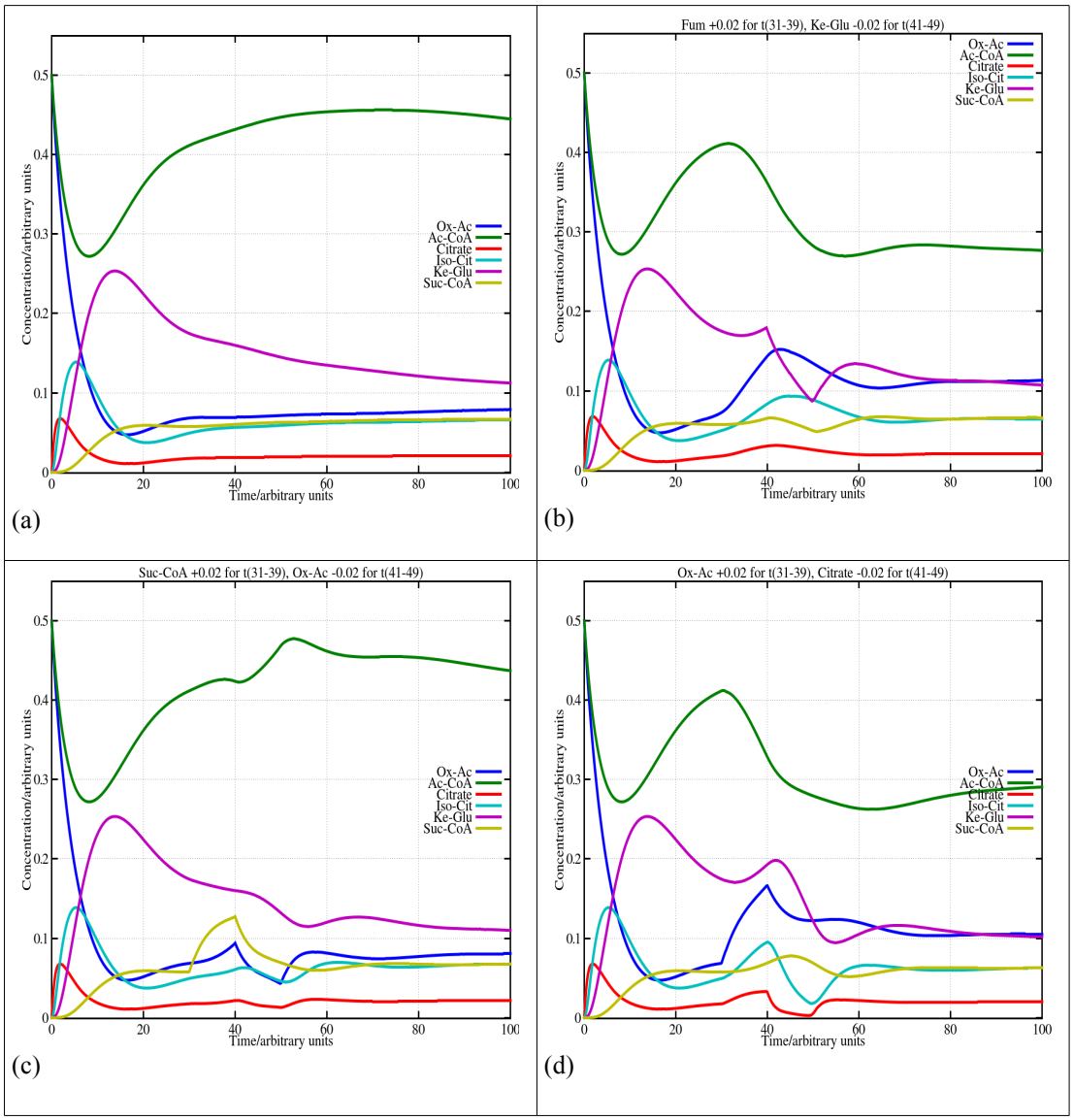

Figure 2.3: The response of the system in different metabolite environment. The first figure (a) corresponds to the native system and has been shown for visual comparison. (b) Fumarate was added to the system for a short duration (nine time points, 31-39) and then after a small gap same amount of α-ketoglutarate was removed for the same duration of time (nine time points, 41-49). Similar tests were done with (c) addition of Succinyl-CoA and removal of oxaloacetate, and (d) with the addition of oxaloacetate and removal of citrate. In all the above cases, even after the perturbation the system tends to return to a steady-state

The Electron Transport Chain (ETC)

The energy stored in NADH and $FADH_2$ formed during the Krebs cycle should be utilised to form ATPs. For this purpose, an electron transport chain is employed, where electrons from these species are transferred to oxygen via a number of redox species. NADH and $FADH_2$ are oxidised by a set of four protein complexes lined on the inner mitochondrial membrane and named as complexes I, II, III and IV. NADH oxidation is facilitated via complexes I, III and IV, and $FADH_2$ oxidation is facilitated by complexes II, III and IV. The first step in both the processes is oxidation by quinone, giving rise to quinol and the oxidised counterpart of NADH and $FADH_2$, i.e. NAD^+ and FAD respectively. The reactions corresponding to each of the complexes are shown in Table 2.5.

Complex I: *Transfer of electrons from NADH to Ubiquinone*- The enzyme **NADH:ubiquinone oxidoreductase** (EC 1.6.99.5) contains 44 separate polypeptide chain and is the largest of the respiratory complexes. Its L-shaped structure includes a large transmembrane domain (consisting around 60 helices) and a hydrophilic domain. Hydrophilic domain includes the NADH binding site, flavin prosthetic group (FMN) and eight iron-sulphur clusters (FeS). Complex I facilitates the exergonic transfer of a hydride ion from NADH along with a proton from the matrix to ubiquinone, thus forming ubiquinol. This reaction results in translocation of up to four protons from the mitochondrial matrix to intermembrane (IM) space (Wikstrom 1984). The protons thus translocated give rise to pH gradient (and protonmotive force) across the inner mitochondrial membrane. However, this also suggests that when pH gradient is sufficiently high, further translocation of proton will be resisted and in such a condition, NADH oxidation would also come to halt. The coupling between NADH oxidation by ubiquinone and proton translocation, thus indicates that the activity of complex I is pH dependent, and the rate of reaction would depend on the pH gradient across the inner mitochondrial membrane.

Complex II: *Transfer of electrons from $FADH_2$ to ubiquinone*- The enzyme **succinate dehydrogenase** is a membrane-bound enzyme in the inner mitochondrial membrane and is shared by both Krebs cycle and the ETC. Complex II consists of two hydrophobic and two hydrophilic subunits. Hydrophobic subunits, SdhC and SdhD, act as membrane anchors. Hydrophilic subunits include a flavoprotein (SdhA) and an iron-sulphur protein (SdhB). Flavoprotein contains a covalently linked FAD and succinate binding site. Iron-sulphur protein includes three iron-sulphur clusters [2Fe-2S], [4Fe-4S], and [3Fe-4S].

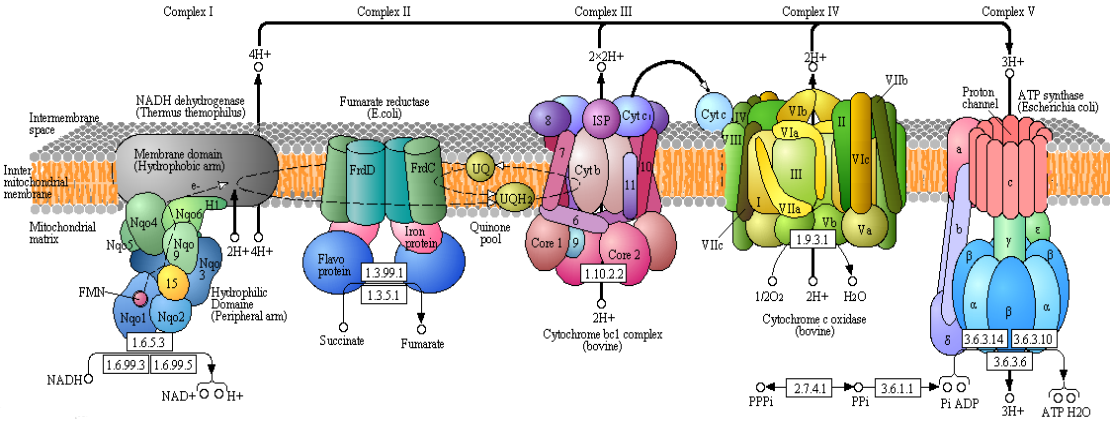

Figure 2.4: Diagrammatic Representation of Oxidative Phosphorylation. It shows the flow of two electrons along the electron transport chain, resulting in the reduction of oxygen. About three molecules of ATP are produced from the oxidation of one molecule of NADH. Figure is taken from http://www.genome.jp/kegg-bin/show_pathway?map00190.

Succinate dehydrogenase catalyses the conversion of succinate to fumarate by reducing FAD to $FADH_2$. This $FADH_2$ is directly channelled to the ETC. FAD and $FADH_2$ are tightly bound to the enzyme, unlike NADH, which is present in the common pool and can be derived from multiple sources. The enzyme further catalyses the transfer of electrons from $FADH_2$ to ubiquinone to form ubiquinol (Cecchini, 2003). There is no proton translocation in this step, and so this enzyme is not particularly pH regulated but is regulated by the Krebs cycle regulators.

Table 2.5: Reactions involved in electron transport chain. The sequence represents the reactions carried out by complexes I, II, III and IV respectively.

$NADH + H^+ + Q \rightarrow NAD^+ + QH_2$	(9)
$FADH_2 + Q \rightarrow FAD + QH_2$	(10)
$QH_2 + 2\text{cyt } c_{(o)} \rightarrow Q + 2\text{cyt } c_{(r)}$	(11)
$O_2 + 4\text{cyt } c_{(r)} + 4H^+ \rightarrow 4\text{cyt } c_{(o)} + 2H_2O$	(12)

Complex III: *Transfer of electrons from ubiquinone to cytochrome c (cyt c)*- The enzyme **ubiquinone:cytochrome c oxidoreductase** transfers electrons from ubiquinone to cyt c, via other cytochromes (cyt b and cyt c_1). Complex III contains eleven subunits: three respiratory subunits, two core proteins and six low-molecular weight proteins (Zhang, Huang, Shulmeister, Chi, Kim, Hung, *et al.*, 1998). Respiratory subunits include cyt b, cyt c_1 and the Rieske iron-sulphur protein subunit.

Cytochrome c is a heme protein, which carry one electron per molecule and therefore two molecules of cytochrome, are required for the oxidation of one molecule of ubiquinol. The half-reactions along with the respective redox potentials are compiled in Table 2.6. This electron transfer is also coupled with the translocation

of up to four protons. This suggests that two protons from ubiquinol and two protons from the matrix are translocated to the IM space. This complex is also regulated by the pH gradient across the inner mitochondrial membrane in a way similar to complex I.

Table 2.6: The list of half-reactions involved in electron transport chain and their respective redox potentials. (*Lehninger, A. L., Nelson, D. L., & Cox, M. M. (2005). Lehninger principles of biochemistry. 2005, 4th edition, WH Freeman.***)**

Redox reaction (half-reaction)	E'° (V)
$NAD^+ + 2H^+ + 2e^- \rightarrow NADH$	0.320
$Ubiquinone + 2H^+ + 2e^- \rightarrow Ubiquinol$	0.045
$Cyt\ b(Fe(III)) + e^- \rightarrow Cyt\ b(Fe(II))$	0.077
$Cyt\ c_1(Fe(III)) + e^- \rightarrow Cyt\ c_1(Fe(II))$	0.22
$Cyt\ c(Fe(III)) + e^- \rightarrow Cyt\ c(Fe(II))$	0.254
$Cyt\ a(Fe(III)) + e^- \rightarrow Cyt\ a(Fe(II))$	0.29
$Cyt\ a_3(Fe(III)) + e^- \rightarrow Cyt\ a_3(Fe(II))$	0.35
$0.5\ O_2 + 2H^+ + 2e^- \rightarrow H_2O$	0.8166

Complex IV: The enzyme, **cytochrome c oxidase**, catalyses the transfer of electrons from reduced cytochrome c to cytochrome a to cytochrome a_3 and then to oxygen. Oxygen acts as the terminal electron acceptor. The half-reactions of these redox reactions are shown in Table 2.6. This step is again tightly coupled with the translocation of up to two protons. This further suggests that the rate of activity of this complex also depends on the pH gradient across the inner mitochondrial membrane. Complete reduction of one molecule of oxygen requires four electrons, and thus four cytochrome c are involved in the reduction of one molecule of oxygen. Protons are also used in the formation of water as a result of the reduction of oxygen in this reaction.

The list of enzymes and the inputs and outputs for individual reactions are listed here in Table 2.7. Unlike Krebs cycle, there are no activators/ inhibitors listed, because the functioning of the ETC mainly depends on the influx of substrates i.e. NADH and $FADH_2$. Further, as discussed earlier, complexes I, III and IV are pH dependent and hence are regulated by the pH gradient across the inner mitochondrial membrane. Also, as seen in Fig. 2.4, most part of these enzymes is present physically inside the matrix and thus are expected to be under direct effect of the matrix pH. Further complex II is also part of the Krebs cycle and is regulated in the cycle.

Table 2.7: The enzymes of the Electron Transport Chain (ETC) with their reactants and products.

Reaction Step	Enzyme (EC number) [5]	Input	Output
NADH to Ubiquinone	NADH:ubiquinone oxidoreductase (EC 1.6.99.5)	NADH, H^+, Q	NAD^+, QH_2
Succinate to Ubiquinone	Succinate dehydrogenase (EC 1.3.5.1)	$FADH_2$, Q	FAD, QH_2
Ubiquinone to Cytochrome c	Ubiquinone: cytochrome c oxidoreductase (EC 1.10.2.2)	QH_2, oxidised cyt c, H^+	Q, reduced cyt c
Cytochrome c to O_2	Cytochrome oxidase (EC 1.9.3.1)	O_2, reduced cyt c, H^+	H_2O, oxidised cyt c

The reactions through complex III and IV are common for NADH and $FADH_2$. The entry point however is different, i.e. they enter from complex I and II respectively. But it is seen that complex II is not involved in proton translocation. So the total number of protons translocated in the oxidation of NADH and $FADH_2$ are not same. Also, this indicates that oxidation of both the species are essentially independent, and presence of either or both of them can lead to functional ETC.

Protons translocated in oxidation of one molecule of NADH = 4 (CI) + 4 (CIII) + 2 (CIV)= 10 protons.

Protons translocated in oxidation of one molecule of $FADH_2$ = 4 (CIII) + 2 (CIV) = 6 protons.

The maximum number of protons translocated in oxidation of one molecule of NADH and FADH2 are ten and six protons respectively.

These protons translocated to the IM space, form the basis of interaction between the ETC and ATP synthesis. The translocated protons create a pH gradient, due to the difference in the number of hydrogen ions on both sides of the membrane. Also due to separation of charges, an electrical gradient is established. Other ions as Ca^{2+}, K^+, Na^+, etc., also contribute to the electrical gradient. The pH gradient and electrical gradient together form the electrochemical gradient also known as the protonmotive force (pmf). This pmf drives complex V, i.e. ATP synthase machinery. It is experimentally difficult to calculate the exact value of individual components of pmf. Soga *et al.* have reported that either of the two components of the pmf can drive ATP synthesis even if the other opposes.

The rate of ATP synthesis is related to the algebraic sum of the two (pmf), and both contribute to the kinetics of ATP synthesis. A combination of ΔpH in the range of -0.3 to 2.2 and $\Delta\Psi$ between -30 and 140 mV resulting in pmf up to 250 mV, irrespective of the individual magnitudes and signs, can lead to ATP synthesis (Soga, Kinosita, Yoshida & Suzuki, 2012). It is only via pmf that the ETC is linked to ATP

synthesis; otherwise there is no physical or molecular connection between the two processes. Therefore, even if ETC is blocked, ATP synthesis can still take place, provided the required pmf is maintained.

Most of the studies related to mitochondrial functions have been carried out using inhibitors. The particular roles of the various subunits present in respiratory complexes have been found out using a combination of inhibitors. The common respiratory chain inhibitors include antimycin A, cyanide, rotenone and thenoyltrifluoroacetone (TTFA). Antimycin A blocks electron transfer in complex III between cytochrome b and cytochrome c_1. It affects oxidation of both NADH and $FADH_2$. Cyanide blocks complex IV, cytochrome oxidase, binds to iron in the complex, thus inhibiting electron the transfer from cytochrome c to oxygen. Rotenone blocks complex I, NADH dehydrogenase, and inhibits the transfer of electrons from complex I to ubiquinone. TTFA blocks complex II, succinate dehydrogenase and therefore does not affect NADH oxidation by the ETC.

Rate equation

The enzymes involved in ETC are complex in their structure with few subunits derived from the mitochondrial genome itself (except for complex II). Seven subunits of complex I, one subunit of complex III and three subunits of complex IV are translated individually from the mitochondrial genome. Also, these complexes are functionally multitasking (redox reaction and proton pump). The detailed mechanisms and information regarding the rate determining steps are not available for these complexes.

As discussed earlier, complexes I, III and IV are regulated by pH across the inner mitochondrial membrane, and these complexes catalyse electron transfer along with proton translocation from the mitochondrial matrix to the intermembrane space. The two phenomena are tightly coupled, therefore if proton translocation cannot take place, then electron transfer also stops. An important challenge in simulating this process is coupling the redox reactions taking place in a given complex and facilitating proton translocation at the same time, followed by appropriately modifying pH on both sides of the membrane. It further implies that if the proton gradient becomes too high, further proton translocation will not take place and so the redox reaction should also stop even in the simulation background. The exact change in pH gradient depends on the number of protons translocated and the volume of the compartment. However, these reactions take place in the folds of inner mitochondrial

membrane and therefore the local pH changes substantially with a small change in proton concentration. Also, as mentioned earlier and seen in Fig. 2.4 too, the active sites in the complexes are in the matrix side. Therefore, the enzyme (complex) activity is expected to be more affected by the pH of the matrix, and this point has been used for writing the script.

In the present simulation, however protons are shown in the reactions, but they are not part of the rate equations but are incorporated in the rate constant and therefore the rate constant is now pH dependent. Redox reactions are essentially reversible; and so are these redox reactions, but the reverse reaction will be no more coupled to proton translocation. The rate equations used for the script for electron transport chain are given in Table 2.8.

Managing change in pH as the redox reactions takes place, pose a challenge in simulating the ETC. Translocation of one proton from the matrix to IM space, result in the decrease in the number of protons in the matrix by 1 and increase in the proton count of IM space. Now in terms of pH gradient there is a difference of two protons, i.e. IM space has two more protons as compared to the matrix. In the present simulation, pH has to be varied after reactions of complexes I, III and IV as these are involved in proton translocation. To meet this purpose, the rate constants for these reactions are varied due to pH by a factor of $1/(1+(\Delta pH)^2)$. Here, ΔpH is the difference between pH in the matrix and the pH within the IM space (Santo-Domingo & Demaurex, 2012).

Table 2.8: Rate equations for the components of electron transport chain

$k = \frac{1}{1+(\Delta pH)^2}$
$\frac{d}{dt}[NADH] = -k\,[NADH]\,[Q]$
$\frac{d}{dt}[FADH_2] = -k\,[FADH_2]\,[Q]$
$\frac{d}{dt}[Q] = -k\,[NADH]\,[Q] - [FADH_2]\,[Q] + k[QH_2]\,[Cyt\,c_{(o)}]$
$\frac{d}{dt}[QH_2] = k\,[NADH][Q] + [FADH_2]\,[Q] - k[QH2]\,[Cyt\,c_{(o)}]$
$\frac{d}{dt}[Cyt\,c_{(o)}] = -k[QH_2]\,[Cyt\,c_{(o)}] + k[Cyt\,c_{(r)}]\,[O_2]$
$\frac{d}{dt}[Cyt\,c_{(r)}] = k[QH_2]\,[Cyt\,c_{(o)}] - k[Cyt\,c_{(r)}]\,[O_2]$
$\frac{d}{dt}[O_2] = k[Cyt\,c_{(r)}]\,[O_2]$

In the present simulation, the pH of the IM space is kept as constant and the matrix pH is varied. It signifies that the pH gradient is important rather than the individual values of pH on the two sides of the inner mitochondrial membrane. So varying pH of any one of the compartment is equally effective and in addition keeps the approach comprehensive. Moreover, since these reactions take place in the folds of inner mitochondrial membrane, transfer of even a few protons will lead to a significant change in local pH. Several calculations were used for computing the pH, and the approach is as follow...

Suppose the matrix pH is *x* and the effective volume of the matrix (cristae region) is *v*

therefore, the hydrogen ion concentration is 10^{-x} and the number of moles of protons in volume *v* is $v.10^{-x}$

If *n* moles of protons are translocated from IM space to the matrix, the concentration of protons in the matrix increases to $10^{-x}+n/v$, and the new pH will be

$$-\log_{10}\left(10^{-x}+\frac{n}{v}\right)=x-\log_{10}\left(1+\frac{10^{x}n}{v}\right) \quad .$$

If the term $10^{x}n/v$ is less than 1, the equation can be linearised to

$$x-\frac{1}{2.303}\,\frac{n}{v}\,10^{x}$$

as the new pH and then the $\Delta pH = -0.4343(n/v)\ 10^{pH}$. Here *n* is known but calculation of *v* is rather approximate. A crude estimation can be made based on the size of mitochondria and the volume of the matrix thereby. Electron microscopy studies indicate the linear size of mitochondrion ~500nm, which is likely to correspond to a volume of $\sim 1 \times 10^{-16}$ l. The matrix volume would be around 50% of this. Using the above formula, it is calculated that one proton translocation can change the matrix pH by 0.04 pH units at pH 7. This value can be further increased to account for the cristae present in the matrix and is arbitrarily chosen to be 0.2 (per proton translocated out of the matrix). As discussed earlier, it was assumed that pH in the IM space is constant, and only the pH in the matrix is increasing thus giving rise to a pH gradient. Further, the IM space pH was kept fixed at 6.

Experimental evidences suggest that the reaction kinetics of the reactions involved in the ETC are strongly pH dependent (Jain & Nath, 2001). This also reflects the facts that the proton translocation is coupled to the redox reactions and once a desired pH gradient is established and if it sustains, further coupled redox reactions would eventually stop. In the previous section, it was suggested that the rate constant is transformed to be pH dependent. The model proposed here to represent

rate constant as a function of pH is given as:

$$k \rightarrow k.\frac{1}{1+(pH-6)^2} = k.\frac{1}{1+(\Delta pH)^2} = k.\frac{1}{1+(0.4343(n/v)10^{pH})^2}$$

Here pH corresponds to the matrix pH, as the IM space pH is kept constant at 6. With the increase in pH, k decreases in a sigmoidal fashion. This supports the experiments conducted by Jain and Nath (Jain & Nath, 2001).

Script

The script written to simulate the electron transport chain is given in Table 2.9. There are seven components in this system, viz. NADH, $FADH_2$, ubiquinone (Q), ubiquinol (QH_2), cytochrome c (oxidised and reduced forms) and oxygen. The initial concentrations of NADH and $FADH_2$ are kept such that their proportion is 3:1, which is same as the output from their output from the Krebs cycle. Also, the constant input for these species is in the same ratio. The initial concentrations of oxidised species as Q and cytochrome c are given initial concentration 1, and their respective reduced counterparts are kept at zero, as they are expected to be formed in the process. Other cytochromes as cyt b, cyt c1, cyt a, cyt a3 are not used in the reactions as these are the internal reactions taking place inside the complexes III and IV and therefore can be ignored for sake of simplicity. The rate constants have been kept at 1.

Table 2.9: Script written for the simulation of electron transport chain.

```
1; % solve the etc constant supply of NADH, FADH2 and O2
function dc=oxip(c)
% c1...c7 are, resp, NADH, Q, QH2, cyt c(oxi), cyt c(red),O2, FADH2.
% 4 rate consts k1,k2,k3,k4 for the reactions of complex I,II,III,IV
% a correspond for delta ph constant with ph values
% 7.78 in mito matrix(pH1) ; 6.88 in im space(pH2);
% a=1/(2-(c2/c1))
k1=1;
k2=1;
k3=1;
k4=1;
a=0.52;
dc=zeros(7,1);
E1=k1*c(1)*c(2)*a;
E2=k2*c(7)*c(2);
E3=k3*c(3)*c(4)*a;
E4=k4*c(5)*c(6)*a;
% the rate equations follow:
dc(1) =-E1+0.06; %NADH
%dc(1) = 0;
dc(2) =-E1-E2+E3; % Q
dc(3) = E1+E2-E3; % QH2
```

```
dc(4) =-E3+E4; % Cyt cox
dc(5) = E3-E4; % cyt c red
dc(6) =-E4+0.08; % O2
dc(7) =-E2+0.02; % FADH2
return
end
% use lsode to solve this set...
lsode_options("relative tolerance",1e-4);
lsode_options("absolute tolerance",1e-3);
t=linspace(0,25,1000);
% supply the initial concentrations ...
c0=[.75,1,0,1,0,1,0.25];
[c,T,MSG]=lsode(@oxip,c0,t);
T
MSG
plot(t,c(:,1),"linewidth",3,t,c(:,2),"linewidth",3,t,c(:,3),"linewid
th",3,t,c(:,4),"linewidth",3,t,c(:,5),"linewidth",3,t,c(:,6),"linewi
dth",3,t,c(:,7),"linewidth",3);
grid on;
set (gca,'FontSize',18);
title ("Both NADH and FADH2 are present\n in 3:1 ratio");
xlabel ("Time/arbitrary units");
ylabel ("Concentration/arbitrary units");
legend("NADH","Q","QH2","cyt c o","cyt c r", "Oxygen", "FADH2",
"location", "northeast");
```

The rate equations, as mentioned in the previous section, are transformed appropriately to be written in the script. Other parameters are set, and the script is run in terminal in Octave environment.

Result

The simulation result of the script given in the previous section is presented here in Fig. 2.5. The figure shows all the components of the system. It is seen that the system reached a steady-state around 15 time points. The curves for Q and QH_2 are complementary, primarily indicating that their total concentration remains same. Similarly for cytochrome c, oxidised and reduced forms are complementary. Concentrations of NADH, $FADH_2$ and oxygen decrease as reactions proceed and reach a steady-state under the given set of increments.

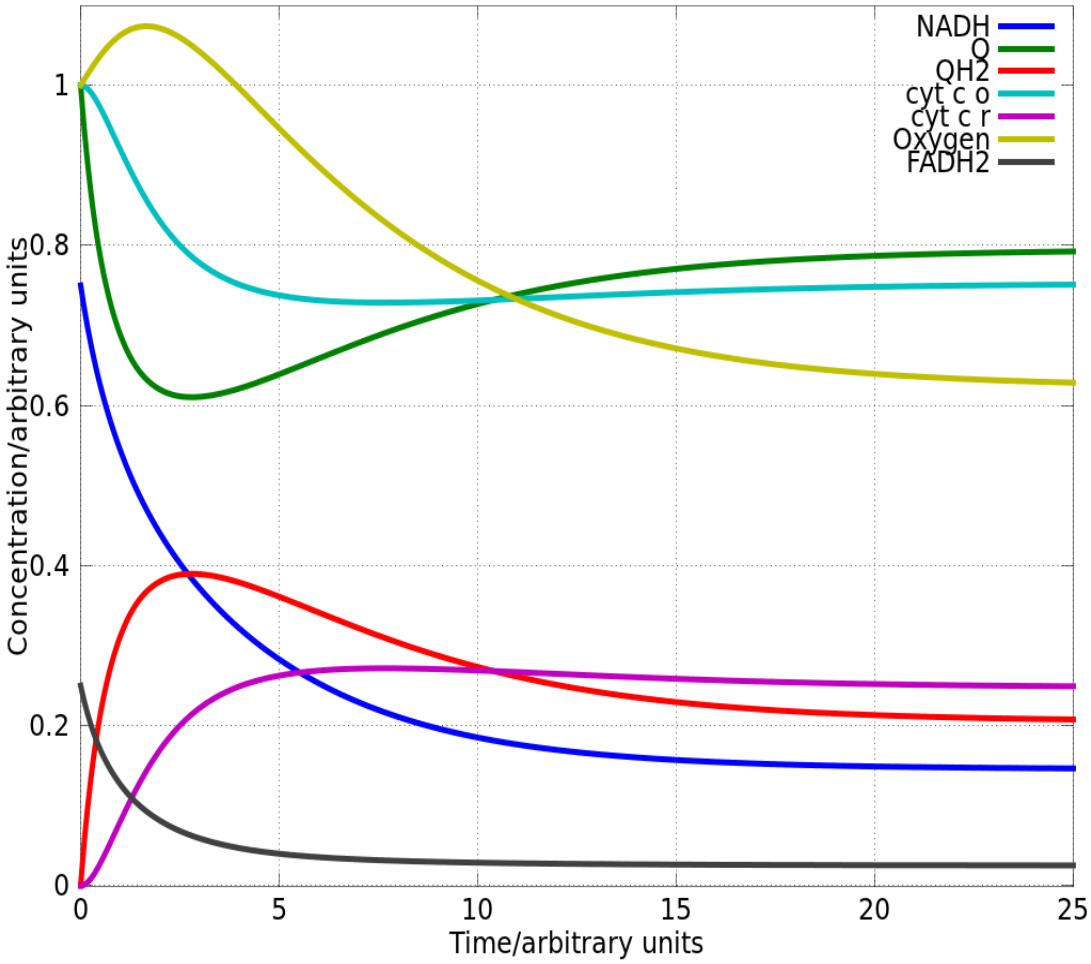

Figure 2.5: Simulation curve for selected components of electron transport chain (Q = Quinone, QH_2 = Quinol, cyt c o = Cytochrome c oxidised form, cyt c r = Cytochrome c reduced form).

ATP Synthesis

The last complex from Fig. 2.4 shows the ATP synthase, which is responsible for ATP synthesis inside the mitochondria. It is seen that ATP synthase, also called the complex V in oxidative phosphorylation is not physically linked to the other four complexes. It is only by the virtue of the chemiosmotic potential (pmf) established across the inner mitochondrial membrane that these complexes are linked. Protons translocated by complexes I, III and IV contribute to protonmotive force along with other ion fluxes across the membrane. This protonmotive force drives ATP synthesis in a mechanism as explained by the binding change mechanism proposed by Boyer (Boyer, 1993). So the ETC is indirectly coupled to ATP synthesis, and the combined process is called as oxidative phosphorylation. Studies with uncouplers have shown that the two processes are physically independent and can function in the absence of each other provided the electrochemical potential (pmf) across the membrane is appropriately maintained. Experimental evidence suggests that P/O ratios of oxidative phosphorylation is about 2.5 with NADH-linked substrates (via complexes I, III and IV) and 1.5 with $FADH_2$ (via complex II, III and IV) (Hinkle, 2005). P/O ratio is defined as the number of ATPs produced per oxygen atom reduced by the respiratory chain. This can be linked to the number of protons translocated in each set, 10 protons in case of NADH-linked substrates and 6 protons for $FADH_2$. This also suggests the relation between the number of protons used up for the generation of one ATP in normal condition. 10 protons are used for generation of 2.5 ATPs, and therefore, four protons are required for generation of one ATP. This also matches with the proton-ATP relation for $FADH_2$, where six protons are translocated, and the P/O ratio is 1.5 ATPs.

Table 2.10: Reactions involved in ATP synthesis.

$P + E + H^+_{out} \rightarrow E-P + H^+_{in}$	(13)
$E-P + MgADP + H^+_{out} \rightarrow E-P-MgADP + H^+_{in}$	(14)
$E-P-MgADP + H^+_{out} \rightarrow E-MgATP + H^+_{in}$	(15)
$E-MgATP + H^+_{out} \rightarrow E + MgATP + H^+_{in}$	(16)
$\boldsymbol{MgADP + P + 4H^+_{out} \rightarrow MgATP + 4H^+_{in}}$	

The details of the reactions involved in ATP Synthesis are shown in Table 2.10 (Weber & Senior, 2003). The last line indicates the overall reaction. E is the

enzyme, and P stands for phosphate. H^+_{out} stands for proton in the IM space, and H^+_{in} denotes protons in the matrix.

Rate equation

Rate of ATP synthesis can be given as,

$k\ [\mathrm{MgADP}]\ [P_i][H^+_{out}]^4$

As discussed previously, the proton concentration is incorporated in the rate constant (k) and therefore k becomes pH dependent. New $k = k\ [H^+_{out}]^4$, which clearly indicates the pH dependence of k. Rate constant here is varied due to pH by a factor of 4. This equation is empirical, but broadly corresponds to the experimental results available in the literature (Jain & Nath, 2001). The functional dependence for ATP synthase is derived in a similar way as was done for the ETC enzymes, and the new k is given as

$$k \rightarrow k.\frac{(pH-6)^4}{1+(pH-6)^4} = k.\frac{(\Delta pH)^4}{1+(\Delta pH)^4}$$

In the present simulation, the efflux (during the ETC) and influx (during ATP synthesis) of protons is mainly responsible for the change of pH of the matrix, however the actual changes depend on the local (and relative) volumes of the cristae (for the matrix) and the intermembrane space. The rate equation thus for the formation of ATP is given as

$$\frac{d}{dt}[ATP] = k.\frac{(\Delta pH)^4}{1+(\Delta pH)^4}\ [ADP][P_i]$$

Script

The rate of formation of ATP, as stated in the previous section, was used to calculate the rate of ATP synthesis at different matrix pH. Table 2.11 shows the script written to calculate ATP production when the matrix pH is 6.5. Similar scripts were used to have a comparative analysis of the amount of ATP synthesis at different matrix pH levels (keeping in consideration that the IM space pH has been kept constant at 6). So for several levels of matrix pH ranging from 6-9.5, a range of pH gradient, ΔpH ranging from 0-3 can be studied. In the script, Line#29, the last entry 6.5, corresponds to the matrix pH. The value of 6.5 was changed to values as 7, 7.5, 8, 8.5, 9, to have a range of ΔpH and to study the behaviour of ATP synthesis at respective ΔpH.

Table 2.11: Script written for the simulation of ATP synthesis when the matrix pH is kept at 6.5

```
1;
% solve for atp synthesis at matrix pH 6.5
function ds=krebs(s)
% s1 is ATP, s2 is ADP, s3 is phosphate , s4 is pH inside.
x= s(4);                        % pH value inside the matrix
k2=((x-6)/2)^4/(1+((x-6)/2)^4);                 %   k2   is   for   ATP
synthase.
ds=zeros(4,1);
% Equation for ATP synthesis
LHS13=k2*s(2)*s(3);
% x= x-(2.303*(10^(-1))*3);
% ATP synthesis rate equation
ds(1) = LHS13;
ds(2) = (-LHS13);
ds(3) = (-LHS13);
ds(4) = 0;
return
end
% use lsode to solve this set...
lsode_options("relative tolerance",1e-4);
lsode_options("absolute tolerance",1e-3);
t=0:0.2:100;
% supply the initial concentrations ...
s0=[0,0.5,0.5,6.5];
[s,T,MSG]=lsode(@krebs,s0,t);
T
MSG
plot(t,s(:,1),"linewidth",3,t,s(:,2),"linewidth",3);
grid on;
title ("pH 6.5");
legend("ATP","ADP","location","northeast");
```

The result obtained from these scripts were used to extract data for ATP concentration and were simultaneously plotted using GNUPLOT to have a comparative study. The GNUPLOT script used for plotting these set of curves is given in Table 2.12.

Table 2.12: Script written for plotting a multiplot showing different levels of ATP synthesis in different levels of matrix pH.

```
set terminal png
set output 'inset2.png'
set multiplot
# Bigger plot options
set xrange [ 0.00000 : 500.000 ]
set yrange [ -0.0100000 : 0.510000 ]
set xtics 100, 100, 500 font "arial, 16"
```

```
set ytics 0, 0.1, 0.5 font "arial, 16"
set size 1,1
set grid
set origin 0,0
set xlabel 'Time (arbitrary unit)' font "sans, 14"
set ylabel 'Concentration (arbitrary unit)' font "sans, 14"
# This plots the big plot
plot "ph6.txt" using 0:1 with lines noti lw 2, "ph65.txt" using 0:1 with lines noti lw 2, "ph7.txt" using 0:1 with lines noti lw 2,  "ph75.txt" using 0:1 with lines noti lw 2, "ph8.txt" using 0:1 with lines noti lw 2, "ph85.txt" using 0:1 with lines noti lw 2, "ph9.txt" using 0:1 with lines noti lw 2, "ph95.txt" using 0:1 with lines noti lw 2

# Now we set the options for the smaller plot
set size 0.4,0.4
set origin 0.55,0.25
set title 'Rate const vs pH' font "sans, 14";
set xrange [6:10]
set yrange [0:1]
set xtics ("6" 6, " " 7, "8" 8, " " 9, "10" 10)
set xtics font "arial, 14"
set ytics font "arial, 14"
set ytics ("0" 0,  " " 0.25, "0.5" 0.5, " "0.75, "1" 1)
unset xlabel
unset ylabel
unset arrow
set grid
# And finally let's plot the same set of data, but in the smaller plot
plot ((x-6)/2)**4/(1+((x-6)/2)**4) noti lw 2
# It's important to close the multiplot environment!!!
unset multiplot
# EOF
```

An inset plot has also been plotted which shows the sigmoidal behaviour of the function.

Result

As discussed earlier, the rate of ATP synthesis depends on the protonmotive force across the inner mitochondrial membrane. A comparative analysis was carried out to study the impact of a range of ΔpH on the rate of ATP synthesis. However, along with ΔpH, which is the chemical component of pmf, the electrical gradient, ΔΨ, also contributes as the electrical component. In the present work, we have not included ΔΨ. This is because the ions as Na^{+}, K^{+}, Mg^{++} and Ca^{++}, which substantially affect the membrane potential, are not involved in any of the reactions under study here. Also, membranes are rich in phosphates, and they act as buffers on the membrane surface and so here we are assuming that the membrane potential remains

constant. Therefore, only the effect of pH was studied, and Fig. 2.6 shows the curves for ATP synthesis at different matrix pH levels.

In Fig. 2.6, there are eight curves in the main plot, and they correspond to different matrix pH levels, the bottom-most corresponding to pH 6 and the top-most corresponding to 9.5. Here, the bottom-most curve shows a straight line parallel to x-axis, indicating no ATP production as the IM space pH is fixed at 6, and therefore ΔpH is practically zero. In the absence of an electrochemical gradient, ATP synthesis cannot take place. However, as the matrix pH level increases, ΔpH also increases and consequently ATP synthesis also increases. At pH 6.5, less than 20% of the product is formed even at 500 time points, however at pH 8, ~90% of the product is formed at 200 time points only. The maximum increase in the ATP production is in the range of 6.5-8. It suggests that oxidative phosphorylation system functions in a narrow range of pH, where maximal productions can be achieved with minimal variations in the pH. However, it is seen that beyond pH 8, the effect of the change in pH on the rate of ATP production is not very significant. Further, this result matches with the earlier studies which report the optimum pH of the mitochondrial matrix as 7.6 and of IM space as 6.88 (Porcelli, Ghelli, Zanna, Pinton, Rizzuto & Rugolo, 2005). This shows that the maximum regulation on the rate of ATP synthesis can be achieved in this range and so the physiological pH is maintained in this range. This fact also validates the model presented here. Another interesting feature is the resemblance of these curves with the Michaelis-Menten curve. Also, an inset curve has been drawn which shows the sigmoidal relationship between rate constant and pH, as was mentioned in the previous section.

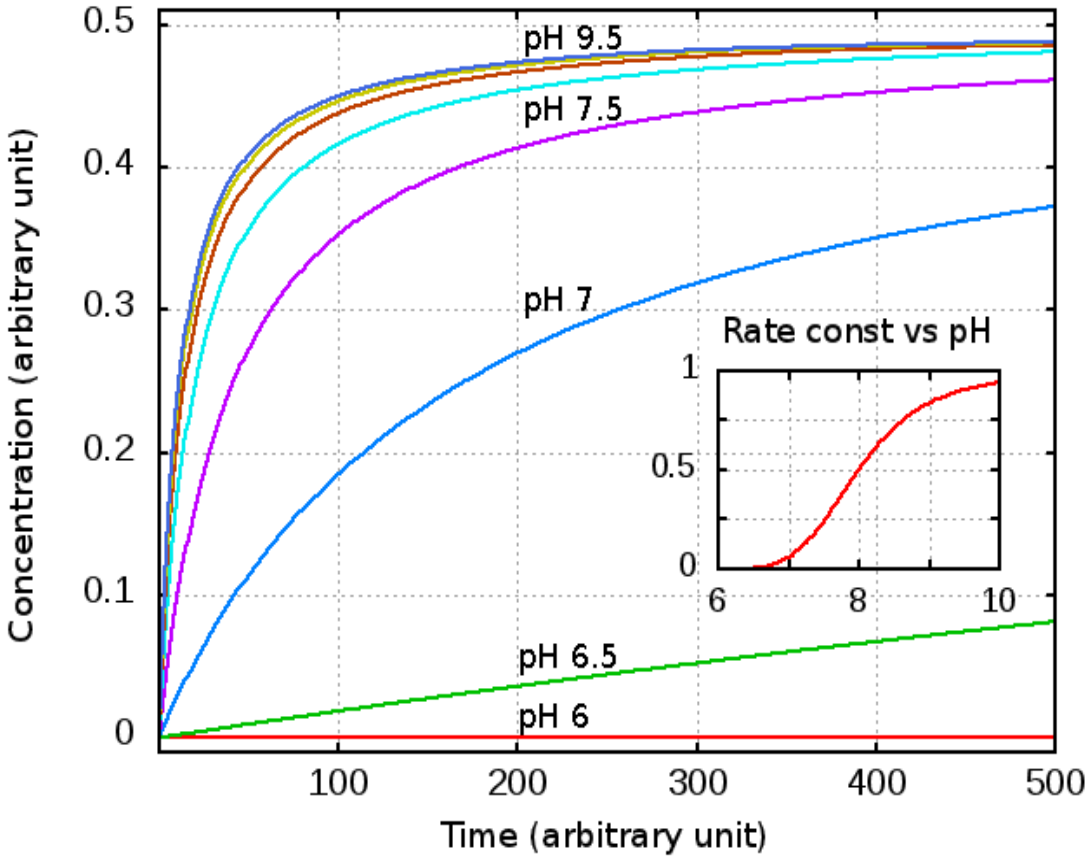

Figure 2.6: The curves for ATP synthesis at different matrix pH levels. The lowest curve corresponds to pH 6, and the subsequently following curves represent increasing pH values in steps of 0.5 units. The inset image shows the curve for rate constant vs pH which shows a sigmoidal dependence.

Combined Simulation

The three subsets described above were simulated individually to standardise internal parameters. The next logical step in the plan was to combine these subsets to have a bigger model of energy machinery inside mitochondria. However, the primary requirement, before it can be combined, was to bring their outputs and inputs at par, i.e. to ensure that the stoichiometry of the three different sets is consistent. It has already been discussed that the outputs of Krebs cycle (NADH and $FADH_2$) act as the input for the ETC. Now, in one round of Krebs cycle, three NADH and one $FADH_2$ is formed. This implies that the ETC should be made to undergo the corresponding number of turns in the same time to maintain the redox balance in the matrix. So, for simultaneous oxidation of three molecules of NADH, the complexes I, III and IV should undergo three sets of reaction. Also, for $FADH_2$, complexes II, III and IV should undergo one set of reaction. So in the whole, by the time Krebs cycle completes one round, complex I should run thrice, complex II should run once and complexes III and IV should run four times.

Further, for the ETC and ATP synthesis, the only connection here is the translocation of protons. Based on this stoichiometric analysis, the following calculations can be made:
Three sets of reactions from complex I would translocate 3*4 protons = 12 protons.
Four sets of reactions from complex III would translocate 4*4 = 16 protons
Similarly, four sets from complex IV would translocate 4*2 = 8 protons

Therefore, for one round of Krebs cycle, a total of 36 protons are translocated. Earlier in the text it was calculated that for every 4 protons translocated, one ATP is formed, so for 36 protons, 9 ATPs would be formed. So, the complex V should undergo nine sets of reaction while Krebs cycle completes one round. These values were appropriately incorporated into the rate equations, to have a reasonably good approximation of the coupling between the three subsets. However, this part of the work represents a tight coupling between the three subsets of energy machinery and this is not the case in the real physiological system. This is because here the pathways are assumed to be a closed system, which is not otherwise correct. Several components as $NADH/NAD^+$, ATP/ADP, malate, oxaloacetate, α-ketoglutarate, etc. are part of the matrix pool and may have more than one sources and sinks. This suggests a loose coupling between the three subsets.

Script

All the components of the three subsets are included to write a giant script given in Table 2.13, which consists of 26 constituents. Scripts of the three subsets were appropriately modified, and a unique nomenclature was followed to consolidate the rate equations. Molar equivalence, as described in the previous sections, was considered, and the stoichiometry was appropriately incorporated to maintain the coupling of the three subsets.

Table 2.13: Script written for combined simulation of the energy machinery, which includes, the Krebs cycle, electron transport chain and ATP synthesis.

```
1;
% solve the Krebs cycle, ETC, ATP synthesis: combined simulation
function ds=krebs(s)
% S1...S10 are respectively, Oxaloacetate, Acetyl-CoA, Citrate,
% Isocitrate, alpha-keto-glutarate, succinyl-CoA, Succinate,
% fumarate, Malate, CoA-SH ; S11 is NAD, S12 is NADH, S13 is CO2
% S14 is GDP, S15 is GTP, S16 is FAD, S17 is FADH2
% KM and VM follow the equation numbers...
% We consider all KM values as 1.
% s18...c22 are, respectively,Q, QH2, cyt c(oxi), cyt c(red),O2.
% s23 is ATP, s24 is ADP, s25 is phosphate , s26 is pH inside.
% 7.6 in mito matrix(pH1->x) ; 6.88 in im space(pH2);

x=s(26);          % pH value inside the matrix, x-6 is used formula
k1=1/(1+(x-6)^2);       % k1 is for complex 1, 3 and 4
k2=((x-6)^4)/(1+(x-6)^4);     % k2 is for ATP synthase.

ds=zeros(26,1);
% Equations for Kreb cycle reactions
LHS1=(s(1)/(1+s(1)))*(s(2)/(1+s(2)))*(1/(1+s(3)))*(1/(1+s(6)));
% this is inhibited by s3; s6; s12; ATP
LHS2=(s(3)/(1+s(3)));
LHS3=(s(4)/(1+s(4)))*(s(11)/(1+s(11))); % this is inhibited by ATP
LHS4=(s(5)/(1+s(5)))*(s(10)/(1+s(10)))*(s(11)/(1+s(11)))*(1/
(1+s(6)));
% this is inhibited by s6; s12
LHS5=(s(6)/(1+s(6)))*(s(14)/(1+s(14)));
LHS6=(s(7)/(1+s(7)))*(s(16)/(1+s(16)));
LHS7=(s(8)/(1+s(8)));
LHS8=(s(9)/(1+s(9)))*(s(11)/(1+s(11)));

% Equations for ETC reactions
LHS9=3*k1*(s(12)/(1+s(12)))*(s(18)/(1+s(18)));
x=(0.2*4*LHS9);
LHS10=(s(17)/(1+s(17)))*(s(18)/(1+s(18)));
% no proton involved
LHS11=4*k1*(s(19)/(1+s(19)))*((s(20))^2/(1+(s(20))^2));
x= x+(0.2*4*LHS11);
```

```
LHS12=4*k1*((s(21))^4/(1+(s(21))^4))*(s(22)/(1+s(22)));
x= x+(0.2*2*LHS12);

% Equation for ATP synthesis
LHS13=k2*(s(24)/(1+s(24)))*(s(25)/(1+s(25)));
x= x-(0.2*4*LHS13);
% the rate equations follow:
ds(1) =-LHS1+LHS8;
ds(2) =-LHS1+0.002;
ds(3) = LHS1-LHS2;
ds(4) = LHS2-LHS3;
ds(5) = LHS3-LHS4;
ds(6) = LHS4-LHS5;
ds(7) = LHS5-LHS6;
ds(8) = LHS6-LHS7;
ds(9) = LHS7-LHS8;
ds(10)= LHS1-LHS4+LHS5;
ds(11)=-LHS3-LHS4-LHS8+LHS9;
% multiplied by 3, because in one cycle of krebs cycle 3NADH is
produced and this reaction will thus occur thrice.
ds(12)= LHS3+LHS4+LHS8-LHS9;
% NAD + NADH are constant values...
% same way FAD/FADH2 and GDP/GTP , ADP/ATP together constant.
ds(13)= LHS3+LHS4;
ds(14)=-LHS5;
ds(15)= LHS5;
% GDP and GTP must be recycled continuously...
ds(16)=-LHS6+LHS10;
ds(17)= LHS6-LHS10; % FAD and FADH2 must be externally recycled...

ds(18) =-LHS9-LHS10+LHS11;
% multiplied by four, because for one round of krebs cycle, complex
3 and 4 should undergo four times(3 for NADH and one for FADH2)
redox reaction.
ds(19) = LHS9+LHS10-LHS11;
ds(20) =-LHS11+LHS12;
ds(21) = LHS11-LHS12;
ds(22) =-LHS12+0.001;
% ATP synthesis rate equation
ds(23) = LHS13;

% multiplied by a factor of nine for one round of krebs cycle, i.e.3
NADH (3*10 protons) and 1 FADH2 (6 protons)= 36 protons are
translocated, and 4protons/ATP released= 9ATPs formed.
ds(24) = -LHS13 +0.0001;
ds(25) = -LHS13 +0.0001;
ds(26) = x;

return
end
% use lsode to solve this set...
lsode_options("relative tolerance",1e-4);
```

```
lsode_options("absolute tolerance",1e-3);
t=0:0.2:200;
% supply the initial concentrations ...
s0=[0.5,0.5,0,0,0,0,0,0,0,0,0.5,0,0,0.5,0,0.5,0,0.5,0,0.5,0,0.5,0,0.
5,0.5,7.6];
[s,T,MSG]=lsode(@krebs,s0,t);
T
MSG
plot(t,s(:,2),"linewidth",5,t,s(:,12),"linewidth",5,t,s(:,17),"linew
idth",5,t,s(:,20),"linewidth",5,t,s(:,22),"linewidth",5,t,s(:,23),"l
inewidth",5);
grid on;
set (gca,'FontSize', 18);
axis([0,100,-0.001,0.55]);
% title ("Simulating 3 in 1");
xlabel ("Time/arbitrary units");
ylabel ("Concentration/arbitrary units");
set (gca,'FontSize', 18)
legend("Ac-CoA","NADH","FADH2","cytcox","Oxygen","ATP",
"location","east");
```

The components that are not regenerated in the reaction system, acetyl-CoA, ADP, phosphate, oxygen, are constantly fed. Cofactors as NAD^+ and FAD are regenerated in the system and therefore are just given once as input and are allowed to be recycled in the system. Here for the present system, the whole energy machinery in a closed system acts as a giant catalyst with four inputs (acetyl-CoA, ADP, phosphate, oxygen) and two outputs (ATP and carbon dioxide).

Result

The combined script was used to study the interaction among the metabolites. The script, as presented in the previous section, was run, and the following results were obtained. In Fig. 2.7, with the decrease in the concentration of acetyl-CoA, the concentration of ATP increases. The steady-state can be seen around 60 time points. Both NAD^+ and $FADH_2$ were given the same initial concentration of 0.5. However the formation of NADH and $FADH_2$ are not in same proportion as the reaction system approaches steady-state. NADH and $FADH_2$ appear to be in proportion of 3:1, which is same as the output of the Krebs cycle. They have achieved a steady-state in the same proportion indicates that at this level the amount of NADH and $FADH_2$ formed can be conveniently oxidised by the subsequent electron transport chain. Other components as cytochrome c (oxidised form) level goes down as the reduced species (NADH) in the matrix have increased. Oxygen level goes down as it is being utilised in the system.

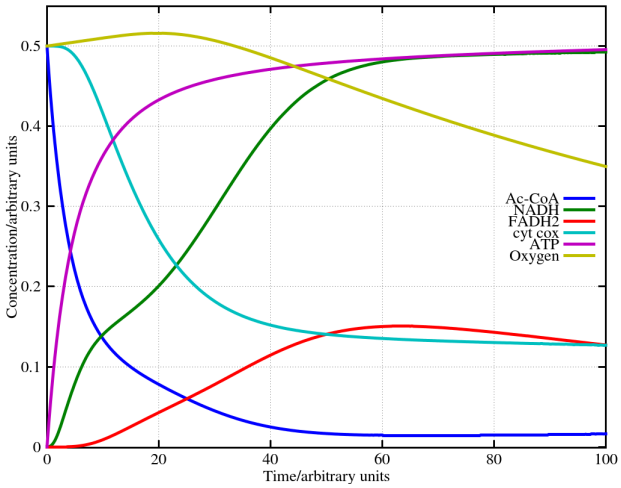

Figure 2.7: Combined Simulation: Curve showing selected components when the three subsets of energy machinery are combined. (Ac-CoA= Acetyl-CoA, cyt-cox=Cyt c oxidised form)

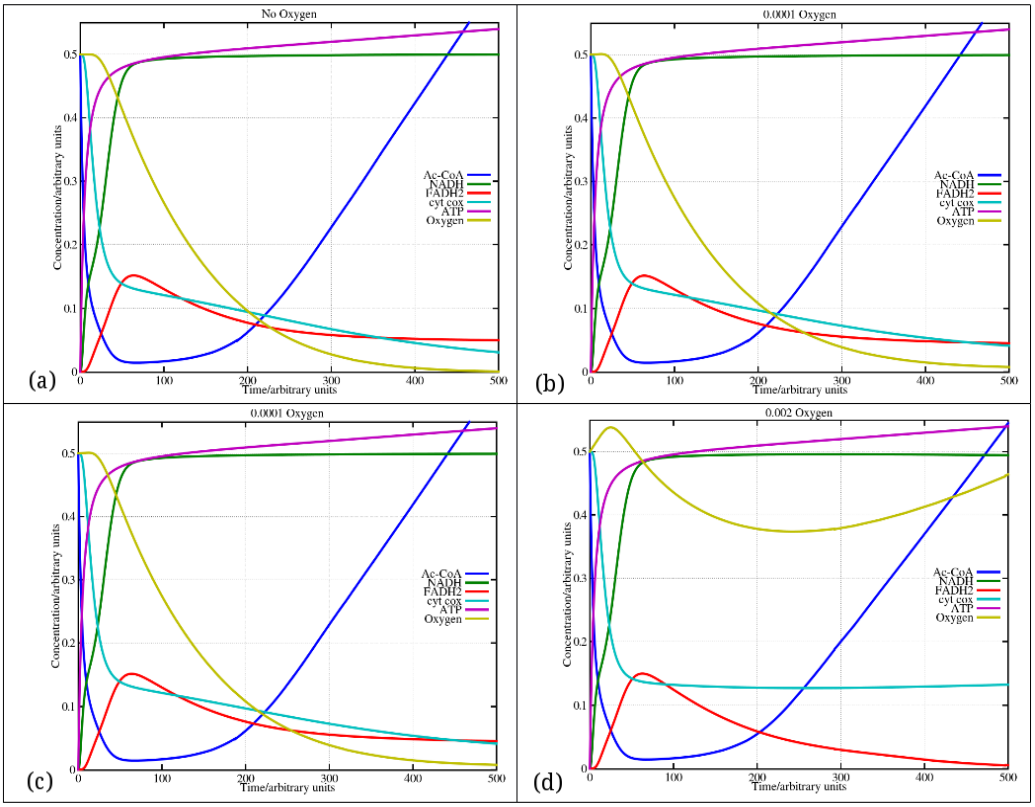

Figure 2.8: Keeping all the other parameters constant, the amount of oxygen given as the constant supply to the system was varied (values mentioned on top of each figure).As the concentration of oxygen pumped increases, there is a decrease in the concentration of NADH & $FADH_2$ (the decrease in NADH is not prominently visible in the figure but indeed there is a change), i.e., NADH & $FADH_2$ are oxidised. Further, concentration of oxygen also has a small impact on the consumption of acetyl-CoA in the system. With the increase in concentration of oxygen, acetyl-CoA concentration decreases. Concentration of oxygen shows its influence on the cytochrome c oxidation state, as expected. As the concentration of oxygen increases, concentration of oxidised form of cytochrome c also increases.

This system enables the study of the impact of a given perturbation on the whole system. Moreover at any given point in time, impact of a single component can be seen on all the other components of the system. A relative study of the effect of different levels of oxygen and acetyl-CoA on the combined system was undertaken, and following results were obtained.

In Fig. 2.8, all the parameters were kept constant, and only the amount of oxygen fed in as a continuous source was changed. As a result of this, changes in the concentrations of other components of the system were observed. With the increase in the increment concentration fed in each cycle, the consumption of acetyl-CoA increased. It is because with more amount of oxygen in the system, the oxidation potential is increased, and correspondingly more amount of acetyl-CoA is oxidised. Further, the concentrations of NADH and $FADH_2$ reduced proportionately. This is because of increased rate of the ETC, as the concentration of terminal electron acceptor is increased. Also, the concentration of oxidised form of cytochrome c increased considerably with the increase in the concentration of oxygen in the system.

In Fig. 2.9, all the parameters were kept constant, and only the amount of acetyl-CoA fed in as a continuous source was changed. As a result of this, changes in the concentrations of other components of the system were observed. It was seen that with the increase in the increment concentration fed in each cycle, the concentration of NADH and $FADH_2$ increases. It is because with more acetyl-CoA, the turnover of the Krebs cycle is expected to increase, leading to increased oxygen consumption.

Another case study, where the reaction corresponding to ATP synthase was blocked, and the effect of this perturbation studied. Fig. 2.10 shows the results, where (a) is the normal simulation result and (b) is the simulation when ATP synthase is blocked. It is seen that when ATP synthase is blocked, ATP concentration goes to zero as expected. Final concentration of oxygen at 100 time point is higher when ATP synthase is blocked. It is essentially because the pH gradient built across the membrane is not *utilised* for ATP synthesis, and it inhibits further transfer of protons from the matrix to IM space, leading to inhibition of the ETC reactions and accumulation of oxygen.

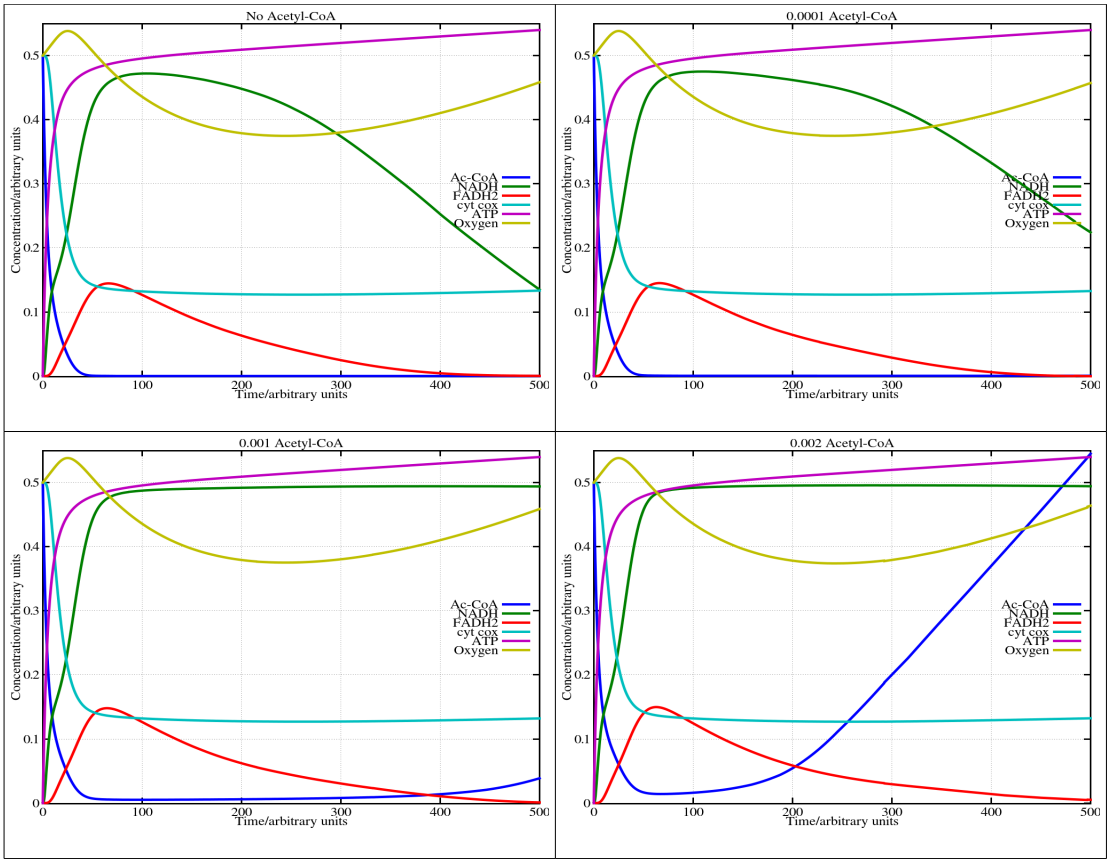

Figure 2.9: Keeping all the other parameters constant, the amount of acetyl-CoA given as the constant supply to the system was varied (values mentioned on top of each figure). The initial concentration of acetyl-CoA is same in all the four cases. Acetyl-CoA was continuously fed into the system. The change in the amount of acetyl-CoA fed after every cycle reflects a change in the other system components. When the concentration of acetyl-CoA is increased, rise in the concentration of NADH (& $FADH_2$) is observed.

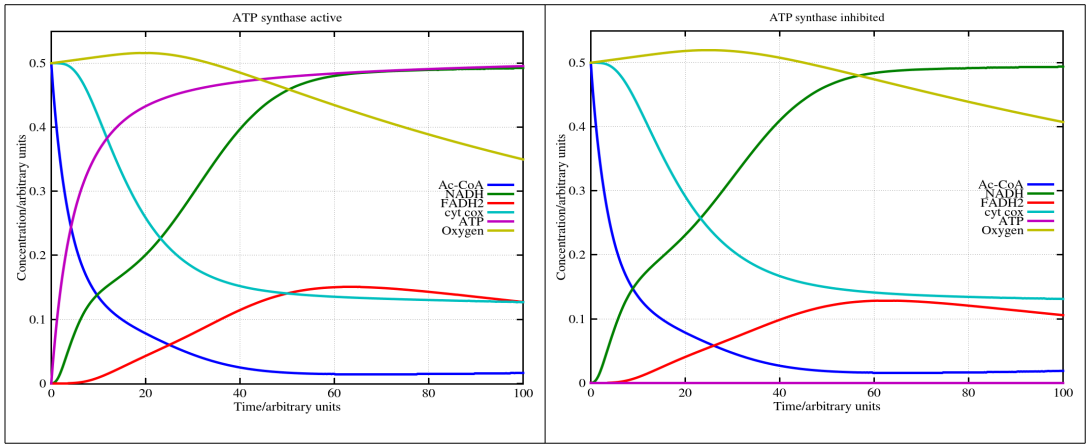

Figure 2.10: The reaction catalysed by ATP synthase is blocked in the Fig (b). The formation of ATP goes to zero. Oxygen concentration increases in Fig. (b), this is essentially because as ATP synthesis stop the upstream reactions also tend to slow down, leading to accumulation of oxygen.

References

Berg, J. M., Tymoczko, J. L., & Stryer, L. (2002). Biochemistry, 5th Edition San Francisco: W.H. Freeman.

Boyer, P. D. (1993). The binding change mechanism for ATP synthase—some probabilities and possibilities. *Biochimica et Biophysica Acta (BBA)-Bioenergetics*, *1140*(3), 215-250.

Cecchini, G. (2003). Function and Structure of Complex II of the Respiratory Chain*. *Annual review of biochemistry*, *72*(1), 77-109.

Hinkle, P. C. (2005). P/O ratios of mitochondrial oxidative phosphorylation. *Biochimica et Biophysica Acta (BBA)-Bioenergetics*, *1706*(1), 1-11.

http://www.brenda-enzymes.org/

http://www.gnu.org/software/octave/

Jain, S., & Nath, S. (2001). Catalysis by ATP synthase: mechanistic, kinetic and thermodynamic characteristics. *Thermochimica acta*, *378*(1), 35-44.

Johnson, J. D., Mehus, J. G., Tews, K., Milavetz, B. I., & Lambeth, D. O. (1998). Genetic evidence for the expression of ATP-and GTP-specific succinyl-CoA synthetases in multicellular eucaryotes. *Journal of Biological Chemistry*, *273*(42), 27580-27586.

Kornberg, H. L. (1966). Anaplerotic sequences and their role in metabolism. *Essays Biochem*, *2*, 1-31.

Lehninger, A. L., Nelson, D. L., & Cox, M. M. (2005). Lehninger principles of biochemistry. 2005, 4th edition, WH Freeman.

Porcelli, A. M., Ghelli, A., Zanna, C., Pinton, P., Rizzuto, R., & Rugolo, M. (2005). pH difference across the outer mitochondrial membrane measured with a green fluorescent protein mutant. *Biochemical and biophysical research communications*, *326*(4), 799-804.

Rellán-Álvarez, R., El-Jendoubi, H., Wohlgemuth, G., Abadía, A., Fiehn, O., Abadía, J., & Álvarez-Fernández, A. (2011). Metabolite profile changes in xylem sap and leaf extracts of strategy I plants in response to iron deficiency and resupply. *Frontiers in plant science*, *2*.

Santo-Domingo, J., & Demaurex, N. (2012). The renaissance of mitochondrial pH. *The Journal of general physiology*, *139*(6), 415-423.

Soga, N., Kinosita, K., Yoshida, M., & Suzuki, T. (2012). Kinetic equivalence of transmembrane pH and electrical potential differences in ATP synthesis. *Journal of Biological Chemistry*, *287*(12), 9633-9639.

Weber, J., & Senior, A. E. (2003). ATP synthesis driven by proton transport in F_1F_0-ATP synthase. *Febs Letters*, *545*(1), 61-70.

Wikström, M. (1984). Two protons are pumped from the mitochondrial matrix per electron transferred between NADH and ubiquinone. *FEBS letters*, *169*(2), 300-304.

Chapter 3 Mitochondrial Shuttles

Transport system in mitochondria

The eukaryotic cell is organised into compartments, and these compartments are specialised for few specific metabolic processes characteristic to them. It implies that individual separate pools of metabolites are maintained in these compartments to aid in the smooth functioning of the corresponding metabolic processes. The relatively restricted exchange or movement of molecules among these compartments presents another level of regulation of the processes interacting in different compartments.

Mitochondrion being a semi-autonomous, double-membraned organelle is one such compartment specialising in metabolic pathways as Krebs cycle, oxidative phosphorylation, fatty acid oxidation, etc. In mitochondria, the inner mitochondrial membrane acts as a barrier against free movement of most of the molecules inside the mitochondria. Those molecules, which can freely cross the inner mitochondrial membrane, include small, uncharged molecules (e.g. CO_2, O_2, H_2O). Besides, there are several specific transporters which assist in the movement of essential ions, metabolites and proteins.

Cells use specialised transporters to regulate metabolite concentrations in different compartments of the cell. This helps in regulating the functionality of individual compartments by maintaining differential concentration of metabolites across the membranes. Some metabolites are not allowed to cross the membrane at all and are maintained as independently regulated pool on both sides of the membrane. This helps in accumulating a particular component at a higher concentration as required by the respective compartment. The maintenance of differential concentration requires transportation and accumulation of metabolites against the concentration gradient. Several transport systems developed by the cell cater to the personalised need of various compartments.

Transporters are membrane proteins that transport molecules across the membrane by using energy already stored in ion gradients, such as proton, sodium or other charge/concentration gradients. Transporters allow the molecules to move across the membrane which otherwise would not move, either because it is impermeable through the membrane or it is to be moved against its concentration gradient. All mitochondrial transporters are encoded by the nuclear genome.

Movement of a molecule against its concentration gradient requires energy and is broadly classified as active transport. Active transport can be further classified as primary and secondary active transport based on the source of energy used in the transport mechanism. If the process uses chemical energy (for example from ATP), it is categorised as primary active transport. It includes transmembrane ATPases, which uses ATP to transport ions across the membrane. Other primary active transporters may use varied forms of energy as redox energy (proton translocation across inner mitochondrial membrane by ETC complexes) or light energy (proton translocation across thylakoid membrane during photosynthesis) to facilitate the transport. In secondary active transport, electrochemical potential difference created by the ion pumps provides the free energy required for transportation (instead of directly using ATPs). The structural basis of secondary active transport mechanism has been widely studied and was reviewed by Forrest *et* al. (Forrest, Krämer & Ziegler, 2011).

Coupled Transport

Sometimes, the transporters facilitate transport of one substance in one direction and at the same time co-transport another substance in either same or the opposite direction. If the movement of one substance necessitates the movement of the coupled substance in the same direction, it is called as symport. When the movement of one substance causes the transport of another substance in the opposite direction, it is termed as antiport. Both antiport and symport are categorised under secondary active transport and are called as coupled transport (or simply co-transport). Here, one of the substance with a higher concentration gradient between the two substances across the membrane will move along its concentration gradient, hence forcing the movement of the other substance in the coupled direction, which may or may not be along latter's concentration gradient (Krupka, 1993). Here, the first substance moving along its concentration gradient is called the driving molecule and the other substance moving uphill of its concentration gradient is known as the driven molecule. So for antiport, the driving molecule will force the movement of driven molecule in the direction opposite to its own direction.

In a case of symport, the transport of driving molecule will result in the movement of the driven molecule in the same direction. The direction of transport is decided by the concentration gradients of the two molecules being transported by the respective transporter. The molecule with a higher concentration gradient, called the driving molecule, will move along its concentration gradient. It supplies the free

energy for the movement of the driven molecule in same or opposite direction for symport and antiport, respectively. The stoichiometry of transport is strictly regulated, and for transport of each driver molecule, one driven molecule is transported in the appropriate direction. Thus the stoichiometry exhibited in coupled transport is essentially 1:1 (Stein, 1986). A compilation of various types of transmembrane transporters and their mechanisms are compiled by Enkavi *et al.* (Enkavi, Li, Mahinthichaichan, Wen, Huang, Shaikh & Tajkhorshid, 2013).

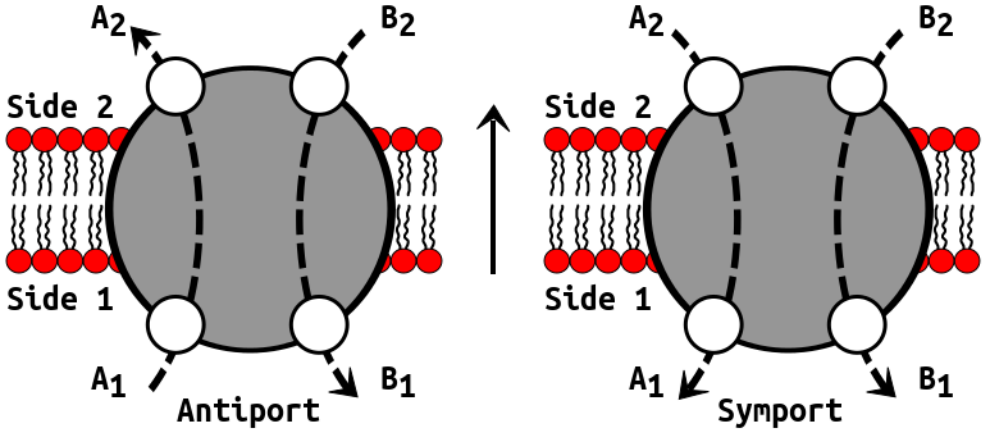

Figure 3.1: Two types of coupled transport: antiport and symport. A_1, A_2 represent the concentrations of the metabolite A in side 1 and side 2 of the membrane respectively. B_1 and B_2 denote the concentrations of metabolite B in side 1 and side 2 of the membrane respectively. White opaque circles on the transporter indicate the binding sites for metabolites, and it is expected that two of the binding sites will be occupied at any given time. There can be six such possibilities when two binding sites are occupied. Of these six possibilities, only two will lead to transportation for a given set. The arrow shown in the centre of the figure shows the positive direction of flux, arbitrarily fixed for the sake of uniformity during scripting.

Fig. 3.1 shows the two types of coupled transport. Here A and B are two molecules which are to be translocated across the membrane.

Simulation

Earlier attempts to explain the kinetics behind co-transport resulted in quite complicated models (Melkikh & Seleznev, 2012; Sanders, Hansen, Gradmann & Slayman, 1983). The overall idea in this section is to simulate individual shuttles and then combine it with Krebs cycle to study the interaction and association among these sets of reactions. The first step is the individual simulation of the two shuttles (malate-aspartate and citrate-pyruvate shuttles). A significant challenge in this direction is to simulate the transporters facilitating the transport.

The transport across the membrane depends on the concentration gradient

of the two metabolites. It is important to note that a given metabolite present on two sides of the membrane is the same species, but for simulation, the metabolite present on two sides has been named differently so that the two pools present on either side of the membrane can be differentiated. It is important to give them a unique name so that the software can treat them as two different species, and their individual concentrations in a particular compartment can be maintained.

In the present simulation for a system with one transporter, there are two metabolites, A and B, which are transported across the membrane. The concentrations of these two metabolites present on the two sides of the membrane, side 1 and side 2, are denoted as A_1, A_2, B_1 and B_2 correspondingly. So considering the transporter to be a protein, E, with four binding sites one each for A and B on both sides of the membrane as seen in Fig. 3.1, several combinations of protein along with the metabolites bound to it are possible. There can be a situation where only one binding site is occupied, and there is no transport expected in this condition. Transport is possible when two of the binding sites are occupied with A and B bound to it in appropriate conformation.

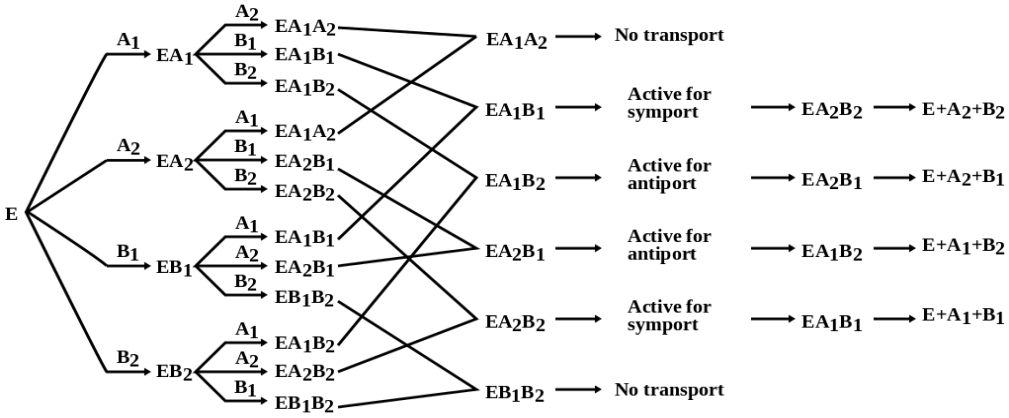

Figure 3.2: The possible intermediates and the probable outcome when two metabolites (A and B) are bound to the transporter (E). Subscripts 1 and 2, denotes the localisation of the metabolite in the two sides of the membrane, side 1 and 2 respectively. Reactions involved in co-transport are not perfect bi-substrate reactions but can be considered taking place via two substrate binding where the substrates can bind in any order. There are six bi-substrate intermediates formed; two are suitable for antiport and two for symport and the remaining two will block one of the channels inhibiting further transport. After transport, the metabolite enters the other side and the subscript changes (1→2 and 2→1) indicating the respective change of side. The intermediates with three and four metabolites bound have not been shown here (included in the simulation script) as they do not lead to transport and are inhibitory in nature.

Depending on the type of transporter, either symport or antiport can be facilitated provided the two metabolites bind appropriately. A brief illustration of this binding and the feasible outcomes is shown in Fig. 3.2. A transporter protein may

have more than two binding sites occupied in a given time; however such a condition would block one of the channels and consequently, coupled transport will be blocked. Binding of three or four species at a given time is not shown in Fig. 3.2 to avoid complexity, but have been considered in the simulation script. The possible intermediates for a system with a transporter (protein) E, and two species, A and B, located on two sides, side 1 and side 2 of a membrane, labelled as A_1, A_2, B_1 and B_2, are shown.

Fig. 3.2 indicates the possible combinations when two of the binding sites are occupied, of those, two are active for antiport (EA_1B_2 and EA_2B_1), and two are active for symport (EA_1B_1 and EA_2B_2). When the correct binding is achieved, transporter protein undergoes a conformational change resulting in transport of metabolites to the opposite side. The transporter can function in a reversible manner depending on the concentration of the metabolites on both sides of the membrane. Also, all the binding sites of the transporters are considered independent and equivalent and thus, all the binding constants used in the current study are considered equal. This approach presents a reasonable assumption and simplifies the numerical calculation for qualitative analysis. However, at any point in time, these binding constants (equilibrium constants here) can be replaced with actual physiological values to obtain exact quantitative results. The rate equations were derived for all possible intermediates.

The important point is the binding mechanism of these metabolites to the transporter, which resembles allosteric binding process, earlier proposed by Monod *et al.* (Monod, Wyman & Changeux, 1965). This primarily demonstrates cooperativity, i.e. after the binding of first metabolite, the binding of the subsequent metabolite is stronger and leads to a change in conformation of other subunits of the transporter complex. However, experimental validation of these intermediate conformational changes in the transporter complex when bound to metabolites is tricky, and hence, experimental data are scant.

Transporter-metabolite binding is quite likely to exhibit a mechanism similar to allostery. With binding of the requisite number of metabolites, the conformation changes leading to the transport of metabolites across the membrane (Jardetzky, 1966). It is also expected that the transporter has a symmetrical structure on two sides of the membrane to facilitate symmetric binding on both sides, which paves a way for reversible nature of these transporters.

Rate equation

The rate equations were derived and were used to calculate the flux using Michaelis-Menten approach (Michaelis & Menten, 1913). In the current simulation, the effect of the electrochemical potential gradient across the membrane has not been taken into consideration. Also, if the metabolites to be exchanged are electrically charged, the membrane potential will play a critical role (Geck & Heinz, 1976; Heinz, Geck & Wilbrandt, 1972). This function of an electrical field across the mitochondrial membrane has not been included in the simulation presented here.

Table 3.1: The intermediate reactions taking place during coupled transport and their rate equations. The states of the transporter with three and four metabolites bound to it are not shown here but are included in the simulation script. The complete set has been included in the equations.

$E + A_1 \Leftrightarrow EA_1$	$k = \frac{[EA_1]}{[E][A_1]}$	$[EA_1] = k[E][A_1]$
$E + A_2 \Leftrightarrow EA_2$	$k = \frac{[EA_2]}{[E][A_2]}$	$[EA_2] = k[E][A_2]$
$E + B_1 \Leftrightarrow EB_1$	$k = \frac{[EB_1]}{[E][B_1]}$	$[EB_1] = k[E][B_1]$
$E + B_2 \Leftrightarrow EB_2$	$k = \frac{[EB_2]}{[E][B_2]}$	$[EB_2] = k[E][B_2]$
$EA_1 + A_2 \Leftrightarrow EA_1A_2$	$k = \frac{[EA_1A_2]}{[EA_1][A_2]}$	$[EA_1A_2] = k[EA_1][A_2] = k^2[E][A_1][A_2]$
$EA_1 + B_1 \Leftrightarrow EA_1B_1$	$k = \frac{[EA_1B_1]}{[EA_1][B_1]}$	$[EA_1B_1] = k[EA_1][B_1] = k^2[E][A_1][B_1]$
$EA_1 + B_2 \Leftrightarrow EA_1B_2$	$k = \frac{[EA_1B_2]}{[EA_1][B_2]}$	$[EA_1B_2] = k^2[EA_1][B_2] = k^2[E][A_1][B_2]$
$EA_2 + B_1 \Leftrightarrow EA_2B_1$	$k = \frac{[EA_2B_1]}{[EA_2][B_1]}$	$[EA_2B_1] = k^2[EA_2][B_1] = k^2[E][A_2][B_1]$
$EA_2 + B_2 \Leftrightarrow EA_2B_2$	$k = \frac{[EA_2B_2]}{[EA_2][B_2]}$	$[EA_2B_2] = k^2[EA_2][B_2] = k^2[E][A_2][B_2]$
$EB_1 + B_2 \Leftrightarrow EB_1B_2$	$k = \frac{[EB_1B_2]}{[EB_1][B_2]}$	$[EB_1B_2] = k^2[EB_1][B_2] = k^2[E][B_1][B_2]$
.....	.....	.....

Following the Michaelis-Menten approach, the total transporter protein concentration was calculated. It includes all the possible forms the transporter protein can display depending on the various combination in which the metabolites bind to different binding sites of the transporter protein.

$$[E^0] = [E] + [EA_1] + [EA_2] + [EB_1] + [EB_2] + [EA_1A_2] + [EA_1B_1] + [EA_1B_2] + [EA_2B_1] + [EA_2B_2] + [EB_1B_2] + [EA_1A_2B_1] + [EA_1A_2B_2] + [EA_1B_1B_2] + [EA_2B_1B_2] + [EA_1A_2B_1B_2]$$

where, [E] is the free transporter protein concentration, and [E^0] is the total transporter protein concentration. Substituting values from the rate equations given in Table 3.1, we get

$$[E^0]=[E]+k[E][A_1]+k[E][A_2]+k[E][B_1]+k[E][B_2]+k^2[E][A_1][A_2]+k^2[E][A_1][B_1]+k^2[E][A_1][B_2]$$
$$+k^2[E][A_2][B_1]+k^2[E][A_2][B_2]+k^2[E][B_1][B_2]+k^3[E][A_1][A_2][B_1]+k^3[E][A_1][A_2][B_2]$$
$$+k^3[E][A_1][B_1][B_2]+k^3[E][A_2][B_1][B_2]+k^4[E][A_1][A_2][B_1][B_2]$$

this equation can be reduced to give,

$$\frac{[E^0]}{[E]}=1+k[A_1]+k[A_2]+k[B_1]+k[B_2]+k^2[A_1][A_2]+k^2[A_1][B_1]+k^2[A_1][B_2]+k^2[A_2][B_1]+k^2[A_2][B_2]$$
$$+k^2[B_1][B_2]+k^3[A_1][A_2][B_1]+k^3[A_1][A_2][B_2]+k^3[A_1][B_1][B_2]+k^3[A_2][B_1][B_2]+k^4[A_1][A_2][B_1][B_2]$$

$\frac{[E^0]}{[E]}=S$ where S depends on A_1, A_2, B_1 and B_2, the expression on the RHS in the equation above.

The concentration of free transporter protein, E can be given as

$$[E]=[E^0]/S$$

This value of E has been further used for equation of symport and antiport.

Symport:

For symport, the rate of transport will be given by

$$symport\ flux=k'[EA_1B_1]-k''[EA_2B_2]$$

since the only conformations that can facilitate transport are A_1B_1 and A_2B_2 (See Figs. 3.1 & 3.2). The negative sign indicates that the two fluxes are in the opposite directions.

The enzyme function is expected to be symmetric, and therefore binding constants of the enzyme for A and B are considered to be same on both sides of the membrane. So, we assume, k'=k", for simulation purposes.

From Table 3.1, we have,

$$[EA_1B_1]=k^2[E][A_1][B_1] \quad \text{and} \quad [EA_2B_2]=k^2[E][A_2][B_2]$$

substituting the value of E, we get

$$[EA_1B_1]=(k^2[E^0][A_1][B_1])/S \quad \text{and} \quad [EA_2B_2]=(k^2[E^0][A_2][B_2])/S$$

substituting these values in the equation for symport flux, we have

$$symport\ flux=(k'k^2[E^0]([A_1][B_1]-[A_2][B_2]))/S$$

Antiport:

For antiport, the rate of transport will be given by

$$antiport\ flux=k'[EA_1B_2]-k''[EA_2B_1]$$

since only two conformations, A_1B_2 and A_2B_1, can lead to antiport, these two terms are included in the above equation.

The enzyme function must be symmetric, and we expect k' and k" to be equal, i.e. k'=k".

From Table 3.1, we have,

$$[EA_1B_2]=k^2[E][A_1][B_2] \quad \text{and} \quad [EA_2B_1]=k^2[E][A_2][B_1]$$

substituting the value of E, we get

$$[EA_1B_2]=(k^2[E^0][A_1][B_2])/S \quad \text{and} \quad [EA_2B_1]=(k^2[E^0][A_2][B_1])/S$$

substituting these values in the equation for antiport flux, we have

$$antiport\ flux=(k'k^2E^0([A_1][B_2]-[A_2][B_1]))/S$$

The equations derived for symport and antiport were used to calculate the flux of each metabolite across the membrane. The flux value obtained from these equations were added or subtracted appropriately in the final rate equations of the metabolites exchanged across the membrane.

Script

A plot was drawn to study the binding behaviour of one of the metabolites when all the metabolites are present in different conditions. A plot of intermediate [EA_1] vs the respective metabolite [A_1] was plotted for three sets of concentrations of all the other metabolites ([A_2], [B_1], [B_2]), i.e. at 0.1, 0.5 and 0.9. The following script (Table 3.2) was written and run in GNUPLOT to visualise the comparative behaviour.

Table 3.2: GNUPLOT script written to plot [EA_1] vs [A_1]

```
set border 31 front linetype -1 linewidth 3.000
set style rectangle back fc  lt -3 fillstyle   solid 1.00 border lt -1
set grid
set key inside right top vertical Right noreverse enhanced autotitles nobox
set style histogram clustered gap 2 title  offset character 0, 0, 0
unset logscale
set origin 0,0
set xzeroaxis linetype -1 linewidth 3.000
set yzeroaxis linetype -1 linewidth 3.000
set zzeroaxis linetype -2 linewidth 1.000
set x2zeroaxis linetype -1 linewidth 3.000
set y2zeroaxis linetype -1 linewidth 3.000
set xtics border in scale 1,0.5 mirror norotate  offset character 0, 0, 0
set xtics autofreq  norangelimit font "arial,14"
set ytics border in scale 1,0.5 mirror norotate  offset character 0, 0, 0
set ytics autofreq  norangelimit font "arial,14"
set xlabel "[A1] / arbitrary unit"
set xlabel  offset character 0, 0, 0 font "arial,14" textcolor lt -1 rotate by -30
set ylabel "[EA1] / arbitrary unit"
set ylabel  offset character 0, 0, 0 font "arial,14" textcolor lt -1 rotate by -270
GNUTERM = "wxt"
set multiplot
set label 1 "A2=B1=B2=0.5" at 7,0.33,0 font "arial,14"
a2=b1=b2=0.5
plot                                                                    x/
```

```
(1+x+a2+b1+b2+x*a2+x*b1+x*b2+a2*b1+a2*b2+b1*b2+x*a2*b1+x*a2*b2+x*b1*b2+a2*b1*b2)
lc 1 lw 3 noti
set label 2 "A2=B1=B2=0.1" at 7,0.73,0 font "arial,14"
a2=b1=b2=0.1
plot x/(1+x+a2+b1+b2+x*a2+x*b1+x*b2+a2*b1+a2*b2+b1*b2+x*a2*b1+x*a2*b2+x*b1*b2+a2*b1*b2)
lc 2 lw 3 noti
set label 3 "A2=B1=B2=0.9" at 7,0.195,0 font "arial,14"
a2=b1=b2=0.9
plot  x/(1+x+a2+b1+b2+x*a2+x*b1+x*b2+a2*b1+a2*b2+b1*b2+x*a2*b1+x*a2*b2+x*b1*b2+a2*b1*b2)
lc 3 lw 3 noti
set label 4 "M-M curve" at 7,0.95,0 font "arial,14"
plot x/(1+x) lc 7 lw 3 noti
unset multiplot
#    EOF
```

Further, the scripts were written to simulate symport and antiport using ode solver in Octave (GNU Octave). The initial concentrations given for the four species, A_1, A_2, B_1, B_2, were given as 0.4, 0.3, 0.1 and 0.6. So the initial concentration gradient of A across the membrane was 0.1 and for B it was 0.5. The script used for symport simulation is given in Table 3.3.

Table 3.3: Script written for simulation of symport.

```
1;
% solve symport
% Equations for symport, the rate equations follow:

ds=zeros(4,1);
s(1) = 0.4; %a1
s(2) = 0.3; %a2
s(3) = 0.1; %b1
s(4) = 0.6; %b2

function ds=sp(s)
t1=1+s(1)+s(2)+s(3)+s(4)+s(1)*s(2)+s(1)*s(3)+s(1)*s(4)+s(2)*s(3)+s(2
)*s(4)+s(3)*s(4)+s(1)*s(2)*s(3)+s(1)*s(2)*s(4)+s(1)*s(3)*s(4)+s(2)*s
(3)*s(4)+s(1)*s(2)*s(3)*s(4);

alpha=(0.1*(s(1)*s(3)-s(2)*s(4)))/t1;
ds(1)= -alpha;
ds(2)= alpha;
ds(3)= -alpha;
ds(4)= alpha;

return
end
% use lsode to solve this set...
lsode_options("relative tolerance",1e-4);
lsode_options("absolute tolerance",1e-3);
t=0:0.1:50;
```

```
% supply the initial concentrations ...
s0=s;

[s,T,MSG]=lsode(@sp,s0,t);
T
MSG
plot(t,s(:,1),"linewidth",5,t,s(:,2),"linewidth",5,t,s(:,3),"linewid
th",5,t,s(:,4),"linewidth",5);

grid on;
set (gca,'FontSize', 20);
axis([0,50,-0.1,1.01]);
% title ("symport");
xlabel ("Time/arbitrary units");
ylabel ("Concentration/arbitrary units");
set (gca,'FontSize', 20)
set(get(gcf,'children'), 'linewidth', 4 )
legend("A1","A2","B1","B2", "location", "northeast");
```

The script used for simulation of an antiport is given in Table 3.4. The initial concentrations of A_1, A_2, B_1 and B_2 are given as 0.4, 0.3, 0.1 and 0.6 respectively.

Table 3.4: Script written for simulation of an antiport.

```
1; %solve antiport
% Equations for antiport
% the rate equations follow:

ds=zeros(4,1);
s(1) = 0.4; %a1
s(2) = 0.3; %a2
s(3) = 0.1; %b1
s(4) = 0.6; %b2

function ds=ap(s)
t1=1+s(1)+s(2)+s(3)+s(4)+s(1)*s(2)+s(1)*s(3)+s(1)*s(4)+s(2)*s(3)+s(2
)*s(4)+s(3)*s(4)+s(1)*s(2)*s(3)+s(1)*s(2)*s(4)+s(1)*s(3)*s(4)+s(2)*s
(3)*s(4)+s(1)*s(2)*s(3)*s(4);
alpha=(0.1*(s(1)*s(4)-s(2)*s(3)))/t1;

ds(1)= -alpha;
ds(2)= alpha;
ds(3)= alpha;
ds(4)= -alpha;

return
end
% use lsode to solve this set...
lsode_options("relative tolerance",1e-4);
lsode_options("absolute tolerance",1e-3);
```

```
t=0:0.1:50;
% supply the initial concentrations ...
s0=s;
[s,T,MSG]=lsode(@ap,s0,t);
T
MSG
plot(t,s(:,1),"linewidth",5,t,s(:,2),"linewidth",5,t,s(:,3),"linewid
th",5,t,s(:,4),"linewidth",5);

grid on;
set (gca,'FontSize', 20);
axis([0,50,-0.1,1.01]);
% title ("antiport");
xlabel ("Time/arbitrary units");
ylabel ("Concentration/arbitrary units");
set (gca,'FontSize', 20)
set(get(gcf,'children'), 'linewidth', 4 )
legend("A1","A2","B1","B2", "location", "northeast");
```

Results and discussion

Transport of metabolites across the mitochondrial membrane via shuttles requires the simulation of these metabolites' fluxes. Once the fluxes are calculated, they can be subsumed in the rate equations of the respective metabolites. However, the flux across the membrane depends on the binding of the metabolite to the concerned transporter protein. The binding is inhibited by the presence of other metabolites, which may bind to transporter protein. For instance, for binding of A_1, concentration of other species as A_2, B_1 and B_2, would inhibit the binding. To study this binding behaviour, the plot shown in Fig. 3.3 was drawn. It is seen in the plot that, higher the concentration of other metabolites, the lower is the concentration of the intermediate EA_1. Also, the Michaelis-Menten curve was plotted for an adequate comparison. It is seen that none of the intermediate curves show hyperbolic behaviour as the Michaelis-Menten curve.

Fig. 3.4 shows the curve plotted using the script given in the previous section for symport and antiport. The concentration gradient of A and B across the membrane is 0.1 and 0.5 respectively. Here, the concentration gradient of B is higher, and so B acts as the driving molecule and A as the driven molecule. The movement of A, however, will depend on the type of transporter. Now, B moves from side 2→side 1, in case of symport, A shall move from side 2→side 1, and for antiport, side 1→side 2.

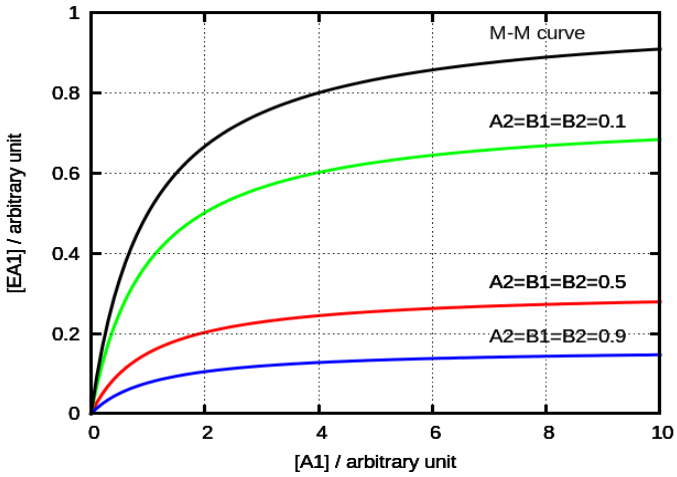

Figure 3.3: This shows the behaviour of metabolite EA_1 when the other three metabolites are kept at same concentration as denoted above the respective curves. The behaviour of the first intermediate EA_1 has been plotted when the concentrations of A_2, B_1 and B_2 were varied. It is an important point to note that the Michaelis-Menten binding (black curve) is hyperbolic in nature. High concentrations of other metabolites inhibit the transporter in a concentration-dependent manner ($A_1=A_2=B_1=B_2=0.9$ gives <0.1 bound EA_1). k'=0.1.

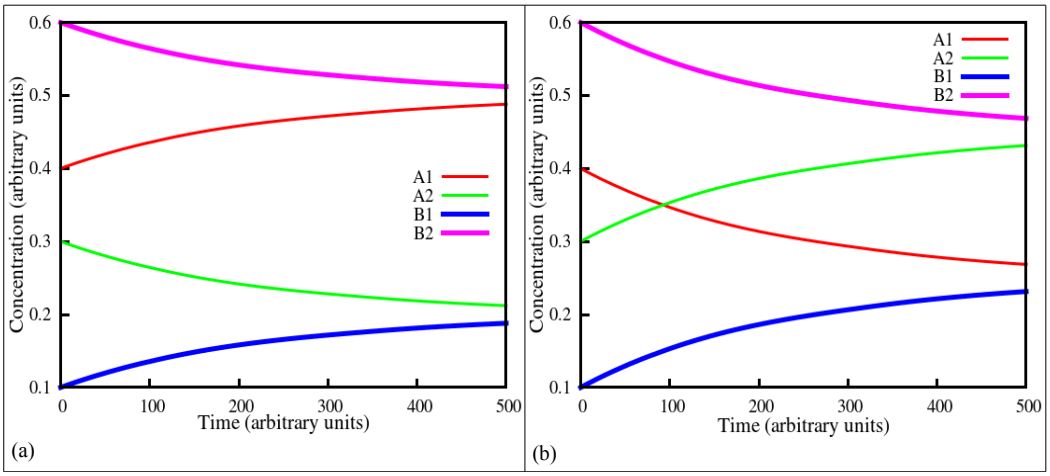

Figure 3.4: Simulation curves for symport and antiport. Red and green curves denote A_1/A_2, and blue and magenta curves denote B_1/B_2. 0.1 and 0.5 are the initial concentration gradients of A and B respectively; the lower concentration is on side 1 of the membrane for both A and B. k'=0.1. (a): Symport: Curves for A_1/A_2 are seen as diverging, whereas curves for B_1/B_2 looks converging, i.e. the concentration gradient is further increasing for A and decreasing for B. Here, the movement of metabolites as seen in the curve, $B_2 \rightarrow B_1$ and $A_2 \rightarrow A_1$. It can be evidently seen that the higher concentration gradient of B (B_2-B_1) is driving the flow of metabolite A (A_1/A_2) against its concentration gradient. (b): Antiport: Curves of A_1/A_2 are seen converging. Their concentrations on both sides of the membrane become equal, and then they start diverging, and the other pair, B_1/B_2 are converging throughout. Here, the concentration gradient of B is seen decreasing consistently, however for A, first it decreases and then increases. The movement of metabolites in the curves are $B_2 \rightarrow B_1$ and $A_1 \rightarrow A_2$, indicating that the higher concentration gradient of B (B_2-B_1) is driving the movement of metabolite A, since the concentration gradient of B is dominating. The movement of A was along the concentration gradient but was later forced to move against its concentration gradient due to the higher concentration gradient of B.

Cooperative binding suggests that with the binding of one substrate to one transporter subunit, the other subunits are stimulated and facilitate the binding of the other substrate. Substrates may exhibit non-cooperativity, positive cooperativity or negative cooperativity. During coupled transport, the substrates are expected to exhibit positive cooperativity.

Symport:

The simulation curve presented in Fig. 3.4a indicates the movement of two metabolites in a symport system based on their concentration gradient across the membrane. As mentioned above, A is expected to move from side 2→side 1, which is evidently seen here. However concentration of A is higher in side 1 and is expected to move from side 1→side 2, but since it is symport and B is the driver molecule, A tends to move against its concentration gradient.

Antiport:

The simulation curve presented in Fig. 3.4b indicates the movement of two metabolites in an antiport system depending on their concentration gradient across the membrane. As mentioned above, A is expected to move from side 1→side 2, which is seen here. The concentration of A is higher in side 1, so its movement to side 2 is justifiable on account of the concentration gradient. However, at ~100 time point, the concentration of A on both sides of the membrane becomes equal and still the movement does not cease. This is because the concentration gradient of B still predominates the movement of A, now against its concentration gradient.

A surface plot has been plotted where the concentrations of A_2 and B_2 were kept constant, and the concentrations of A_1 and B_1 were varied in the range of 1 to 10. The surface plot for symport (a) and antiport (b) are shown in Fig. 3.5. In Fig. 3.5a, it can be clearly seen that at (0,0) concentration of both A1 and B1 is rising. It indicates their transport from side 2→side1, and as expected both the metabolites are moving in the same direction. However, in Fig. 3.5b, the concentration of A_1 is increasing and of B_1 is decreasing. This shows their movement in the opposite direction and fits the expected behaviour of an antiport.

This section provides the fundamental framework for simulating coupled transport across a biological membrane. It can be used for simulating antiports and symports, and the respective flux can be added to the rate equations of metabolites. In the following sections, the two shuttle systems present on the mitochondrial membrane are discussed in details. These shuttles were simulated individually and were then combined with Krebs cycle to study the interaction and association.

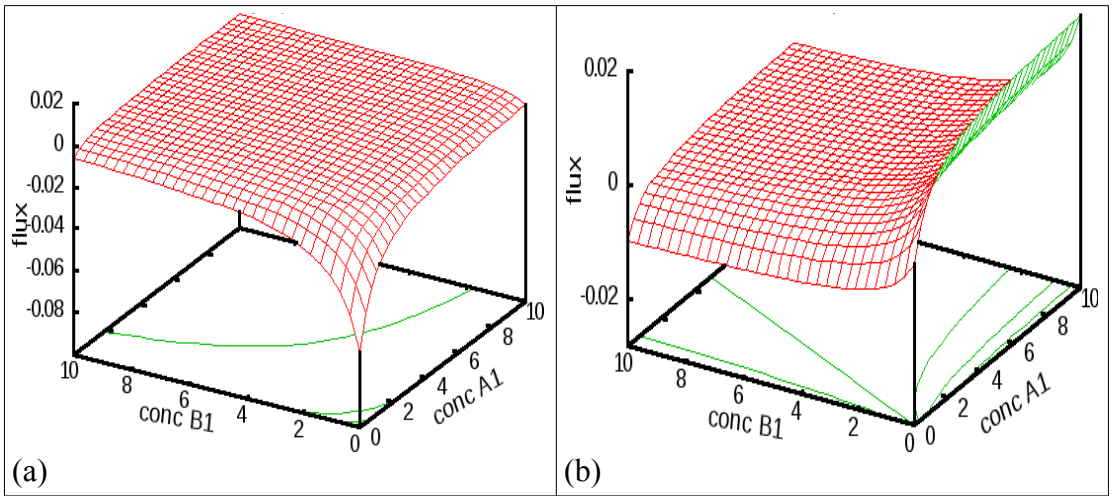

Figure 3.5: The surface plot has been generated by plotting concentrations of A_1 and B_1 varying in the range of 1 to 10. However, the concentrations of A_2 and B_2 were kept constant at 3 and 6 respectively for the two plots. k'=0.1. Here, the contours are projected on the xy plane. (a) Surface plot for symport flux. (b) Surface plot for antiport flux.

Introduction for shuttles

Several processes as Krebs cycle, ATP synthesis, fatty acid oxidation, ketone bodies synthesis, take place inside mitochondria. Most of the proteins, metabolites, raw materials required for these processes are essentially imported from the cytoplasm. The transport system across the mitochondrial membrane consists of several transporters. The two most widely studied shuttle systems are malate-aspartate and citrate-pyruvate shuttle. Malate-aspartate shuttle is used to transport reducing equivalents across the mitochondrial membrane. Citrate-pyruvate shuttle is used to shuffle carbon skeleton across the mitochondrial depending upon the needs and availability of these metabolites in cytoplasm and the mitochondrial matrix. In the present work, these two shuttles were simulated individually and were combined with Krebs cycle (Chapter 2). These mitochondrial shuttles mentioned here function in close association with Krebs cycle, by virtue of the components involved in them.

Shuttles play a significant role in maintaining suitable metabolite concentrations on both sides of the inner mitochondrial membrane. However, appropriate metabolite concentrations do not necessarily indicate equal concentrations but indicate the optimal concentrations required to meet the needs of the respective compartments. These shuttles, therefore, consist of several parts which can be combined in various combinations to facilitate movement of metabolites on either side of the membrane as per the requirements. Metabolites, like malate, can be transported by more than one independent transporters and the concentrations in such cases can be rather complex.

Various approaches used to simulate these systems can be found in the literature. A model based on detailed kinetics and thermodynamically balanced reaction mechanisms was proposed by Wu *et al.* (Wu, Yang, Vinnakota & Beard, 2007). A model integrating the dynamics of respiratory chain, Krebs cycle, the fatty acid β-oxidation and the inner membrane metabolite transport system was presented by Yugi and Tomita (2004). Another report by Lu *et al.* presents the role of malate-aspartate shuttle on the metabolic response to myocardial ischemia (Lu, Zhou, Stanley, Cabrera, Saidel & Yu, 2008). However, these reports are confined to a particular set of conditions, whereas the approach presented in this chapter is quite general and can be easily extrapolated to address particular problems.

Malate-Aspartate Shuttle

In the previous chapter, energy machinery inside the mitochondria was dealt in detail. NADH and $FADH_2$ are oxidised in mitochondria to build up electrochemical potential gradient ($\Delta\psi$ +ΔpH) across the inner mitochondrial membrane which is used by ATP synthase to produce ATP from ADP and P_i. In the earlier simulation, NADH and $FADH_2$ were shown to be exclusively derived from the Krebs cycle. However, a substantial amount of NADH is also produced in the cytoplasm. This NADH is required to be transported to mitochondria for its oxidation and to regenerate back NAD^+ in the cytoplasm to be used in glycolysis and other metabolic processes (Dawson, 1979). This NADH generated in the cytoplasm can be fed into the ETC to contribute for electrochemical potential gradient. Mitochondrial membrane is impermeable to NADH/NAD^+ (Purvis & Lowenstein, 1961). This can be considered as a part of cellular regulatory mechanism, where the cell intends to maintain two independently regulated pools of NADH/NAD^+. However, it is essential to oxidise NADH, to regenerate NAD^+, and this is achieved by using shuttle transport system (Williamson, Safer, LaNoue, Smith & Walajtys, 1973). In shuttles, the reducing equivalents rather than NADH/NAD^+ directly, are transported across the mitochondrial membrane. This maintains the two independently regulated pools and also facilitates the oxidation of NADH by the ETC in the mitochondrial matrix.

Malate-aspartate shuttle is the most widely used shuttle for this purpose (Barron, Gu & Parrillo, 1998). It consists of two transporters viz. malate-α-ketoglutarate transporter and glutamate-aspartate transporter, and both of them are antiports, i.e. transport equal molar equivalents of metabolites move in the opposite direction. These transporters are not physically coupled but are coupled by the virtue of the biochemical reactions among the metabolites transported through them (Nelson & Cox, 2004). Malate-α-ketoglutarate antiport transporter is responsible for transport of malate and α-ketoglutarate across the inner mitochondrial membrane in the opposite direction. The transfer of one mole of malate from intermembrane space (IM) to the mitochondrial matrix (M) facilitates the transfer of one mole of α-ketoglutarate in the opposite direction and vice versa. Similarly, glutamate-aspartate transporter facilitates transport of glutamate and aspartate across the membrane.

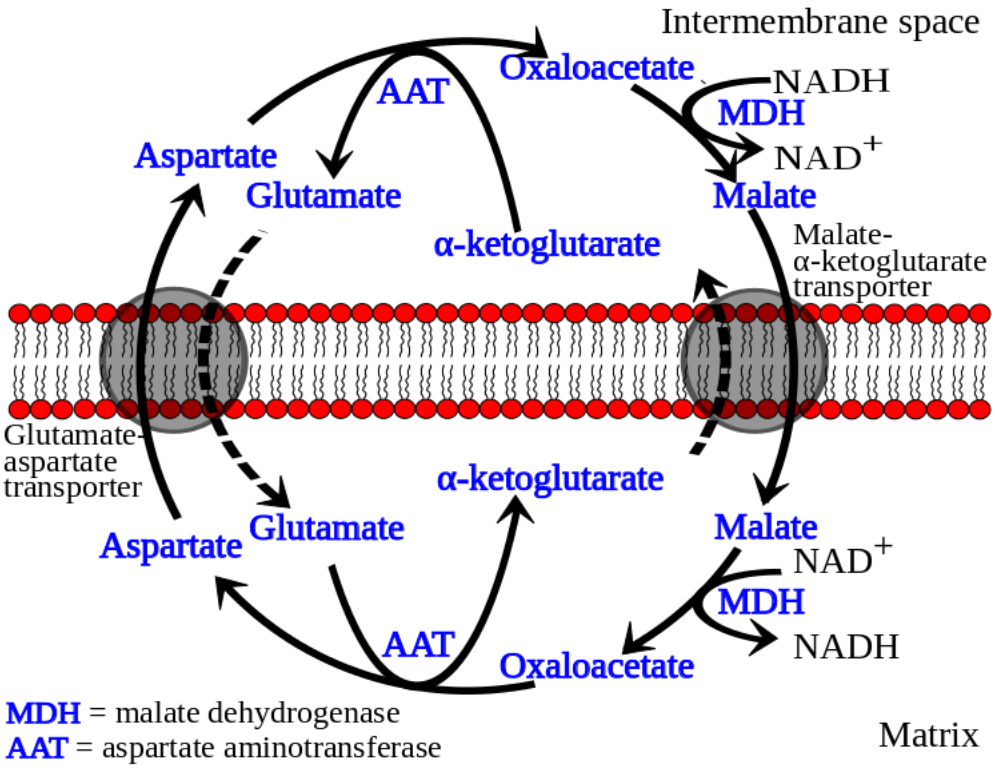

Figure 3.6: Pictorial representation of malate-aspartate shuttle. The shuttle consists of two transporters, (aspartate-glutamate antiport transporter and malate-α-ketoglutarate antiport transporter) and the reaction scheme used for transferring reducing equivalents between two sides of the inner mitochondrial membrane. The diagram contains two circles, (i) moving clockwise and the other (ii) moving anti-clockwise, and these two circles are connected at two points by aspartate aminotransferase. The reaction scheme is completely symmetric on both sides as drawn. However, oxaloacetate, α-ketoglutarate and malate can enter Krebs cycle and can control the rate of the Krebs cycle.

The strategy followed by malate-aspartate shuttle to transfer reducing equivalents start with the activity of malate dehydrogenase, where oxaloacetate is converted to malate accompanied by oxidation of one NADH. Here the electrons are now transferred to malate. This malate is exchanged with α-ketoglutarate, which moves out of the mitochondrial matrix. Malate inside the matrix is now oxidised to oxaloacetate and in turn reducing NAD^+ to NADH. So it can be seen that electrons picked up from NADH in the cytosolic side are used in the matrix to reduce NAD^+ and in the process oxaloacetate is formed again. Oxaloacetate may react with glutamate in a reaction catalysed by aspartate aminotransferase to form aspartate and α-ketoglutarate. This α-ketoglutarate thus formed may be exchanged with influx of malate into the matrix, and itself is being transported to the intermembrane space via malate- α-ketoglutarate transporter. Similarly, aspartate is exchanged with glutamate, where glutamate enters the matrix, and aspartate is transported to the intermembrane space. Aspartate in the intermembrane space can combine with α-ketoglutarate

transported by malate-α-ketoglutarate transporter, to form oxaloacetate and glutamate. Oxaloacetate can form malate again and glutamate can be transported to the matrix in exchange of aspartate (Brand & Chappell, 1974). This cycle is balanced on both sides of the membrane, and the net effect is the transfer of electrons from NADH via malate in the directions as shown in Fig. 3.6. However, all the reactions in this set are reversible, and the whole shuttle can be reversed if the need arises.

The direction of the flux through a transporter is determined by concentration gradient of the two metabolites to be transported across the membrane. Metabolite with higher concentration gradient will flow along its concentration gradient, i.e., from the higher concentration to the lower concentration side. Consequently, the metabolite with lower concentration gradient will flow in the opposite direction irrespective of its own concentration gradient.

The reactions taking place in both intermembrane and the matrix sides are taken into consideration, and the flux across the membrane is calculated as described in the previous section. The reactions of malate-aspartate shuttle are listed in Table 3.5.

Table 3.5: The reactions involved in malate-aspartate shuttle. The suffix "-im" and "-m" indicates the localisation of the respective metabolite in the intermembrane space and the matrix respectively.

Aspartate-im + α-ketoglutarate-im → Oxaloacetate-im + Glutamate-im
Oxaloacetate-im + NADH-im → malate-im + NAD^+-im
Malate-m + NAD^+-m → Oxaloacetate-m + NADH-m
Oxaloacetate-m + Glutamate-m → Aspartate-m + α-ketoglutarate-m

All the reactions shown here are ideally reversible and are hence considered reversible in the script also.

Simulation

The simulation of malate-aspartate shuttle included simulating fluxes across the two transporters and incorporated them to the rate equations of the respective metabolites. The two fluxes alpha and beta were added and subtracted to the rate equation of the four metabolites depending on their flux as seen in Fig. 3.6 for malate-aspartate shuttle presented earlier.

Rate equation

The rate equations used for writing the script for simulation of malate-aspartate shuttle is given in Table 3.6. Fluxes (alpha and beta) are included in the rate equations (derived by using the same approach as followed for simulating antiport in the previous section).

Table 3.6: The list of metabolites and their rate equations derived from the reactions given in Table 3.5. The fluxes, alpha and beta, added in the rate equations are obtained using the same approach used for antiport simulation.

$\frac{d}{dt}[Asp-\mathrm{im}] = -\frac{[Asp-\mathrm{im}]}{1+[Asp-\mathrm{im}]}.\frac{[Akg-\mathrm{im}]}{1+[Akg-\mathrm{im}]}+\frac{[Oaa-\mathrm{im}]}{1+[Oaa-\mathrm{im}]}.\frac{[Glu-\mathrm{im}]}{1+[Glu-\mathrm{im}]} + alpha$
$\frac{d}{dt}[Akg-\mathrm{im}] = -\frac{[Asp-\mathrm{im}]}{1+[Asp-\mathrm{im}]}.\frac{[Akg-\mathrm{im}]}{1+[Akg-\mathrm{im}]}+\frac{[Oaa-\mathrm{im}]}{1+[Oaa-\mathrm{im}]}.\frac{[Glu-\mathrm{im}]}{1+[Glu-\mathrm{im}]} + beta$
$\frac{d}{dt}[Oaa-\mathrm{im}] = \frac{[Asp-\mathrm{im}]}{1+[Asp-\mathrm{im}]}.\frac{[Akg-\mathrm{im}]}{1+[Akg-\mathrm{im}]}-\frac{[Oaa-\mathrm{im}]}{1+[Oaa-\mathrm{im}]}.\frac{[Glu-\mathrm{im}]}{1+[Glu-\mathrm{im}]}-\frac{[Oaa-\mathrm{im}]}{1+[Oaa-\mathrm{im}]}.\frac{[NADH-\mathrm{im}]}{1+[NADH-\mathrm{im}]}+\frac{[Mal-\mathrm{im}]}{1+[Mal-\mathrm{im}]}.\frac{[NAD^+-\mathrm{im}]}{1+[NAD^+-\mathrm{im}]}$
$\frac{d}{dt}[Glu-\mathrm{im}] = \frac{[Asp-\mathrm{im}]}{1+[Asp-\mathrm{im}]}.\frac{[Akg-\mathrm{im}]}{1+[Akg-\mathrm{im}]}-\frac{[Oaa-\mathrm{im}]}{1+[Oaa-\mathrm{im}]}.\frac{[Glu-\mathrm{im}]}{1+[Glu-\mathrm{im}]} - alpha$
$\frac{d}{dt}[NADH-\mathrm{im}] = -\frac{[Oaa-\mathrm{im}]}{1+[Oaa-\mathrm{im}]}.\frac{[NADH-\mathrm{im}]}{1+[NADH-\mathrm{im}]}+\frac{[Mal-\mathrm{im}]}{1+[Mal-\mathrm{im}]}.\frac{[NAD^+-\mathrm{im}]}{1+[NAD^+-\mathrm{im}]}$
$\frac{d}{dt}[Mal-\mathrm{im}] = \frac{[Oaa-\mathrm{im}]}{1+[Oaa-\mathrm{im}]}.\frac{[NADH-\mathrm{im}]}{1+[NADH-\mathrm{im}]}-\frac{[Mal-\mathrm{im}]}{1+[Mal-\mathrm{im}]}.\frac{[NAD^{+'}-\mathrm{im}]}{1+[NAD^+-\mathrm{im}]} - beta$
$\frac{d}{dt}[NAD^+-\mathrm{im}] = \frac{[Oaa-\mathrm{im}]}{1+[Oaa-\mathrm{im}]}.\frac{[NADH-\mathrm{im}]}{1+[NADH-\mathrm{im}]}-\frac{[Mal-\mathrm{im}]}{1+[Mal-\mathrm{im}]}.\frac{[NAD^{+'}-\mathrm{im}]}{1+[NAD^+-\mathrm{im}]}$
$\frac{d}{dt}[Mal-\mathrm{m}] = -\frac{[Mal-\mathrm{m}]}{1+[Mal-\mathrm{m}]}.\frac{[NAD^+-\mathrm{m}]}{1+[NAD^+-\mathrm{m}]}+\frac{[Oaa-\mathrm{m}]}{1+[Oaa-\mathrm{m}]}.\frac{[NADH-\mathrm{m}]}{1+[NADH-\mathrm{m}]} + beta$
$\frac{d}{dt}[NAD^+-\mathrm{m}] = -\frac{[Mal-\mathrm{m}]}{1+[Mal-\mathrm{m}]}.\frac{[NAD^+-\mathrm{m}]}{1+[NAD^+-\mathrm{m}]}+\frac{[Oaa-\mathrm{m}]}{1+[Oaa-\mathrm{m}]}.\frac{[NADH-\mathrm{m}]}{1+[NADH-\mathrm{m}]}$
$\frac{d}{dt}[Oaa-\mathrm{m}] = \frac{[Mal-\mathrm{im}]}{1+[Mal-\mathrm{im}]}.\frac{[NAD^+-\mathrm{im}]}{1+[NAD^+-\mathrm{im}]}-\frac{[Oaa-\mathrm{im}]}{1+[Oaa-\mathrm{im}]}.\frac{[NADH-\mathrm{im}]}{1+[NADH-\mathrm{im}]}-\frac{[Oaa-\mathrm{im}]}{1+[Oaa-\mathrm{im}]}.\frac{[Glu-\mathrm{im}]}{1+[Glu-\mathrm{im}]}+\frac{[Asp-\mathrm{im}]}{1+[Asp-\mathrm{im}]}.\frac{[Akg-\mathrm{im}]}{1+[Akg-\mathrm{im}]}$
$\frac{d}{dt}[NADH-\mathrm{m}] = \frac{[Mal-\mathrm{m}]}{1+[Mal-\mathrm{m}]}.\frac{[NAD^+-\mathrm{m}]}{1+[NAD^+-\mathrm{m}]}-\frac{[Oaa-\mathrm{m}]}{1+[Oaa-\mathrm{m}]}.\frac{[NADH-\mathrm{m}]}{1+[NADH-\mathrm{m}]}$
$\frac{d}{dt}[Glu-\mathrm{m}] = -\frac{[Oaa-\mathrm{m}]}{1+[Oaa-\mathrm{m}]}.\frac{[Glu-\mathrm{m}]}{1+[Glu-\mathrm{m}]}+\frac{[Asp-\mathrm{m}]}{1+[Asp-\mathrm{m}]}.\frac{[Akg-\mathrm{m}]}{1+[Akg-\mathrm{m}]} + alpha$
$\frac{d}{dt}[Asp-\mathrm{m}] = \frac{[Oaa-\mathrm{m}]}{1+[Oaa-\mathrm{m}]}.\frac{[Glu-\mathrm{m}]}{1+[Glu-\mathrm{m}]}-\frac{[Asp-\mathrm{m}]}{1+[Asp-\mathrm{m}]}.\frac{[Akg-\mathrm{m}]}{1+[Akg-\mathrm{m}]} - alpha$
$\frac{d}{dt}[Akg-\mathrm{m}] = \frac{[Oaa-\mathrm{m}]}{1+[Oaa-\mathrm{m}]}.\frac{[Glu-\mathrm{m}]}{1+[Glu-\mathrm{m}]}-\frac{[Asp-\mathrm{m}]}{1+[Asp-\mathrm{m}]}.\frac{[Akg-\mathrm{m}]}{1+[Akg-\mathrm{m}]} - beta$

Alpha is calculated for glutamate-aspartate transporter, and beta is for malate-α-ketoglutarate transporter. No additional factor has been added to oxaloacetate, NADH, NAD^+, and this indicates that these metabolites are not transported across the membrane. These metabolites are maintained as independent pools on both sides of the membrane.

Script

The script used for simulating malate-aspartate shuttle is given in Table 3.7.

Table 3.7: Script used for simulation of malate-aspartate shuttle. Alpha and beta are fluxes calculated for glutamate-aspartate and malate-α-ketoglutarate transporter.

```
1;

% solve the malate-aspartate shuttle
% alpha= aspartate/glutamate direction and rate
% beta = malate/ketoglutarate direction and rate

% Rate equations for malate-aspartate shuttle

ds=zeros(14,1);
s(1) = 0.1;  %  1=Asp-im
s(2) = 0.3;  %  2=akg-im
s(3) = 0.1;  %  3=oaa-im
s(4) = 0.4;  %  4=glu-im
s(5) = 0.5;  %  5=NADH-im
s(6) = 0.8;  %  6-mal-im
s(7) = 0.1;  %  7= NAD-im
s(8) = 0.2;  %  8=mal-m
s(9) = 0.5;  %  9=NAD-m
s(10)= 0.2;  %  10=oaa-m
s(11)= 0.1;  %  11=NADH-m
s(12)= 0.1;  %  12=glu-m
s(13)= 0.9;  %  13-asp-m
s(14)= 0.7;  %  14=akg-m

function ds=mas(s)

LHS1= (s(1)/(1+s(1)))*(s(2)/(1+s(2)));
RHS1= (s(3)/(1+s(3)))*(s(4)/(1+s(4)));
LHS2= (s(3)/(1+s(3)))*(s(5)/(1+s(5)));
RHS2= (s(6)/(1+s(6)))*(s(7)/(1+s(7)));
LHS3= (s(8)/(1+s(8)))*(s(9)/(1+s(9)));
RHS3= (s(10)/(1+s(10)))*(s(11)/(1+s(11)));
LHS4= (s(10)/(1+s(10)))*(s(12)/(1+s(12)));
```

```
RHS4= (s(13)/(1+s(13)))*(s(14)/(1+s(14)));

t1=1+s(1)+s(13)+s(4)+s(12)+s(1)*s(13)+s(1)*s(4)+s(1)*s(12)+s(13)*s(4
)+s(13)*s(12)+s(4)*s(12)+s(1)*s(13)*s(4)+s(1)*s(13)*s(12)+s(1)*s(4)*
s(12)+s(13)*s(4)*s(12)+s(1)*s(13)*s(4)*s(12);

alpha=(s(1)*s(12)-s(13)*s(4))/t1; % alpha= aspartate/glutamate
direction and rate
% s1=asp-im, s12=glu-m, s13=asp-m, s4=glu-im

t1=1+s(6)+s(8)+s(2)+s(14)+s(6)*s(8)+s(6)*s(2)+s(6)*s(14)+s(8)*s(2)+s
(8)*s(14)+s(2)*s(14)+s(6)*s(8)*s(2)+s(6)*s(8)*s(14)+s(6)*s(2)*s(14)+
s(8)*s(2)*s(14)+s(6)*s(8)*s(2)*s(14);
beta=(s(6)*s(14)-s(8)*s(2))/t1; % beta = malate/ketoglutarate
direction and rate
% s6=mal-im, s14=akg-m, s8=mal-m, s2=akg-im

ds(1)= -LHS1+RHS1 -alpha;
ds(2)= -LHS1+RHS1 +beta;
ds(3)=  LHS1-RHS1-LHS2+RHS2;
ds(4)=  LHS1-RHS1 +alpha;
ds(5)= -LHS2+RHS2+0.01;
ds(6)=  LHS2-RHS2 -beta;
ds(7)=  LHS2-RHS2;
ds(8)= -LHS3+RHS3 +beta;
ds(9)= -LHS3+RHS3+0.01;
ds(10)= LHS3-RHS3-LHS4+RHS4;
ds(11)= LHS3-RHS3;
ds(12)= -LHS4+RHS4 -alpha;
ds(13)= LHS4-RHS4 +alpha;
ds(14)= LHS4-RHS4 -beta;
return
end

% use lsode to solve this set...
lsode_options("relative tolerance",1e-4);
lsode_options("absolute tolerance",1e-3);
t=0:0.01:10;
s0=s; % supply the initial concentrations
[s,T,MSG]=lsode(@mas,s0,t);
T
MSG

plot(t,s(:,8),"linewidth",5,t,s(:,13),"linewidth",5,t,s(:,6),"linewi
dth",5,t,s(:,12),"linewidth",5,t,s(:,2),"linewidth",5,t,s(:,14),"lin
ewidth",5);
grid on;

set (gca,'FontSize', 20);
set (gca, 'FontName', 'Times')
axis([0,10,0,1]);
% title ("malate-aspartate shuttle");
```

```
xlabel ("Time/arbitrary units");
ylabel ("Concentration/arbitrary units");
set (gca,'FontSize', 20);
set( get(gcf,'children'), 'linewidth',4 );
legend("mal-m","asp-m","mal-im","glu-m","akg-im","akg-m",
"location", "northeast");
```

This includes the fluxes (alpha and beta) across the two transporters, which has been incorporated in the rate equations of the respective metabolites which are transported across the mitochondrial membrane.

Result

Fig. 3.7 shows the curve obtained using the script given in the previous section. It can be clearly seen that the metabolites with higher concentration are decreasing, and those with lower concentration are increasing. This essentially suggests that the transporters are facilitating the exchange of components across the mitochondrial membrane.

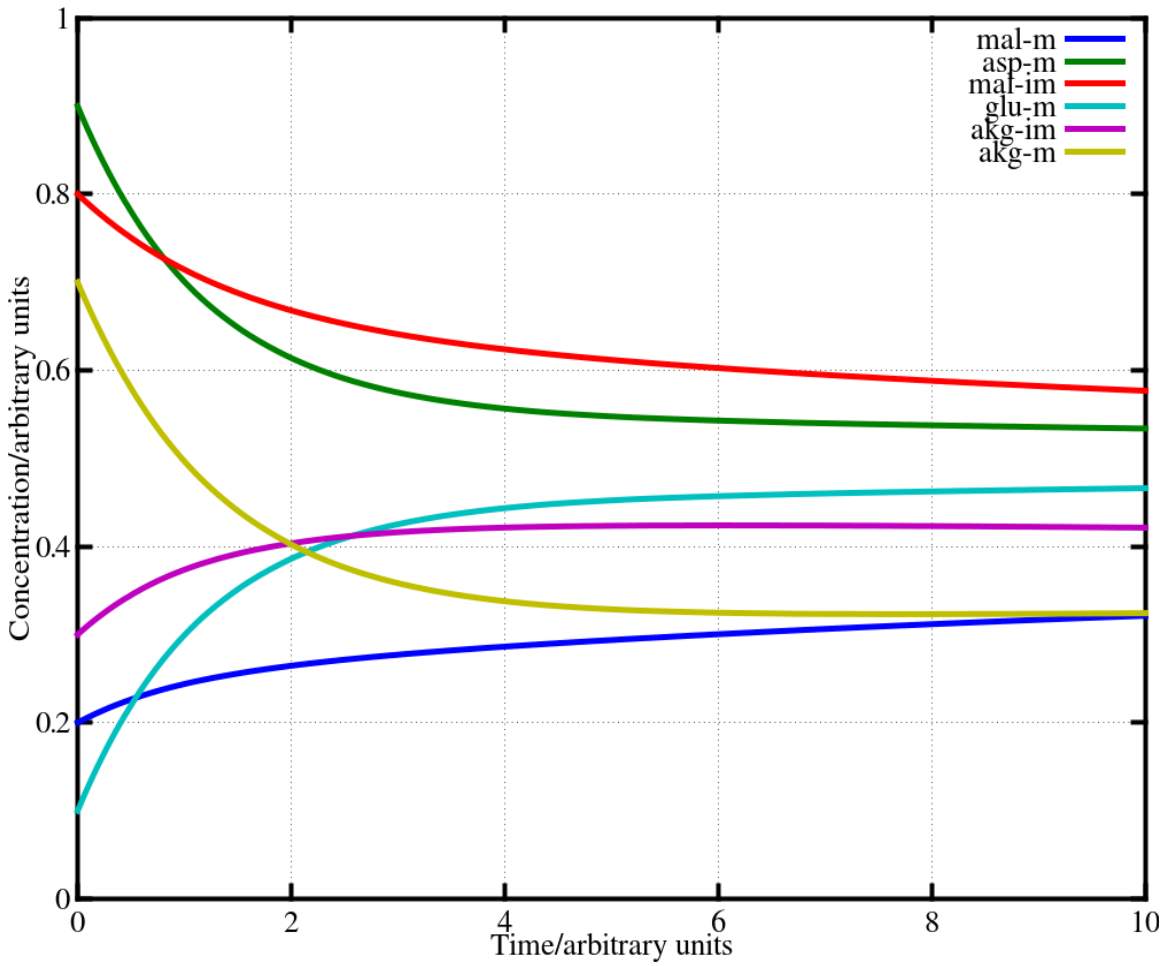

Figure 3.7: The simulation result showing progress curves of selected metabolites of malate-aspartate shuttle. The suffix "-im" and "-m" indicates the localisation of the respective metabolite in the intermembrane space and the matrix respectively. Transport stops when both concentration gradients become equal.

Citrate-Pyruvate shuttle

Citrate-pyruvate shuttle is used for the movement of carbon skeleton across the mitochondrial membrane. It consists of two exchangers (citrate/malate exchanger and malate/phosphate exchanger) and a pyruvate pump. Pyruvate pump functions as a symport transporting pyruvate and H^+ ions (or OH^- in the opposite direction) from IM space to the mitochondrial matrix, thus maintaining charge balance across the membrane (Halestrap, 1975). Pyruvate formed in the cytoplasm (mostly during glycolysis) is transported to the matrix for its further oxidation. Pyruvate can enter Krebs cycle in the form of acetyl-CoA or oxaloacetate.

There are six enzymes involved in this shuttle, which are distributed on both sides of the membrane. In the matrix, pyruvate, that enters through pyruvate pump, enters Krebs cycle via, acetyl-CoA, and formed by oxidative decarboxylation by pyruvate dehydrogenase or oxaloacetate, formed by carboxylation reaction mediated by pyruvate carboxylase. This shuttle also serves another important function, i.e. to transport (indirectly) excess of acetyl-CoA in the matrix to the cytosolic side. There are no transporters known for transporting acetyl-CoA, the cell has adopted an alternative mechanism, where acetyl-CoA is converted to citrate by combining with oxaloacetate, reaction catalysed by citrate synthase. This citrate is now transported to the intermembrane space via citrate/malate exchanger, where one mole of citrate is transported to the intermembrane space in exchange with one mole of malate. In the intermembrane space, ATP citrate lyase cleaves this citrate in an ATP-dependent manner to release oxaloacetate and acetyl-CoA. The acetyl-CoA formed here may be used for fatty acid synthesis in the cytoplasm. Moreover, oxaloacetate formed by ATP citrate lyase is reduced to malate by the action of malate dehydrogenase, oxidising NADH in the process. Malate can be used for conversion of NADP to NADPH, forming pyruvate in the process, which can be further transported via pyruvate pump (Fig. 3.8). Alternatively, malate formed in the previous step can directly be transported to the matrix via malate-α-ketoglutarate transporter, thus transporting reducing equivalent across the mitochondrial membrane (as seen under malate-aspartate shuttle).

Common metabolites as malate, oxaloacetate, citrate, etc. which are involved in multiple processes are part of the pool and can follow any reaction path, thus interrelating several metabolic processes.

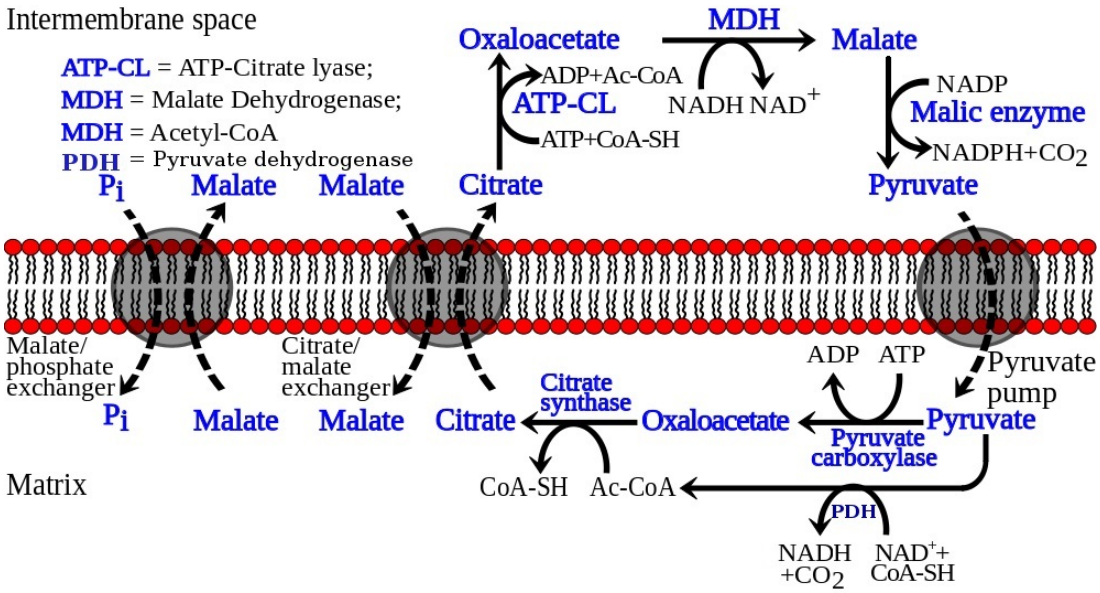

Figure 3.8: Pictorial representation of citrate-pyruvate shuttle. The figure shows six enzymes (ATP-citrate lyase, malate dehydrogenase, malic enzyme, pyruvate carboxylase, pyruvate dehydrogenase and citrate synthase), two antiport transporters, citrate/malate and malate/phosphate, and pH-dependent pyruvate pump.

Citrate-pyruvate shuttle presents an elegant mechanism for shuffling carbon skeleton across the mitochondrial membrane to meet the individual requirements on both sides of the membrane. There is pyruvate pump which can pump in 3-carbon molecule, pyruvate. Moreover, there is citrate/malate exchanger which exchanges a 6-carbon molecule with a 4-carbon molecule, resulting in the net transfer of a 2-carbon molecule. Also malate, a 4-carbon molecule, can be exchanged with a phosphate, resulting in the net transfer of 4-carbon molecule. Further, malate-α-ketoglutarate transporter, which was mentioned under malate-aspartate shuttle, can facilitate the exchange of malate, 4-carbon compound, with α-ketoglutarate, which is a 5-carbon compound. This suggests a weak coupling among these transporters by the virtue of the metabolites they transport as these metabolites are part of the common pool and can opt any of the available options.

The reactions taking place in both intermembrane space and the matrix side are taken into consideration, and the flux across the membrane is calculated as described in the previous section. The reactions of citrate-pyruvate shuttle are listed in Table 3.8.

Table 3.8: The reactions involved in citrate-pyruvate shuttle. The suffix "-im" and "-m" indicates the localisation of the respective metabolite in the intermembrane space and the matrix respectively (Reaction 2 given in bold is a reversible reaction).

Citrate-im + ATP-im + CoA-SH-im → OAA-im + acetyl-CoA-im + ADP-im + Pi-im
OAA-im + NADH-im → malate-im + NAD^+-im
Malate-im + NADP-im → Pyruvate-im + NADPH-im + CO_2
Pyruvate-m + ATP-m + CO_2 → Oxaloacetate-m + ADP-m + Pi-m
Acetyl-CoA-m + Oxaloacetate-m → Citrate-m + CoASH-m

Simulation

In the present simulation, pH and membrane potential across the membrane are assumed to be constant. However, a non-zero membrane potential would regulate the kinetics of the transport process along with the metabolite's concentration gradient. Pyruvate pump is modelled as a one-way transporter and is governed by its own concentration gradient across the mitochondrial membrane. A constant factor, flux, is also introduced to incorporate the effect of pH and membrane potential.

Rate equation

The rate equations used for writing the script for simulation of citrate-pyruvate shuttle are given in Table 3.9. Fluxes (alpha and beta) are included in the rate equations and are derived using the same approach as followed for simulating antiport in the previous section. Alpha is used for the flux for citrate/malate exchanger, and beta is similarly for malate/phosphate exchanger. pH and membrane potential have been considered constant in the simulation.

Table 3.9: The list of metabolites and their rate equations derived from the reactions given in Table 3.8. The term "flux" added in the rate equation is derived using the same approach used for antiport simulation. The suffix "-im" and "-m" indicates the localisation of the respective metabolite in the intermembrane space and the matrix respectively.

$\frac{d}{dt}[Cit-\mathrm{im}] = -\frac{[Cit-\mathrm{im}]}{1+[Cit-\mathrm{im}]}.\frac{[ATP-\mathrm{im}]}{1+[ATP-\mathrm{im}]}.\frac{[CoA-SH-\mathrm{im}]}{1+[CoA-SH-\mathrm{im}]} + alpha$
$\frac{d}{dt}[ATP-\mathrm{im}] = -\frac{[Cit-\mathrm{im}]}{1+[Cit-\mathrm{im}]}.\frac{[ATP-\mathrm{im}]}{1+[ATP-\mathrm{im}]}.\frac{[CoA-SH-\mathrm{im}]}{1+[CoA-SH-\mathrm{im}]}$

$$\frac{d}{dt}[CoA-SH-\mathrm{im}] = -\frac{[Cit-\mathrm{im}]}{1+[Cit-\mathrm{im}]}\cdot\frac{[ATP-\mathrm{im}]}{1+[ATP-\mathrm{im}]}\cdot\frac{[CoA-SH-\mathrm{im}]}{1+[CoA-SH-\mathrm{im}]}$$

$$\frac{d}{dt}[Oaa-\mathrm{im}] = \frac{[Cit-\mathrm{im}]}{1+[Cit-\mathrm{im}]}\cdot\frac{[ATP-\mathrm{im}]}{1+[ATP-\mathrm{im}]}\cdot\frac{[CoA-SH-\mathrm{im}]}{1+[CoA-SH-\mathrm{im}]} - \frac{[Oaa-\mathrm{im}]}{1+[Oaa-\mathrm{im}]}\cdot\frac{[NADH-\mathrm{im}]}{1+[NADH-\mathrm{im}]} + \frac{[Mal-\mathrm{im}]}{1+[Mal-\mathrm{im}]}\cdot\frac{[NAD^{+}-\mathrm{im}]}{1+[NAD^{+}-\mathrm{im}]}$$

$$\frac{d}{dt}[Ac-CoA-\mathrm{im}] = \frac{[Cit-\mathrm{im}]}{1+[Cit-\mathrm{im}]}\cdot\frac{[ATP-\mathrm{im}]}{1+[ATP-\mathrm{im}]}\cdot\frac{[CoA-SH-\mathrm{im}]}{1+[CoA-SH-\mathrm{im}]}$$

$$\frac{d}{dt}[ADP-\mathrm{im}] = \frac{[Cit-\mathrm{im}]}{1+[Cit-\mathrm{im}]}\cdot\frac{[ATP-\mathrm{im}]}{1+[ATP-\mathrm{im}]}\cdot\frac{[CoA-SH-\mathrm{im}]}{1+[CoA-SH-\mathrm{im}]}$$

$$\frac{d}{dt}[NADH-\mathrm{im}] = -\frac{[Oaa-\mathrm{im}]}{1+[Oaa-\mathrm{im}]}\cdot\frac{[NADH-\mathrm{im}]}{1+[NADH-\mathrm{im}]} + \frac{[Mal-\mathrm{im}]}{1+[Mal-\mathrm{im}]}\cdot\frac{[NAD^{+}-\mathrm{im}]}{1+[NAD^{+}-\mathrm{im}]}$$

$$\frac{d}{dt}[Mal-\mathrm{im}] = \frac{[Oaa-\mathrm{im}]}{1+[Oaa-\mathrm{im}]}\cdot\frac{[NADH-\mathrm{im}]}{1+[NADH-\mathrm{im}]} - \frac{[Mal-\mathrm{im}]}{1+[Mal-\mathrm{im}]}\cdot\frac{[NAD^{+}-\mathrm{im}]}{1+[NAD^{+}-\mathrm{im}]} - \frac{[Mal-\mathrm{im}]}{1+[Mal-\mathrm{im}]}\cdot\frac{[NADP-\mathrm{im}]}{1+[NADP-\mathrm{im}]} + alpha + beta$$

$$\frac{d}{dt}[NAD^{+}-\mathrm{im}] = -\frac{[Mal-\mathrm{im}]}{1+[Mal-\mathrm{im}]}\cdot\frac{[NAD^{+}-\mathrm{im}]}{1+[NAD^{+}-\mathrm{im}]} + \frac{[Oaa-\mathrm{im}]}{1+[Oaa-\mathrm{im}]}\cdot\frac{[NADH-\mathrm{im}]}{1+[NADH-\mathrm{im}]}$$

$$\frac{d}{dt}[NADP-\mathrm{im}] = -\frac{[Mal-\mathrm{im}]}{1+[Mal-\mathrm{im}]}\cdot\frac{[NADP-\mathrm{im}]}{1+[NADP-\mathrm{im}]}$$

$$\frac{d}{dt}[Pyr-\mathrm{im}] = \frac{[Mal-\mathrm{im}]}{1+[Mal-\mathrm{im}]}\cdot\frac{[NADP-\mathrm{im}]}{1+[NADP-\mathrm{im}]} - flux$$

$$\frac{d}{dt}[NADPH-\mathrm{im}] = \frac{[Mal-\mathrm{im}]}{1+[Mal-\mathrm{im}]}\cdot\frac{[NADP-\mathrm{im}]}{1+[NADP-\mathrm{im}]}$$

$$\frac{d}{dt}[Pyr-\mathrm{m}] = -\frac{[Pyr-\mathrm{m}]}{1+[Pyr-\mathrm{m}]}\cdot\frac{[ATP-\mathrm{m}]}{1+[ATP-\mathrm{m}]} + flux$$

$$\frac{d}{dt}[ATP-\mathrm{m}] = -\frac{[Pyr-\mathrm{m}]}{1+[Pyr-\mathrm{m}]}\cdot\frac{[ATP-\mathrm{m}]}{1+[ATP-\mathrm{m}]}$$

$$\frac{d}{dt}[Oaa-\mathrm{m}] = -\frac{[Pyr-\mathrm{m}]}{1+[Pyr-\mathrm{m}]}\cdot\frac{[ATP-\mathrm{m}]}{1+[ATP-\mathrm{m}]} - \frac{[Oaa-\mathrm{m}]}{1+[Oaa-\mathrm{m}]}\cdot\frac{[Ac-CoA-\mathrm{m}]}{1+[Ac-CoA-\mathrm{m}]}$$

$$\frac{d}{dt}[ADP-\mathrm{m}] = \frac{[Pyr-\mathrm{m}]}{1+[Pyr-\mathrm{m}]}\cdot\frac{[ATP-\mathrm{m}]}{1+[ATP-\mathrm{m}]}$$

$$\frac{d}{dt}[Ac-CoA-\mathrm{m}] = -\frac{[Oaa-\mathrm{m}]}{1+[Oaa-\mathrm{m}]}\cdot\frac{[Ac-CoA-\mathrm{m}]}{1+[Ac-CoA-\mathrm{m}]}$$

$$\frac{\mathrm{d}}{\mathrm{dt}}[\mathrm{Cit}-\mathrm{m}] = \frac{[\mathrm{Oaa}-\mathrm{m}]}{1+[\mathrm{Oaa}-\mathrm{m}]}\cdot\frac{[\mathrm{Ac}-\mathrm{CoA}-\mathrm{m}]}{1+[\mathrm{Ac}-\mathrm{CoA}-\mathrm{m}]} - \mathrm{flux}$$

$$\frac{\mathrm{d}}{\mathrm{dt}}[\mathrm{CoA}-\mathrm{SH}-\mathrm{m}] = \frac{[\mathrm{Oaa}-\mathrm{m}]}{1+[\mathrm{Oaa}-\mathrm{m}]}\cdot\frac{[\mathrm{Ac}-\mathrm{CoA}-\mathrm{m}]}{1+[\mathrm{Ac}-\mathrm{CoA}-\mathrm{m}]}$$

Pyruvate pump has been simulated as a one-way transporter, which is regulated by its own concentration gradient across the inner mitochondrial membrane. A non-zero membrane potential will affect pyruvate transport across the

mitochondrial membrane. It can be seen that additional factor has not been added to acetyl-CoA, CoA-SH, oxaloacetate, NADH, NAD^+, which indicates that these metabolites are not transported across the membrane and are maintained as independent pools on both sides of the membrane.

Script

The script used for simulation of citrate-pyruvate shuttle is given Table 3.10. Fluxed are included for the two exchangers in this system, citrate/malate exchanger and malate/phosphate exchanger.

Table 3.10: Script used for simulation of citrate-pyruvate shuttle.

```
1;
% solve the citrate shuttle

% 1=cit-im, 2=ATP-im, 3=oaa-im, 4=CoASH-im, 5=NADH-im, 6-mal-im, 7=
NAD-im, 8=Ac-CoA-im, 9=NADP-im, 10=oaa-m, 11=Pyruvate-im, 12=NADPH-
im, 13-ADP-im, 14=pyr-m, 15=ATP-m, 16=ADP-m, 17=acetyl-CoA-m,
18=citrate-m, 19=CoA-SH-m , 20=mal-m, 21=phos-im, 22=phos-m

% Equations for citrate shuttle
% the rate equations follow:

ds=zeros(22,1);

s(1) = 1; %initial concentrations of various components
s(2) = 1; s(3) = 0.1; s(4) = 1; s(5) = 1; s(6) = 0.3; s(7) = 0.1;
s(8) = 0.1; s(9) = 1; s(10)= 0.1; s(11)= 0.1; s(12)= 0.1; s(13)=
0.1; s(14)= 0.5; s(15)= 1; s(16)= 0.1; s(17)= 1; s(18)= 0.2; s(19)=
0.1; s(20)= 0.5; s(21)= 0.6;s(22)= 0.4;

function ds=cs(s)

LHS1= (s(1)/(1+s(1)))*(s(2)/(1+s(2)))*(s(4)/(1+s(4)));
LHS2= (s(3)/(1+s(3)))*(s(5)/(1+s(5)));
RHS2= (s(6)/(1+s(6)))*(s(7)/(1+s(7)));
LHS3= (s(6)/(1+s(6)))*(s(9)/(1+s(9)));
LHS4= (s(14)/(1+s(14)))*(s(15)/(1+s(15)));
LHS5= (s(10)/(1+s(10)))*(s(17)/(1+s(17)));

% citrate/malate exchanger

j=1+s(6)+s(20)+s(1)+s(18)+s(6)*s(20)+s(6)*s(1)+s(6)*s(18)+s(20)*s(1)
+s(20)*s(18)+s(1)*s(18)+s(6)*s(20)*s(1)+s(6)*s(20)*s(18)+s(6)*s(1)*s
(18)+s(20)*s(1)*s(18)+s(6)*s(20)*s(1)*s(18);
alpha=0.1*(s(6)*s(18)-s(20)*s(1))/j;
% s6=mal-im, s18=cit-m, s20=mal-m, s1=cit-im
```

```
% malate/phosphate exchanger

k=1+s(6)+s(20)+s(21)+s(22)+s(6)*s(20)+s(6)*s(21)+s(6)*s(22)+s(20)*s(
21)+s(20)*s(22)+s(21)*s(22)+s(6)*s(20)*s(21)+s(6)*s(20)*s(22)+s(6)*s
(21)*s(22)+s(20)*s(21)*s(22)+s(6)*s(20)*s(21)*s(22);
beta=0.1*((s(6)*s(22))-(s(20)*s(21)))/k;
% s6=mal-im, s22=phos-m, s20=mal-m, s21=phos-im

ds(1)= -LHS1+alpha;
ds(2)= -LHS1;
ds(3)=  LHS1-LHS2;
ds(4)= -LHS1;
ds(5)= -LHS2+RHS2;
ds(6)=  LHS2-RHS2-LHS3-alpha+beta;
ds(7)=  LHS2-RHS2;
ds(8)=  LHS1;
ds(9)= -LHS3;
ds(10)= LHS4-LHS5;
ds(11)= LHS3-0.01*s(11);
ds(12)= LHS3;
ds(13)= LHS1;
ds(14)=-LHS4+0.01*s(11);
ds(15)=-LHS4;
ds(16)= LHS4;
ds(17)=-LHS5;
ds(18)= LHS5-alpha;
ds(19)= LHS5;
ds(20)= alpha-beta;
ds(21)= LHS1-beta;
ds(22)= LHS4+beta;
return
end

% use lsode to solve this set...
lsode_options("relative tolerance",1e-4);
lsode_options("absolute tolerance",1e-3);
t=0:0.2:10;
% supply the initial concentrations ...
s0=s;
%   1  2  3  4  5  6  7  8
%   0  0  0  0  0  0  0  0
[s,T,MSG]=lsode(@cs,s0,t);
T
MSG
plot(t,s(:,1),"linewidth",5,t,s(:,18),"linewidth",5,t,s(:,11),"linew
idth",5,t,s(:,14),"linewidth",5,t,s(:,6),"linewidth",5,t,s(:,20),"li
newidth",5);

grid on;
```

```
set (gca,'FontSize', 20);
set (gca, 'FontName', 'Times')
axis([0,10,.001,1.01]);
% title ("citrate shuttle");
xlabel ("Time/arbitrary units");
ylabel ("Concentration/arbitrary units");
set (gca,'FontSize', 20)
set( get(gcf,'children'), 'linewidth',4 );
legend("cit-im","cit-m","pyr-im","pyr-m","mal-im","mal-
m","location", "northeast");
```

Result

The script in the previous section when run on an Octave environment gave the following graph shown in Fig. 3.9 as the result.

Concentrations of selected metabolites from citrate-pyruvate shuttle are plotted in Fig. 3.9. It can be seen that citrate concentration in the intermembrane space goes down, despite its input from the matrix. This decrease can be attributed to the reaction catalysed by ATP-citrate lyase, where oxaloacetate and acetyl-CoA are formed.

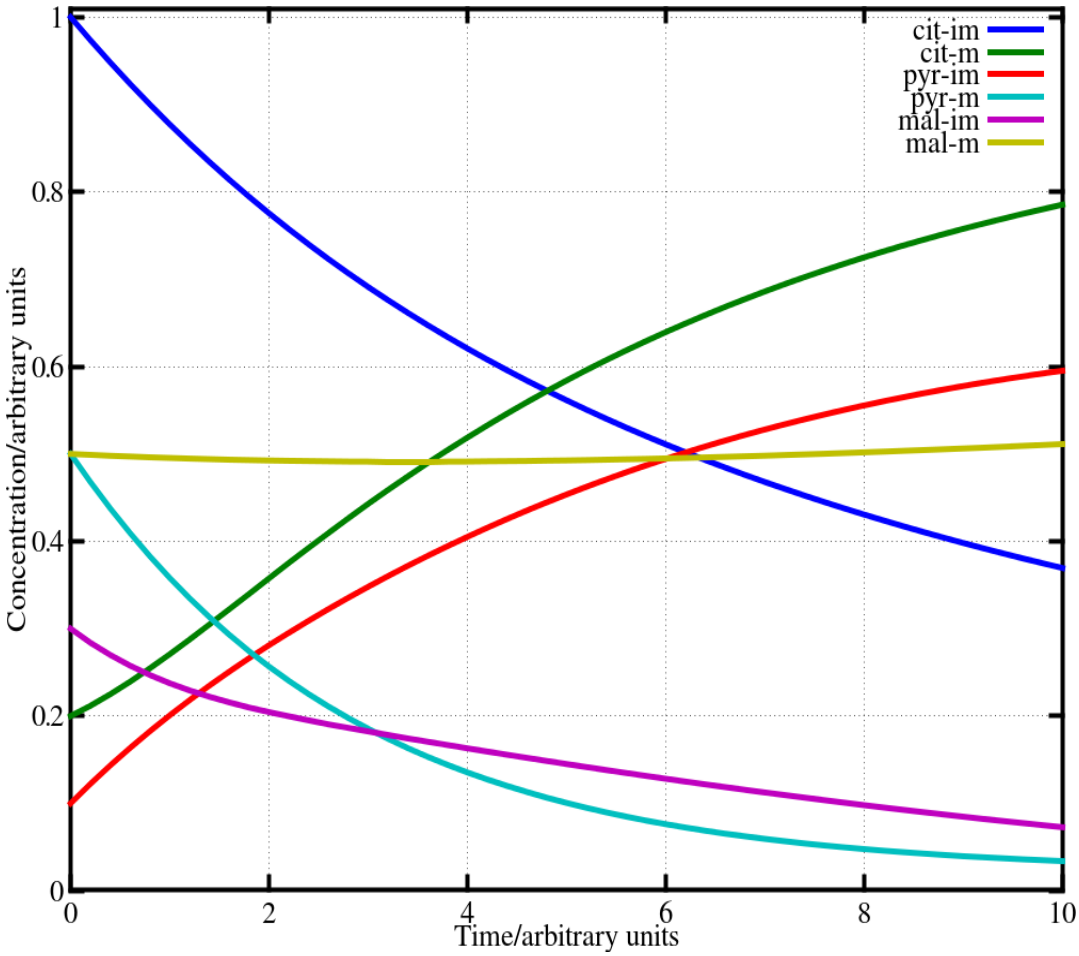

Figure 3.9: The progress curves for selected metabolites of citrate-pyruvate shuttle are shown here.

Associating Krebs cycle with shuttles

Several common components among Krebs cycle and two shuttles discussed above indicates close interdependence among them. This sharing of metabolites among the different set of reactions provides these metabolites with several paths, which they can follow to reach a steady-state under a given set of conditions. Several paths here indicate several independent sources and sinks for any particular metabolite and also presents alternative mechanisms for the cells. The complete set of reactions including Krebs cycle, malate-aspartate shuttle and citrate-pyruvate shuttle are illustrated in Fig. 3.10.

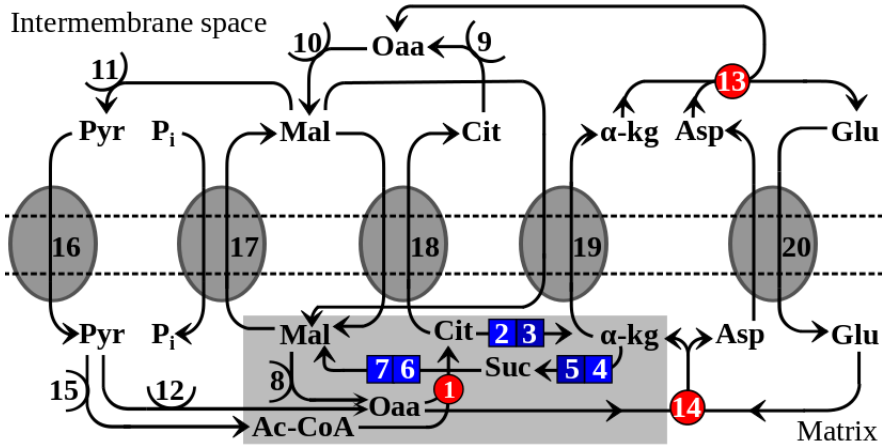

Figure 3.10: Schematic diagram representing Krebs cycle (enclosed in grey rectangular box) and transporters involved with malate-aspartate and citrate-pyruvate shuttles. [Pyr = Pyruvate, Mal = malate, α-kg = α-ketoglutarate, Cit = citrate, Glu = glutamate, Asp = aspartate, Oaa = oxaloacetate, P_i = phosphate, Suc = succinate, Ac-CoA = acetyl-CoA]. The numbers marked on the reaction lines indicate the reaction serial number from Table 3.11. 16 corresponds to pyruvate pump, 17-20 correspond to malate-phosphate, malate-citrate, malate-α-ketoglutarate and aspartate-glutamate transporters respectively

Fig. 3.10 represents an overall system where several metabolites are interconnected. Cells can use a combination of different metabolites and alternate paths to regulate cellular processes. This close association among the three sets of reactions in terms of regulation and function paves way for an intricate system which can be modelled to gain insights into their metabolic inter-connectivity.

The list of reactions included in this simulation is given in Table 3.11. There are a few reactions common among these set of reactions, and they have been compiled avoiding any repetition. These reactions were used for writing rate equations for the metabolites involved in them.

Table 3.11: List of reactions included in the present study. The table includes reactions of Krebs cycle, malate-aspartate and citrate-pyruvate shuttle. Reactions in bold indicate reversible reactions.

1.	Acetyl-CoA-m + Oxaloacetate-m → Citrate-m + CoASH-m 2 +1 → 3+ 10
2.	Citrate-m → Isocitrate-m 3 → 4
3.	Isocitrate-m + NAD^+-m → α-ketoglutarate-m+ NADH-m + CO_2 4+11 → 5 + 12 + 13
4.	α-ketoglutarate-m + CoASH-m + NAD^+-m → Succinyl CoA-m + NADH-m + CO_2-m 5+10+11 → 6+12+13
5.	Succinyl CoA-m + GDP-m + Phos-m → Succinate-m + GTP-m + CoASH-m 6+14+38 → 7 + 15+10
6.	Succinate-m + FAD-m → Fumarate-m + $FADH_2$-m 7+16 → 8+17
7.	Fumarate-m + H_2O → Malate-m 8 → 9
8.	**Malate-m + NAD^+-m → Oxaloacetate-m + NADH-m** 9+11 → 1+ 12
9.	Citrate-im + ATP-im + CoA-SH-im → OAA-im + acetyl-CoA-im + ADP-im + Pi-im 25+26+27 → 34 +28+29+39
10.	**OAA-im + NADH-im → malate-im + NAD^+-im** 34+35 → 20+36
11.	Malate-im + NADP-im → Pyruvate-im + NADPH-im + CO_2 20+30 → 31+32
12.	Pyruvate-m + ATP-m + CO_2 → Oxaloacetate-m + ADP-m + Pi-m 33+18+13 → 1+37+38
13.	**Aspartate-im + α-ketoglutarate-im → Oxaloacetate-im + Glutamate-im** 19+21 → 34+22
14.	**Oxaloacetate-m + Glutamate-m → Aspartate-m + α-ketoglutarate-m** 1+23 → 24+5
15.	Pyruvate-m + NAD^+-m + CoASH-m → Acetyl-CoA-m + CO_2-m +NADH-m 33+11+10 → 2+13+12

A combination of these mechanisms suggests that apart from ATP synthesis, mitochondria also have considerable biosynthetic activity. It is determined by the energy state of the cell and is regulated by the activities of shuttles, Krebs cycle and ATP synthesis. The reducing equivalents required for functioning of the ETC can be derived both from inside mitochondria and cytosol. However, in the absence of shuttle systems, mitochondria will be left with only one source of reducing equivalents, i.e., Krebs cycle, which may not meet the ATP needs of the cell. Thus, shuttles play a critical role in regulation and maintenance of routine cellular metabolism.

Rate equation

The rate equations used for writing the script for combined simulation of Krebs cycle, malate-aspartate shuttle and citrate-pyruvate shuttle are given in Table 3.12. Fluxes (alpha, beta, gamma, delta) are added in the rate equation which is derived by using the same approach as followed for simulating antiport in the previous section. Here alpha denotes the flux across glutamate-aspartate transporter and beta is for malate-α-ketoglutarate transporter. Gamma is the flux for malate/citrate exchanger and delta is for malate/phosphate exchanger Flux is the flux of pyruvate through pyruvate pump.

Table 3.12: The list of metabolites and their rate equations derived from the reactions given in Table 11. The terms "alpha, beta, gamma, delta and flux" added in the rate equation is derived using the same approach used for antiport simulation. The suffix "-im" and "-m" indicates the localisation of the respective metabolite in the intermembrane space and the matrix respectively.

$\frac{d}{dt}[Oaa-\mathrm{m}] = -\frac{[Ac-CoA-\mathrm{m}]}{1+[Ac-CoA-\mathrm{m}]}\cdot\frac{[Oaa-\mathrm{m}]}{1+[Oaa-\mathrm{m}]}\cdot\frac{1}{1+[Cit]}\cdot\frac{1}{1+[SucCoA]}+\frac{[Mal-\mathrm{m}]}{1+[Mal-\mathrm{m}]}\cdot\frac{[NAD^+-\mathrm{m}]}{1+[NAD^+-\mathrm{m}]}-\frac{[Oaa-\mathrm{m}]}{1+[Oaa-\mathrm{m}]}\cdot\frac{[NADH-\mathrm{m}]}{1+[NADH-\mathrm{m}]}-\frac{[Oaa-\mathrm{m}]}{1+[Oaa-\mathrm{m}]}\cdot\frac{[Glu-\mathrm{m}]}{1+[Glu-\mathrm{m}]}+\frac{[Asp-\mathrm{m}]}{1+[Asp-\mathrm{m}]}\cdot\frac{[Akg-\mathrm{m}]}{1+[Akg-\mathrm{m}]}+\frac{[Pyr-\mathrm{m}]}{1+[Pyr-\mathrm{m}]}\cdot\frac{[ATP-\mathrm{m}]}{1+[ATP-\mathrm{m}]}\cdot\frac{[CO_2-\mathrm{m}]}{1+[CO_2-\mathrm{m}]}$
$\frac{d}{dt}[Ac-CoA-\mathrm{m}] = -\frac{[Ac-CoA-\mathrm{m}]}{1+[Ac-CoA-\mathrm{m}]}\cdot\frac{[Oaa-\mathrm{m}]}{1+[Oaa-\mathrm{m}]}\cdot\frac{1}{1+[Cit]}\cdot\frac{1}{1+[SucCoA]}+\frac{[Pyr-\mathrm{m}]}{1+[Pyr-\mathrm{m}]}\cdot\frac{[NAD^+-\mathrm{m}]}{1+[NAD^+-\mathrm{m}]}\cdot\frac{[CoASH-\mathrm{m}]}{1+[CoASH-\mathrm{m}]}$
$\frac{d}{dt}[Cit-\mathrm{m}] = \frac{[Ac-CoA-\mathrm{m}]}{1+[Ac-CoA-\mathrm{m}]}\cdot\frac{[Oaa-\mathrm{m}]}{1+[Oaa-\mathrm{m}]}\cdot\frac{1}{1+[Cit]}\cdot\frac{1}{1+[SucCoA]}-\frac{[Iso-cit-\mathrm{m}]}{1+[Iso-cit-\mathrm{m}]} - gamma$
$\frac{d}{dt}[Isocit-\mathrm{m}] = \frac{[Cit-\mathrm{m}]}{1+[Cit-\mathrm{m}]}-\frac{[Isocit-\mathrm{m}]}{1+[Isocit-\mathrm{m}]}\cdot\frac{[NAD^+-\mathrm{m}]}{1+[NAD^+-\mathrm{m}]}$
$\frac{d}{dt}[Akg-\mathrm{m}] = \frac{[Iso-cit-\mathrm{m}]}{1+[Iso-cit-\mathrm{m}]}\cdot\frac{[NAD^+-\mathrm{m}]}{1+[NAD^+-\mathrm{m}]}-\frac{[Akg-\mathrm{m}]}{1+[Akg-\mathrm{m}]}\cdot\frac{[CoASH-\mathrm{m}]}{1+[CoASH-\mathrm{m}]}\cdot\frac{[NAD^+-\mathrm{m}]}{1+[NAD^+-\mathrm{m}]}\cdot\frac{1}{1+[SucCoA]}+\frac{[Oaa-\mathrm{m}]}{1+[Oaa-\mathrm{m}]}\cdot\frac{[Glu-\mathrm{m}]}{1+[Glu-\mathrm{m}]}-\frac{[Asp-\mathrm{m}]}{1+[Asp-\mathrm{m}]}\cdot\frac{[Akg-\mathrm{m}]}{1+[Akg-\mathrm{m}]} - beta$
$\frac{d}{dt}[SucCoA-\mathrm{m}] = \frac{[Akg-\mathrm{m}]}{1+[Akg-\mathrm{m}]}\cdot\frac{[CoASH-\mathrm{m}]}{1+[CoASH-\mathrm{m}]}\cdot\frac{[NAD^+-\mathrm{m}]}{1+[NAD^+-\mathrm{m}]}\cdot\frac{1}{1+[SucCoA]}-\frac{[SucCoA-\mathrm{m}]}{1+[SucCoA-\mathrm{m}]}\cdot\frac{[GDP-\mathrm{m}]}{1+[GDP-\mathrm{m}]}\cdot\frac{[Phos-\mathrm{m}]}{1+[Phos-\mathrm{m}]}$
$\frac{d}{dt}[Suc-\mathrm{m}] = -\frac{[SucCoA-\mathrm{m}]}{1+[SucCoA-\mathrm{m}]}\cdot\frac{[GDP-\mathrm{m}]}{1+[GDP-\mathrm{m}]}\cdot\frac{[Phos-\mathrm{m}]}{1+[Phos-\mathrm{m}]}-\frac{[Suc-\mathrm{m}]}{1+[Suc-\mathrm{m}]}\cdot\frac{[FAD-\mathrm{m}]}{1+[FAD-\mathrm{m}]}$
$\frac{d}{dt}[Fum-\mathrm{m}] = \frac{[Suc-\mathrm{m}]}{1+[Suc-\mathrm{m}]}\cdot\frac{[FAD-\mathrm{m}]}{1+[FAD-\mathrm{im}]}-\frac{[Fum-\mathrm{m}]}{1+[Fum-\mathrm{m}]}$
$\frac{d}{dt}[Mal-\mathrm{m}] = \frac{[Fum-\mathrm{m}]}{1+[Fum-\mathrm{m}]}-\frac{[Mal-\mathrm{m}]}{1+[Mal-\mathrm{m}]}\cdot\frac{[NAD^+-\mathrm{m}]}{1+[NAD^+-\mathrm{m}]}+\frac{[Oaa-\mathrm{m}]}{1+[Oaa-\mathrm{m}]}\cdot\frac{[NADH-\mathrm{m}]}{1+[NADH-\mathrm{m}]} + beta + gamma - delta$
$\frac{d}{dt}[CoASH-\mathrm{m}] = -\frac{[AcCoA-\mathrm{m}]}{1+[AcCoA-\mathrm{m}]}\cdot\frac{[Oaa-\mathrm{m}]}{1+[Oaa-\mathrm{m}]}\cdot\frac{1}{1+[Cit]}\cdot\frac{1}{1+[SucCoA]}-\frac{[Akg-\mathrm{m}]}{1+[Akg-\mathrm{m}]}\cdot\frac{[CoASH-\mathrm{m}]}{1+[CoASH-\mathrm{m}]}\cdot\frac{[NAD^+-\mathrm{m}]}{1+[NAD^+-\mathrm{m}]}\cdot\frac{1}{1+[SucCoA]}+\frac{[SucCoA-\mathrm{m}]}{1+[SucCoA-\mathrm{m}]}\cdot\frac{[GDP-\mathrm{m}]}{1+[GDP-\mathrm{m}]}\cdot\frac{[Phos-\mathrm{m}]}{1+[Phos-\mathrm{m}]}-\frac{[Pyr-\mathrm{m}]}{1+[Pyr-\mathrm{m}]}\cdot\frac{[NAD^+-\mathrm{m}]}{1+[NAD^+-\mathrm{m}]}\cdot\frac{[CoASH-\mathrm{m}]}{1+[CoASH-\mathrm{m}]}$

$$\frac{d}{dt}[NAD^+ - \mathrm{m}] = -\frac{[Isocit - \mathrm{m}]}{1+[Isocit - \mathrm{m}]}\cdot\frac{[NAD^+ - \mathrm{m}]}{1+[NAD^+ - \mathrm{m}]} - \frac{[Akg - \mathrm{m}]}{1+[Akg - \mathrm{m}]}\cdot\frac{[CoASH - \mathrm{m}]}{1+[CoASH - \mathrm{m}]}\cdot\frac{[NAD^+ - \mathrm{m}]}{1+[NAD^+ - \mathrm{m}]}\cdot\frac{1}{1+[SucCoA]}$$
$$-\frac{[Mal - \mathrm{m}]}{1+[Mal - \mathrm{m}]}\cdot\frac{[NAD^+ - \mathrm{m}]}{1+[NAD^+ - \mathrm{m}]} + \frac{[Oaa - \mathrm{m}]}{1+[Oaa - \mathrm{m}]}\cdot\frac{[NADH - \mathrm{m}]}{1+[NADH - \mathrm{m}]} - \frac{[Pyr - \mathrm{m}]}{1+[Pyr - \mathrm{m}]}\cdot\frac{[NAD^+ - \mathrm{m}]}{1+[NAD^+ - \mathrm{m}]}\cdot\frac{[CoASH - \mathrm{m}]}{1+[CoASH - \mathrm{m}]}$$

$$\frac{d}{dt}[NADH - \mathrm{m}] = \frac{[Isocit - \mathrm{m}]}{1+[Isocit - \mathrm{m}]}\cdot\frac{[NAD^+ - \mathrm{m}]}{1+[NAD^+ - \mathrm{m}]} + \frac{[Akg - \mathrm{m}]}{1+[Akg - \mathrm{m}]}\cdot\frac{[CoASH - \mathrm{m}]}{1+[CoASH - \mathrm{m}]}\cdot\frac{[NAD^+ - \mathrm{m}]}{1+[NAD^+ - \mathrm{m}]}\cdot\frac{1}{1+[SucCoA]}$$
$$+\frac{[Mal - \mathrm{m}]}{1+[Mal - \mathrm{m}]}\cdot\frac{[NAD^+ - \mathrm{m}]}{1+[NAD^+ - \mathrm{m}]}\cdot\frac{[Oaa - \mathrm{m}]}{1+[Oaa - \mathrm{m}]}\cdot\frac{[NADH - \mathrm{m}]}{1+[NADH - \mathrm{m}]} + \frac{[Pyr - \mathrm{m}]}{1+[Pyr - \mathrm{m}]}\cdot\frac{[NAD^+ - \mathrm{m}]}{1+[NAD^+ - \mathrm{m}]}\cdot\frac{[CoASH - \mathrm{m}]}{1+[CoASH - \mathrm{m}]}$$

$$\frac{d}{dt}[CO_2 - \mathrm{m}] = \frac{[Iso - cit - \mathrm{m}]}{1+[Iso - cit - \mathrm{m}]}\cdot\frac{[NAD^+ - \mathrm{m}]}{1+[NAD^+ - \mathrm{m}]} + \frac{[Akg - \mathrm{m}]}{1+[Akg - \mathrm{m}]}\cdot\frac{[CoASH - \mathrm{m}]}{1+[CoASH - \mathrm{m}]}\cdot\frac{[NAD^+ - \mathrm{m}]}{1+[NAD^+ - \mathrm{m}]}\cdot\frac{1}{1+[SucCoA]}$$
$$+\frac{[Pyr - \mathrm{m}]}{1+[Pyr - \mathrm{m}]}\cdot\frac{[NAD^+ - \mathrm{m}]}{1+[NAD^+ - \mathrm{m}]}\cdot\frac{[CoASH - \mathrm{m}]}{1+[CoASH - \mathrm{m}]}$$

$$\frac{d}{dt}[GDP - \mathrm{m}] = -\frac{[SucCoA - \mathrm{m}]}{1+[SucCoA - \mathrm{m}]}\cdot\frac{[GDP - \mathrm{m}]}{1+[GDP - \mathrm{m}]}\cdot\frac{[Phos - \mathrm{m}]}{1+[Phos - \mathrm{m}]}$$

$$\frac{d}{dt}[GTP - \mathrm{m}] = \frac{[SucCoA - \mathrm{m}]}{1+[SucCoA - \mathrm{m}]}\cdot\frac{[GDP - \mathrm{m}]}{1+[GDP - \mathrm{m}]}\cdot\frac{[Phos - \mathrm{m}]}{1+[Phos - \mathrm{m}]}$$

$$\frac{d}{dt}[FAD - \mathrm{m}] = -\frac{[SucCoA - \mathrm{m}]}{1+[SucCoA - \mathrm{m}]}\cdot\frac{[FAD - \mathrm{m}]}{1+[FAD - \mathrm{m}]}$$

$$\frac{d}{dt}[FADH_2 - \mathrm{m}] = -\frac{[SucCoA - \mathrm{m}]}{1+[SucCoA - \mathrm{m}]}\cdot\frac{[FAD - \mathrm{m}]}{1+[FAD - \mathrm{m}]}$$

$$\frac{d}{dt}[ATP - \mathrm{m}] = -\frac{[Pyr - \mathrm{m}]}{1+[Pyr - \mathrm{m}]}\cdot\frac{[ATP - \mathrm{m}]}{1+[ATP - \mathrm{m}]}\cdot\frac{[CO_2 - \mathrm{m}]}{1+[CO_2 - \mathrm{m}]}$$

$$\frac{d}{dt}[Asp - \mathrm{im}] = -\frac{[Asp - \mathrm{im}]}{1+[Asp - \mathrm{im}]}\cdot\frac{[Akg - \mathrm{im}]}{1+[Akg - \mathrm{im}]} + \frac{[Oaa - \mathrm{im}]}{1+[Oaa - \mathrm{im}]}\cdot\frac{[Glu - \mathrm{im}]}{1+[Glu - \mathrm{im}]} + alpha$$

$$\frac{d}{dt}[Mal - \mathrm{im}] = \frac{[Oaa - \mathrm{im}]}{1+[Oaa - \mathrm{im}]}\cdot\frac{[NADH - \mathrm{im}]}{1+[NADH - \mathrm{im}]} - \frac{[Mal - \mathrm{im}]}{1+[Mal - \mathrm{im}]}\cdot\frac{[NAD^+ - \mathrm{im}]}{1+[NAD^+ - \mathrm{im}]} - \frac{[Mal - \mathrm{im}]}{1+[Mal - \mathrm{im}]}\cdot\frac{[NADP - \mathrm{im}]}{1+[NADP - \mathrm{im}]}$$
$$- beta - gamma + delta$$

$$\frac{d}{dt}[Akg - \mathrm{im}] = -\frac{[Asp - \mathrm{im}]}{1+[Asp - \mathrm{im}]}\cdot\frac{[Akg - \mathrm{im}]}{1+[Akg - \mathrm{im}]} + \frac{[Oaa - \mathrm{im}]}{1+[Oaa - \mathrm{im}]}\cdot\frac{[Glu - \mathrm{im}]}{1+[Glu - \mathrm{im}]} + beta$$

$$\frac{d}{dt}[Glu - \mathrm{im}] = \frac{[Asp - \mathrm{im}]}{1+[Asp - \mathrm{im}]}\cdot\frac{[Akg - \mathrm{im}]}{1+[Akg - \mathrm{im}]} - \frac{[Oaa - \mathrm{im}]}{1+[Oaa - \mathrm{im}]}\cdot\frac{[Glu - \mathrm{im}]}{1+[Glu - \mathrm{im}]} - alpha$$

$$\frac{d}{dt}[Glu - \mathrm{m}] = -\frac{[Oaa - \mathrm{m}]}{1+[Oaa - \mathrm{m}]}\cdot\frac{[Glu - \mathrm{m}]}{1+[Glu - \mathrm{m}]} + \frac{[Asp - \mathrm{m}]}{1+[Asp - \mathrm{m}]}\cdot\frac{[Akg - \mathrm{m}]}{1+[Akg - \mathrm{m}]} + alpha$$

$$\frac{d}{dt}[Asp - \mathrm{m}] = \frac{[Oaa - \mathrm{m}]}{1+[Oaa - \mathrm{m}]}\cdot\frac{[Glu - \mathrm{m}]}{1+[Glu - \mathrm{m}]} - \frac{[Asp - \mathrm{m}]}{1+[Asp - \mathrm{m}]}\cdot\frac{[Akg - \mathrm{m}]}{1+[Akg - \mathrm{m}]} - alpha$$

$$\frac{d}{dt}[Cit - \mathrm{im}] = -\frac{[Cit - \mathrm{im}]}{1+[Cit - \mathrm{im}]}\cdot\frac{[ATP - \mathrm{im}]}{1+[ATP - \mathrm{im}]}\cdot\frac{[CoASH - \mathrm{im}]}{1+[CoASH - \mathrm{im}]}$$

$$\frac{d}{dt}[ATP - \mathrm{im}] = -\frac{[Cit - \mathrm{im}]}{1+[Cit - \mathrm{im}]}\cdot\frac{[ATP - \mathrm{im}]}{1+[ATP - \mathrm{im}]}\cdot\frac{[CoASH - \mathrm{im}]}{1+[CoASH - \mathrm{im}]}$$

$$\frac{d}{dt}[CoASH - \mathrm{im}] = -\frac{[Cit - \mathrm{im}]}{1+[Cit - \mathrm{im}]}\cdot\frac{[ATP - \mathrm{im}]}{1+[ATP - \mathrm{im}]}\cdot\frac{[CoASH - \mathrm{im}]}{1+[CoASH - \mathrm{im}]}$$

$$\frac{d}{dt}[Ac - CoA - \mathrm{im}] = \frac{[Cit - \mathrm{im}]}{1+[Cit - \mathrm{im}]}\cdot\frac{[ATP - \mathrm{im}]}{1+[ATP - \mathrm{im}]}\cdot\frac{[CoASH - \mathrm{im}]}{1+[CoASH - \mathrm{im}]}$$

$$\frac{d}{dt}[ADP - \mathrm{im}] = \frac{[Cit - \mathrm{im}]}{1+[Cit - \mathrm{im}]}\cdot\frac{[ATP - \mathrm{im}]}{1+[ATP - \mathrm{im}]}\cdot\frac{[CoASH - \mathrm{im}]}{1+[CoASH - \mathrm{im}]}$$

$$\frac{d}{dt}[NADP - \mathrm{im}] = -\frac{[Mal - \mathrm{im}]}{1+[Mal - \mathrm{im}]}\cdot\frac{[NADP - \mathrm{im}]}{1+[NADP - \mathrm{im}]}$$

$$\frac{d}{dt}[Pyr-\text{im}] = \frac{[Mal-\text{im}]}{1+[Mal-\text{im}]}.\frac{[NADP-\text{im}]}{1+[NADP-\text{im}]} - flux$$

$$\frac{d}{dt}[NADPH-\text{im}] = \frac{[Mal-\text{im}]}{1+[Mal-\text{im}]}.\frac{[NADP-\text{im}]}{1+[NADP-\text{im}]}$$

$$\frac{d}{dt}[Pyr-\text{m}] = -\frac{[Pyr-\text{m}]}{1+[Pyr-\text{m}]}.\frac{[ATP-\text{m}]}{1+[ATP-\text{m}]}.\frac{[CO_2-\text{m}]}{1+[CO_2-\text{m}]} - \frac{[Pyr-\text{m}]}{1+[Pyr-\text{m}]}.\frac{[NAD^+-\text{m}]}{1+[NAD^+-\text{m}]}.\frac{[CoASH-\text{m}]}{1+[CoASH-\text{m}]} + flux$$

$$\frac{d}{dt}[Oaa-\text{im}] = -\frac{[Oaa-\text{im}]}{1+[Oaa-\text{im}]}.\frac{[NADH-\text{im}]}{1+[NADH-\text{im}]} + \frac{[Mal-\text{im}]}{1+[Mal-\text{im}]}.\frac{[NAD^+-\text{im}]}{1+[NAD^+-\text{im}]}\frac{[Asp-\text{im}]}{1+[Asp-\text{im}]}.\frac{[Akg-\text{im}]}{1+[Akg-\text{im}]} - \frac{[Oaa-\text{im}]}{1+[Oaa-\text{im}]}.\frac{[Glu-\text{im}]}{1+[Glu-\text{im}]} + \frac{[Cit-\text{im}]}{1+[Cit-\text{im}]}.\frac{[ATP-\text{im}]}{1+[ATP-\text{im}]}.\frac{[CoASH-\text{im}]}{1+[CoASH-\text{im}]}$$

$$\frac{d}{dt}[NADH-\text{im}] = -\frac{[Oaa-\text{im}]}{1+[Oaa-\text{im}]}.\frac{[NADH-\text{im}]}{1+[NADH-\text{im}]} + \frac{[Mal-\text{im}]}{1+[Mal-\text{im}]}.\frac{[NAD^+-\text{im}]}{1+[NAD^+-\text{im}]}$$

$$\frac{d}{dt}[NAD^+-\text{im}] = \frac{[Oaa-\text{im}]}{1+[Oaa-\text{im}]}.\frac{[NADH-\text{im}]}{1+[NADH-\text{im}]} - \frac{[Mal-\text{im}]}{1+[Mal-\text{im}]}.\frac{[NAD^+-\text{im}]}{1+[NAD^+-\text{im}]}$$

$$\frac{d}{dt}[ADP-\text{m}] = \frac{[Pyr-\text{m}]}{1+[Pyr-\text{m}]}.\frac{[ATP-\text{m}]}{1+[ATP-\text{m}]}.\frac{[CO_2-\text{m}]}{1+[CO_2-\text{m}]}$$

$$\frac{d}{dt}[Phos-\text{m}] = \frac{[Pyr-\text{m}]}{1+[Pyr-\text{m}]}.\frac{[ATP-\text{m}]}{1+[ATP-\text{m}]}.\frac{[CO_2-\text{m}]}{1+[CO_2-\text{m}]} + \frac{[Cit-\text{im}]}{1+[Cit-\text{im}]}.\frac{[ATP-\text{im}]}{1+[ATP-\text{im}]}.\frac{[CoASH-\text{im}]}{1+[CoASH-\text{im}]} + delta$$

$$\frac{\text{d}}{\text{dt}}[\text{Phos}-\text{im}] = \frac{[\text{Cit}-\text{im}]}{1+[\text{Cit}-\text{im}]}.\frac{[\text{ATP}-\text{im}]}{1+[\text{ATP}-\text{im}]}.\frac{[\text{CoASH}-\text{im}]}{1+[\text{CoASH}-\text{im}]} - \text{delta}$$

Additional factor has not been added to acetyl-CoA, CoA-SH, oxaloacetate, NADH, NAD^+, etc. and this indicates that these metabolites are not transported across the membrane. These metabolites are maintained as independent pools on both sides of the membrane.

Script

The script used for combined simulation of Krebs cycle, malate-aspartate shuttle and citrate-pyruvate shuttle is given in Table 3.13. All the four transporters and pyruvate pumps have been simulated.

Table 3.13: Script used for simulation of Krebs cycle along with malate-aspartate and citrate-pyruvate shuttles.

```
1; % solve the Krebs cycle + shuttles
ds=zeros(39,1);
s(1) = 0.5;             % oxaloacetate-m
s(2) = 0.5;             % acetyl-CoA-m
s(3) = 0.1;             % citrate-m
s(4) = 0.1;             % isocitrate-m
s(5) = 0.2;             % ketoglutarate-m
s(6) = 0.1;             % succinyl-CoA-m
s(7) = 0.1;             % succinate-m
s(8) = 0.1;             % fumarate-m
s(9) = 0.1;             % malate-m
```

```
s(10)= 0.5;             % CoA-SH-m
s(11)= 0.1;             % NAD-m
s(12)= 0.1;             % NADH-m
s(13)= 0.1;             % CO2
s(14)= 0.1;             % GDP
s(15)= 0.1;             % GTP
s(16)= 0.1;             % FAD
s(17)= 0.1;             % FADH2
s(18)= 0.2;             % ATP-m
s(19)= 0.3;             % Aspartate-im
s(20)= 0.5;             % malate-im
s(21)= 0.5;             % ketoglutarate-im
s(22)= 0.5;             % glutamate-im
s(23)= 0.2;             % glutamate-m
s(24)= 0.1;             % Aspartate-m
s(25)= 0.1;             % citrate-im
s(26)= 0.2;             % ATP-im
s(27)= 0.5;             % CoA-SH-im
s(28)= 0.1;             % Acetyl-CoA-im
s(29)= 0.1;             % ADP-im
s(30)= 0.5;             % NADP-im
s(31)= 0.3;             % Pyruvate-im
s(32)= 0.1;             % NADPH-im
s(33)= 0.2;             % Pyruvate-m
s(34)= 0.5;             % oxaloacetate-im
s(35)= 0.2;             % NADH-im
s(36)= 0.1;             % NAD-im
s(37)= 0.1;             % ADP-m
s(38)= 0.5;             % phos-m
s(39)= 0.6;             % phos-im

function ds=shukr(s)
% Equations for Kreb cycle reactions
LHS1=(s(1)/(1+s(1)))*(s(2)/(1+s(2)))*(1/(1+s(3)))*(1/(1+s(6)))*(1/
(1+s(12)))*(1/(1+s(18)));
      % this is inhibited by s3; s6; s12; ATP
LHS2= 0.2*(s(3)/(1+s(3)));
LHS3= 0.2*(s(4)/(1+s(4)))*(s(11)/(1+s(11)))*(1/(1+s(18)));
      % this is inhibited by ATP
LHS4=      0.2*(s(5)/(1+s(5)))*(s(10)/(1+s(10)))*(s(11)/(1+s(11)))*(1/
(1+s(6)))*(1/(1+s(12)));
      % this is inhibited by s6; s12
LHS5= (s(6)/(1+s(6)))*(s(14)/(1+s(14)))*(s(38)/(1+s(38)));
LHS6= (s(7)/(1+s(7)))*(s(16)/(1+s(16)));
LHS7= 0.2*(s(8)/(1+s(8)));
LHS8= (s(9)/(1+s(9)))*(s(11)/(1+s(11)));
RHS8= (s(1)/(1+s(1)))*(s(12)/(1+s(12)));
LHS15= (s(33)/(1+s(33)))*(s(11)/(1+s(11)))*(s(10)/(1+s(10)));

% Equations for shuttle reactions
LHS9 =(s(27)/(1+s(27)))*(s(25)/(1+s(25)))*(s(26)/(1+s(26)));
LHS10=(s(34)/(1+s(34)))*(s(35)/(1+s(35)));
```

```
RHS10=(s(20)/(1+s(20)))*(s(36)/(1+s(36)));
LHS11=(s(20)/(1+s(20)))*(s(30)/(1+s(30)));
LHS12=(s(33)/(1+s(33)))*(s(18)/(1+s(18)))*(s(13)/(1+s(13)));
LHS13=(s(19)/(1+s(19)))*(s(21)/(1+s(21)));
RHS13=(s(34)/(1+s(34)))*(s(22)/(1+s(22)));
LHS14=(s(1)/(1+s(1)))*(s(23)/(1+s(23)));
RHS14=(s(24)/(1+s(24)))*(s(5)/(1+s(5)));

port = 0.05;
% alpha= aspartate/glutamate direction and rate
a=1+s(19)+s(24)+s(22)+s(23)+s(19)*s(24)+s(19)*s(22)+s(19)*s(23)+s(24)*
s(22)+s(24)*s(23)+s(22)*s(23)+s(19)*s(24)*s(22)+s(19)*s(24)*s(23)+s(19
)*s(22)*s(23)+s(24)*s(22)*s(23)+s(19)*s(24)*s(22)*s(23);
alpha=port*((s(22)*s(24))-(s(19)*s(23)))/a;
% s19=asp-im, s23=glu-m, s24=asp-m, s22=glu-im

% beta = malate/ketoglutarate direction and rate
b=1+s(20)+s(9)+s(21)+s(5)+s(20)*s(9)+s(20)*s(21)+s(20)*s(5)+s(9)*s(21)
+s(9)*s(5)+s(21)*s(5)+s(20)*s(9)*s(21)+s(20)*s(9)*s(5)+s(20)*s(21)*s(5
)+s(9)*s(21)*s(5)+s(20)*s(9)*s(21)*s(5);
beta=port*((s(20)*s(5))-(s(9)*s(21)))/b;
% s20=mal-im, s5=akg-m, s9=mal-m, s21=akg-im

% malate citrate exchanger
 j=1+s(20)+s(9)+s(25)+s(3)+s(20)*s(9)+s(20)*s(25)+s(20)*s(3)+s(9)*s(25
)+s(9)*s(3)+s(25)*s(3)+s(20)*s(9)*s(25)+s(20)*s(9)*s(3)+s(20)*s(25)*s(
3)+s(9)*s(25)*s(3)+s(20)*s(9)*s(25)*s(3);
gamma=port*((s(20)*s(3))-(s(9)*s(25)))/j;
% s20=mal-im, s3=cit-m, s9=mal-m, s25=cit-im

% malate phosphate exchanger
k=1+s(20)+s(9)+s(39)+s(38)+s(20)*s(9)+s(20)*s(39)+s(20)*s(38)+s(9)*s(3
9)+s(9)*s(38)+s(39)*s(38)+s(20)*s(9)*s(39)+s(20)*s(9)*s(38)+s(20)*s(39
)*s(38)+s(9)*s(39)*s(38)+s(20)*s(9)*s(39)*s(38);
delta=port*((s(9)*s(39))-(s(20)*s(38)))/k;
% s20=mal-im, s38=phos-m, s9=mal-m, s39=phos-im

%alpha=beta=gamma=delta=0;
flux = 0.02*(s(31)-s(33));
% rate equations
ds(1) = -LHS1+LHS8-RHS8+LHS12-LHS14+RHS14;
ds(2) = -LHS1+LHS15;
ds(3) =  LHS1-LHS2-gamma;
ds(4) =  LHS2-LHS3;
ds(5) =  LHS3-LHS4+LHS14-RHS14-beta;
ds(6) =  LHS4-LHS5;
ds(7) =  LHS5-LHS6;
ds(8) =  LHS6-LHS7;
ds(9) =  LHS7-LHS8+RHS8+beta+gamma-delta;
ds(10)=  LHS1-LHS4+LHS5-LHS15;
ds(11)=0;
%ds(11)= -LHS3-LHS4-LHS8+RHS8-LHS15;
```

```
ds(12)=0;
%ds(12)=  LHS3+LHS4+LHS8-RHS8+LHS15;
ds(13)=0;
%ds(13)=  LHS4-LHS12+LHS15;
ds(14)= 0;
%ds(14)= -LHS5;
ds(15)= 0;
%ds(15)=  LHS5;
ds(16) = 0;
%ds(16)= -LHS6;
ds(17) = 0;
%ds(17)= LHS6;
ds(18)=0;
%ds(18)= -LHS12;
ds(19)= -LHS13+RHS13+alpha;
ds(20)=  LHS10-RHS10-LHS11-beta-gamma+delta;
ds(21)= -LHS13+RHS13+beta;
ds(22)=  LHS13-RHS13-alpha;
ds(23)= -LHS14+RHS14+alpha;
ds(24)=  LHS14-RHS14-alpha;
ds(25)= -LHS9+gamma;
ds(26)= 0;
%ds(26)= -LHS9;
ds(27)= 0;
%ds(27)= -LHS9;
ds(28)= 0;
%ds(28)= LHS9;
ds(29)=0;
%ds(29)= LHS9;
ds(30)= 0;
%ds(30)= -LHS11;
ds(31)=  LHS11-flux;
ds(32)= 0;
%ds(32)=  LHS11;
ds(33)= -LHS12-LHS15+flux;
ds(34)=  LHS9-LHS10+RHS10+LHS13-RHS13;
ds(35)= -LHS10+RHS10;
ds(36)=  LHS10-RHS10;
ds(37)=0;
%ds(37)=  LHS12;
ds(38)= -LHS5+LHS12+delta;
ds(39)=  LHS9-delta;
return
end
% use lsode to solve this set...
lsode_options("relative tolerance",1e-7);
lsode_options("absolute tolerance",1e-6);
t=0:1:900;

% supply the initial concentrations ...
s0=s;
```

```
[s,T,MSG]=lsode(@shukr,s0,t);
T
MSG

plot(t,s(:,4),"linewidth",5,t,s(:,5),"linewidth",5,t,s(:,9),"linewidth
",5,t,s(:,23),"linewidth",5,t,s(:,24),"linewidth",5,t,s(:,33),"linewid
th",5,t,s(:,31),"linewidth",5);
grid on;
set (gca,'FontSize', 20);
set (gca, 'FontName', 'Times');
axis([000,500,.001,1.01]);
% title ("Krebs cycle and shuttle");
xlabel ("Time/arbitrary units");
ylabel ("Concentration/arbitrary units");
set (gca,'FontSize', 20);
set( get(gcf,'children'), 'linewidth',4 );
legend("Isocit-m","Keglu-m","Mal-m","Glu-m","Asp-m","Pyr-m","Pyr-im",
"location", "east");
```

Result

Simulation of a combined system of Krebs cycle in conjunction with the shuttles provides insight to the carbon skeleton shuffling across the mitochondrial membrane and ATP synthesis using reducing equivalents from within mitochondria and from cytoplasm.

Fig. 3.11 shows the simulation result of the shuttles along with the Krebs cycle. Most of the metabolites attain a steady-state around 200 time points. The initial parts of the graph indicate random initial concentrations provided in the script to execute the program, however as the time passes, the metabolites tend to approach a steady-state. The initial state resembles a condition where a system existing in steady-state experiences a perturbation due to change in concentration of one or more metabolites, and it tries to restore a steady-state.

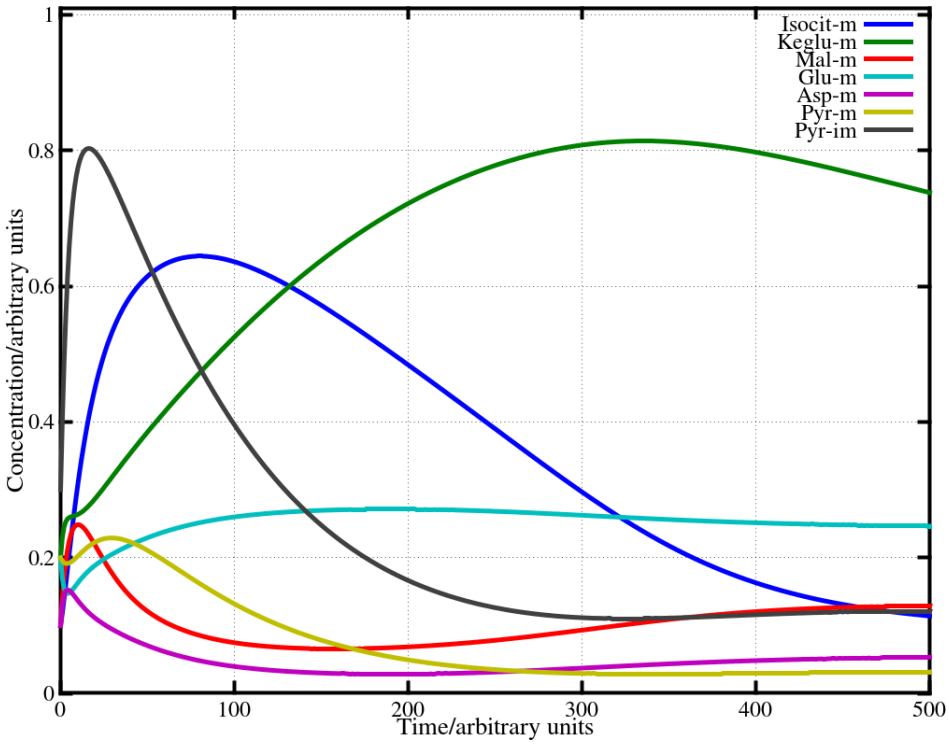

Figure 3.11: Simulation curves for selected components of Krebs cycle-shuttle system. Isocit = Isocitrate, Keglu = α-ketoglutarate, Mal = malate, Glu = glutamate, Asp = aspartate, Pyr = pyruvate. Suffix '-m' and '-im' indicate that the presence of component in the matrix and intermembrane space respectively.

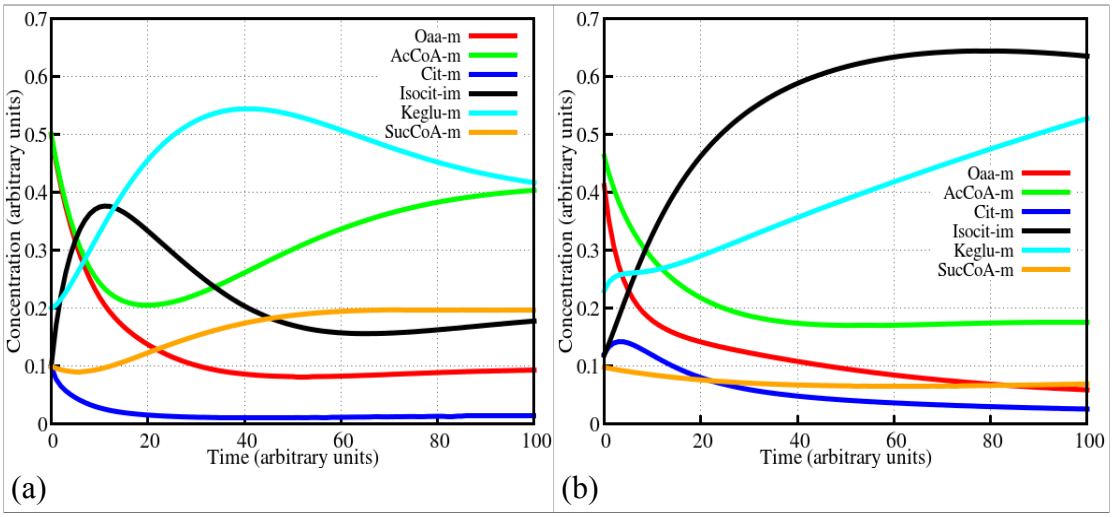

Figure 3.12: Simulation curves for (a) Krebs cycle alone (b) Krebs cycle + malate-aspartate and citrate-pyruvate shuttles. [Oaa = oxaloacetate, AcCoA = acetyl-CoA, Cit = citrate, Isocit = isocitrate, Keglu = α-ketoglutarate, SucCoA = succinyl-coA].

An important aspect, that can be illustrated using this simulation, can be achieved by having a comparative analysis of various systems. One such comparison is illustrated in the set of graphs in Fig. 3.12. Fig. 3.12a shows few key components of Krebs cycle, when only Krebs cycle was simulated. Fig. 3.12b displays the behaviour of the same components, when Krebs cycle was simulated along with malate-aspartate and citrate-pyruvate shuttle. It can be seen that same components behave differently in different environments. An important observation from these figures was the steady-state behaviour of the same components in two different environments when similar initial conditions were provided. The metabolites tend to attain steady-state in both the systems, but the time taken to reach a steady-state concentration for the metabolites is comparatively less in case of the combined system (Fig. 3.12b). This essentially suggests that with a larger network among the metabolites assists them in attaining steady-state earlier. A larger network also ensures multiple paths to reach the destination, thus providing the system with branching alternatives. This creates multiple paths and several sources and sinks for a given metabolite, which helps it to reach its steady-state earlier after a perturbation. It can be proposed that the rate of attainment of steady-state is related qualitatively to the respective number of paths available for a given metabolite to reach its destination. In other words, a larger network among a given set of metabolites imparts robustness to the system. It also suggests that metabolic pathways tend to exist at a steady-state rather than in a state of equilibrium. This steady-state, however is not accurately defined as a point rather is more likely to exist as a region or basin where the metabolites are in steady-state over a small range of concentration.

In Chapter 2, it was suggested that Krebs cycle works like a giant catalyst. However, when combined with shuttles, Krebs cycle no more acts as a giant catalyst as the intermediate components of the system can now be involved in more than one reaction at the same time. So Krebs cycle can now be considered as a source for metabolites as citrate, malate, α-ketoglutarate, oxaloacetate, etc., to facilitate several anaplerotic reactions inside the cell. Also, this represents an elegant relation among these systems, which are regulated internally based on the cellular requirements at a given time. The common metabolites act as a branch point where a decision can be made regarding which path should be followed by the given metabolite, keeping view the cellular environment and requirements.

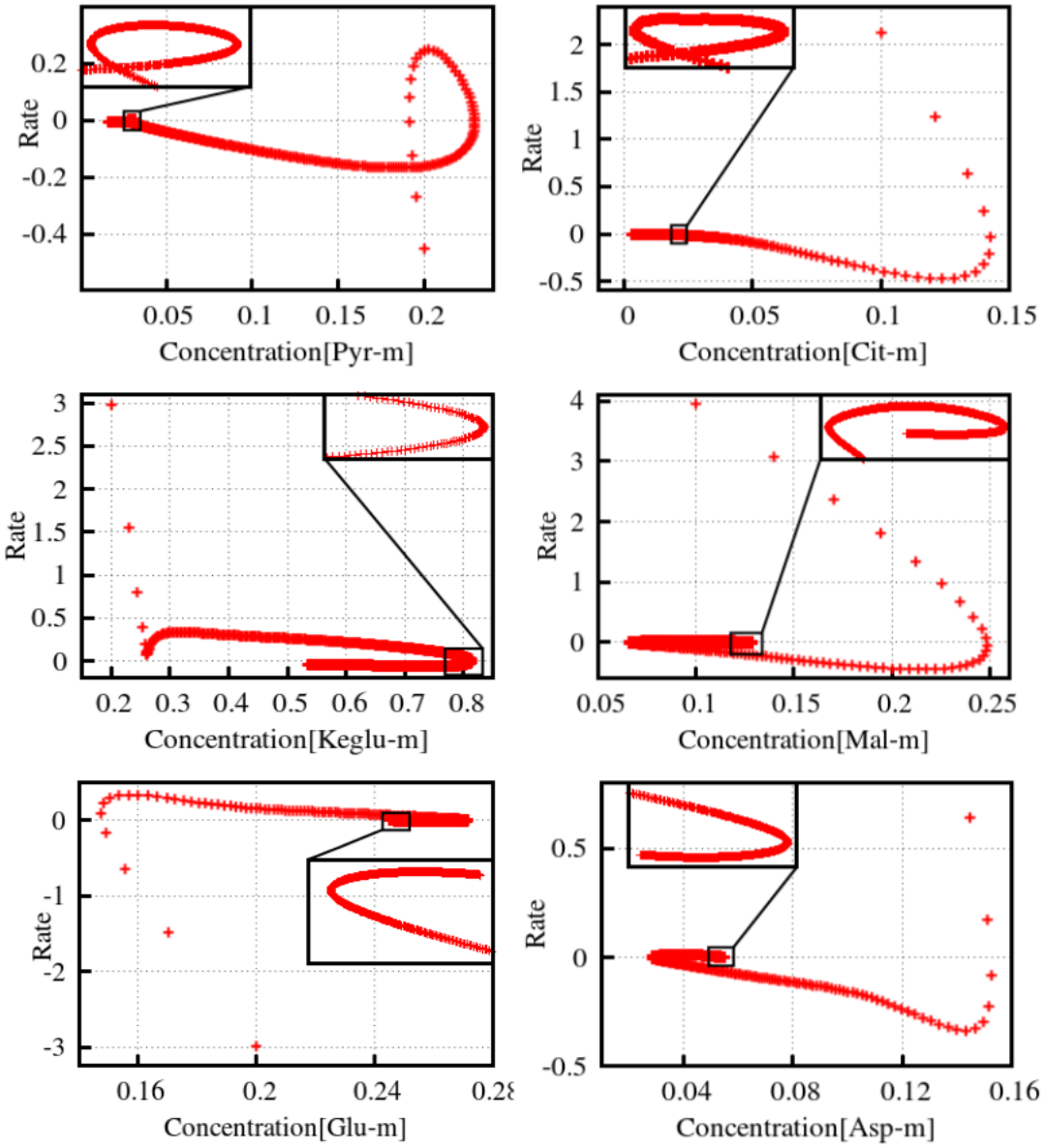

Figure 3.13: Phase diagram for selected important metabolites present in the mitochondrial matrix. [Pyr = Pyruvate, Mal = Malate, Keglu = α-ketoglutarate, Cit = Citrate, Glu = Glutamate, Asp = Aspartate]. Inset figure shows the magnified view of the selected region. The y-axis represents the rate of transformation of the corresponding substrate as indicated on the abscissa. The concentrations and time are expressed in arbitrary units.

Fig. 3.13 shows phase curves for selected metabolites from the mitochondrial matrix. Here the rates of change in concentrations of the given metabolites are plotted against their respective concentration. The curves start from the initial concentration of the respective metabolites and include 900 data points. It can be seen that the majority of them tend to cluster towards the end. The region close to the end was expanded to portray a closer perspective.

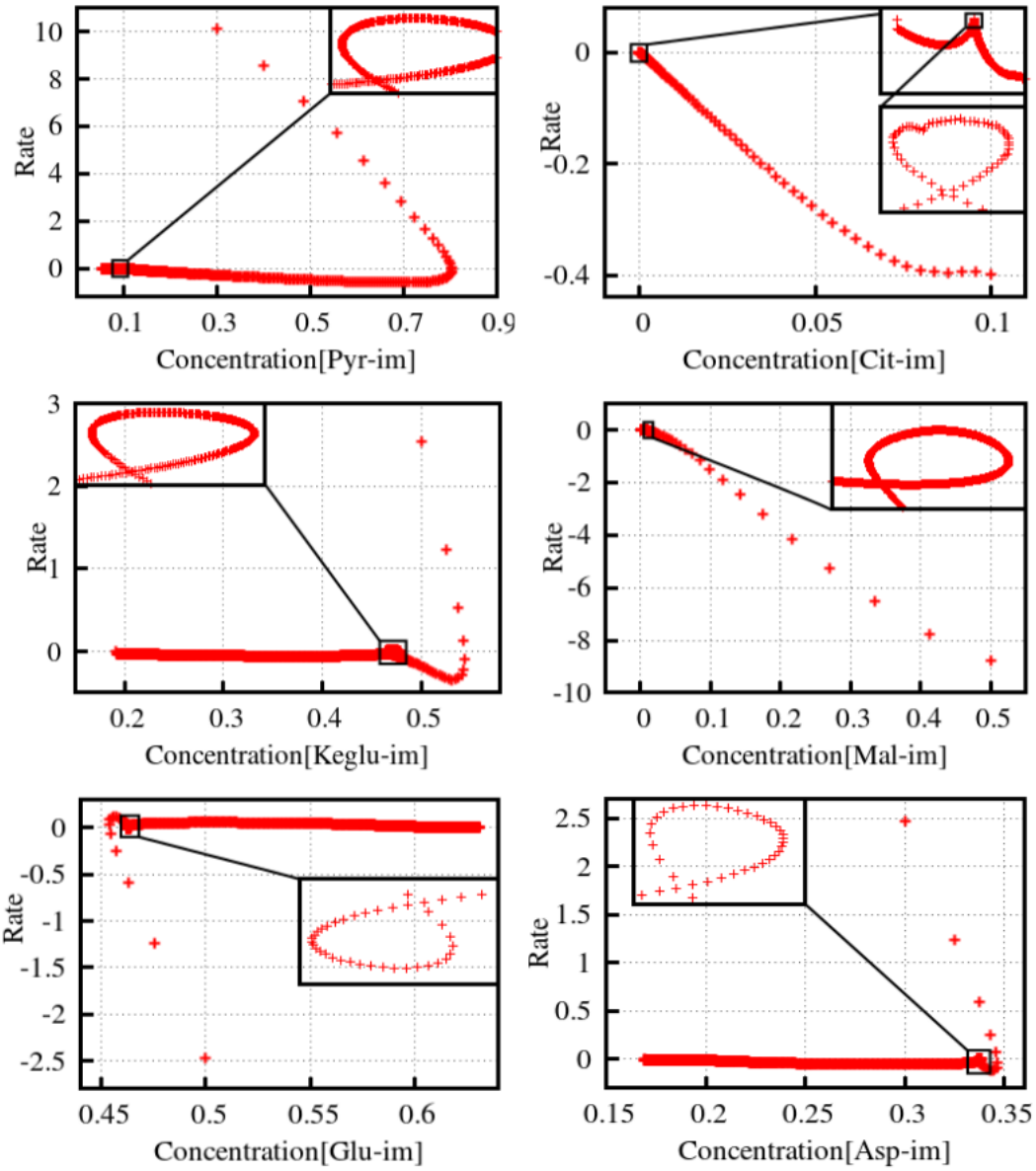

Figure 3.14: Phase diagram for selected important metabolites present in the intermembrane space. [Pyr = Pyruvate, Mal = Malate, Keglu = α-ketoglutarate, Cit = Citrate, Glu = Glutamate, Asp = Aspartate]. Inset figure shows the magnified view of the selected region. The y-axis represents the rate of transformation of the corresponding substrate as indicated on the abscissa. The concentrations and time are expressed in arbitrary units.

The inset graphs show the twisted paths taken by the metabolite near the steady-state region. The loops seen in the inset figures proposes that the steady-state is not a point, but a region spanning multiple sets of concentrations of various metabolites involved. It indicates that the concentrations localise in a small region with very slight changes in concentrations as it approaches nearer to the steady-state.

Fig. 3.14 shows phase curves for selected metabolites from the intermembrane space. A system in steady-state when perturbed by change in the concentration of at least one of the metabolites will tend to restore its steady-state. The return to steady-state follows a path similar to those shown in these phase curves. The return to steady-state is not monotonic, rather follows a curved trajectory, with the variations in concentrations decreasing at each time point, as it approaches nearer to the steady-state.

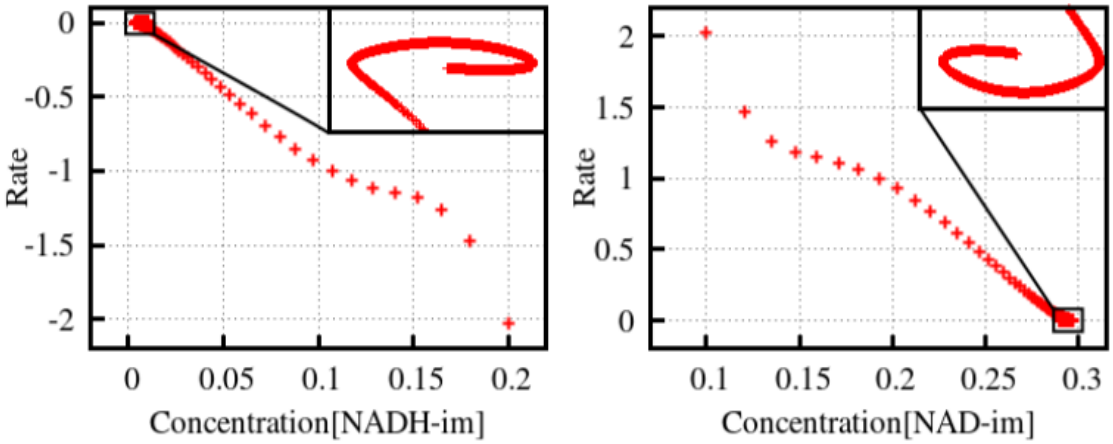

Figure 3.15: Phase diagram for NADH-im and NAD^+-im. The curves are complementary since they are inter-convertible species. Inset figure shows the magnified view of the selected region. The y-axis represents the rate of transformation of the corresponding substrate as indicated on the abscissa. The concentrations and time are expressed in arbitrary units.

Fig. 3.15 shows the phase curves for NADH and NAD^+ from the IM space. The total concentration of two species combined will always be same, which is evident even from their complementary phase curves. The curve starts at the initial concentration point, i.e. NADH-im at 0.2 and for NAD^+-im at 0.1. They approach the steady-state region within 20 time points and towards the end all the data points tend to cluster in the same region.

Comparison with experimental data

The results obtained from the simulation model of Krebs cycle with the two shuttles was compared with the experimental results reported by Bennett *et al.* (2009). The absolute metabolite concentrations of several metabolites present in *E.coli* were reported by the authors. These concentrations were compared with the concentrations of the selected metabolites present in the intermembrane space obtained by using the simulation model. Near steady-state concentrations were used for comparison and, therefore, the concentrations at 500 time point were taken.

However, the concentrations obtained by the simulation scheme are reduced by a factor of their respective K_M values, therefore to obtain absolute concentrations, the concentrations from the simulation results were multiplied by their K_M values.

Table 3.14: List of metabolites, enzymes and metabolite concentrations under the experimental and simulated conditions (calculated using corresponding K_M for the reactions).

Metabolite	Enzyme	Experimental concentration (Moles/L)	K_M (Moles/L)	Simulated concentration	K_M*Simulated concentration (Moles/L)
Aspartate	Aspartate transaminase	4.2e-03	2.22e-03	1.94e-01	0.434e-03
Citrate	Citrate lyase	2.0e-03	1.60e-04	2.56e-05	4.096e-09
Glutamate	Aspartate transaminase	9.6e-02	1.50e-02	6.06e-01	0.909e-02
α-Ketoglutarate	Aspartate transaminase	4.4e-04	2.47e-04	3.78e-01	0.934e-04
Malate	Malate dehydrogenase	1.7e-03	2.60e-03	5.26e-03	0.0137e-03
NAD^+	Malate dehydrogenase	2.6e-03	2.60e-04	2.9e-01	0.0754e-03
NADH	Malate dehydrogenase	8.3e-05	6.10e-05	9.98e-03	0.0609e-05
$NADH/NAD^+$	-------	8.3e-05/2.6e-03			0.0609e-05/0.0754e-03

Table 3.14 contains the list of metabolites, respective enzymes, absolute metabolite concentration obtained from the experiments and simulation. The experimental and simulated concentrations are plotted as a histogram for visual comparison (Fig. 3.16).

It is seen that the concentrations obtained from the simulation result are lower the corresponding experimental values. The concentrations of all the metabolites except malate and citrate vary within a factor of 10, which appears to be a good match. The anomaly seen for malate and citrate can be due to the presence of other sources and sink outside mitochondria which are not included in the simulation scheme. The results presented in Fig. 3.16 indicate applicability of the simulation scheme. The differences in the concentration sets of NADH and NAD^+ are quite similar, and therefore, their ratios seem to be closely related for the two concentration sets. Also, it is the ratio ($NADH/NAD^+$) which is considered as an important parameter for regulation and the difference in the ratio in the two sets is smaller than the differences between the individual components (NADH, NAD^+).

The experimental data has been obtained from *E.coli* that lacks mitochondria, which can further explain the variability seen in the results. The outcome of the comparison is particularly encouraging, keeping in view the fact that minimal assumptions were made in the simulation model and yet the results show fair agreement with the experimental data.

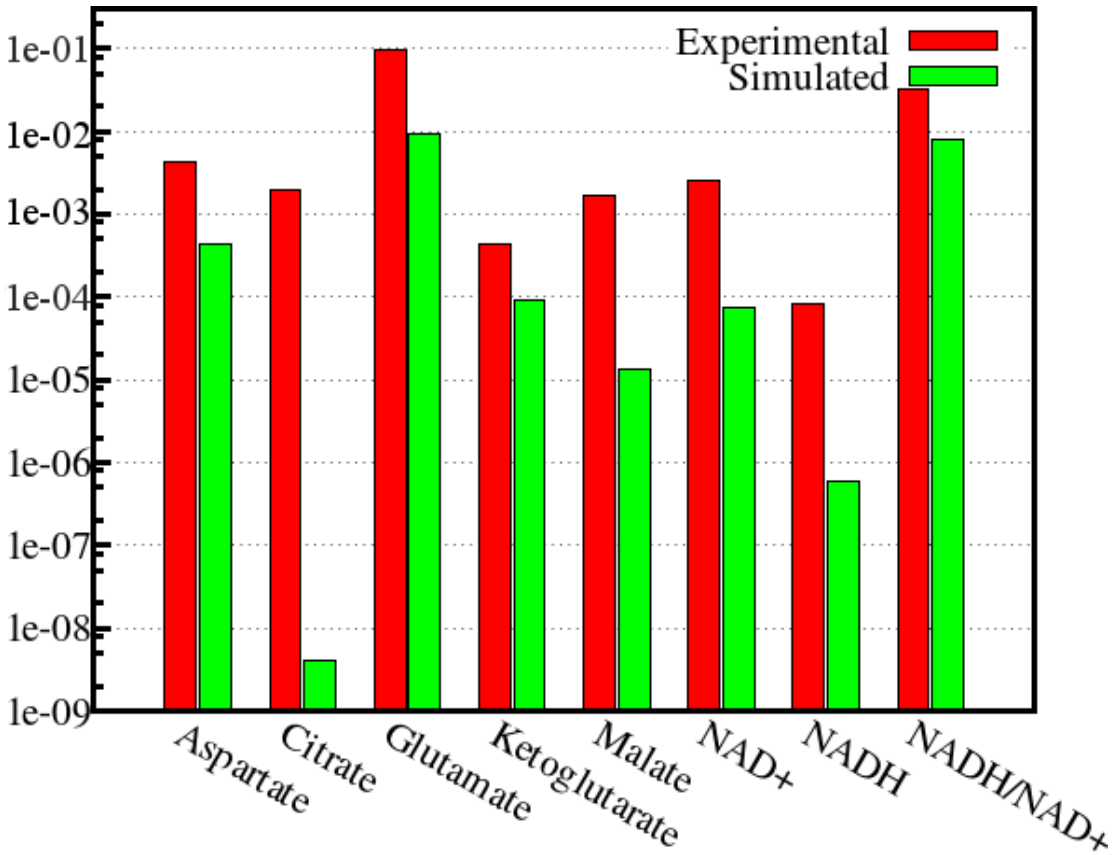

Figure 3.16: Comparative analysis of experimental and simulated metabolite concentrations. The experimental data was taken from Bennett *et al*. (2009).

References

Barron, J. T., Gu, L., & Parrillo, J. E. (1998). Malate-aspartate shuttle, cytoplasmic NADH redox potential, and energetics in vascular smooth muscle. *Journal of molecular and cellular cardiology*, *30*(8), 1571-1579.

Bennett, B. D., Kimball, E. H., Gao, M., Osterhout, R., Van Dien, S. J., & Rabinowitz, J. D. (2009). Absolute metabolite concentrations and implied enzyme active site occupancy in *Escherichia coli*. *Nature chemical biology*, *5*(8), 593-599.

Brand, M. D., & Chappell, J. B. (1974). Glutamate and aspartate transport in rat brain mitochondria. *Biochem. J*, *140*, 205-210.

Dawson AG. (1979) Oxidation of cytosolic NADH formed during aerobic metabolism in mammalian cells. Trends Biochem Sci 4(8): 171-176.

Enkavi, G., Li, J., Mahinthichaichan, P., Wen, P. C., Huang, Z., Shaikh, S. A., & Tajkhorshid, E. (2013). Simulation studies of the mechanism of membrane transporters. In *Biomolecular Simulations* (pp. 361-405). Humana Press.

Forrest, L. R., Krämer, R., & Ziegler, C. (2011). The structural basis of secondary active transport mechanisms. *Biochimica et Biophysica Acta (BBA)-Bioenergetics*, *1807*(2), 167-188.

Geck, P., & Heinz, E. (1976). Coupling in secondary transport effect of electrical potentials on the kinetics of ion linked co-transport. *Biochimica et Biophysica Acta (BBA)-Biomembranes*, *443*(1), 49-63.

GNU Octave: http://www.gnu.org/software/octave/

Halestrap, A. P. (1975). The mitochondrial pyruvate carrier. Kinetics and specificity for substrates and inhibitors. *Biochem. J*, *148*, 85-96.

Heinz, E., Geck, P., & Wilbrandt, W. (1972). Coupling in secondary active transport: Activation of transport by co-transport and/or counter-transport with the fluxes of other solutes. *Biochimica et Biophysica Acta (BBA)-Biomembranes*, *255*(2), 442-461.

Jardetzky, O. (1966). Simple allosteric model for membrane pumps. *Nature, 211*, 969–970.

Krupka, R. M. (1993). Coupling mechanisms in active transport. *Biochimica et*

Biophysica Acta (BBA)-Bioenergetics, *1183*(1), 105-113.

Lu, M., Zhou, L., Stanley, W. C., Cabrera, M. E., Saidel, G. M., & Yu, X. (2008). Role of the malate–aspartate shuttle on the metabolic response to myocardial ischemia. *Journal of theoretical biology*, *254*(2), 466-475.

Melkikh, A. V., & Seleznev, V. D. (2012). Mechanisms and models of the active transport of ions and the transformation of energy in intracellular compartments. *Progress in Biophysics and Molecular Biology*, *109*(1), 33-57.

Michaelis, L., & Menten, M. L. (1913). Die kinetik der invertinwirkung. *Biochem. Z*, *49*(333-369), 352.

Monod, J., Wyman, J., & Changeux, J. P. (1965). On the nature of allosteric transitions: a plausible model. *Journal of molecular biology*, *12*(1), 88-118.

Nelson DL, Cox MM, Freeman (ed.). (2004) Lehninger Principles of Biochemistry, Fourth Edition.

Purvis, J. L., & Lowenstein, J. M. (1961). The relation between intra-and extramitochondrial pyridine nucleotides. *Journal of Biological Chemistry*, *236*(10), 2794-2803.

Sanders, D., Hansen, U. P., Gradmann, D., & Slayman, C. L. (1983). Generalized kinetic analysis of ion-driven cotransport systems: A unified interpretation of selective ionic effects on Michaelis parameters. *The Journal of membrane biology*, *77*(2), 123-152.

Stein, W. (1986). *Transport and diffusion across cell membranes*.

Williamson, J. R., Safer, B. R. I. A. N., LaNOUE, K. F., Smith, C. M., & Walajtys, E. (1973). Mitochondrial-cytosolic interactions in cardiac tissue: role of the malate-aspartate cycle in the removal of glycolytic NADH from the cytosol. In *Symposia of the Society for Experimental Biology* (Vol. 27, p. 241).

Wu, F., Yang, F., Vinnakota, K. C., & Beard, D. A. (2007). Computer modeling of mitochondrial tricarboxylic acid cycle, oxidative phosphorylation, metabolite transport, and electrophysiology. *Journal of Biological Chemistry*, *282*(34), 24525-24537.

Yugi, K., & Tomita, M. (2004). A general computational model of mitochondrial metabolism in a whole organelle scale. *Bioinformatics*, *20*(11), 1795-1796.

Chapter 4 Reactive Oxygen Species

Reactive Oxygen Species

Mitochondrion is the major site of ROS generation in the cell. Oxygen is the terminal electron acceptor and is subject to reduction by incoming electrons, one electron at a time. Oxygen is reduced at complex IV, which ensures its full reduction to form water. However, electrons may leak from other redox centres (as complexes I and III) inside mitochondria leading to a partial reduction of oxygen to form superoxide anion ($O_2^{\bullet -}$). Oxygen molecule is a biradical but is relatively chemically inert and can be reduced only by strong electron donors as complex I (Korshunov & Imlay, 2006). Most of the ROS are generated when oxygen is reduced.

Mitochondria are the source of almost 90% of the ROS generated inside the cell (Balaban, Nemoto, & Finkel, 2005). Other cellular sources of ROS include NADPH oxidases, lipid metabolism within peroxisomes, activity of cytosolic enzymes as cyclooxygenases, etc. However, the major contributors to mitochondrial ROS are complexes I and III of the electron transport chain (ETC). There are other sources connected to mitochondria, which include several enzymes. A list of enzymes is given in Table 4.1.

Table 4.1: List of sources of ROS.

Source	Localisation	Mechanism	Reference
Cytochrome b5 reductase	Outer mitochondrial membrane	Oxidises cytoplasmic NADPH and reduces cytochrome b5 in the outer membrane. Can produce superoxide with a high rate of 300nmol/min/mg protein	Whatley *et al*., 1998
Monoamine oxidase	Outer mitochondrial membrane	Oxidation of biogenic amines accompanied by release of H_2O_2, which may exceed other mitochondrial sources	Simonson *et al*., 1993
Dihydroorotate dehydrogenase	Outer surface of inner mitochondrial membrane	Conversion of dihydroorotate to orotate. *In vitro* produces H_2O_2 in absence of natural electron acceptor, Q.	Löffler, Becker, Wegerle & Schuster, 1996
α-glycerophosphate dehydrogenase	Outer surface of inner mitochondrial membrane	Oxidation of G-3-P to DHAP. In drosophila, H_2O_2 produced by this enzyme, of which 30% was at complex I due to RET	Miwa, St-Pierre, Patridge & Brand, 2003
Aconitase	Mitochondrial matrix	Catalyses citrate to isocitrate conversion. It is inactivated by superoxide, induces production of hydroxyl radical.	Vasquez-Vivar, Kalyanaraman & Kennedy, 2000
α-ketoglutarate	Matrix side of	Oxidation of α-ketoglutarate to succinyl-	Tretter & Adam-

dehydrogenase	inner mitochondrial membrane	CoA. Dihydrolipoamide dehydrogenase (dld), a component of this enzyme complex is responsible for ROS generation. Stimulated by low availability of its natural electron acceptor, NAD^+	Vizi, 2004, Starkov *et al.*, 2004
Complex I and Complex III	spans inner mitochondrial membrane		

Complexes I and III are the primary sources of ROS inside mitochondria and are, therefore, explicitly considered in the present simulation.

Superoxide, peroxide and hydroxyl radical are the most widely occurring ROS. They are generated when oxygen is reduced:

$$O_2 + e^- \rightarrow O_2^{\bullet -} \text{ (superoxide)}$$
$$O_2^{\bullet -} + e^- \rightarrow O_2^{2-} \text{ (peroxide)}$$
$$O_2^{2-} + 2H^+ \rightarrow 2HO^{\bullet} \text{ (hydroxyl radical)}$$
$$HO^{\bullet} + e^- + H^+ \rightarrow H_2O \text{ (not a ROS)}$$

ROS generation by Complex I

The matrix $NADH/NAD^+$ ratio (the reduction potential) and the protonmotive force (contributed by pH gradient and electrical potential) across the inner mitochondrial membrane are considered as the main factors that determine ROS generation by complex I (Andreyev, Kushnareva & Starkov, 2005).

In complex I, NADH is oxidised to NAD^+ and the electrons are used to reduce quinone to quinol. The electrons from NADH are first transferred to flavin mononucleotide (FMN) and then transferred to quinone via a series of Fe-S clusters. In the current reaction scheme, the transfer from NADH to quinone is mediated by complex I. Complex I includes FMN, Fe-S clusters, etc. as redox centres. It acquires two electrons from NADH and these electrons are transferred one at a time to quinone. In this process, when the electrons are localised in complex I, it is termed as $C_{1(red)\backslash}$. The transfer of one electron to quinone leads to the formation of semiubiquinone, and complex I with one electron and is denoted as $C_{1(semi)}$. After the transfer of the second electron from $C_{1(semi)}$, it is denoted as $C_{1(ox)}$ in the present simulation scheme. The related reactions are shown in Table 4.3. The semiubiquinone formed in this process is highly reactive and may transfer its electron to oxygen, giving rise to superoxide ion.

ROS generation by Complex III

Complex III catalyses the transfer of electrons from ubiquinol to cytochrome c. Cytochrome c can carry only one electron at a time, so the electrons from one molecule of ubiquinol is transferred to two molecules of cytochrome c. After transfer of one electron to cytochrome c, ubiquinol is converted to transient semiubiquinone, which then transfers the second electron to another cytochrome c molecule, leading to regeneration of ubiquinone. This process is called as the **Q-cycle** (Chance & Hollunger, 1961). Here, the transient formation of semiubiquinone radical, may lead to the formation of superoxide as discussed in the previous section.

Reverse electron transfer (RET)

ROS may be generated in a mitochondrion powered by succinate by a mechanism known as reverse electron transfer (Adam-Vizi & Chinopoulos, 2006). This is exclusively mediated by complex I (Rigoulet, Yoboue & Devin, 2011). In a situation where ATP/ADP ratio is high, membrane potential across the inner mitochondrial membrane is high, along with a high redox potential. In such a case, the energy from pmf is used to reduce NAD^+ or $NADP^+$ by driving electrons in reverse direction via complex I. Here due to high pmf across the inner mitochondrial membrane, a weak reducing agent as succinate acts as the electron donor. The mechanism behind ROS generation associated with RET is not entirely understood. Fully reduced FMN, iron–sulphur centers and semiubiquinone formed at the complex I as a result of RET may be the possible sites for ROS generation (Schönfeld, Więckowski, Lebiedzińska & Wojtczak, 2010).

RET is inhibited by energy requiring processes as RET can take place only at in energy-rich environment. This process is included in the simulation by considering reactions via complexes I and III as reversible (shown in reactions 1-5 in Table 4.3).

ROS-induced ROS release

ROS can cause damage to membrane lipids, which may lead to increased permeability of the mitochondrial membrane. Despite the presence of several scavenging and repair mechanisms inside mitochondria to combat ROS, the damage once caused cannot be repaired effectively. Mitochondrial membrane being in the

vicinity of the site of ROS generation (enzymes of electron transport chain, complexes I and III, reside in mitochondrial membrane) are prone to maximum damage caused due to ROS.

The damage once caused to membrane cannot be eliminated by removing the ROS from the site, rather, these damages tend to accumulate over time. Over a period of time, this may lead to opening of one of the selective channels thus leading to a drop in membrane potential. This will result in the release of ROS into the cytosol, which will aggravate ROS generation from neighbouring mitochondria. These ROS are generated as a consequence of the already present ROS, and this is called as ROS-induced ROS release (RIRR).

RIRR acts as a measure of cell's health and in extreme cases may lead to programmed mitochondrial destruction and apoptosis (Zorov, Juhaszova & Sollott, 2006). However, these are not the primary sources of ROS generation and can be considered as the after effects of ROS generation, and are, therefore, not included in the present simulation.

Superoxide

Superoxides are primarily formed in both complexes I and III. 2-5 % of total cellular oxygen is used for superoxide generation (Rigoulet, Yoboue & Devin, 2011). 70-80% of these superoxides are formed during Q-cycle operation in complex III (Chance & Hollunger, 1961). It cannot cross inner mitochondrial membrane in its anionic form as it is too strongly charged. All the superoxide generated from complex I are released in the mitochondrial matrix, and no traces are detected in the cytosolic side of an intact mitochondrion (Muller, Liu, & Van Remmen, 2004). Contrary to the anionic form, the protonated form of superoxide, hydroperoxyl radical, is uncharged and can readily cross the mitochondrial membrane. Studies report that in a typical cell, 0.3% of superoxide exists in its protonated form (de Grey, 2002). However, this protonated form may cross the membrane and on deprotonation can turn reactive, leading to damage in the cytosolic side.

Superoxides are also found to activate uncouplers. Also, mild uncoupling leads to a reduced ROS generation from mitochondria, thus suggesting a feedback mechanism, where ROS interact with uncouplers leading to their activation, which in turn would decrease ROS generation in mitochondria. This presents a protective mechanism by decreasing ROS production (Brand *et al*., 2004).

Peroxide

Superoxides are removed by the action of superoxide dismutase, leading to the formation of peroxide, commonly found as hydrogen peroxide, an electrically neutral dismutation product.

Damage caused by ROS

ROS mostly cause damage to lipids, proteins and DNA. Lipids react with hydroxyl radical to form lipid radical, which can further react with oxygen to form lipid peroxyl radical. This lipid peroxyl radical may disintegrate to give small molecules as malondialdehyde and 4-hydroxynonenal (MDA, 4-HNE), etc. (Schaur, 2003). These small molecules (4-HNE) may further initiate protein carbonylation (of proteins with side chains of lysine, histidine and cysteine residues) through Michael addition reactions (Petersen & Doorn, 2004; Grimsrud, Xie, Griffin & Bernlohr, 2008).

Lipid peroxidation: $HO^{\bullet} + L\ (lipid) \rightarrow L^{\bullet} + H_2O$

$L^{\bullet} + O_2 \rightarrow LOO^{\bullet}$

$LOO^{\bullet} \rightarrow MDA + 4\text{-}HNE$

Alternatively, ROS can lead to inactivation of a functional protein by direct protein carbonylation and amino acid oxidation. Site specific damage caused to some susceptible amino acids of protein has been considered as the prime cause of metabolic dysfunction during cellular pathology (Bandyopadhyay, Das & Banerjee, 1999). ROS can interact with nucleic acids resulting in permanent or transient damage (Hemnani & Parihar, 1998; Seifried, Anderson, Fisher & Milner, 2007). This aspect has not been included in the present study.

An imbalance between ROS generation and defence mechanisms in the cell leads to oxidative damage, ultimately resulting in pathological conditions.

mtDNA vs nuclear DNA

The damage caused to proteins and lipid can be rectified or they can be regenerated. On the other hand, the damage caused to DNA may lead to mutation which can be inherited and may become permanent (Bohr & Dianov, 1999). mtDNA is small and exposed, and therefore is comparatively at a higher risk than nuclear DNA in acquiring oxidative damage. They also lack an efficient repair system and are critically prone to damage by ROS (Yakes & Van Houten, 1997). This damage is more profound and last longer than nuclear DNA damage, and therefore mtDNA is

said to accumulate more oxidative DNA damage. Research shows that mtDNA contains a higher steady-state amount of oxidative DNA damage than nuclear DNA, due to their proximity to ROS sources. Due to relatively high oxidative damage in mitochondria, the existence of efficient DNA repair mechanisms to eliminate DNA damage caused by ROS is must. Oxidative DNA lesions tend to accumulate with age; however it has been seen that their accumulation is higher in mitochondrial DNA when compared to nuclear DNA (Richter, 1995).

Defence against ROS

The formation of ROS resulting from routine metabolic process demands efficient defence mechanism against ROS. A set of enzymes and scavenging molecules are used against ROS in the cell. These are specialised for their actions in specified locations in the cell as the mitochondrial matrix, mitochondrial membrane, intermembrane space, cytoplasm, etc. The enzymes and scavenging molecules pertaining to mitochondria are given in Table 4.2. The reactions involving superoxide dismutase, glutathione (Glutathione-S-transferase, glutathione peroxidase, glutathione reductase) and catalase have been included in the present simulation study. The reactions are given in Table 4.3 (Reactions 7-9).

Table 4.2: List of defence mechanisms against ROS in mitochondria.

Scavenger	Location	Mechanism	Reference
α-tocopherol	Lipid soluble free radical scavenger in mitochondrial membrane	Reduces lipid radicals and can be regenerated by reduced quinone	Packer, Weber & Rimbach, 2001
Phospholipid hydroperoxide glutathione peroxidase	Mitochondrial membrane of kidney, intestine, cortex and testes	Reduce peroxidised phospholipids within membranes	Imai & Nakagawa, 2003; Knopp, Arndt, Eng, Caldwell, LeBoeuf, Deeb & O'Brien, 1999; Pushpa-Rekha, Burdsall, Oleksa, Chisolm & Driscoll, 1995
Manganese superoxide dismutase (MnSOD)	Mitochondrial matrix	Dismutation of superoxide radical to H_2O_2	
Cytochrome c	IM space	Superoxide removal	McCord & Fridovich, 1970
Catalase	Mitochondrial matrix	Converts H_2O_2 to oxygen and water.	Ho, Xiong, Ma, Spector & Ho, 2004
Glutathione	~10-12% of the total cell's GSH is present in matrix	Antioxidant with -SH of cysteine as the active group	Pastore, Federici, Bertini & Piemonte, 2003; Dringen, 2000

Glutathione-S-transferase	Mitochondrial matrix-several isoforms	Catalyses the conjugation reaction of GSH with several toxins (as 4-HNE)	Singh, Coronella, Beneš, Cochrane & Zimniak, 2001, Singhal, Zimniak, Awasthi, Piper, He, Teng, *et al*., 1994
Glutathione reductase	Mitochondrial matrix	Reduction of GSSG to GSH	
Glutathione peroxidase	Mitochondrial matrix	Utilises GSH for the reduction of H_2O_2 to H_2O	
Peroxiredoxin (Prx3 and Prx5)		Reduce H_2O_2 and lipid peroxidases	Fujii & Ikeda, 2002; Wood, Schröder, Robin Harris & Poole, 2003

Functions of ROS

Besides causing damage lipids, proteins and DNA, ROS have been attributed to several cellular functions. They have been established as intracellular signalling molecules (Holmström & Finkel, 2014). They have been shown to activate transcription factors. Cell culture studies have demonstrated a significant role of ROS in regulation of cellular processes as proliferation, differentiation, death and migration. Also, ROS is involved in regulation of developmental processes as spermatogenesis and oogenesis, morphogenesis, angiogenesis and cell migration (Covarrubias, Hernández-García, Schnabel, Salas-Vidal & Castro-Obregón, 2008)

Simulation

Simulation is carried out for ROS generation and scavenging in close association with the ETC. A major part of ROS are generated by complexes I and III of the ETC and are, therefore, included in the present simulation. The corresponding reactions are shown in Table 4.3. A number of scavenging measures used by mitochondria are already listed in the text. The major scavenging mechanisms include glutathione, superoxide dismutase and catalase activity. They have been appropriately represented in the simulation presented. All the reactions used for simulation are listed in Table 4.3, and the scope of simulation is restricted to generation and scavenging of ROS through these reactions.

Table 4.3: List of reactions used for simulation of ROS along with reactions of electron transport chain.

1.	$NADH + C_{1(ox)} \rightarrow NAD^+ + C_{1(red)}$	Complex I reaction
2.	$Q + C_{1(red)} \rightarrow HQ^{\bullet} + C_{1(semi)}$	Complex I reaction
3.	$HQ^{\bullet} + C_{1(semi)} \rightarrow QH_2 + C_{1(ox)}$	Complex I reaction

4.	$QH_2 + cytc_{(o)} \rightarrow HQ^{\bullet} + cytc_{(r)}$	Complex III reaction
5.	$HQ^{\bullet} + cytc_{(o)} \rightarrow Q + cytc_{(r)} + H^+$	Complex III reaction
6.	$HQ^{\bullet} + O_2 \rightarrow Q + H^+ + O_2^{\bullet -}$	Superoxide production
7.	$O_2^{\bullet -} + O_2^{\bullet -} + 2H^+ \rightarrow H_2O_2 + O_2$	Superoxide dismutase
8.	$H_2O_2 + NADPH + H^+ \rightarrow 2H_2O + NADP$	Glutathione
9.	$2H_2O_2 \rightarrow 2H_2O + O_2$	Catalase
10.	$O_2 + 4cytc_{(r)} + 4H^+ \rightarrow 4cytc_{(o)} + 2H_2O$	Complex IV reaction

As already explained in the previous chapters, all the components are given a unique number and then a rate equation is written for each of these components. Reversible nature of these reactions is taken into consideration while writing the rate equations. In Table 4.3, the reactions 1-5 are reversible. The rate equations are reversible reactions were written for both forward and reverse reactions, represented as LHS and RHS (denoting the reactants of left and right hand side of the reaction) in Table 4.4 and in the script given in Table 4.5.

Rate Equations

The rate equations used in the simulation of ROS generation and scavenging in association with the ETC are given in Table 4.4.

Table 4.4: The rate equations for both forward and reverse reactions (LHS and RHS respectively) of the reactions given in Table 4.3. The rate equation for each component of the system is also given.

$LHS1 = \frac{[NADH]}{1+[NADH]} \cdot \frac{[C_1(ox)]}{1+[C_1(ox)]}$	$RHS1 = a * \frac{[NAD^+]}{1+[NAD^+]} \cdot \frac{[C_1(\mathrm{red})]}{1+[C_1(\mathrm{red})]}$
$LHS2 = \frac{[Q]}{1+[Q]} \cdot \frac{[C_1(\mathrm{red})]}{1+[C_1(\mathrm{red})]}$	$RHS2 = a * \frac{[QH^{\cdot}]}{1+[QH^{\cdot}]} \cdot \frac{[C_1(semi)]}{1+[C_1(semi)]}$
$LHS3 = \frac{[QH^{\cdot}]}{1+[QH^{\cdot}]} \cdot \frac{[C_1(semi)]}{1+[C_1(semi)]}$	$RHS3 = a * \frac{[QH_2]}{1+[QH_2]} \cdot \frac{[C_1(ox)]}{1+[C_1(ox)]}$
$LHS4 = d * \frac{[QH_2]}{1+[QH_2]} \cdot \frac{[cytc_{(o)}]}{1+[cytc_{(o)}]}$	$RHS4 = a * \frac{[QH^{\cdot}]}{1+[QH^{\cdot}]} \cdot \frac{[cytc_{(\mathrm{red})}]}{1+[cytc_{(\mathrm{red})}]}$
$LHS5 = (1-d) * \frac{[QH^{\cdot}]}{1+[QH^{\cdot}]} \cdot \frac{[cytc_{(ox)}]}{1+[cytc_{(ox)}]}$	$RHS5 = a * \frac{[Q]}{1+[Q]} \cdot \frac{[cytc_{(\mathrm{red})}]}{1+[cytc_{(\mathrm{red})}]}$
$LHS6 = b * \frac{[QH^{\cdot}]}{1+[QH^{\cdot}]} \cdot \frac{[O_2]}{1+[O_2]}$	$LHS7 = \frac{[O_2^{-\cdot}]}{1+[O_2^{-\cdot}]} \cdot \frac{[O_2^{-\cdot}]}{1+[O_2^{-\cdot}]}$
$LHS8 = c * \frac{[H_2O_2]}{1+[H_2O_2]} \cdot \frac{[NADPH]}{1+[NADPH]}$	$LHS9 = (1-c) * \frac{[H_2O_2]}{1+[H_2O_2]} \cdot \frac{[H_2O_2]}{1+[H_2O_2]}$
$LHS10 = (1-b) * \frac{[O_2]^{1/2}}{1+[O_2]^{1/2}} \cdot \frac{[cytc_{(\mathrm{red})}]^2}{1+[cytc_{(\mathrm{red})}]^2}$	
$\frac{d}{dt}[NADH] = -\frac{[NADH]}{1+[NADH]} \cdot \frac{[C_1(ox)]}{1+[C_1(ox)]} + \frac{[NAD^+]}{1+[NAD^+]} \cdot \frac{[C_1(\mathrm{red})]}{1+[C_1(\mathrm{red})]}$	

$$\frac{d}{dt}[NAD^+] = \frac{[NADH]}{1+[NADH]}.\frac{[C_1(ox)]}{1+[C_1(ox)]} - \frac{[NAD^+]}{1+[NAD^+]}.\frac{[C_1(\mathrm{red})]}{1+[C_1(\mathrm{red})]}$$

$$\frac{d}{dt}[C_1(ox)] = -\frac{[NADH]}{1+[NADH]}.\frac{[C_1(ox)]}{1+[C_1(ox)]} + \frac{[NAD^+]}{1+[NAD^+]}.\frac{[C_1(\mathrm{red})]}{1+[C_1(\mathrm{red})]} + \frac{[QH^\cdot]}{1+[QH^\cdot]}.\frac{[C_1(semi)]}{1+[C_1(semi)]} - \frac{[QH_2]}{1+[QH_2]}.\frac{[C_1(ox)]}{1+[C_1(ox)]}$$

$$\frac{d}{dt}[C_1(semi)] = \frac{[NADH]}{1+[NADH]}.\frac{[C_1(ox)]}{1+[C_1(ox)]} - \frac{[NAD^+]}{1+[NAD^+]}.\frac{[C_1(\mathrm{red})]}{1+[C_1(\mathrm{red})]} - \frac{[QH^\cdot]}{1+[QH^\cdot]}.\frac{[C_1(semi)]}{1+[C_1(semi)]} + \frac{[QH_2]}{1+[QH_2]}.\frac{[C_1(ox)]}{1+[C_1(ox)]}$$

$$\frac{d}{dt}[C_1(\mathrm{red})] = \frac{[NADH]}{1+[NADH]}.\frac{[C_1(ox)]}{1+[C_1(ox)]} - \frac{[NAD^+]}{1+[NAD^+]}.\frac{[C_1(\mathrm{red})]}{1+[C_1(\mathrm{red})]} - \frac{[Q]}{1+[Q]}.\frac{[C_1(\mathrm{red})]}{1+[C_1(\mathrm{red})]} + \frac{[QH^\cdot]}{1+[QH^\cdot]}.\frac{[C_1(semi)]}{1+[C_1(semi)]}$$

$$\frac{d}{dt}[QH^\cdot] = \frac{[NADH]}{1+[NADH]}.\frac{[C_1(ox)]}{1+[C_1(ox)]} - \frac{[NAD^+]}{1+[NAD^+]}.\frac{[C_1(\mathrm{red})]}{1+[C_1(\mathrm{red})]} - \frac{[QH^\cdot]}{1+[QH^\cdot]}.\frac{[C_1(semi)]}{1+[C_1(semi)]} + \frac{[QH_2]}{1+[QH_2]}.\frac{[C_1(ox)]}{1+[C_1(ox)]} + \frac{[QH_2]}{1+[QH_2]}.\frac{[cytc_{(ox)}]}{1+[cytc_{(ox)}]} - \frac{[QH^\cdot]}{1+[QH^\cdot]}.\frac{[cytc_{(\mathrm{red})}]}{1+[cytc_{(\mathrm{red})}]} - \frac{[QH^\cdot]}{1+[QH^\cdot]}.\frac{[cytc_{(ox)}]}{1+[cytc_{(ox)}]} + \frac{[Q]}{1+[Q]}.\frac{[cytc_{(\mathrm{red})}]}{1+[cytc_{(\mathrm{red})}]} - \frac{[QH^\cdot]}{1+[QH^\cdot]}.\frac{[O_2]}{1+[O_2]}$$

$$\frac{d}{dt}[QH_2] = \frac{[QH^\cdot]}{1+[QH^\cdot]}.\frac{[C_1(semi)]}{1+[C_1(semi)]} - \frac{[QH_2]}{1+[QH_2]}.\frac{[C_1(ox)]}{1+[C_1(ox)]} - \frac{[QH_2]}{1+[QH_2]}.\frac{[cytc_{(ox)}]}{1+[cytc_{(ox)}]} + \frac{[QH^\cdot]}{1+[QH^\cdot]}.\frac{[cytc_{(\mathrm{red})}]}{1+[cytc_{(\mathrm{red})}]}$$

$$\frac{d}{dt}[Q] = -\frac{[NADH]}{1+[NADH]}.\frac{[C_1(ox)]}{1+[C_1(ox)]} - \frac{[NAD^+]}{1+[NAD^+]}.\frac{[C_1(\mathrm{red})]}{1+[C_1(\mathrm{red})]} + \frac{[QH^\cdot]}{1+[QH^\cdot]}.\frac{[cytc_{(ox)}]}{1+[cytc_{(ox)}]} - \frac{[Q]}{1+[Q]}.\frac{[cytc_{(\mathrm{red})}]}{1+[cytc_{(\mathrm{red})}]}$$

$$\frac{d}{dt}[cytc_{(ox)}] = -\frac{[QH_2]}{1+[QH_2]}.\frac{[cytc_{(ox)}]}{1+[cytc_{(ox)}]} + \frac{[QH^\cdot]}{1+[QH^\cdot]}.\frac{[cytc_{(\mathrm{red})}]}{1+[cytc_{(\mathrm{red})}]} - \frac{[QH^\cdot]}{1+[QH^\cdot]}.\frac{[cytc_{(ox)}]}{1+[cytc_{(ox)}]} + \frac{[Q]}{1+[Q]}.\frac{[cytc_{(\mathrm{red})}]}{1+[cytc_{(\mathrm{red})}]} + \frac{[O_2]^{1/2}}{1+[O_2]^{1/2}}.\frac{[cytc_{(\mathrm{red})}]^2}{1+[cytc_{(\mathrm{red})}]^2}$$

$$\frac{d}{dt}[cytc_{(\mathrm{red})}] = \frac{[QH_2]}{1+[QH_2]}.\frac{[cytc_{(ox)}]}{1+[cytc_{(ox)}]} - \frac{[QH^\cdot]}{1+[QH^\cdot]}.\frac{[cytc_{(\mathrm{red})}]}{1+[cytc_{(\mathrm{red})}]} + \frac{[QH^\cdot]}{1+[QH^\cdot]}.\frac{[cytc_{(ox)}]}{1+[cytc_{(ox)}]} - \frac{[Q]}{1+[Q]}.\frac{[cytc_{(\mathrm{red})}]}{1+[cytc_{(\mathrm{red})}]} - \frac{[O_2]^{1/2}}{1+[O_2]^{1/2}}.\frac{[cytc_{(\mathrm{red})}]^2}{1+[cytc_{(\mathrm{red})}]^2}$$

$$\frac{d}{dt}[O_2] = -\frac{[QH^\cdot]}{1+[QH^\cdot]}.\frac{[O_2]}{1+[O_2]} + \frac{[O_2^{-\cdot}]}{1+[O_2^{-\cdot}]}.\frac{[O_2^{-\cdot}]}{1+[O_2^{-\cdot}]} - \frac{[O_2]^{1/2}}{1+[O_2]^{1/2}}.\frac{[cytc_{(\mathrm{red})}]^2}{1+[cytc_{(\mathrm{red})}]^2}$$

$$\frac{d}{dt}[O_2^{-\cdot}] = \frac{[QH^\cdot]}{1+[QH^\cdot]}.\frac{[O_2]}{1+[O_2]} - \frac{[O_2^{-\cdot}]}{1+[O_2^{-\cdot}]}.\frac{[O_2^{-\cdot}]}{1+[O_2^{-\cdot}]}$$

$$\frac{d}{dt}[H_2O_2] = \frac{[O_2^{-\cdot}]}{1+[O_2^{-\cdot}]}.\frac{[O_2^{-\cdot}]}{1+[O_2^{-\cdot}]} - \frac{[H_2O_2]}{1+[H_2O_2]}.\frac{[NADPH]}{1+[NADPH]} - \frac{[H_2O_2]}{1+[H_2O_2]}.\frac{[H_2O_2]}{1+[H_2O_2]}$$

$$\frac{d}{dt}[NADPH] = -\frac{[H_2O_2]}{1+[H_2O_2]}.\frac{[NADPH]}{1+[NADPH]}$$

$$\frac{d}{dt}[NADP] = \frac{[H_2O_2]}{1+[H_2O_2]}.\frac{[NADPH]}{1+[NADPH]}$$

Script

The script used for simulation of ROS generation and scavenging in association with the ETC is presented in Table 4.5.

For simulation, four factors have been used, whose values were fixed manually based on the previous studies and the values given in the literature. These have been denoted using variables, a, b, c and d. The first variable “a” has been used to control the rate of the reverse reactions and has been fixed at 0.2. This indicates that the forward reaction will be favoured five times over the reverse reaction. Another factor “b” regulates the amount of oxygen channelled to superoxide

production in the reaction scheme. It has been shown that 2-5% of total oxygen consumed is used for superoxide production, so based on this, in the present scheme, 3% of the total oxygen is channelled for superoxide production. The next factor "c" is used for giving weights to the two parallel reactions which utilize H_2O_2, i.e., the oxidation reaction via catalase and glutathione (reaction 8 and 9 in Table 4.3). The last factor "d" is used to account for the reactions by complex III, where cytochrome c can react with ubiquinol or semiubiquinone (reaction 4 and 5 in Table 4.3). Here both the above cases of parallel reactions have been given equal weight, i.e., the values of both "c" and "d" are kept at 0.5. This value can be changed if the preference of a given tissue or cell type under study of either of the two reactions is known. This approach renders the flexibility to the kinetic scheme presented and thus it can be adapted to a wide range of systems. Modifications were made to this script to study the behaviour in various conditions.

Table 4.5: Script used for simulation of ROS in association with electron transport chain.

```
1;
% solve ROS formation and scavenging-H2O2 weight 0.5, no H2O2 pulse
function ds=ros(s,t)
% 1=NADH; 2=NAD+; 3=C1(ox); 4=C1(semi);5=C1(red);6=QH(.); 7=QH2;8=Q;
%9=cytc(ox);10=cyctc(red);11=O2;12=O2(.-);13=H2O2;14=NADPH; 15=NADP;
% Equations for mitochondrial translation termination reactions

a=0.2;      % factor to control reverse reactions
b=0.03;     % portion of oxygen used for superoxide formation
c=0.5;      % weights for H2O2 parallel reactions (GSH)
d=0.5;      % weights for cytc(o) parallel reactions (complex III)

% Complex I reactions
LHS1=(s(1)/(1+s(1)))*(s(3)/(1+s(3)));
RHS1=a*(s(2)/(1+s(2)))*(s(5)/(1+s(5)));
LHS2=(s(8)/(1+s(8)))*(s(5)/(1+s(5)));
RHS2=a*(s(6)/(1+s(6)))*(s(4)/(1+s(4)));
LHS3=(s(6)/(1+s(6)))*(s(4)/(1+s(4)));
RHS3=a*(s(7)/(1+s(7)))*(s(3)/(1+s(3)));

% Complex III reactions
LHS4=d*(s(7)/(1+s(7)))*(s(9)/(1+s(9)));
RHS4=a*(s(6)/(1+s(6)))*(s(10)/(1+s(10)));
LHS5=(1-d)*(s(6)/(1+s(6)))*(s(9)/(1+s(9)));
RHS5=a*(s(8)/(1+s(8)))*(s(10)/(1+s(10)));
%Complex IV reaction
LHS10=(1-b)*(s(11)/(1+s(11)))*((s(10)/(1+s(10)))^4);
% superoxide formation
LHS6=b*(s(6)/(1+s(6)))*(s(11)/(1+s(11)));
```

```
% Scavenging reactions
LHS7=(s(12)/(1+s(12)))*(s(12)/(1+s(12))); % Superoxide dismutase
LHS8=c*(s(13)/(1+s(13)))*(s(14)/(1+s(14))); % glutathione
LHS9=(1-c)*((s(13)/(1+s(13)))^2); % catalase reaction

ds=zeros(15,1);
ds(1)= -LHS1+RHS1+0.005;
ds(2)=  LHS1-RHS1-(0.1*s(2));
ds(3)= -LHS1+RHS1+LHS3-RHS3;
ds(4)=  LHS2-RHS2-LHS3+RHS3;
ds(5)=  LHS1-RHS1-LHS2+RHS2;
ds(6)=  LHS2-RHS2-LHS3+RHS3+LHS4-RHS4-LHS5+RHS5-LHS6;
ds(7)=  LHS3-RHS3-LHS4+RHS4;
ds(8)= -LHS2+RHS2+LHS5-RHS5+LHS6;
ds(9)= -LHS4+RHS4-LHS5+RHS5+LHS10;
ds(10)= LHS4-RHS4+LHS5-RHS5-LHS10;
ds(11)=-LHS6+LHS7-LHS10+0.008;
ds(12)= LHS6-LHS7;
ds(13)= LHS7-LHS8-LHS9;
ds(14)=-LHS8+0.001;
ds(15)= LHS8-(0.1*s(15));
return
end

% use lsode to solve this set...
lsode_options("relative tolerance",1e-4);
lsode_options("absolute tolerance",1e-3);
t=0:1:200;
% supply the initial concentrations ...
s0=[0.1,0.1,0.3,0.1,0.1,0.1,0.1,0.5,0.3,0.1,0.2,0.1,0.1,0.2,0.1]; ;
%     0   0   0   0   0   0   0   0   0   1   1   1   1   1   1
%     1   2   3   4   5   6   7   8   9   0   1   2   3   4   5
[s,T,MSG]=lsode(@ros,s0,t);
T
MSG
plot(t,s(:,1),"linewidth",5,t,s(:,6),"linewidth",5,t,s(:,11),"linewi
dth",5,t,s(:,12),"linewidth",5,t,s(:,13),"linewidth",5,t,s(:,14),"li
newidth",5,t,s(:,15),"linewidth",5);
grid on;
set (gca, 'FontName', 'Times');
set (gca,'FontSize',20);
axis([0,200,.001,1.05]);
title ("No H2O2 pulse");
xlabel ("Time/arbitrary units");
ylabel ("Concentration/arbitrary units");
set (gca,'FontSize', 20);
set( get(gcf,'children'), 'linewidth',4 );
legend("NADH","QH.", "O2","O2.-","H2O2", "NADPH","NADP", "location",
"east")
```

Result

The simulation of reactive oxygen species was carried out in association with the ETC. The simulation result has been presented along with comparisons in the concentration levels of selected metabolites when there is a sudden change in the concentration of H_2O_2 and O_2. This has been achieved by their addition or removal for a limited time, and the impact has been represented graphically.

In Fig. 4.1, three conditions were studied apart from the basic simulation result obtained by running the script given in Table 4.5. An additional input of H_2O_2 was given for three different time slots, i.e., 50-75 time units, 100-125 time units and 50-125 time units. The changes in the concentration of most of the components are not obvious from the graph, but the change in the behaviour of NADPH and NADPH/NADP are prominently visible. With the addition of H_2O_2, NADPH concentration decreases and NADP concentration increases. This can be explained in a simple way that as H_2O_2 concentration increases, the scavenging mechanism via glutathione catalysed by glutathione peroxidase and glutathione reductase reduces H_2O_2 to water and oxidises NADPH to NADP, thus decreasing the concentration of NADPH. An interesting observation is that in all the three cases the concentration of H_2O_2 does not rise beyond 0.5 concentration unit, irrespective of the duration of the pulse. This could be possibly due to the action of enzymes as catalase, glutathione peroxidase and glutathione reductase, which maintains a low level of H_2O_2 concentration. Also, it is important to note that with the withdrawal of pulse, the system attains the earlier state with low level of H_2O_2.

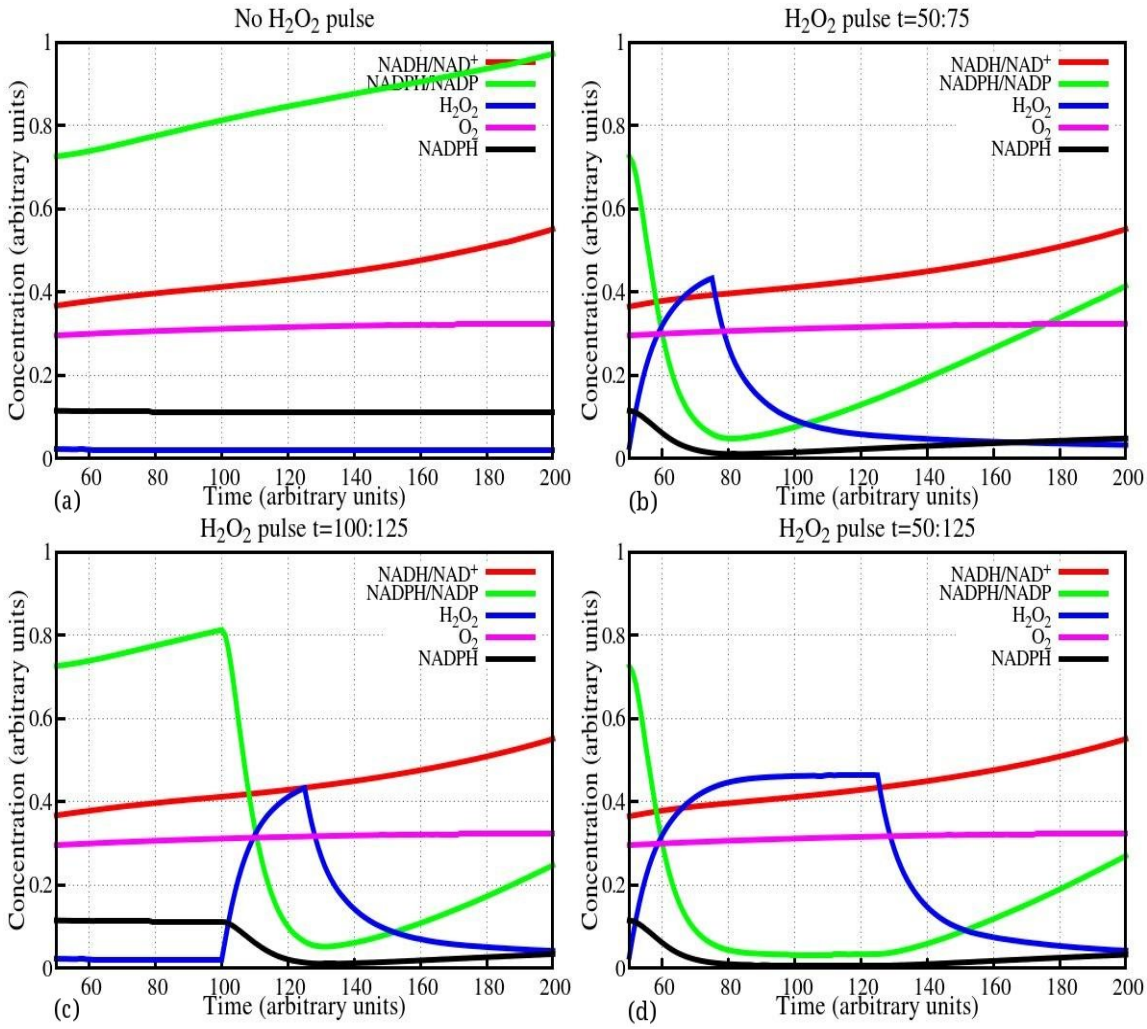

Figure 4.1: The effect of a pulse of H_2O_2 in the reaction system including the ETC and ROS. (a) The native state, with no additional H_2O_2 input, (b) H_2O_2 pulse given for a duration of 25 time units between 50-75 time units, (c) H_2O_2 pulse for time duration between 100-125 time units and, (d) an elongated H_2O_2 pulse for 75 time units ranging from 50-125 time units. It can be clearly seen that an intermittent pulse of H_2O_2 @0.05 for a specified duration results in a peak in H_2O_2 concentration and then it is consumed as the pulse is withdrawn. Also, it is interesting to note that the highest point in the peak is always around 0.5 concentration unit. The graphs are plotted for 50-200 time points duration as the initial time regions are same for all the four cases. The x-axis represents time in arbitrary units, and the y-axis represents concentrations in arbitrary units.

Similar analyses were done by addition and removal of O_2 leading to three different combinations. The results are shown in Fig. 4.2. The three combinations include (i) removal of oxygen for a duration of 25 time units (50-75 time units), (ii) addition of O_2 for 25 time units (100-125 time units) and (iii) both the addition and removal combined, i.e. removal from 50:75 time units followed by addition for 100-125 time units. The change in the final concentration (end of the curve @200 time point) can be clearly seen in all the four cases, the first one being the basic simulation result obtained from the script given in Table 4.5. It is interesting to note that when both the conditions, addition and removal, are combined the final concentrations of all the components are close to the basic curve.

With the addition of O_2, the concentration of NADPH decreases. This effect can be explained by the oxidizing capabilities of O_2. The increase in concentration of O_2 results in the increase in ROS levels, including H_2O_2. It results in increased utilisation of NADPH for H_2O_2 scavenging via glutathione, thus decreasing NADPH concentration. Also, concentration of NADP increases as more and more NADPH is oxidised. This presents a ripple effect, which is clearly evident in the graphical representation.

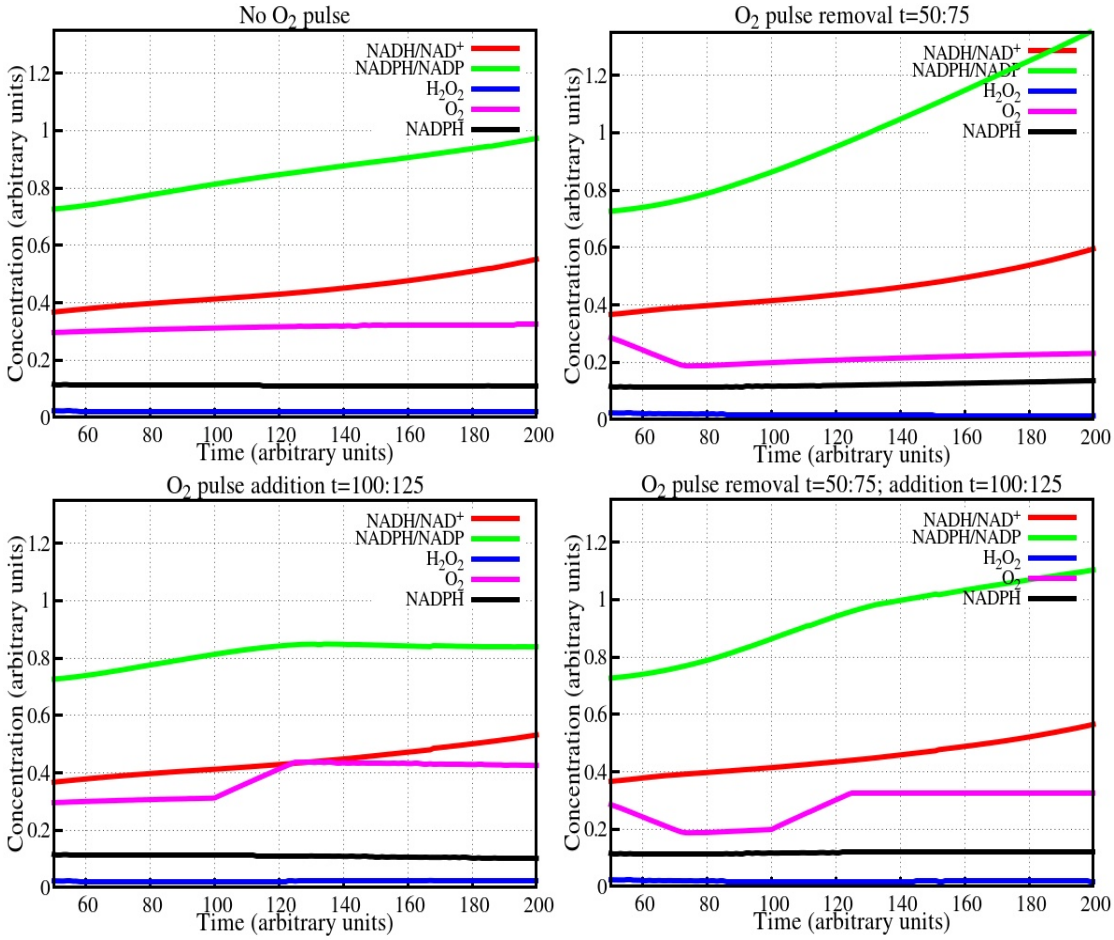

Figure 4.2: These figures illustrate the effect of a pulse of O_2 on the reaction system and the concentrations of its components. (a) No O_2 addition or removal: native state, (b) Removal of O_2 form a duration of 25 time units, from 50-75 time points, (c) addition of O_2 ranging from 100-125 time points and, (d) removal for 25 time units (50-75 time points) followed by addition of 25 time units 100-125 time points. It can be clearly seen that an intermittent pulse of addition of O_2 results in a peak in O_2 concentration and then it is consumed as the pulse is withdrawn. It can be seen that with the change in concentration of oxygen the concentration curves of other components change. The x-axis represents time in arbitrary units, and the y-axis represents concentrations in arbitrary units.

Phase Diagrams: The phase diagrams are rate of change in concentration vs concentration curve for a given metabolite. They resemble the basic Michaelis-Menten curve, which is also a rate vs concentration curve.

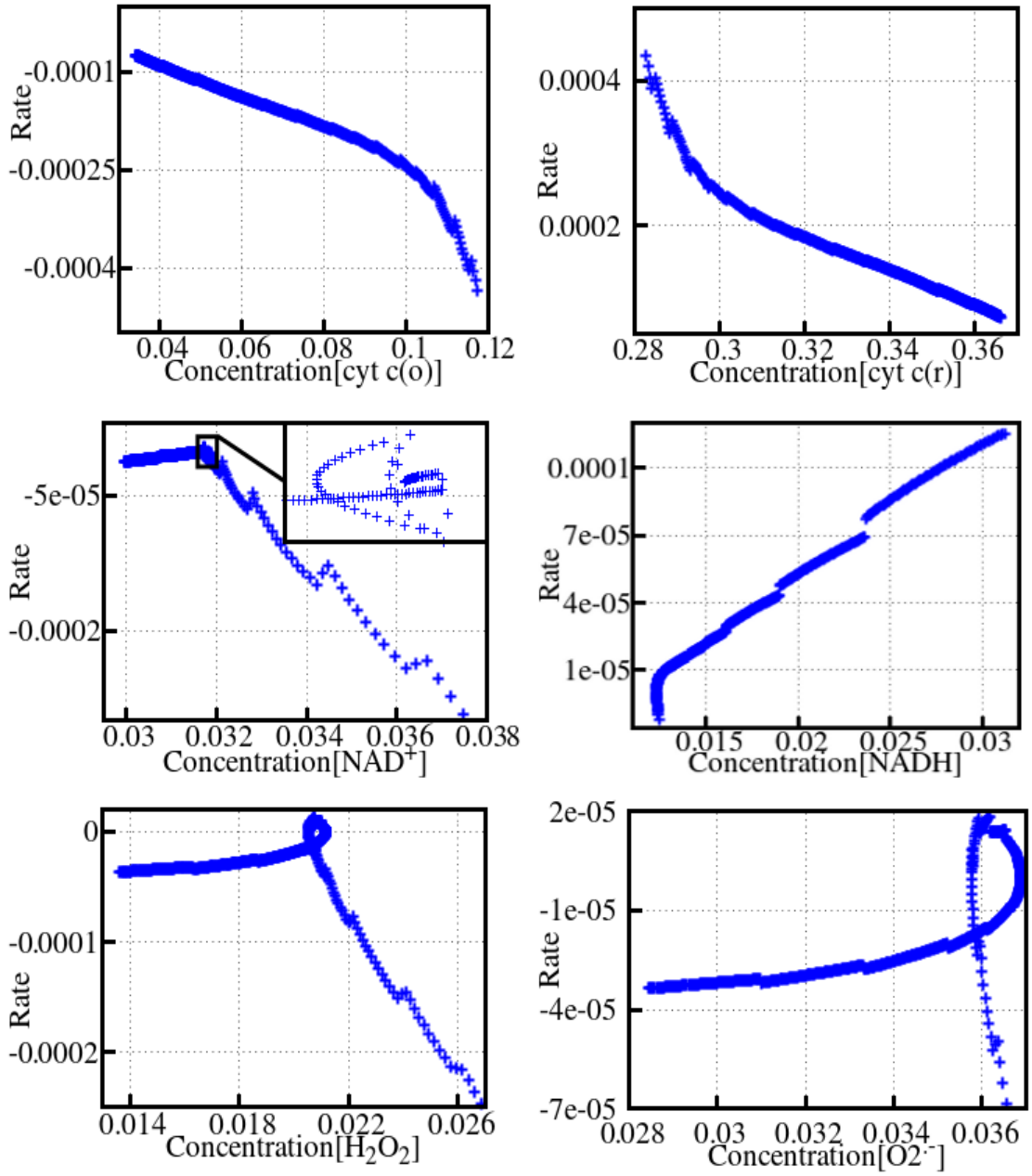

Figure 4.3: Phase diagrams for selected metabolites. [cyt c(o): cytochrome c oxidised form, cyt c (r): cytochrome c reduced form]. The inset graph shows the magnified version of enclosed area. The y-axis represents the rate of transformation of the corresponding substrate as indicated on the abscissa. The concentrations and rates are expressed in arbitrary units.

Fig. 4.3 represents phase diagrams for selected metabolites. 400 data points are plotted in each of these curves. It can be clearly seen that more than 300 data points are clustered in a small region. This region has been shown in magnified form in the inset image. This suggests that as the concentration of a metabolite reaches steady-state concentration, the rates become very less.

The curves for cytochrome c oxidised and reduced forms show complementary behaviour. Similarly, curves for quinone and quinol also appear broadly complementary, and the slight differences can be explained by the presence of an intermediate species, semiubiquinone, at a low concentration at any point in time. The curve for H_2O_2 consists of a small loop suggesting the stabilising of concentration in that particular region. A similar pattern is seen in NAD^+ concentration where the concentration tends to be bound in a small region.

Combined Simulation

The simulation for ROS generation and scavenging was further extended to include Krebs cycle, ATP synthesis and malate-aspartate and citrate-pyruvate shuttles. The combined simulation consists of all the components of these metabolic pathways involved and thus the impact of perturbations caused by one or more components can be studied in a qualitative and semi-quantitative way. The total number of components in this case was 53.

Comparison with physiological experimental data: The simulation results obtained from the combined simulation were compared with the experimental work reported by Mamer *et al*. (2013). The experimental data presented the complete targeted profile of the metabolic intermediates of Krebs cycle. The authors have treated an untransformed mouse mammary epithelial cell line with inhibitors of oxidative phosphorylation, viz., rotenone, which blocks complex I (NADH dehydrogenase), antimycin A, which blocks complex III between cytochrome b and cytochrome c_1, and oligomycin, which blocks ATP synthesis by F_0/F_1 ATPase and reported data showing the change in concentrations of the Krebs cycle intermediates. This data was correlated with the data obtained by blocking the respective reactions in the combined simulation including Krebs cycle, oxidative phosphorylation (along with reactive oxygen species generation and scavenging) and mitochondrial shuttles presented earlier (Chapters 2 and 3).

Rate equations

The rate equations were obtained by combining the rate equations used in the previous sections. The six sets of equations were combined viz. Krebs cycle, the ETC, ATP synthesis, malate-aspartate shuttle, citrate-pyruvate shuttle and ROS scavenging and generation.

Script

The script used here is a combination of the six sets of scripts already presented in the previous chapters (Table 4.6). All the variables were appropriately combined, and the rate equations were critically analysed to avoid repetitions. The simulation results were compared with experimental work (Mamer *et al*., 2013) conducted on mouse cell lines using respiratory chain inhibitors (rotenone, antimycin A and oligomycin). To reproduce the effect of inhibitors in the simulation, the corresponding reactions were blocked 80% for a duration of 350 time units (t=50:400) and readings taken at 500 time point. The initial concentrations used in this script were near steady-state concentrations to mimic the physiological conditions.

Rotenone inhibits electron transfer from iron-sulfur centres in complex I to quinone, and has no effect on oxidation of NADH by complex I. In this case, 80% block has been put in the reaction 2 shown in Table 4.3, where complex I transfers the electrons to quinone. Thus it can be seen in the script that "p", complex I blocking factor, has been incorporated in LHS21 (which correspond to reaction 2 of Table 4.3).

Table 4.6: Script for combined simulation including Krebs cycle, electron transport chain, ATP synthesis, ROS generation and scavenging, malate-aspartate shuttle and citrate-pyruvate shuttle.

```
1; % solve the Krebs cycle + ETC + ATP + Shuttles + ROS , pH
revisited, no additional factors, final script, with @200 steady-
state initial conc

ds=zeros(53,1);
s(1)=       4.06762706e-02;         % oxaloacetate-m
s(2)=       5.41150858e-02;         % acetyl-CoA-m
s(3)=       1.36479148e-03;         % citrate-m
s(4)=       1.30120600e-01;         % isocitrate-m
s(5)=       6.49494655e-01;         % ketoglutarate-m
s(6)=       1.90077480e-01;         % succinyl-CoA-m
s(7)=       2.52000261e-01;         % succinate-m
s(8)=       6.40000549e-04;         % fumarate-m
s(9)=       3.04701742e-01;         % malate-m
s(10)=      8.55807434e-01;         % CoA-SH-m
```

```
s(11)=      1.34850500e-02;          % NAD-m
s(12)=      1.86514950e-01;          % NADH-m
s(13)=      5.30647232e-01;          % CO2
s(14)=      1.00000000e-01;          % GDP
s(15)=      1.00000000e-01;          % GTP
s(16)=      3.17776953e-03;          % FAD
s(17)=      1.96822230e-01;          % FADH2
s(18)=      4.31824438e-02;          % ATP-m
s(19)=      2.80659445e-01;          % Aspartate-im
s(20)=      1.03660114e-02;          % malate-im
s(21)=      3.49702454e-01;          % ketoglutarate-im
s(22)=      5.19340555e-01;          % glutamate-im
s(23)=      2.74689310e-01;          % glutamate-m
s(24)=      2.53106896e-02;          % Aspartate-m
s(25)=      9.02575749e-06;          % citrate-im
s(26)=      2.00000000e-01;          % ATP-im
s(27)=      5.00000000e-01;          % CoA-SH-im
s(28)=      1.00000000e-01;          % Acetyl-CoA-im
s(29)=      1.00000000e-01;          % ADP-im
s(30)=      5.00000000e-01;          % NADP-im
s(31)=      4.75716178e-01;          % Pyruvate-im
s(32)=      1.00000000e-01;          % NADPH-im
s(33)=      2.68433710e-01;          % Pyruvate-m
s(34)=      2.02778865e-01;          % oxaloacetate-im
s(35)=      1.37216611e-02;          % NADH-im
s(36)=      2.86278339e-01;          % NAD-im
s(37)=      2.56817556e-01;          % ADP-m
s(38)=      1.71089959e-01;          % phos-m
s(39)=      2.13138504e-01;          % phos-im
s(40)=      3.73909749e-03;          % Q
s(41)=      5.95838504e-01;          % QH2
s(42)=      3.78298398e-02;          % cyt c(oxi)
s(43)=      3.62170160e-01;          % cyt c(red)
s(44)=      1.82560783e-01;          % O2
s(45)=      2.28021649e-04;          % H+ conc
s(46)=      1.75587375e-02;          % complex I (ox)
s(47)=      2.99827181e-02;          % complex I (semi)
s(48)=      9.52458544e-01;          % complex (red)
s(49)=      1.00422399e-01;          % QH.
s(50)=      2.27827686e-02;          % O2-.
s(51)=      8.69672964e-03;          % H2O2
s(52)=      1.39426788e-01;          % NADPH-m
s(53)=      5.51128696e-03;          % NADP-m

function ds=kears(s,t)

% 7.6 in mito matrix(pH1->x) ; 6.88 in im space(pH2);
if (s(45)<1e-10) s(45)=1e-9; endif
x=-log10(s(45));              % pH value inside the matrix
if ((x < 7.5) | (x > 8.5)) k1=0.1; else k1=((x-6.9)/(x-5.9)); endif
% x-6.9 is used in the formula, k1= x/1+x
```

```
a=0.2;            % factor to control reverse reactions
b=0.03;           % portion of oxygen used for superoxide formation
c=0.5;            % weights for H2O2 parallel reactions (GSH)
d=0.5;            % weight for cyt c(o) parallel reaction

% Equations for Kreb cycle reactions
LHS1=(s(1)/(1+s(1)))*(s(2)/(1+s(2)))*(1/(1+s(3)))*(1/(1+s(6)))*(1/
(1+s(12)))*(1/(1+s(18)));
      % this is inhibited by s3; s6; s12; ATP
LHS2= (s(3)/(1+s(3)));
LHS3= (s(4)/(1+s(4)))*(s(11)/(1+s(11)))*(1/(1+s(18)));
      % this is inhibited by ATP
LHS4=         (s(5)/(1+s(5)))*(s(10)/(1+s(10)))*(s(11)/(1+s(11)))*(1/
(1+s(6)))*(1/(1+s(12)));
      % this is inhibited by s6; s12
LHS5= (s(6)/(1+s(6)))*(s(14)/(1+s(14)))*(s(38)/(1+s(38)));
LHS6= (s(7)/(1+s(7)))*(s(16)/(1+s(16)));
LHS7= (s(8)/(1+s(8)));
LHS8= (s(9)/(1+s(9)))*(s(11)/(1+s(11)));
RHS8= (s(1)/(1+s(1)))*(s(12)/(1+s(12)));
LHS15= (s(33)/(1+s(33)))*(s(11)/(1+s(11)))*(s(10)/(1+s(10)));

% Equations for shuttle reactions
LHS9 =(s(27)/(1+s(27)))*(s(25)/(1+s(25)))*(s(26)/(1+s(26)));
LHS10=(s(34)/(1+s(34)))*(s(35)/(1+s(35)));
RHS10=(s(20)/(1+s(20)))*(s(36)/(1+s(36)));
LHS11=(s(20)/(1+s(20)))*(s(30)/(1+s(30)));
LHS12=(s(33)/(1+s(33)))*(s(18)/(1+s(18)))*(s(13)/(1+s(13)));
LHS13=(s(19)/(1+s(19)))*(s(21)/(1+s(21)));
RHS13=(s(34)/(1+s(34)))*(s(22)/(1+s(22)));
LHS14=(s(1)/(1+s(1)))*(s(23)/(1+s(23)));
RHS14=(s(24)/(1+s(24)))*(s(5)/(1+s(5)));

port = 0.05;
% alpha= aspartate/glutamate direction and rate
e=1+s(19)+s(24)+s(22)+s(23)+s(19)*s(24)+s(19)*s(22)+s(19)*s(23)+s(24
)*s(22)+s(24)*s(23)+s(22)*s(23)+s(19)*s(24)*s(22)+s(19)*s(24)*s(23)+
s(19)*s(22)*s(23)+s(24)*s(22)*s(23)+s(19)*s(24)*s(22)*s(23);
alpha=port*((s(22)*s(24))-(s(19)*s(23)))/e;
% s19=asp-im, s23=glu-m, s24=asp-m, s22=glu-im

% beta = malate/ketoglutarate direction and rate
f=1+s(20)+s(9)+s(21)+s(5)+s(20)*s(9)+s(20)*s(21)+s(20)*s(5)+s(9)*s(2
1)+s(9)*s(5)+s(21)*s(5)+s(20)*s(9)*s(21)+s(20)*s(9)*s(5)+s(20)*s(21)
*s(5)+s(9)*s(21)*s(5)+s(20)*s(9)*s(21)*s(5);
beta=port*((s(20)*s(5))-(s(9)*s(21)))/f;
% s20=mal-im, s5=akg-m, s9=mal-m, s21=akg-im

% malate citrate exchanger
 j=1+s(20)+s(9)+s(25)+s(3)+s(20)*s(9)+s(20)*s(25)+s(20)*s(3)+s(9)*s(
25)+s(9)*s(3)+s(25)*s(3)+s(20)*s(9)*s(25)+s(20)*s(9)*s(3)+s(20)*s(25
```

```
)*s(3)+s(9)*s(25)*s(3)+s(20)*s(9)*s(25)*s(3);
gamma=port*((s(20)*s(3))-(s(9)*s(25)))/j;
% s20=mal-im, s3=cit-m, s9=mal-m, s25=cit-im

% malate phosphate exchanger
k=1+s(20)+s(9)+s(39)+s(38)+s(20)*s(9)+s(20)*s(39)+s(20)*s(38)+s(9)*s
(39)+s(9)*s(38)+s(39)*s(38)+s(20)*s(9)*s(39)+s(20)*s(9)*s(38)+s(20)*
s(39)*s(38)+s(9)*s(39)*s(38)+s(20)*s(9)*s(39)*s(38);
delta=port*((s(9)*s(39))-(s(20)*s(38)))/k;
% s20=mal-im, s38=phos-m, s9=mal-m, s39=phos-im
%alpha=beta=gamma=delta=0;
flux = 0.02*(s(31)-s(33));
% Equations for ETC reactions
% Inhibitors of ETC
if ((t > 50) | (t < 400)) r=0.2; else r=1; endif
p=1;        % rotenone complex I block
q=1;        % antimycin A complex III block
% r=1;      % oligomycin complex V block

% Complex I reactions
LHS16=(s(12)/(1+s(12)))*(s(46)/(1+s(46)));
RHS16=a*(s(11)/(1+s(11)))*(s(48)/(1+s(48)));
LHS21=p*(s(40)/(1+s(40)))*(s(48)/(1+s(48)));
% rotenone blocks transfer of electrons from complex I to uniquinone
RHS21=a*(s(49)/(1+s(49)))*(s(47)/(1+s(47)));
LHS22=(s(49)/(1+s(49)))*(s(47)/(1+s(47)));
RHS22=a*(s(41)/(1+s(41)))*(s(46)/(1+s(46)));;

% Complex II reaction
LHS17=(s(17)/(1+s(17)))*(s(40)/(1+s(40)));
% Complex III reactions
LHS18=q*d*(s(41)/(1+s(41)))*(s(42)/(1+s(42)));
RHS18=a*(s(49)/(1+s(49)))*(s(43)/(1+s(43)));
LHS23=q*(1-d)*(s(49)/(1+s(49)))*(s(42)/(1+s(42)));
RHS23=a*(s(40)/(1+s(40)))*(s(43)/(1+s(43)));

% Complex IV reaction
LHS19=k1*(1-b)*((s(43))^2/(1+(s(43))^2))*(s(44)^(1/2)/
(1+s(44)^(1/2)));

% superoxide formation
LHS24=b*(s(49)/(1+s(49)))*(s(44)/(1+s(44)));

% Scavenging reactions
LHS25=(s(50)/(1+s(50)))*(s(50)/(1+s(50))); % Superoxide dismutase
LHS26=c*(s(51)/(1+s(51)))*(s(52)/(1+s(52))); % glutathione
LHS27=(1-c)*((s(51)/(1+s(51)))^2); % catalase reaction

% Equation for ATP synthesis
LHS20=r*k1*(s(37)/(1+s(37)))*(s(38)/(1+s(38)));

% rate equations
```

```
ds(1) = -LHS1+LHS8-RHS8+LHS12-LHS14+RHS14;
ds(2) = -LHS1+LHS15;
ds(3) =  LHS1-LHS2-gamma;
ds(4) =  LHS2-LHS3;
ds(5) =  LHS3-LHS4+LHS14-RHS14-beta;
ds(6) =  LHS4-LHS5;
ds(7) =  LHS5-LHS6;
ds(8) =  LHS6-LHS7;
ds(9) =  LHS7-LHS8+RHS8+beta+gamma-delta;
ds(10)=  LHS1-LHS4+LHS5-LHS15;
ds(11)= -LHS3-LHS4-LHS8+RHS8-LHS15+LHS16-RHS16;
ds(12)=  LHS3+LHS4+LHS8-RHS8+LHS15-LHS16+RHS16;
ds(13)=  LHS4-LHS12+LHS15;
ds(14)= 0;
%ds(14)= -LHS5;
ds(15)= 0;
%ds(15)=  LHS5;
ds(16)= -LHS6+LHS17;
ds(17)=  LHS6-LHS17;
ds(18)= -LHS12+LHS20;
ds(19)= -LHS13+RHS13+alpha;
ds(20)=  LHS10-RHS10-LHS11-beta-gamma+delta;
ds(21)= -LHS13+RHS13+beta;
ds(22)=  LHS13-RHS13-alpha;
ds(23)= -LHS14+RHS14+alpha;
ds(24)=  LHS14-RHS14-alpha;
ds(25)= -LHS9+gamma;
ds(26)= 0;
%ds(26)= -LHS9;
ds(27)= 0;
%ds(27)= -LHS9;
ds(28)= 0;
%ds(28)= LHS9;
ds(29)=0;
%ds(29)= LHS9;
ds(30)= 0;
%ds(30)= -LHS11;
ds(31)=  LHS11-flux;
ds(32)= 0;
%ds(32)=  LHS11;
ds(33)= -LHS12-LHS15+flux;
ds(34)=  LHS9-LHS10+RHS10+LHS13-RHS13;
ds(35)= -LHS10+RHS10;
ds(36)=  LHS10-RHS10;
ds(37)=  LHS12-LHS20;
ds(38)= -LHS5+LHS12-LHS20+delta;
ds(39)=  LHS9-delta;
ds(40)= -LHS21+RHS21-LHS17+LHS23-RHS23+LHS24;
ds(41)=  LHS22-RHS22+LHS17-LHS18+RHS18;
ds(42)= -LHS18+RHS18+LHS19-LHS23+RHS23;
ds(43)=  LHS18-RHS18-LHS19+LHS23-RHS23;
```

```
ds(44)= -LHS19-LHS24+LHS25+LHS27+0.0015;
ds(45)=                              (-(0.02*4*LHS16)-(0.02*4*LHS23)-
(0.02*2*LHS19)+(0.2*4*LHS20))*0.001;
% ds(45) = 0;
ds(46)= -LHS16+RHS16+LHS22-RHS22;
ds(47)=  LHS21-RHS21-LHS22+RHS22;
ds(48)=  LHS16-RHS16-LHS21+RHS21;
ds(49)=  LHS21-RHS21-LHS22+RHS22+LHS18-RHS18-LHS23+RHS23-LHS24;
ds(50)=  LHS24-LHS25;
ds(51)=  LHS25-LHS26-LHS27;
ds(52)= -LHS26+0.001;
ds(53)=  LHS26-(0.1*s(53));
return
end

% use lsode to solve this set...
lsode_options("relative tolerance",1e-7);
lsode_options("absolute tolerance",1e-6);
t=0:1:500;
% supply the initial concentrations ...
s0=s;
[s,T,MSG]=lsode(@kears,s0,t);
T
MSG
%
plot(t,s(:,43),"linewidth",5,t,s(:,44),"linewidth",5,t,s(:,46),"line
width",5,t,s(:,47),"linewidth",5,t,s(:,48),"linewidth",5,t,s(:,49),"
linewidth",5,t,s(:,50),"linewidth",5);
grid on;

set (gca,'FontSize', 20);
set (gca, 'FontName', 'Times');
axis([000,100,.001,1.01]);
% title ("KEAS");
xlabel ("Time/arbitrary units");
ylabel ("Concentration/arbitrary units");
set (gca,'FontSize', 20);
set( get(gcf,'children'), 'linewidth',4 );
legend("43","44","45","18","40","41","42", "location", "east");
```

Antimycin A blocks the transfer of electron to cytochrome c. In case of complex III, both the reactions (reactions 4 and 5 shown in Table 4.3 and LHS18 and LHS23 in Table 4.6) are transferring electrons to cytochrome c, therefore the factor “q”, complex III blocking factor, has been incorporated in both the reactions. The factor “r” is used to impart block in complex V reaction, i.e., ATP synthesis (LHS20 in Table 4.6).

Result

The concentrations of selected metabolic intermediates of Krebs cycle for the two sets, viz., simulated and experimental, are shown in Table 4.7. The values shown under experimental set are measured in nanomoles/10^6 cells. The values shown under simulated values are the concentrations in arbitrary units as obtained from the simulation.

Table 4.7: Concentrations of selected metabolites under experimental and simulated conditions. The concentrations belong to four different environments viz., DMSO, antimycin A, rotenone and oligomycin. (In the original report, the metabolites have been referenced by their acid form.)

	Experimental values				Simulated values			
Metabolite	**DMSO**	**Antimycin A**	**Rotenone**	**Oligomycin**	**DMSO**	**Antimycin A**	**Rotenone**	**Oligomycin**
Oxaloacetate	0.0034	0.0027	0.006	0.0063	0.0087308	0.0090020	0.0088405	0.0039128
Citrate	0.58	0.09	0.27	0.30	2.3207e-04	2.3571e-04	1.9122e-04	2.3067e-04
Isocitrate	0.0062	0.0013	0.0034	0.0038	0.097519	0.097489	0.10927	0.13545
α-Ketoglutarate	0.59	0.43	0.9	0.73	0.63888	0.64006	0.79063	0.62538
Succinate	0.22	15.0	0.08	0.14	0.50839	0.608608	0.31140	0.49063
Fumarate	0.33	0.79	0.45	0.50	2.3994e-04	5.3666e-04	2.4016e-04	2.3766e-04
Malate	1.00	0.55	1.66	1.57	0.53358	0.54669	0.78437	0.23853
Pyruvate	0.18	0.13	0.39	0.44	0.22532	0.22131	0.22782	0.44385

The data obtained by simulation has to be calibrated so as to be comparable to the experimental data. The data was calibrated taking the DMSO values as 1 (as uninhibited reaction rate), and all the other concentrations were scaled accordingly for plotting graphs. Similarly for the values obtained by simulation, the concentration under DMSO condition is taken to be 1 and all the other concentrations were accordingly calculated. The experimental values were derived from the box plots illustrated in the original article. Therefore, the values taken for this comparison are the median values and may have considerable variations from the actual data points of the samples studied.

The graphs shown in Figs. 4.4 and 4.5 show the comparison of experimental and simulated data when the concentration values are scaled using the concentrations under DMSO condition as 1. A significant correlation can be seen in most of the cases, when the concentrations of selected components were plotted alongside.

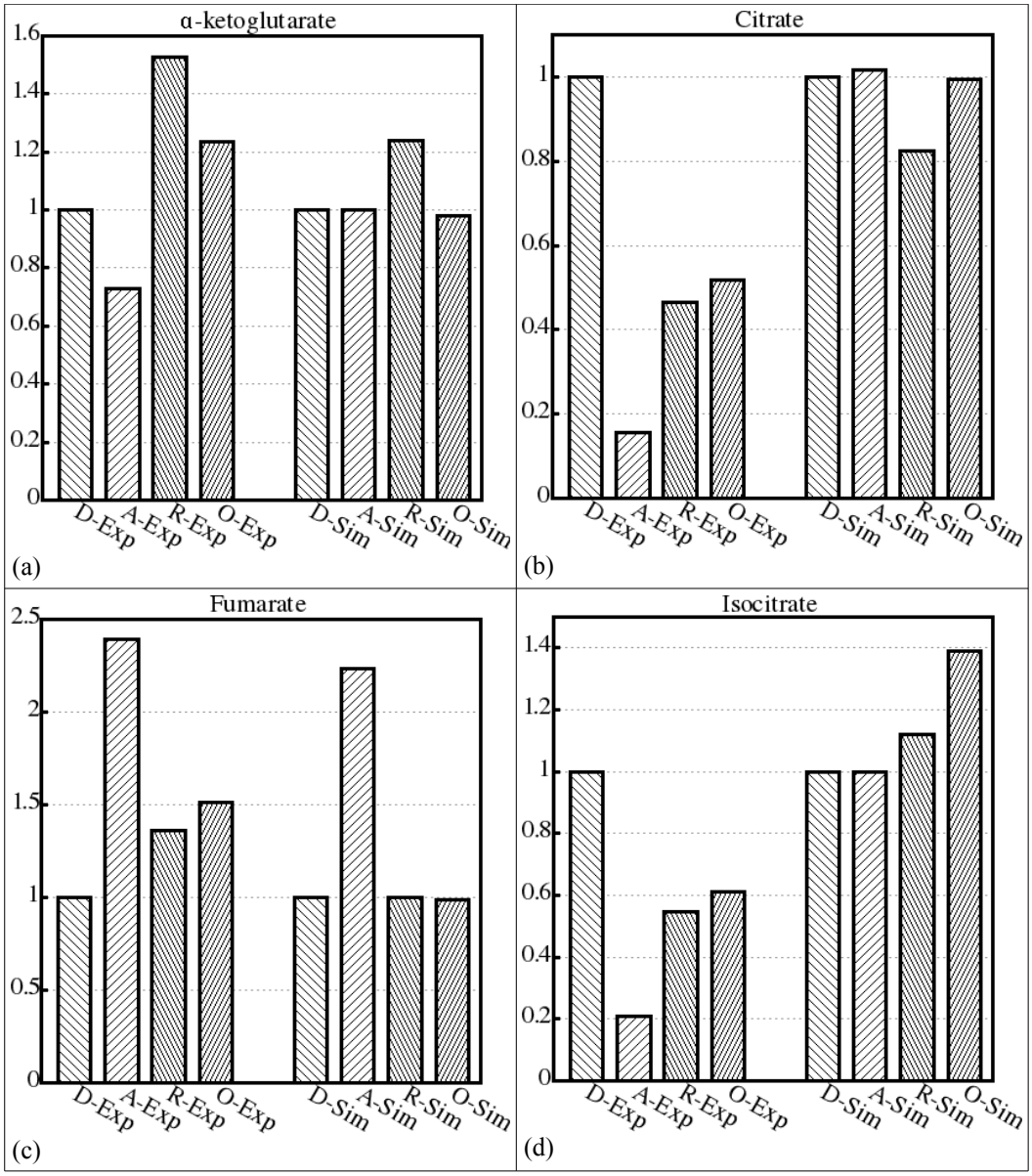

Figure 4.4: Comparison of the simulation results with the experimental data presented by Mamer *et al.* (2013) for α-ketoglutarate, citrate, fumarate and isocitrate. The exact values are given in Table 4.7. The experiments were conducted on an untransformed mouse cell line with inhibitors of oxidative phosphorylation, viz. Antimycin A, rotenone and oligomycin. The x-axis represents the four conditions abbreviated as D=DMSO, A=Antimycin A, R=Rotenone and O=Oligomycin, for two datasets, Exp=experimental values and Sim=Simulation values. The y-axis indicates the fold change calibrated using the concentration under DMSO condition, which was scaled to 1 and the other concentrations were scaled accordingly.

It is important to note that the experimental data used for comparison was obtained from untransformed mouse cell line and no specific parameters (as K_M, V_{max}) pertaining to this system were used for simulation. In such a scenario, the correlation observed between the two datasets is considerable, and a perfect match was never expected.

α-Ketoglutarate: It is clearly seen that the concentration under rotenone in both the cases is highest of all. The concentration under oligomycin is lower than that of rotenone quite proportionally in both the datasets. Concentrations under antimycin A and oligomycin are closer to the DMSO values, thus showing broadly similar trend in both cases.

Citrate: Concentrations of citrate in presence of rotenone and oligomycin behave similarly under both experimental and simulation conditions. The concentration under rotenone is lower than the concentration under oligomycin in both the cases, and both these values are lower than the DMSO values. The concentration under antimycin A is anomalous.

Fumarate: Concentration of fumarate under antimycin A stands out in both the datasets and is higher than all the other concentrations. The concentrations under rotenone and oligomycin are close to that under DMSO presenting a good correlation between the two datasets.

Isocitrate: The figure shows a similar trend for the concentrations in the presence of inhibitors. The concentrations under oligomycin being the highest followed by rotenone and oligomycin, in both the datasets.

Malate: It can be seen that the concentration under rotenone is the highest in both the datasets. The concentration under antimycin A is close to the DMSO control, and the concentration under oligomycin is anomalous here.

Oxaloacetate: It is seen that the concentrations do not follow any trend in this case. All the concentrations in the simulated set are close to the DMSO values, which can be inferred as a stabilising effect. The system is seen to behave in such a way that in the presence of any perturbation the concentration of the given component tends to be in the same region. This can be correlated to the steady-state region seen under phase curves.

Pyruvate: The concentrations of pyruvate behave similar to oxaloacetate under DMSO, antimycin A and rotenone (i.e. when compared with corresponding values). It can be due to the reaction where pyruvate is redirected to oxaloacetate, which enters the Krebs cycle and this behaves as a one-way reaction without any branch point. The concentration under oligomycin is highest of all in both the datasets, thus presenting a fair agreement.

Succinate: The data shows a similar trend for the two datasets. The experimental data under DMSO, rotenone and oligomycin closely resemble the simulated results. The concentration of succinate under antimycin A in experimental dataset is exceptionally high, i.e., ~15 nanomoles/10^6 cells. It does not match the

simulated dataset, however it is seen that the concentration under antimycin A is the highest of all in both the datasets.

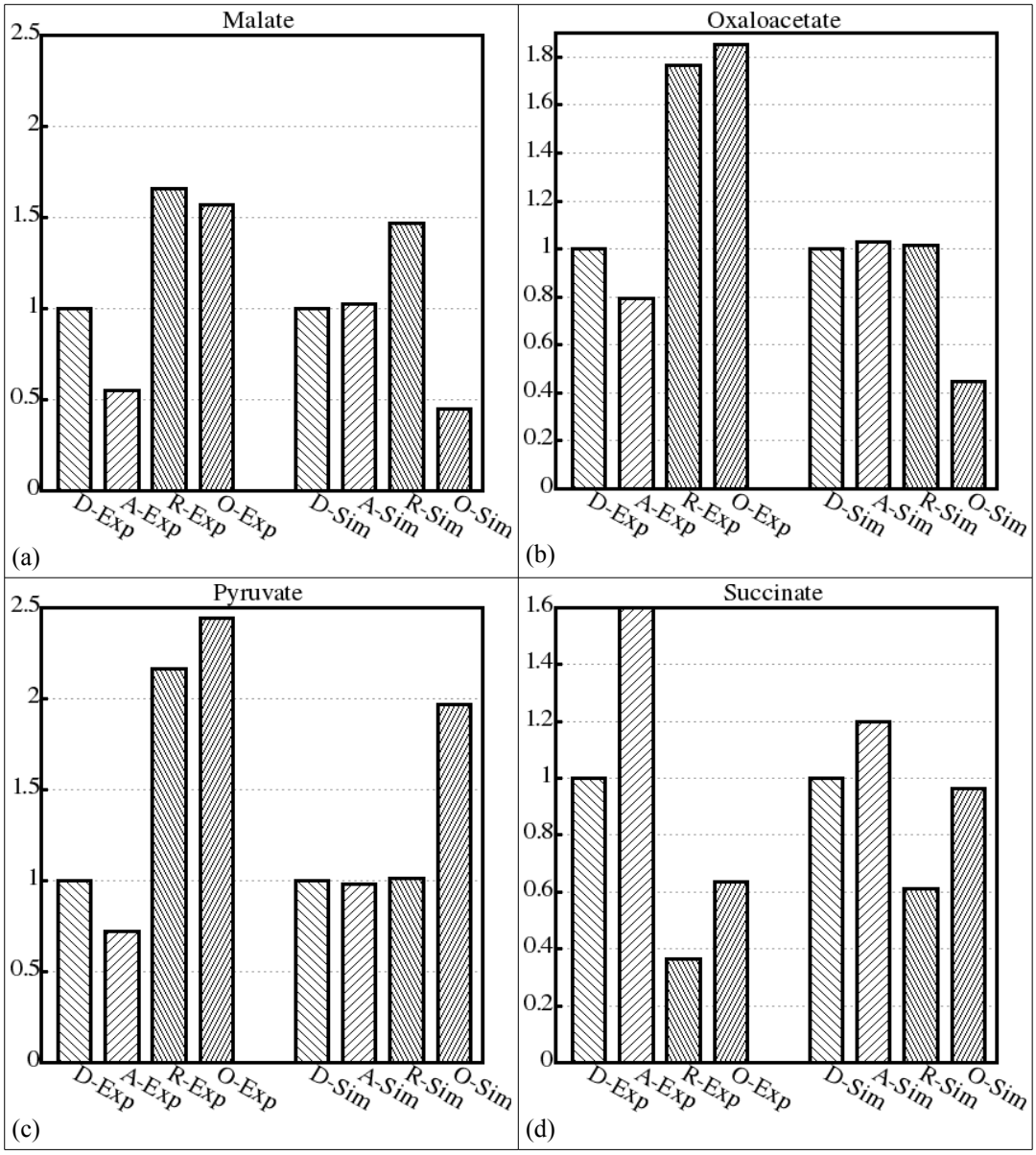

Figure 4.5: Comparison of the simulation results with the experimental data presented by Mamer *et al.* (2013) for malate, oxaloacetate, pyruvate and succinate. The exact values are given in Table 4.7. The experiments were conducted on an untransformed mouse mammary epithelial cell line with inhibitors of oxidative phosphorylation, viz. Antimycin A, rotenone and oligomycin. The x-axis represents the four conditions abbreviated as D=DMSO, A=Antimycin A, R=Rotenone and O=Oligomycin, for two datasets, Exp=experimental values and Sim=Simulation values. The y-axis indicates the fold change calibrated using the concentration under DMSO condition, which was scaled to 1 and the other concentrations were scaled accordingly.

The comparison of simulated results with experimental dataset presents an excellent correlation, despite the fact that no specific kinetic parameters were used for simulation. This basic model can be appropriately modified and customised to suit the experimental system under study, and a prediction about the expected outcomes can be made.

Analysis of all the systems together

The kinetic systems studied in this chapter and the previous two chapters can be compiled in a single figure as shown in Fig. 4.6. Four components viz., oxaloacetate, citrate, α-ketoglutarate and malate, have been studied for their behaviour under four different simulation environments.

The metabolites are common for all the four simulation environments, (I) Krebs cycle, (II) Krebs cycle + ETC + ATP synthesis, (III) Krebs cycle + ETC + ATP synthesis + citrate-pyruvate shuttle + malate-aspartate shuttle and (IV) Krebs cycle + ETC + ATP synthesis + citrate-pyruvate shuttle + malate-aspartate shuttle + reactive oxygen species. The initial concentrations of all the components in the respective systems were kept same to obtain an unbiased result. Starting with the same initial concentrations, the progress curves for the first 100 time points are shown here. It can be seen that the final concentrations (concentration at 100 time point) are broadly comparable for the four metabolites indicating that their general behaviours are related. Malate concentrations range between 0.1-0.3 (with two out of the four values being ~0.2). The concentrations of oxaloacetate are close to 0.8; concentrations of citrate lie close to zero in all the four environments. The concentrations of α-ketoglutarate are in the range of 0.5-0.6. When the reaction network is extended with the addition of few more metabolites and reaction pathways, minor changes are observed in the progress curves of the respective metabolites.

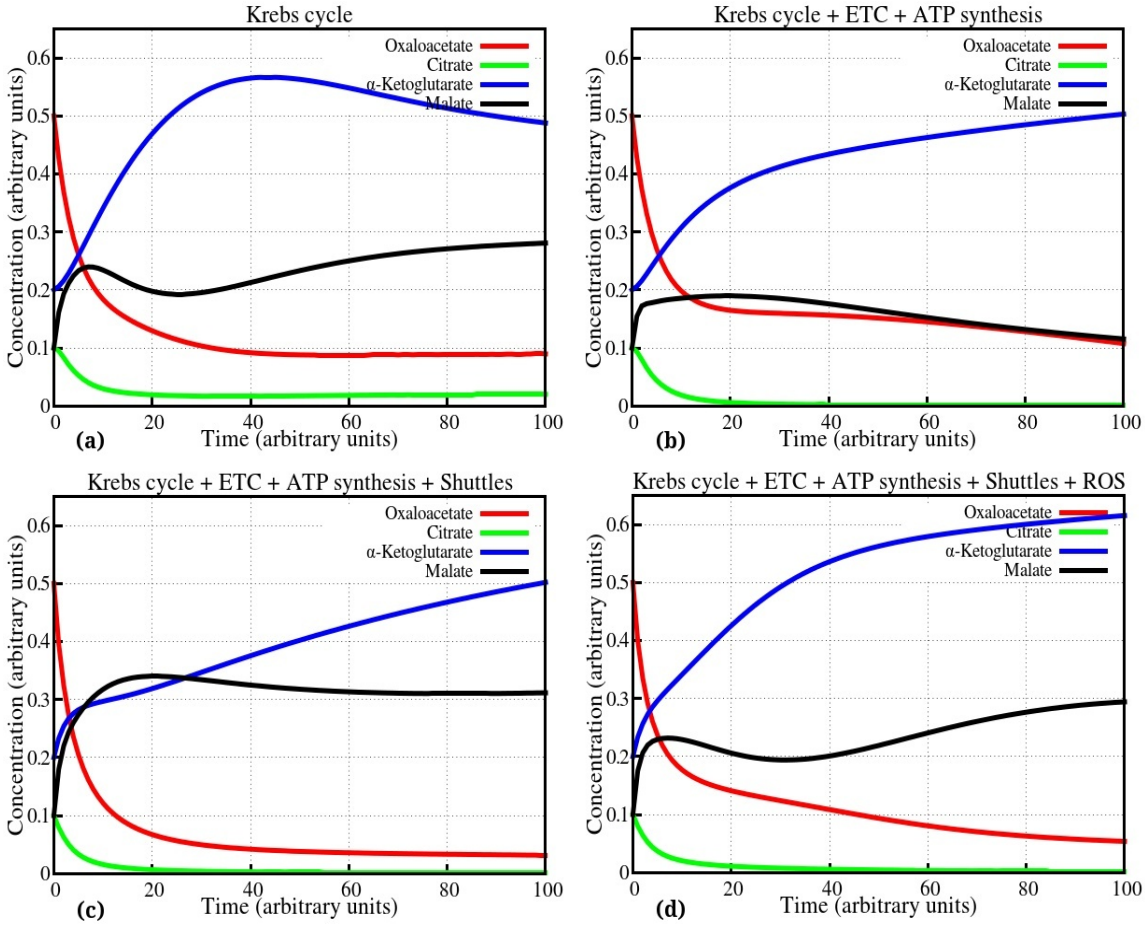

Figure 4.6: The progress curves of four metabolites, viz., oxaloacetate, citrate, α-ketoglutarate and malate plotted under four different environments, (a) Krebs cycle, (b) Krebs cycle combined with the ETC and ATP synthesis, (c) Krebs cycle combined with the ETC, ATP synthesis and citrate-pyruvate and malate-aspartate shuttles, and (d) Krebs cycle combined with the ETC, ATP synthesis, citrate-pyruvate and malate-aspartate shuttles and ROS. The concentrations and rates are expressed in arbitrary units.

References

Adam-Vizi, V., & Chinopoulos, C. (2006). Bioenergetics and the formation of mitochondrial reactive oxygen species. *Trends in pharmacological sciences*, *27*(12), 639-645.

Andreyev, A. Y., Kushnareva, Y. E., & Starkov, A. A. (2005). Mitochondrial metabolism of reactive oxygen species. *Biochemistry (Moscow)*, *70*(2), 200-214.

Balaban, R. S., Nemoto, S., & Finkel, T. (2005). Mitochondria, oxidants, and aging. *Cell*, *120*(4), 483-495.

Bandyopadhyay, U., Das, D., & Banerjee, R. K. (1999). Reactive oxygen species: oxidative damage and pathogenesis. *Current science*, *77*(5), 658-666.

Bohr, V. A., & Dianov, G. L. (1999). Oxidative DNA damage processing in nuclear and mitochondrial DNA. *Biochimie*, *81*(1-2), 155-160.

Brand, M. D., Affourtit, C., Esteves, T. C., Green, K., Lambert, A. J., Miwa, S., Pakay, J. L., & Parker, N. (2004). Mitochondrial superoxide: production, biological effects, and activation of uncoupling proteins. *Free Radical Biology and Medicine*, *37*(6), 755-767.

Chance, B., & Hollunger, G. (1961). The interaction of energy and electron transfer reactions in mitochondria I. General properties and nature of the products of succinate-linked reduction of pyridine nucleotide. *Journal of Biological Chemistry*, *236*(5), 1534-1543.

Covarrubias, L., Hernández-García, D., Schnabel, D., Salas-Vidal, E., & Castro-Obregón, S. (2008). Function of reactive oxygen species during animal development: passive or active? *Developmental biology*, *320*(1), 1-11.

de Grey, A. D. (2002). HO_2: The forgotten radical. *DNA and cell biology*, *21*(4), 251-257.

Dringen, R. (2000). Metabolism and functions of glutathione in brain. *Progress in neurobiology*, *62*(6), 649-671.

Fujii, J., & Ikeda, Y. (2002). Advances in our understanding of peroxiredoxin, a multifunctional, mammalian redox protein. *Redox Report*, *7*(3), 123-130.

Grimsrud, P. A., Xie, H., Griffin, T. J., & Bernlohr, D. A. (2008). Oxidative stress and covalent modification of protein with bioactive aldehydes. *Journal of Biological Chemistry*, *283*(32), 21837-21841.

Hemnani, T., & Parihar, M. S. (1998). Reactive oxygen species and oxidative DNA damage. *Indian journal of physiology and pharmacology*, *42*(4), 440-452.

Ho, Y. S., Xiong, Y., Ma, W., Spector, A., & Ho, D. S. (2004). Mice lacking catalase develop normally but show differential sensitivity to oxidant tissue injury. *Journal of Biological Chemistry*, *279*(31), 32804-32812.

Holmström, K. M., & Finkel, T. (2014). Cellular mechanisms and physiological consequences of redox-dependent signalling. *Nature Reviews Molecular Cell Biology*, *15*(6), 411-421.

Imai, H., & Nakagawa, Y. (2003). Biological significance of phospholipid hydroperoxide glutathione peroxidase (PHGPx, GPx4) in mammalian cells. *Free Radical Biology and Medicine*, *34*(2), 145-169.

Knopp, E. A., Arndt, T. L., Eng, K. L., Caldwell, M., LeBoeuf, R. C., Deeb, S. S., & O'Brien, K. D. (1999). Murine phospholipid hydroperoxide glutathione peroxidase: cDNA sequence, tissue expression, and mapping. *Mammalian genome*, *10*(6), 601-605.

Korshunov, S., & Imlay, J. A. (2006). Detection and quantification of superoxide formed within the periplasm of Escherichia coli. *Journal of bacteriology*, *188*(17), 6326-6334.

Löffler, M., Becker, C., Wegerle, E., & Schuster, G. (1996). Catalytic enzyme histochemistry and biochemical analysis of dihydroorotate dehydrogenase/oxidase and succinate dehydrogenase in mammalian tissues, cells and mitochondria. *Histochemistry and cell biology*, *105*(2), 119-128.

Mamer, O., Gravel, S. P., Choinière, L., Chénard, V., St-Pierre, J., & Avizonis, D. (2013). The complete targeted profile of the organic acid intermediates of the citric acid cycle using a single stable isotope dilution analysis, sodium borodeuteride reduction and selected ion monitoring GC/MS. *Metabolomics*, *9*(5), 1019-1030.

McCord, J. M., & Fridovich, I. (1970). The utility of superoxide dismutase in

studying free radical reactions II. The mechanism of the mediation of cytochrome c reduction by a variety of electron carriers. *Journal of Biological Chemistry*, *245*(6), 1374-1377.

Miwa, S., St-Pierre, J., Partridge, L., & Brand, M. D. (2003). Superoxide and hydrogen peroxide production by *Drosophila* mitochondria. *Free Radical Biology and Medicine*, *35*(8), 938-948.

Muller, F. L., Liu, Y., & Van Remmen, H. (2004). Complex III releases superoxide to both sides of the inner mitochondrial membrane. *Journal of Biological Chemistry*, *279*(47), 49064-49073.

Packer, L., Weber, S. U., & Rimbach, G. (2001). Molecular aspects of α-tocotrienol antioxidant action and cell signalling. *The Journal of nutrition*, *131*(2), 369S-373S.

Pastore, A., Federici, G., Bertini, E., & Piemonte, F. (2003). Analysis of glutathione: implication in redox and detoxification. *Clinica chimica acta*, *333*(1), 19-39.

Petersen, D. R., & Doorn, J. A. (2004). Reactions of 4-hydroxynonenal with proteins and cellular targets. *Free Radical Biology and Medicine*, *37*(7), 937-945.

Pushpa-Rekha, T. R., Burdsall, A. L., Oleksa, L. M., Chisolm, G. M., & Driscoll, D. M. (1995). Rat phospholipid-hydroperoxide glutathione peroxidase cDNA cloning and identification of multiple transcription and translation start sites. *Journal of Biological Chemistry*, *270*(45), 26993-26999.

Richter, C. (1995). Oxidative damage to mitochondrial DNA and its relationship to ageing. *The international journal of biochemistry & cell biology*, *27*(7), 647-653.

Rigoulet, M., Yoboue, E. D., & Devin, A. (2011). Mitochondrial ROS generation and its regulation: mechanisms involved in H_2O_2 signaling. *Antioxidants & redox signaling*, *14*(3), 459-468.

Schaur, R. J. (2003). Basic aspects of the biochemical reactivity of 4-hydroxynonenal. *Molecular aspects of medicine*, *24*(4), 149-159.

Schönfeld, P., Więckowski, M. R., Lebiedzińska, M., & Wojtczak, L. (2010). Mitochondrial fatty acid oxidation and oxidative stress: lack of reverse electron transfer-associated production of reactive oxygen species. *Biochimica et Biophysica Acta (BBA)-Bioenergetics*, *1797*(6), 929-938.

Seifried, H. E., Anderson, D. E., Fisher, E. I., & Milner, J. A. (2007). A review of the interaction among dietary antioxidants and reactive oxygen species. *The Journal of nutritional biochemistry*, *18*(9), 567-579.

Simonson, S. G., Zhang, J., Canada, A. T., Su, Y. F., Benveniste, H., & Piantadosi, C. A. (1993). Hydrogen peroxide production by monoamine oxidase during ischemia-reperfusion in the rat brain. *Journal of Cerebral Blood Flow & Metabolism*, *13*(1), 125-134.

Singh, S. P., Coronella, J. A., Beneš, H., Cochrane, B. J., & Zimniak, P. (2001). Catalytic function of Drosophila melanogaster glutathione S-transferase DmGSTS1-1 (GST-2) in conjugation of lipid peroxidation end products. *European Journal of Biochemistry*, *268*(10), 2912-2923.

Singhal, S. S., Zimniak, P., Awasthi, S., Piper, J. T., He, N. G., Teng, J. I., ... & Awasthi, Y. C. (1994). Several closely related glutathione S-transferase isozymes catalyzing conjugation of 4-hydroxynonenal are differentially expressed in human tissues. *Archives of biochemistry and biophysics*, *311*(2), 242-250.

Stadtman, E. R., & Levine, R. L. (2003). Free radical-mediated oxidation of free amino acids and amino acid residues in proteins. *Amino acids*, *25*(3-4), 207-218.

Starkov, A. A., Fiskum, G., Chinopoulos, C., Lorenzo, B. J., Browne, S. E., Patel, M. S., & Beal, M. F. (2004). Mitochondrial α-ketoglutarate dehydrogenase complex generates reactive oxygen species. *The Journal of neuroscience*, *24*(36), 7779-7788.

Tretter, L., & Adam-Vizi, V. (2004). Generation of reactive oxygen species in the reaction catalyzed by α-ketoglutarate dehydrogenase. *The Journal of neuroscience*, *24*(36), 7771-7778.

Vásquez-Vivar, J., Kalyanaraman, B., & Kennedy, M. C. (2000). Mitochondrial aconitase is a source of hydroxyl radical an electron spin resonance investigation. *Journal of Biological Chemistry*, *275*(19), 14064-14069.

Whatley, S. A., Curti, D., Das, G. F., Ferrier, I. N., Jones, S., Taylor, C., & Marchbanks, R. M. (1998). Superoxide, neuroleptics and the ubiquinone and cytochrome b5 reductases in brain and lymphocytes from normals and schizophrenic patients. *Molecular psychiatry*, *3*(3), 227-237.

Wood, Z. A., Schröder, E., Robin Harris, J., & Poole, L. B. (2003). Structure, mechanism and regulation of peroxiredoxins. *Trends in biochemical sciences*, *28*(1), 32-40.

Yakes, F. M., & Van Houten, B. (1997). Mitochondrial DNA damage is more extensive and persists longer than nuclear DNA damage in human cells following oxidative stress. *Proceedings of the National Academy of Sciences*, *94*(2), 514-519.

Zorov, D. B., Juhaszova, M., & Sollott, S. J. (2006). Mitochondrial ROS-induced ROS release: an update and review. *Biochimica et Biophysica Acta (BBA)-Bioenergetics*, *1757*(5), 509-517.

Chapter 5 Mitochondrial Protein Translation

Mitochondrial translation

Mitochondria possess their own genome that may be present in multiple copies (Robin & Wong, 1988). They carry out replication, transcription and translation of the respective genes. Mitochondrial DNA (mtDNA) is a double-stranded, circular DNA approximately 16.5kb long. The two strands are classified as heavy and light strand, based on their nucleotide content. The guanine rich strand is termed as the heavy strand, and the cytosine rich strand is called as the light strand. The heavy strand encodes for 28 genes that include two rRNAs, 14 tRNAs, and 12 polypeptides. The light strand encodes for nine genes, which consists of eight tRNAs and a single polypeptide (Taanman, 1999). So on the whole, the mtDNA codes for 37 genes. There are 13 protein-coding genes, 22 genes for tRNAs and two genes for rRNA (Anderson *et al*., 1981).

Recent reports suggest that some tRNAs are imported from cytosol, which are used for translation inside mitochondria (Salinas *et al.*, 2012). All the other proteins required for translation by mitochondria are imported from the cytosol. The 13 protein-coding genes encode for the subunits of the oxidative phosphorylation complexes in mitochondria; however the other subunits are imported from the cytosol and are assembled within mitochondria. These complexes are localised in the inner mitochondrial membrane and assist in proton translocation and electron transfer. The 13 subunits include seven subunits of complex I (NADH:ubiquinone oxidoreductase), one subunit of complex III (ubiquinone:cytochrome *c* oxidoreductase), three subunits of complex IV (cytochrome *c*:oxygen oxidoreductase) and two subunits of complex V (ATP synthase), the details of which are given in Table 5.1.

Table 5.1: The details of 12 protein-coding genes in mitochondria (Ref: http://www.genenames.org/genefamilies/mitocomplex)

Respiratory Complex	Approved Symbol	Approved Name	Number of amino acids
Mitochondrial subunits in complex I	MT-ND1	mitochondrially encoded NADH dehydrogenase 1	318
	MT-ND2	mitochondrially encoded NADH dehydrogenase 2	347
	MT-ND3	mitochondrially encoded NADH dehydrogenase 3	115
	MT-ND4	mitochondrially encoded NADH dehydrogenase 4	450
	MT-ND4L	mitochondrially encoded NADH dehydrogenase 4L	98
	MT-ND5	mitochondrially encoded NADH dehydrogenase 5	603
	MT-ND6	mitochondrially encoded NADH dehydrogenase 6	174

Mitochondrial subunits in complex III	MT-CYB	mitochondrially encoded cytochrome b	380
Mitochondrial subunits in complex IV	MT-CO1	mitochondrially encoded cytochrome c oxidase I	513
	MT-CO2	mitochondrially encoded cytochrome c oxidase II	227
	MT-CO3	mitochondrially encoded cytochrome c oxidase III	261
Mitochondrial subunits in complex V	MT-ATP6	mitochondrially encoded ATP synthase 6	226
	MT-ATP8	mitochondrially encoded ATP synthase 8	68

The two rRNAs encoded by the mitochondrial genome are *MT-RNR1* (12S) and *MT-RNR2* (16S) rRNAs. *MT-RNR2* also codes for a small peptide, humanin (Muzumdar *et al.*, 2009) The 22 tRNAs coded by the mitochondrial genome include all the tRNAs required for mitochondrial translation. However, some tRNAs are still imported from the cytosol to meet the requirements of mitochondria.

The remaining mitochondrial oxidative phosphorylation proteins, the metabolic enzymes, the DNA and RNA polymerases, the ribosomal proteins and the mtDNA regulatory factors required by mitochondria are all encoded by nuclear genes. These metabolites are synthesised in the cytosol and then imported into the organelle. Replication, transcription and translation of the mitochondrial genome takes place within the mitochondrial matrix only. The proteins and accessory molecules required for these processes are imported from cytosol as mentioned earlier, via several specific and non-specific transporters.

Several variations have been reported in the genetic code used by mitochondria during mitochondrial translation when compared to the cytosolic system. In cytosolic system, AUA codes for isoleucine, whereas it codes for methionine in the mitochondrial system. One of the stop codons (in translation in cytosol), UGA, codes for tryptophan in the mitochondrial system (Barrell, Bankier, & Drouin, 1979). It was earlier reported that AGA and AGG, which codes for arginine in the cytosolic system, acts as stop codon in the mitochondrial system, in addition to UAA and UAG. Recent reports suggest that there are two mRNAs where AGA and AGG act as stop codons and apparently they have a preceding U in both the cases. A -1 frameshift leads to positioning of UAG at the A-site during translation, which then acts as a regular stop codon (Temperley, Richter, Dennerlein, Lightowlers, & Chrzanowska-Lightowlers, 2010). Apart from the two aforementioned mRNAs, the other mRNAs have either UAA or UAG as the stop codon.

The process of protein synthesis takes place in three phases, initiation, elongation and termination. Of which, initiation and termination are one-step processes, and elongation consists of repeated incorporation amino-acids

corresponding to the codon placed at the A-site of the mitoribosome. Translation starts with initiation, where the initiator tRNA (fMet-tRNA) binds to the mRNA at the P-site of the mitoribosome (RajBhandary, 1994). During the elongation process, the codons following the start codon are read sequentially, and the corresponding amino acids are incorporated in the growing polypeptide chain. Once the whole mRNA is read and the stop codon is placed at the A-site of the mitoribosome, the elongation complex enters the termination phase. The completed polypeptide is released and the mitoribosome is recycled in the termination phase. The recycled mitoribosome can now start a new set of translation. Each of these phases requires a set of protein factors that are required for the sequential appropriate positioning of the components to form the respective complexes. A number of these steps have been successfully demonstrated *in vitro*, but till date no *in vitro* system capable of carrying out the whole mitochondrial translation process could be established (Smits, Smeitink, & van den Heuvel, 2010; Koc & Spremulli, 2002).

It has been suggested that the cytoplasmic and mitochondrial translation machineries are localised in close proximity on either side of the mitochondrial membranes, thereby allowing efficient assembly of oxidative phosphorylation complexes as it involves subunit from both the cytosolic system and mitochondrial system proteins (Smits *et al*., 2010).

Simulation of Protein Translation

The first step towards simulation is a detailed analysis of the individual steps involved in the three processes and their characteristic features. Previously Chu *et al.* have reported a preliminary computational tool to model translation (Chu, Zabet, & von der Haar, 2012). The model includes a representation of exhaustible tRNA pools, ribosome–ribosome interactions and differential initiation rates for different mRNA species. In the present work, a model of mitochondrial translation has been presented. Most of the data used in this work has been taken from the mammalian system.

Octave was used for modelling the three phases of mitochondrial translation individually. Rate equations were derived for all the components involved in all the three phases. These rate equations were simulated using ode solver in Octave. Of the three phases of translation, elongation is a set of repetitive events, which was taken into special consideration. Monte Carlo simulation was used for simulating the repetitive events with appropriate loops and conditions incorporated

into the script. Proper initial conditions and constraints were used to reproduce the randomness as observed in the biological system.

Table 5.2: List of all the components used for mitochondrial translation along with their symbolic names (Figs. 1, 2 and 3 mentioned in the table refers to Figs. 5.1, 5.2 and 5.3).

Symbolic name	Octave number	Component	Figure Reference
A	s1	mtIF3	Figure 1
BC	s2	Mitoribosome LSU:SSU	Figure 1 and 3
AC	s3	mtIF3:SSU	Figure 1
B	s4	LSU	Figure 1
D	s5	mtIF2	Figure 1
E	s6	SSU:mtIF3:mtIF2	Figure 1
F	s7	mRNA	Figure 1 and 3
G	s8	SSU:mtIF3:mtIF2:mRNA	Figure 1
H	s9	Aminoacyl-tRNA (aa-tRNA)	Figure 1 and 2
I	s10	SSU:mtIF3:mtIF2:mRNA: aa-tRNA	Figure 1
J	s11	SSU:LSU:mRNA:aa-tRNA	Figure 1, 2 and 3
X	s12	mtEFTu:GTP:aa-tRNA	Figure 2
K	s13	SSU:LSU:mRNA: aa-RNA: mtEFTu:GTP:aa-tRNA	Figure 2
L	s14	SSU:LSU:mRNA: aa-tRNA:aa-tRNA	Figure 2
L'		SSU:LSU:mRNA: tRNA:peptidyl-tRNA	Figure 2
M	s15	mtEFG1	Figure 2
N	s16	SSU:LSU:mRNA:tRNA:peptidyl-tRNA:mtEFG1	Figure 2
R	s17	Deacyl-tRNA	Figure 2 and 3
S	s18	mtRF1a	Figure 3
T	s19	SSU:LSU:mRNA:$(aa)_n$tRNA:mtRF1a	Figure 3
U	s20	SSU:LSU:mRNA:tRNA	Figure 3
V	s21	Polypeptide	Figure 3
W	s22	mtRRF1	Figure 3
Y	s23	mtRRF2	Figure 3
Z	s24	SSU:LSU:mRNA:tRNA:mtRRF1:mtRRF2	Figure 3
P1		GTP	Figure 1, 2 and 3
P2		GDP	Figure 1, 2 and 3

All the components used for simulation were given a unique symbolic name, and the same name was used throughout to maintain the consistency in the simulation process. A list of all the components and their symbolic names is presented in Table 5.2.

Initial conditions and concentrations

In the present system, all the reactants in the first reaction and the auxiliary factors were given an initial concentration of 1; all the other intermediates and products were kept at an initial concentration of 0. In the elongation phase, a constant concentration of source and sink was provided for tRNA in the script using ode solver. The aminoacylation process, where a deacylated tRNA is aminoacylated with its respective amino acid, was not included in this simulation. A special strategy was used to keep a track of the rate of amino acid incorporation in the polypeptide chain where formation of deacyl-tRNA was used as an indicator for amino acid incorporation.

Assumptions

The present simulation includes the reactions of mitochondrial translation and therefore all components are shown to be conserved in the system. It is quite possible that in the biological system, these components may have other sources and sinks, which are not considered in the given system. Small molecules as GTP, GDP, ATP, etc. are not involved in simulation, assuming that their concentrations do not change substantially and thus can be considered as constant. The emphasis was given to the key reactants, intermediates, factors and products.

Initiation

Mammalian mitochondrial ribosomes (mitoribosomes) are 55S ribosomes with two subunits: 39S large subunit (LSU) and 28S small subunit (SSU) (O'Brien, 2003). Mitochondrial DNA encodes for 13 protein-coding genes, which are synthesised by nine monocistronic and two dicistronic mRNAs. The dicistronic mRNAs contain overlapping reading frames and have internal start sites (Anderson *et al*., 1981). These mitochondrial mRNAs do not include 5' and 3' untranslated regions. They are assumed to be recognised by their unstructured 5' sequences, as there are no reports validating the presence of Shine-Dalgarno sequence or 7-methyl guanylate cap (Grohmann, Amalric, Crews, & Attardi, 1978). Mitochondrial translation system is quite simple when compared to eukaryotic cytosolic translation system, where a number of auxiliary factors are involved in all the three phases of translation.

Initiation in mitochondrial translation involves only two homologues of cytosolic translation initiation factors, mtIF2 and mtIF3 (Grasso, Christian, Spencer, & Spremulli, 2007). The first mitochondrial initiation factor involved in the process is mtIF3, which catalyses dissociation of mitoribosome into its two subunits (Koc & Spremulli, 2002). mtIF3 remains bound to SSU and LSU is released. The second initiation factor, mtIF2 bound with GTP, binds to SSU. mtIF2 acts as a substitute for the roles of both bacterial IF1 and IF2 (Gaur *et al*., 2008). No homologue for IF1 has been reported for the mitochondrial system. Further, it was shown that insertion of a conserved 37 amino acids sequence in mtIF2 enables it to carry out functions of both bacterial IF1 and IF2. Presence of mtIF3 assists mRNA binding to SSU in the correct orientation so as to ensure proper positioning of start codon (Fig. 5.1).

Once mRNA is bound to SSU, mtIF2 facilitates the entry of fMet-tRNA at the P-site of mitoribosome (Spencer & Spremulli, 2004). mtIF3 allows binding of fMet-tRNA to ribosome, only in the presence of mtIF2 and mRNA, and thus prevents premature binding of LSU, mtIF2 and fMet-tRNA (Koc & Spremulli, 2002). After fMet-tRNA binds to the ribosome, LSU binds to the SSU initiation complex and mtIF2 hydrolyses GTP to GDP. This is followed by release of mtIF2 and mtIF3. The complex thus formed with mRNA and fMet-tRNA bound to both subunits of mitoribosome is the initiation complex. It is the product of the initiation subset and will be the input in the elongation subset (Fig. 5.1).

The final complex derived from the initiation phase has both subunits of ribosome, mRNA and fMet-tRNA positioned at the P-site in mitoribosome. Since the final complex does not include either of the initiation factors, it can be concluded that mtIF3 and mtIF2 act as catalysts. They enable a series of reactions in a sequential manner, so as to form the initiation complex with all the aforesaid components placed in the correct position and orientation. The initiation complex, thus formed, can be carried over to the next phase, i.e. elongation. The first four reactions as shown in Fig. 5.1 are reversible. However, GTP hydrolysis in the last step makes the reaction irreversible, and the conformation of the initiation complex is locked, preventing the system from reverting. Stepwise sequential progression allows mRNA and fMet-tRNA to align correctly at the P-site and mtIF3 further checks the premature binding of components in each step. It is evident that the process exhibits several checks to ensure correct position and orientation of all the components of the final initiation complex.

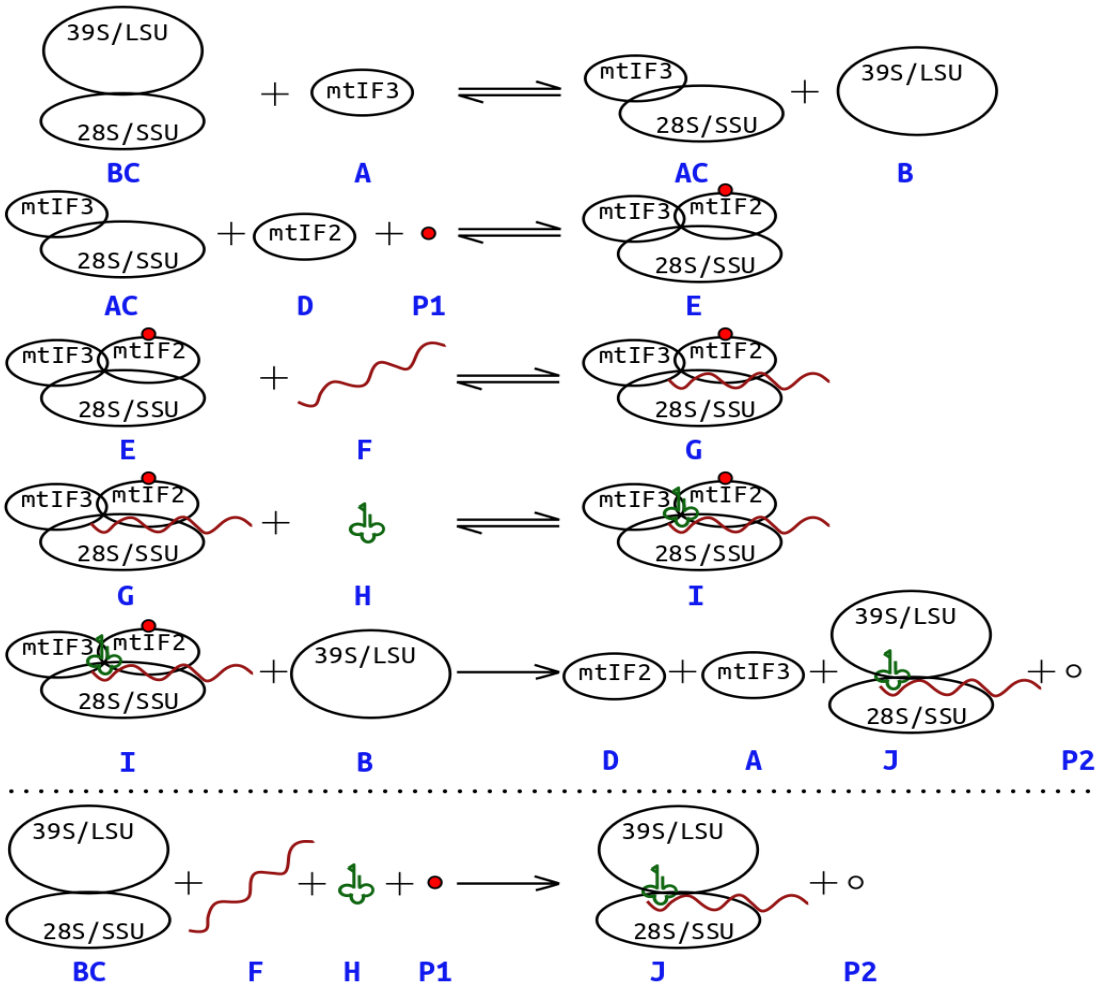

Figure 5.1: Pictorial representation of mitochondrial translation initiation: mtIF3: (A) mitochondrial initiation factor 3, LSU (B) and SSU (C) are the two subunits of mitoribosome (BC), mtIF2: (D) mitochondrial initiation factor 2 (may be bound to GTP (red solid circle-P1) or GDP (hollow circle-P2)), F: mRNA, H: aminoacyl-tRNA. mtIF3 catalyses the dissociation of mitoribosome to LSU and SSU, and it remains bound to SSU (AC). GTP-bound mtIF2 binds to this complex (AC), giving complex E. Complex E next binds to the mRNA (F) and leads to appropriate positioning of mRNA (G). The first aminoacyl-tRNA is fMet-tRNA, which binds to this complex (G). LSU (B) next triggers the hydrolysis of GTP-bound mtIF2 in complex I and mtIF2 (D': GDP-bound mtIF2) is released from the complex. LSU binds to the complex and simultaneously A is released, and J is formed. The initiation complex (J) is the input for the next step of translation, i.e., elongation. Here the first four steps are reversible, while the last step is irreversible, since it is accompanied by GTP hydrolysis. This step locks the conformation after J complex is formed, and the process cannot revert after this step. The components as D, F and H enters the system only when a particular complex (AC, E and G respectively) is formed and not prior to that. The overall reaction is represented in the end (below the dotted line). The initiation factors and other intermediate complexes are not seen in the overall reaction, suggesting that they act only as catalysts. The whole process of assembly proceeds in a desired sequential manner. All the components of final J complex are incorporated in the correct orientation, which would not have been possible if the components were mixed randomly in a reaction pool to react.

Simulation

The reactions shown in Fig. 5.1 were simulated using ode solver in Octave. The initial concentrations for mtIF3, mitoribosome, mRNA, mtIF2 and fMet-tRNA (A, BC, F, D and H) were given as 1. All the other species seen in the figure were eventually formed in the system, and hence their initial concentrations were kept as 0. The first four reactions facilitate the correct positioning of the various components of the final initiation complex. These four reactions are reversible and therefore the rate equations included both forward and backward reactions. For the fifth reaction, the rate equation includes only the forward reaction. As mentioned earlier, GTP and GDP were not included in the rate equations. They are assumed to be present in bulk (comparatively high concentrations) and therefore a small change in their concentrations will not affect the rate of the reaction. In Fig. 5.1 the last reaction drawn below the dotted line, J is the initiation complex which is carried forward in the next set of reactions, i.e., elongation.

Rate Equations

Rate equations used for simulation of mitochondrial translation initiation are given in Table 5.3. A given complex with multiple components is shown in square brackets.

Table 5.3: Rate equations used for simulation of mitochondrial translation initiation. Multiple components present in a single complex are enclosed by square brackets.

$\frac{d}{dt}[mtIF3] = -[mtIF3].[39S+28S]+[mtIF3+28S].[39S]+[mtIF3+28S+mRNA+mtIF2+tRNA-met].[39S]$
$\frac{d}{dt}[39S+28S] = -[mtIF3].[39S+28S]+[mtIF3+28S].[39S]$
$\frac{d}{dt}[mtIF3+28S] = [mtIF3].[39S+28S]-[mtIF3+28S].[39S]-[mtIF3+28S].[mtIF2]+[mtIF3+28S+mtIF2]$
$\frac{d}{dt}[39S] = [mtIF3].[39S+28S]-[mtIF3+28S].[39S]-[mtIF3+28S+mRNA+mtIF2+tRNA-met].[39S]$
$\frac{d}{dt}[mtIF2] = -[mtIF3+28S].[mtIF2]+[mtIF3+28S+mtIF2]+[mtIF3+28S+mRNA+mtIF2+tRNA-met].[39S]$
$\frac{d}{dt}[mtIF3+28S+mtIF2] = [mtIF3+28S].[mtIF2]-[mtIF3+28S+mtIF2].[mRNA]-[mtIF3+28S+mtIF2]+[mtIF3+28S+mtIF2+mRNA]$
$\frac{d}{dt}[mRNA] = -[mtIF3+28S+mtIF2].[mRNA]+[mtIF3+28S+mtIF2+mRNA]$
$\frac{d}{dt}[mtIF3+28S+mtIF2+mRNA] = [mtIF3+28S+mtIF2].[mRNA]-[mtIF3+28S+mtIF2+mRNA].[tRNA-met]-[mtIF3+28S+mtIF2+mRNA]+[mtIF3+28S+mRNA+mtIF2+tRNA-met]$

$$\frac{d}{dt}[tRNA-met] = -[mtIF3+28S+mtIF2+mRNA].[tRNA-met]+[mtIF3+28S+mRNA+mtIF2+tRNA-met]$$

$$\frac{d}{dt}[mtIF3+28S+mRNA+mtIF2+tRNA-met] = [mtIF3+28S+mtIF2+mRNA].[tRNA-met] - [mtIF3+28S+mRNA+mtIF2+tRNA-met].[39S] - [mtIF3+28S+mRNA+mtIF2+tRNA-met]$$

$$\frac{d}{dt}[28S+39S+mRNA+tRNA-met] = [mtIF3+28S+mRNA+mtIF2+tRNA-met].[39S]$$

Script

Table 5.4 shows the script used for simulation of mitochondrial translation initiation phase. It uses the rate equations given in the previous section and simulates using ode solver.

Table 5.4: Script used for simulation of mitochondrial translation initiation.

```
1;
% solve the initiation of mitochondrial translation
function ds=mtini(s)
% 1=mtIF3; 2=39S+28S; 3=mtIF3+28S; 4=39S;
5=mtIF2;6=mtIF3+28S+mtIF2;7=mRNA;
%  8=mtIF3+28S+mtIF2+mRNA;9=tRNA-met;  10=mtIF3+28S+mRNA+mtIF2+tRNA-
met;
% 11=28S+39S+mRNA+tRNA-met
% the rate equations for mito translation initiation reactions
follow:

ds(1) =-s(1)*s(2)+s(3)*s(4)+s(10)*s(4);
ds(2) =-s(1)*s(2)+s(3)*s(4);
ds(3) = s(1)*s(2)-s(3)*s(4)-s(3)*s(5)+s(6);
ds(4) = s(1)*s(2)-s(3)*s(4)-s(10)*s(4);
ds(5) =-s(3)*s(5)+s(6)+s(10)*s(4);
ds(6) = s(3)*s(5)-s(6)-s(6)*s(7)+s(8);
ds(7) =-s(6)*s(7)+s(8);
ds(8) = s(6)*s(7)-s(8)-s(8)*s(9)+s(10);
ds(9) =-s(8)*s(9)+s(10);
ds(10)= s(8)*s(9)-s(10)-s(10)*s(4);
ds(11)= s(10)*s(4);
return
end

% use lsode to solve this set...
lsode_options("relative tolerance",1e-4);
lsode_options("absolute tolerance",1e-3);
t=0:0.2:200;
ds=zeros(11,1);
% supply the initial concentrations ...
s0=[1, 1, 0, 0, 1, 0, 1, 0, 1, 0, 0];
%   0  0  0  0  0  0  0  0  0  1  1
%   1  2  3  4  5  6  7  8  9  0  1
```

```
[s,T,MSG]=lsode(@mtini,s0,t);
T
MSG
plot(t,s(:,1),"linewidth",5,t,s(:,2),"linewidth",5,t,s(:,7),"linewid
th",5,t,s(:,5),"linewidth",5,t,s(:,9),"linewidth",5,t,s(:,11),"linew
idth",5);
grid on;
set (gca,'FontSize', 20);
set (gca, 'FontName', 'Times');
axis([0,100,.001,1.01]);
xlabel ("Time/arbitrary units");
ylabel ("Concentration/arbitrary units");
set (gca,'FontSize', 20);
set( get(gcf,'children'), 'linewidth',4 );
legend("mtIF3","ribo","mRNA","mtIF2","fMet-tRNA","ini
comp","location","northeast");
```

Result

Fig. 5.2 shows the simulation curves obtained using the script given in the previous section. In this phase the two mitochondrial translation initiation factors, mtIF3 and mtIF2, sequentially bind to the mitoribosome and assist in the formation of the final initiation complex. The progress curves for selected components are shown. It can be seen that the concentrations of mitoribosome, mRNA and fMet-tRNA falls indicating the decrease in the concentration of their free species in the mitochondrial matrix. Since these components are now in a bound state in the system (complexes seen in Fig. 5.1), and therefore, no more exhibit their native state.

Concentrations of both the initiation factors fall initially indicating their binding to the ribosome subunit, i.e., they are not available as free species in the system. However, since these components are released in the subsequent reactions, their concentrations rise again towards the end of the process. Also, it can be seen that not all the initiation factors are released, indicating some residual binding to the intermediate complexes which could not complete the whole process. The concentration of the initiation complex rises indicating its formation, and a small lag phase can be seen early in the graph, indicating the time taken for execution of the first four preparatory reactions. The reduced concentrations of mitoribosome, mRNA and fMet-tRNA towards the end of the process here indicate that they are now bound together in the initiation complex.

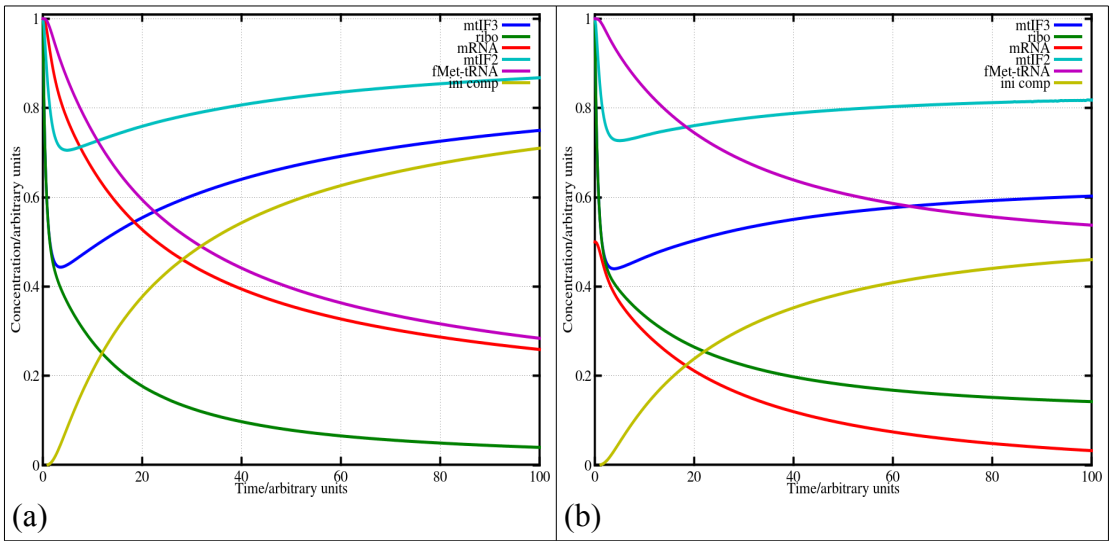

Figure 5.2: Simulation curves for mitochondrial translation initiation; (a) with mRNA initial concentration 1; (b) with mRNA initial concentration 0.5. ribo: 55S mitoribosome; ini comp: initiation complex made up of 55S mitoribosome, mRNA and fMet-tRNA positioned at the P-site. The shift in the position of the curve, obtained by changing the initial concentration of mRNA, indicates the impact of mRNA on their concentration. With the decrease in initial concentration of mRNA, the final concentrations of initiation factors, mtIF2 and mtIF3, and initiation complex decreases, whereas the concentrations of ribosome and fMet-tRNA increase.

It can be seen that in Fig. 5.2a, after 100 arbitrary time units, 95% of ribosome remains in the bound state, whereas only 75% of mRNA is in the bound state. This essentially indicates that in steady-state, approximately 75% of ribosomes are bound to mRNA and 5% of ribosomes are free. The rest of 20% of ribosomes exist in form of intermediates AC, B and E (see Fig. 5.1). These ratios will change if the availability of any of the system component is altered; an example is shown in Fig. 5.2b, where the initial concentration of mRNA is halved (0.5 instead of 1), the concentrations of the various components change accordingly. Since a lesser concentration of mRNA is used keeping all the concentrations of all the other components same, the final concentration of mRNA is lower as compared to Fig. 5.2a.

Elongation

Initiation is followed by elongation, which is a set of repetitive events. The triplet codons following the start codon in mRNA are read one at a time, and corresponding aminoacyl-tRNA (aa-tRNA) carrying the appropriate amino acid is incorporated at the A-site. This is followed by peptide bond formation between the previous amino acid at the P-site and the one at the A-site, thus elongating the peptide chain. Specific elongation factors are recruited in a cyclic fashion to facilitate the whole process of elongation. Mitochondrial elongation factor Tu, mtEFTu, is the first factor involved directly in the process. Its activated form (carrying GTP) binds to aa-tRNA to form mtEFTu ternary complex (mtEFTu-GTP-aa-tRNA) (Cai, Bullard, Thompson, & Spremulli, 2000). This ternary complex is responsible for carrying aa-tRNA to the A-site and wait for codon-anticodon interaction. Here the triplet codon at the A-site is decoded, and if the amino acid on the aa-tRNA corresponds to this codon, then codon-anticodon interaction takes place. In the absence of codon-anticodon interaction, this ternary complex leaves mitoribosome and another mtEFTu complex bound with another aa-tRNA enters the A-site.

Since there are 22 different tRNAs in the mitochondrial matrix, there will be 22 such mtEFTu-GTP-aa-tRNA complexes, each with a different amino acid bound to it. This process continues till cognate codon-anticodon interaction takes place. Following successful codon-anticodon interaction, mtEFTu hydrolyses GTP to GDP, and this reaction becomes irreversible and the aa-tRNA is locked within ribosome. This step releases mtEFTu now bound to GDP, which binds to another elongation factor, mtEFTs to form mtEFTu-mtEFTs complex. mtEFTs facilitates

exchange of GDP to GTP releasing GTP-bound mtEFTu, which can be used further in the next round of elongation (Schwartzbach & Spremulli, 1989). aa-tRNA cannot enter mitoribosome complex on its own and needs mtEFTu as a carrier. aa-tRNA preferably binds to GTP-bound mtEFTu rather than GDP-bound mtEFTu or just mtEFTu. Therefore, the concentration of mtEFTu-GTP also controls the rate of translation. Alternatively, the activity of mtEFTs in converting mtEFTu-GDP to mtEFTu-GTP (so that it can bind and carry aa-tRNA to mitoribosome complex) regulates the process of translational elongation.

The complex formed after successful codon-anticodon interaction now consists of fMet-tRNA at P-site and aa-tRNA corresponding to the next codon in the mRNA at the A-site. The next step is the formation of the peptide bond between the amino acids present on the two aforementioned tRNAs. Formation of the peptide bond between the amino acid bound to tRNA at A-site and amino acid bound to initiator tRNA (fMet-tRNA) is catalysed by mitoribosome itself. This reaction takes place in the peptidyl transferase centre (PTC) inside ribosome and leaves deacylated-tRNA (deacyl-tRNA) at the P-site and peptidyl-tRNA which is one amino acid longer at the A-site (Polacek & Mankin, 2005).

Another mitochondrial growth factor, mtEFG1, mitochondrial elongation factor G1, bound with GTP catalyses translocation step. It removes deacyl-tRNA from the P-site and peptidyl-tRNA moves from the A-site to the P-site in GTP-dependent reaction (Bhargava, Templeton, & Spremulli, 2004). This step leaves A-site vacant for the entry of next aa-tRNA. With the translocation of peptidyl-tRNA from A-site to P-site, mRNA also moves by one codon.

Another mtEFTu-GTP-bound to appropriate aa-tRNA (corresponding to the codon at the A-site) enters at the A-site to continue elongation. This translocation, to occupy the P-site along with the movement of mRNA, is very crucial to maintain the unidirectional reading so that the next triplet is read instead of the previous one. In the process of incorporation of one amino acid to the growing peptide chain, two GTPs are hydrolysed (from mtEFTu and mtEFG1).

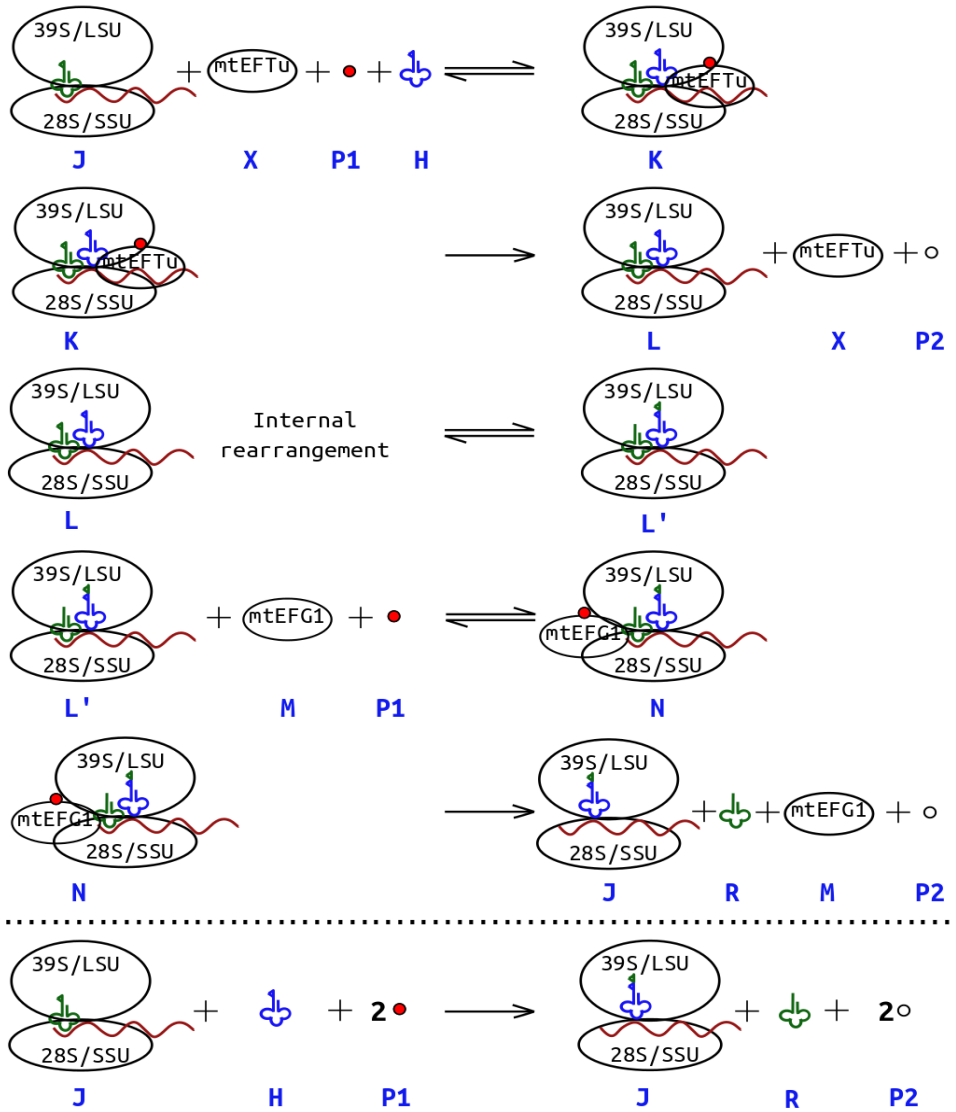

Figure 5.3: Pictorial representation of mitochondrial translation elongation: J complex (LSU+SSU+mRNA+fMet-tRNA) is derived from the initiation subset (Fig. 5.1). mtEFTu: (X) mitochondrial elongation factor Tu. mtEFTu (X) binds to GTP (P1) first and then to aminoacyl-tRNA (H) and carries it to the J complex. The J complex interacts with X to produce K, which after successful codon-anticodon interaction, releases mtEFTu via an irreversible reaction (accompanied by GTP hydrolysis). The main product of this reaction is complex L, and mtEFTu is released along with GDP. There are 22 variants of H and EFTu carrying tRNA. The next step is the internal rearrangement, which takes place at peptidyl transferase centre in mitoribosome. Here, amino acid (or peptide chain) from the tRNA at P-site shifts to the aa-tRNA on the A-site to form L' complex. GTP-bound mtEFG1 (M) binds to L' complex to give rise to N. Complex N dissociates to release deacyl-tRNA (R), GDP-bound mtEFG1 and thus forming complex J'. The complex J' has the A-site tRNA now shifted to the P-site. This has the same conformational form like J and can continue in the cycle. The overall reaction (shown below the dotted line) shows that J complex reacts with aa-tRNA to release deacyl-tRNA, forming complex J'. J' is further renamed as J, so that it can enter the loop to repeat the addition of amino acids in the growing polypeptide chain. In this process, the two tRNAs have been exchanged and the tRNA now present in the ribosome carries an extra amino acid in the growing polypeptide chain.

The GTPs used in the system can be attributed various functions simultaneously. They are used to form strong interactions as the slipping of components from the complex is not desired. The molecular interactions may be weak otherwise and might compromise the efficiency of the system. Since the molecular interactions in such processes decide the fate of the complex, the bindings should be strong enough so as to avoid escape. Moreover, covalent bonds are not preferred, since they might block further progression of the complex. Also, reaction accompanied by GTP hydrolysis becomes irreversible, thus locking the conformation so that the system cannot revert from that point. These steps involving GTP hydrolysis appear as checkpoints in the process. A careful look at the steps, where GTP hydrolysis is involved, indicates that it is only when the correct conformation is achieved, GTP is hydrolysed (Fig. 5.3). This set of reactions continues till A-site encounters a stop codon, where the system enters the termination phase (Fig. 5.6).

Simulation

Simulation of elongation was done using two methods, the ode solver method and the Monte Carlo simulation. The ode solver method used the rate equations obtained using the reactions mentioned in Fig. 5.3. The first reaction, binding of mtEFTu-GTP-aa-tRNA to the initiation complex is a reversible reaction, and so both forward and reverse reaction rates were taken into account while deriving rate equations. The next reaction is codon-anticodon interaction, which releases mtEFTu-GDP, is accompanied by GTP hydrolysis. It is an irreversible reaction, and rate equations were written accordingly. The internal rearrangement step was not included in the simulation as there are no external factors involved, and the process is self-driven. The fourth reaction is the binding of mtEFG1-GTP and is also a reversible reaction. The last reaction is the translocation step which is facilitated by mtEFG1, accompanied by GTP hydrolysis and is an irreversible step.

Formation of J in the last step of the elongation phase allows the system to repeat the set of reactions where J enters again in the first reaction. The complex formed in the last step has been considered equivalent to the J that is used in the first reaction It is because the former (J') has peptidyl-tRNA at P-site now, instead of fMet-tRNA in the latter (J in the initiation subset). The only difference between J' and J is an added amino acid to tRNA at P-site and mRNA moved forward by one triplet codon. Also, eventually the J formed in the last step has to enter the same loop again until a stop codon enters the A-site. So for all practical purposes the two species can be considered equivalent.

The initiation complex and the elongation factors are given as input in the system with their initial concentration kept at 1. An unlimited supply of aa-tRNA was provided in the script, which implied a constant increase in concentration of deacyl-tRNA. All the other intermediates and products were kept at an initial concentration 0.

Monte Carlo simulation

Monte Carlo method solves a problem by generating suitable random numbers and observing that fraction of the numbers obeying some property or properties. It is useful for obtaining numerical solutions to problems which are too complicated to solve analytically (Wolfram). In the present system, this approach of random number generation was used to simulate the codon-anticodon interaction scheme, where a number of aa-tRNAs carried by mtEFTu enter A-site individually to look for successful codon-anticodon interaction.

In the simulation script here, the mRNA sequence translating to protein sequence of *MTND4L* (Table 5.1) was simulated. This mRNA consists of 297 nucleotide bases corresponding to 98 amino acids and a stop codon in the end. The mRNA sequence taken from ENSEMBL database (www.ensembl.org) is given below:

"AUGCCCCUCAUUUACAUAAAUAUUAUACUAGCAUUUACCAUCUCACUUC
UAGGAAUACUAGUAUAUCGCUCACACCUCAUAUCCUCCCUACUAUGCCUA
GAAGGAAUAAUACUAUCGCUGUUCAUUAUAGCUACUCUCAUAACCCUCAA
CACCCACUCCCUCUUAGCCAAUAUUGUGCCUAUUGCCAUACUAGUCUUUG
CCGCCUGCGAAGCAGCGGUGGGCCUAGCCCUACUAGUCUCAAUCUCCAAC
ACAUAUGGCCUAGACUACGUACAUAACCUAAACCUACUCCAAUGCUAA".

In the script, mRNA is read three nucleotide bases, i.e. one triplet codon at a time, and this codon is checked against a table of corresponding aminoacyl-tRNA. The table identifies the correct tRNA codon based on the mRNA codon, which is then included in the growing peptide chain. The selection of tRNA to be checked with the mRNA codon placed at the A-site is done using a random number algorithm. If the selected tRNA matches with the mRNA codon present at A-site, it enters, and the amino acid is subsequently added to the growing polypeptide chain. If the selected tRNA do not match, it is rejected, and a new tRNA is selected. Despite the outcome of the match, be it successful or unsuccessful, it utilises some time in the biological system. Also, in the script, one time unit is consumed for each trial by the selected tRNA. All the amino acids may not take the same time for elongation, and it depends on their chance selection.

In the present study, all 22 distinct tRNAs (including the start codon) have been considered as having same initial concentration, which may not be the case in the biological system. At the A-site of the ribosome, all the 22 aa-tRNAs are potential candidates for binding. Based on the codon-anticodon interaction, only one of the 22 aa-tRNAs will be considered to be an appropriate match, whereas the remaining tRNAs act as potential inhibitors. This presents a case of competitive inhibition, so this will reduce the K_M. This aspect is considered in Monte Carlo simulation where a random tRNA taken out of the pool of 22 tRNAs is selected, evaluated and accepted/rejected based on mRNA codon at A-site. However, in the biological system the tRNAs are present in unequal concentrations and therefore translation proceeds with a non-uniform rate of incorporation of amino acids to the growing polypeptide chain.

Rate Equations

Table 5.5 shows the rate equations derived from the reactions shown in Fig. 5.3. These rate equations were used to simulate mitochondrial translation elongation by using the ode solver method.

Table 5.5: Rate equations for simulation of mitochondrial translation elongation.

$\frac{d}{dt}[28S+39S+mRNA+tRNA-met] = -[28S+39S+mRNA+tRNA-met].[mtEFTu].[aatRNA]$ $+[28S+39S+mRNA+tRNA-met+mtEFTu+aatRNA]+[28S+39S+mRNA+tRNA-met+aatRNA+EFG1]$
$\frac{d}{dt}[mtEFTu] = -[28S+39S+mRNA+tRNA-met].[mtEFTu].[aatRNA]+[28S+39S+mRNA+tRNA-met+mtEFTu+aatRNA]$ $+[28S+39S+mRNA+tRNA-met+aatRNA+EFG1]$
$\frac{d}{dt}[28S+39S+mRNA+tRNA-met+mtEFTu+aatRNA] = [28S+39S+mRNA+tRNA-met].[mtEFTu].[aatRNA]$ $-[28S+39S+mRNA+tRNA-met+mtEFTu+aatRNA]-[28S+39S+mRNA+tRNA-met+aatRNA+EFG1]$
$\frac{d}{dt}[28S+39S+mRNA+tRNA-met+aatRNA] = -[28S+39S+mRNA+tRNA-met+aatRNA].[mtEFG1]$ $+[28S+39S+mRNA+tRNA-met+aatRNA+EFG1]+[28S+39S+mRNA+tRNA-met+mtEFTu+aatRNA]$
$\frac{d}{dt}[mtEFG1] = -[28S+39S+mRNA+tRNA-met+aatRNA].[mtEFG1]+[28S+39S+mRNA+tRNA-met+aatRNA+EFG1]$ $+[28S+39S+mRNA+tRNA-met+aatRNA+EFG1]$
$\frac{d}{dt}[28S+39S+mRNA+tRNA-met+aatRNA+EFG1] = -[28S+39S+mRNA+tRNA-met+aatRNA+EFG1]$ $-[28S+39S+mRNA+tRNA-met+aatRNA+EFG1]+[28S+39S+mRNA+tRNA-met+aatRNA].[mtEFG1]$
$\frac{d}{dt}[28S,39S,mRNA,tRNAaa+met] = [28S+39S+mRNA+tRNA-met+aatRNA+EFG1]$
$\frac{d}{dt}[deacyltRNA] = [28S+39S+mRNA+tRNA-met+aatRNA+EFG1]$
$\frac{d}{dt}[aatRNA] = [28S+39S+mRNA+tRNA-met+aatRNA+EFG1]$

Script

The scripts used for simulation of mitochondrial translation elongation are given in Table 5.6. Two methods were used for simulation of this complicated process.

The script below uses the rate equations mentioned above and simulates them using ode solver in Octave.

Table 5.6: Script used for simulating mitochondrial translation elongation using the ode solver method.

```
1;
% solve the elongation of mitochondrial translation
function ds=mtelo(s)

% 1-(28S+39S+mRNA+tRNA-met=J), 2-mtEFTu,
% 3-28S+39S+mRNA+tRNA-met+mtEFTu+aatRNA
% 4-28S+39S+mRNA+tRNA-met+aatRNA, 5-mtEFG1,
% 6-28S+39S+mRNA+tRNA-met+aatRNA+EFG1,
% 7-(28S,39S,mRNA,tRNAaa+met)-elo comp,
% 8-deacyl tRNA, 9-aatRNA

% Equations for mitochondrial translation elongation reactions
% the rate equations follow:

ds=zeros(9,1);

ds(1)= -s(1)*s(2)*s(9)+s(3)+s(6);
ds(2)= -s(1)*s(2)*s(9)+s(3)+s(3);
ds(3)=  s(1)*s(2)*s(9)-s(3)-s(3);
ds(4)=  s(3)-s(4)*s(5)+s(6);
ds(5)= -s(4)*s(5)+s(6)+s(6);
ds(6)=  s(4)*s(5)-s(6)-s(6);
% ds(7)=  s(6);
ds(7)=0;
ds(8)=  s(6);
ds(9)=  0;

return
end

% use lsode to solve this set...
lsode_options("relative tolerance",1e-4);
lsode_options("absolute tolerance",1e-3);
t=0:0.2:100;

% supply the initial concentrations ...
s0=[  1, 1, 0, 0, 1, 0, 0, 0, 1];
%     0  0  0  0  0  0  0  0  0
```

```
%     1   2   3   4   5   6   7   8   9
[s,T,MSG]=lsode(@mtelo,s0,t);
T
MSG
plot(t,s(:,1),"linewidth",5,t,s(:,2),"linewidth",5,t,s(:,8),"linewid
th",5);
grid on;
set (gca, 'FontName', 'Times');
set (gca,'FontSize', 20);
axis([0,100,.001,1.2]);
% title ("mito trans elo");
xlabel ("Time/arbitrary units");
ylabel ("Concentration/arbitrary units");
set (gca,'FontSize', 20);
set( get(gcf,'children'), 'linewidth',4 );
legend("ini comp","mtEFTu","tRNA", "location", "northeast");
```

The screenshot below shows the steps used to reset the concentration of deacyl-tRNA to zero after successful incorporation of each amino acid to the growing polypeptide chain.

```
octave:16> elo
T =  2
MSG = successful exit
octave:17> size (s(:,8))
ans =

   501     1

octave:18> for i=1:501
> s(i,8)=mod(s(i,8),1);
> endfor
octave:19> plot(t,s(:,1),"linewidth",5,t,s(:,2),"linewidth",5,t,s(:,8),"linewidt
h",5);
```

The script given in Table 5.7 was used to incorporate the randomness using Monte Carlo simulation for simulating mitochondrial elongation, where a random number generator was used. The 22 tRNAs formed by the mitochondrial genome coding for 20 amino acids were included in the script.

Table 5.7: Script used for Monte Carlo simulation of mitochondrial translation elongation.

```
1;
% the amino acid pool concentration is allowed to decrease as each amino acid is used up in the
synthesis.
% there must be sufficient number of aa to start with for the translation to be successful
% the total number of amino acids initially present is naa; same for all
% the 22 aa (excluding stop codon) after each amino acid is used up the number is reduced by 1.
trna = ["AAR";"AAY";"ACN";"AGY";"UCN";"AUR";"AUY";"CAR";"CAY";"CCN";"CGN";\
"CUN";"UUR";"GAR";"GAY";"GCN";"GGN";"GUN";"UAY";"UGR";"UGY";"UUY";"UAR"];
```

```
% the last tRNA is not a tRNA, it is a stop codon.
aa = ["K";"N";"T";"S";"S";"M";"I";"Q";"H";"P";"R";"L";"L";
"E";"D";"A";"G";"V";"Y";"W";"C";"F";""];
% last amino acid is null; corresponding to the stop codon. There are duplicates as they have multiple
tRNAs.
resno=0;
time=1;
naa=50; % the number of amino acids present to start with...
mrna = \
"AUGCCCCUCAUUUACAUAAAUAUUAUACUAGCAUUUACCAUCUCACUUCUAGGAAU\
ACUAGUAUAUCGCUCACACCUCAUAUCCUCCCUACUAUGCCUAGAAGGAAUAAUACU\
AUCGCUGUUCAUUAUAGCUACUCUCAUAACCCUCAACACCCACUCCCUCUUAGCCAA\
UAUUGUGCCUAUUGCCAUACUAGUCUUUGCCGCCUGCGAAGCAGCGGUGGGCCUAGC\
CCUACUAGUCUCAAUCUCCAACACAUAUGGCCUAGACUACGUACAUAACCUAAACCU\
ACUCCAAUGCUAA";
% this mRNA sequence is taken from ensembl database.
function codonmatch = matches (x,y)
% x is trna codon; y is mrna codon; the order should be preserved. Multiple mrna codons can
correspond to one trna codon.
codonmatch=0;
        if (x(1) != y(1)) return; endif
        if (x(2) != y(2)) return; endif
        if ((x(3) == y(3)) | (x(3)=='R' & y(3)=='A') | (x(3)=='R' & y(3)=='G') |
        (x(3)=='Y' & y(3)=='C') |(x(3)=='Y' & y(3)=='U') | (x(3)=='N')) codonmatch = 1;
        % printf ("x(1) is %c, x(2) is %c, x(3) is %c\n", x(1), x(2), x(3));
        return;
        endif
endfunction
% main prog begins here...
d="";
protseq=fopen('p5.txt','w');
tot_aa=linspace(1,23,23);
cum=linspace(1,23,23);
% initialises the tot_aa array with naa at each position...
i=1;
        while (i<24) tot_aa(i)=naa; i=i+1; endwhile
% compute the cumulative total till 23:
        while(1)
        d=mrna(resno*3+1:resno*3+3);
                if (matches ("UAR",d) == 1) break; endif
                while(1)
                cum(1)=0; i=2;
                        while(i<24) cum(i)=cum(i-1)+tot_aa(i-1); i=i+1; endwhile
                max_no=cum(23);
                number=unidrnd(max_no);
                i=1;
                        while(!((number>cum(i)) & (number<=cum(i+1)))) i=i+1; endwhile
                number=i;
                c=trna(number,:);
                time=time+1;
                a = matches (c,d);
```

```
                % printf ("The string x=%s and y=%s matches %d\n", d,c,a)
                        if (a==1) resno=resno+1;
                        tot_aa(number)=tot_aa(number)-1;
                        var=number;
                                if (number>=4) var=number-1; endif
                                if (number>=12) var=number-2; endif
                        fprintf(protseq, "%d aa %c %d\n", time,aa(number),var+1);
                        break;
                        endif
                endwhile
                %printf ("Residue: %s at time: %d \n",c,time);
        endwhile
fclose(protseq)
```

Result

Mitochondrial translation elongation is an extensive process and was simulated using two methods to account for the random repetitive process. One method used the ode solver, and the other used the Monte Carlo simulation. Both the results are presented here in Figs. 5.4 and 5.5.

Fig. 5.4 is the outcome of the script given in Table 5.6 in the scripts section. Here the rate equations given in Table 5.5 were simulated using ode solver in Octave. With the addition of each amino acid to the growing polypeptide chain, one deacyl-tRNA was formed and in the script it was reset to zero after each cycle (red curve). This indicates the successful incorporation of one amino acid to the growing polypeptide chain. So in Fig. 5.4, it shows incorporation of 14 amino acids to the polypeptide chain. Other component shown in the figure is the initiation complex which is utilised in the reaction system. The mitochondrial elongation factor Tu, mtEFTu, is used initially and is regenerated as the reaction proceeds and acts as a catalyst in the system.

Monte Carlo simulation was used to incorporate the randomness of the biological system in the model. An important feature of elongation step is codon-anticodon interaction. In the mitochondrial matrix, several aminoacyl-tRNAs are present at a given time. The binding of the correct aminoacyl-tRNA at the A-site is subject to its chance interaction with the codon present at the A-site. At any given point in time, all types of aminoacyl-tRNAs can access the A-site codon. However only the correct match will lead to codon-anticodon interaction and can be called as successful encounter. However, there can be several unsuccessful encounters preceding the desired successful encounter. It is important to take the time utilised in those unsuccessful encounters, and this was achieved by Monte Carlo simulation.

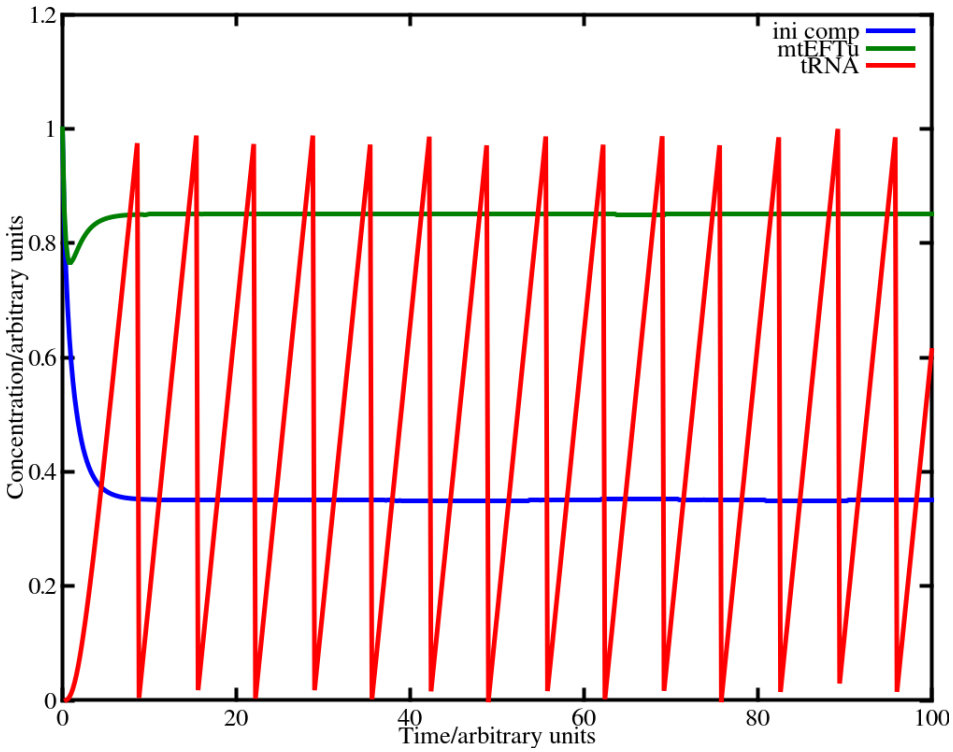

Figure 5.4: Simulation curves for mitochondrial translation elongation. Ini comp: initiation complex derived from initiation subset containing fMet-tRNA, 55S ribosome and mRNA template (Fig. 5.1). The curve for tRNA represents the incorporation of amino acid in the growing polypeptide chain, and this value is reset at the end of one cycle of elongation. This plot shows incorporation of 12 amino acids into the chain, and the process is incomplete. mtEFTu: mitochondrial elongation factor Tu curve shows that a large amount of it is present in the bound form in the steady-state condition. Initiation complex (blue curve) initially starts with unit concentration but rapidly reaches steady-state concentration of 0.3, the remaining amount being present in the elongation loop complexes (see Fig. 5.3: Complexes K, L, L' and N).

In Monte Carlo simulation, an individual tRNA is selected by a random number algorithm and tested for codon-anticodon match. The amino acid is accepted and incorporated only after a successful match. The results show the translation for mRNA sequence of *mtND4L*. Fig. 5.5 shows the time taken for the incorporation of each amino acid (the width of the bar) and the progress in the formation of complete peptide. The height of the bar indicates the respective amino acid shown in the y1 axis. The green line shows the cumulative addition of amino acid and the total time taken for the incorporation of 98 amino acids.

The process was randomised and the time taken for a successful interaction was based on chance. The initial amino acid concentration was same for all the aminoacids, but was decreasing in the system depending on utilisation. The initial concentration of all the aa-tRNA was kept as 50, and after each successful codon-anticodon interaction, when the amino acid from aa-tRNA is incorporated to the growing peptide chain, the count of that particular amino acid decreased by one. Every time an aa-tRNA tries to match with the codon at the A-site, irrespective of the outcome of the match, be it successful or unsuccessful, it was made to consume one time unit. The four figures shown in Fig. 5.5 were generated using the same script. Every time the script was run a different graph was produced. This essentially indicates that the generation of a particular peptide chain in the biological system does not necessarily take exactly same time, and this would depend on the availability of amino acids to be incorporated.

Here the time taken for four sets of simulation is 2263, 2342, 2445 and 2269 time units for (a), (b), (c) and (d) respectively. However, the average time for incorporation of each amino acid is 23.1, 23.9, 24.9 and 23.1 time units, which are quite similar in all the cases.

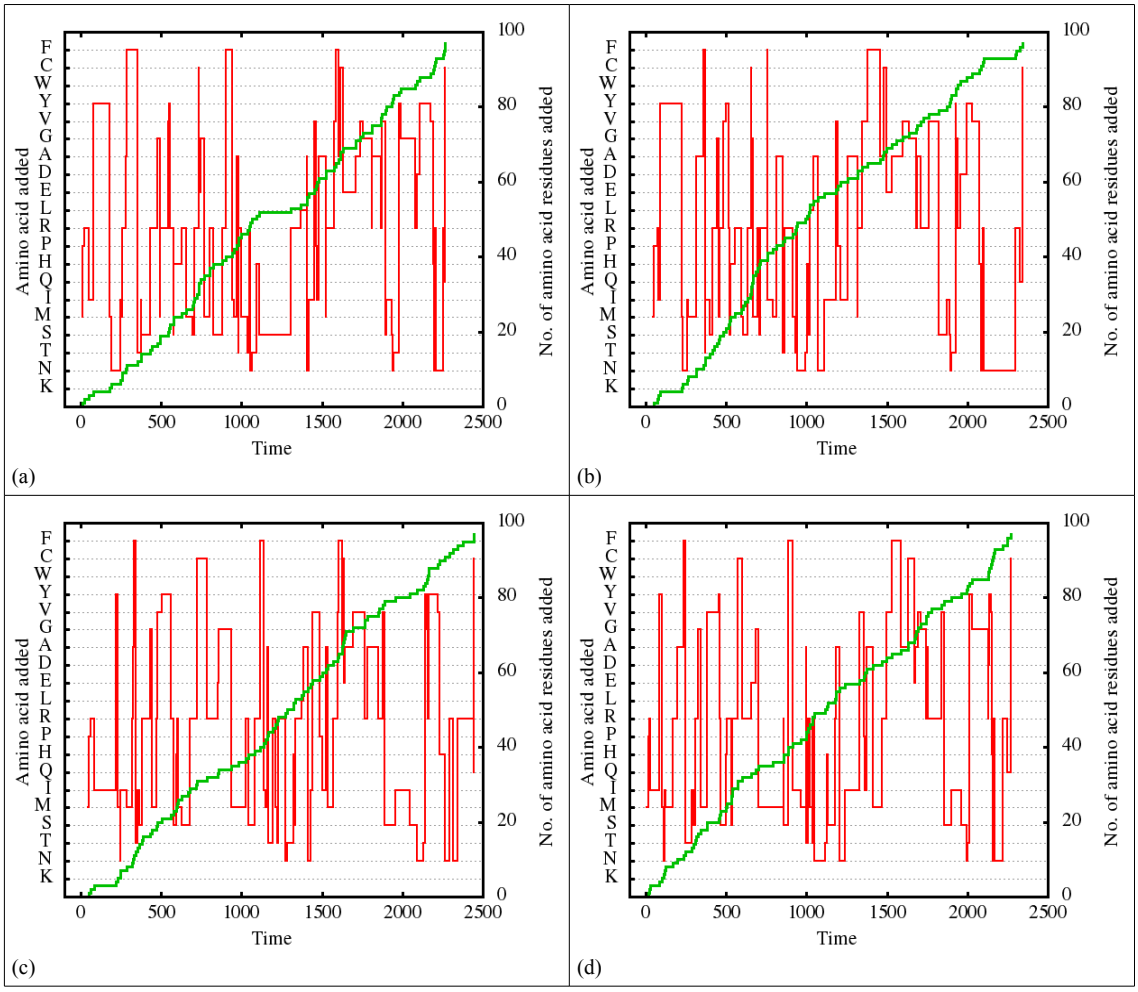

Figure 5.5: The Monte Carlo simulation of the protein synthesis process. These four figures correspond to peptide elongation process from the same mRNA. The initial concentrations of the 20 amino acids in the system were kept constant for all the figures, but were allowed to decrease as the elongation process progresses. This signifies that each time the same mRNA is translated, the time taken for the incorporation of any given amino acid is not constant, considering the randomness of the system. Each aminoacyl-tRNA is a potential candidate for a binding at the A-site of the ribosome, but the success or failure is ultimately decided by the codon-anticodon match. It has been assumed that all unsuccessful binding of the aminoacyl-tRNA takes the same time to be terminated, and the process continues till successful codon-anticodon match is obtained. Here, each horizontal break in the graph signifies one amino acid addition to the growing polypeptide chain. Therefore, we see 98 such breaks in all the four graphs. However, each horizontal break is of different width suggesting that multiple tRNAs need to be tried to locate the "matching one". All the four graphs produce the same protein but take different time due to the random nature of the process. The total time taken for adding all amino acids in these graphs are 2263, 2342, 2445 and 2269 time units for (a), (b), (c) and (d) respectively. The average time taken for the incorporation of each amino acid is 23.1, 23.9, 24.9 and 23.1 time units. The cumulative process (shown in the green curve) shows the addition of an amino acid to the elongating polypeptide chain.

Termination

When a stop codon, UAA or UAG, is placed at the A-site, there are no corresponding aminoacyl-tRNA for these codons and are thus called stop codons. They are recognised by a special protein called as the mitochondrial release factor 1a (mtRF1a). mtRF1a binds to the elongation complex and initiates the termination phase (Nozaki, Matsunaga, Ishizawa, Ueda, & Takeuchi, 2008; Rorbach *et al*., 2007). The ORFs of the two mitochondrial transcripts, MTCO1 and MTND6, terminate in AGA and AGG respectively. mtRF1a failed to recognize AGA and AGG as the stop codon. In both these transcripts the last codon is preceded by U. The recent studies indicated that these two mRNAs undergo a -1 frameshift, such that the standard stop codon, UAG, is placed at the A-site. In the ORFs of the other eleven mRNAs, the standard stop codons are present.

mtRF1a has three functional domains, which are responsible for two major functions, (a) recognition of stop codon at the A-site and, (b) consequent hydrolysis of the ester bond between the tRNA present at the P-site and the last amino acid of the growing polypeptide chain linked to the tRNA. mtRF1a is bound to GTP and polypeptide release from the P-site triggers GTP hydrolysis. Thus at the end of this step, polypeptide along with mtRF1a-GDP is released (Fig. 5.6).

The complex (complex U) now consists of deacyl-tRNA bound to mRNA which is placed between the two subunits of mitoribosome. The next step is the release of native mitoribosome so that it is available for another set of translation, called as the ribosome recycling.

Ribosome recycling is facilitated by the use of two other protein factors called as mitochondrial ribosome release factors1 and 2, mtRRF1 and mtRRF2. mtRRF2 was earlier known as mtEFG2 but was later found to have no role in elongation and was renamed as mtRRF2. These ribosome release factors bind to the complex U in a reversible manner. They facilitate the release of mRNA and deacyl-tRNA, thus regenerating the native 55S mitoribosome accompanied by GTP hydrolysis (Tsuboi *et al*., 2009).

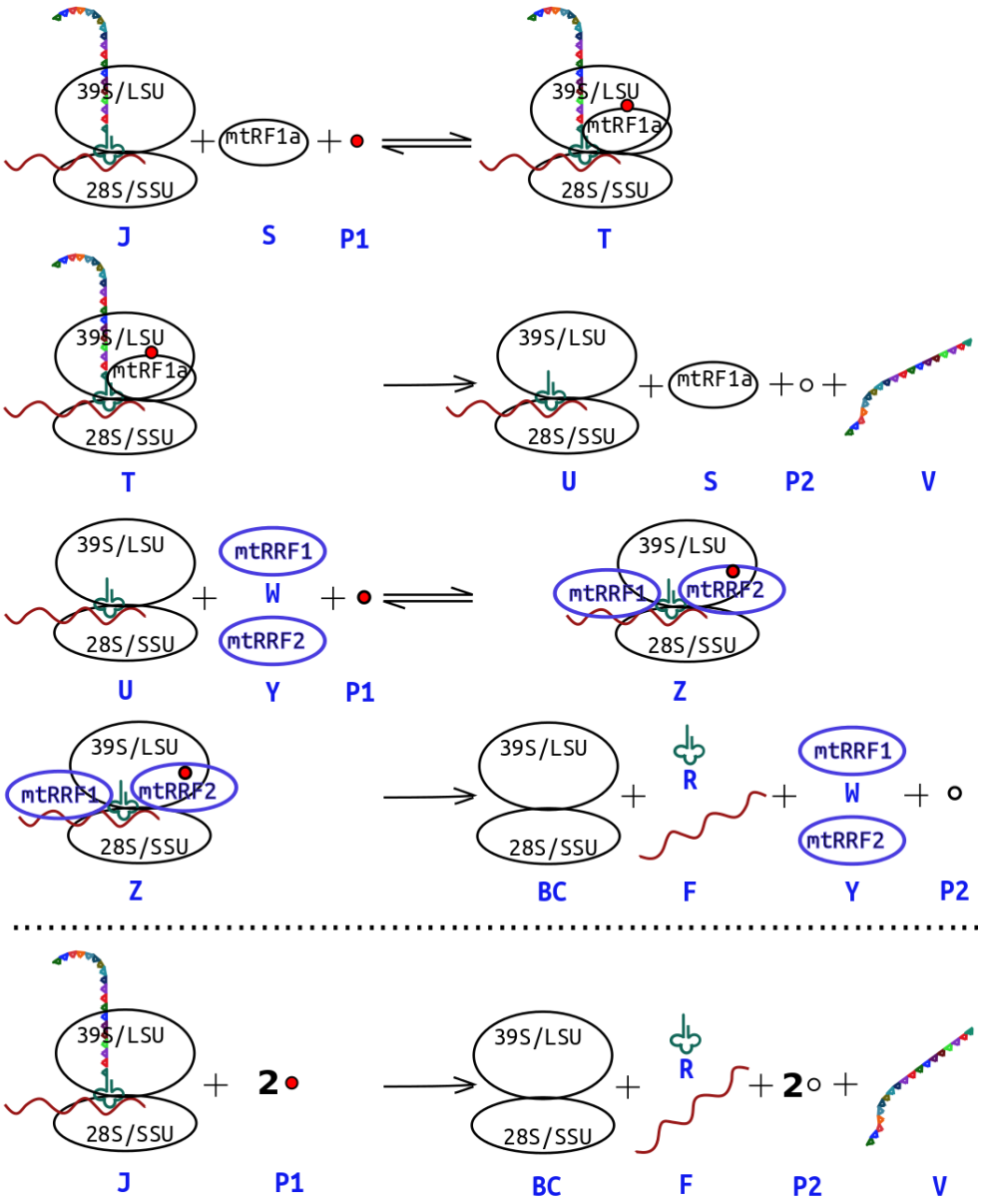

Figure 5.6: Pictorial representation of mitochondrial translation termination: mtRF1a: (S) mitochondrial release factor 1a (may be bound to GTP (red solid circle) or GDP (hollow circle)). J complex derived from elongation (Fig. 5.2) has aa-tRNA linked to the growing polypeptide chain at the P-site. When a stop codon, UAA or UAG, enters the A-site, it is recognised by a protein factor mtRF1a (S) to form T complex. This T complex dissociates to release polypeptide chain in a GTP-dependent irreversible reaction, along with GDP-bound mtRF1a and complex U. Complex U consists of LSU, SSU, mRNA and deacyl-tRNA. mtRRF1: (W) mitochondrial ribosome release factor 1. mtRRF2: (Y) mitochondrial ribosome release factor 2 (may be bound to GTP (red solid circle) or GDP (hollow circle)). W and Y bind to U complex to give Z complex. Z complex undergoes an irreversible reaction, accompanied by GTP hydrolysis to release deacyl-tRNA, mRNA, mtRRF1, GDP-bound mtRRF2 along with native mitoribosome (LSU+SSU).

Simulation

Termination starts with binding of mtRF1a to the elongation complex, when the stop codon is placed at the A site. Here in this step inputs are mtRF1a and the elongation complex, so for simulation these components were fed in the system with an initial concentration of 1. The reaction scheme seen in Fig. 5.6 clearly indicates that the first and the third reactions are reversible, and therefore rate equations were written accordingly. The second reaction, where the peptide is released, is a GTP-dependent hydrolysis of the ester bond and is an irreversible reaction. The three intermediate complexes T, U and Z are formed and utilised in the reaction set and therefore don't appear in the final reaction. The initial concentrations of these components were kept at zero. Also, the peptide is released in the second reaction, and its initial concentration was also kept at 0. In the third reaction, after the release of peptide, complex U enters the ribosome recycling step. The two ribosome release factors bind to complex U, and facilitate the release of deacyl-tRNA, mRNA and recycled 55S mitoribosome. Here the initial concentrations of both the ribosome release factors were kept at 1, to initiate the reaction. The final dissociation step is an irreversible step and was simulated appropriately.

Rate Equations

The rate equations used for simulation of the termination step of mitochondrial translation are listed in Table 5.8. The rate equations are based on the reactions as shown in Fig. 5.6.

Table 5.8: Rate equations used for simulation of termination of mitochondrial translation.

$\frac{d}{dt}[28S+39S+mRNA+tRNA+peptide] = -[28S+39S+mRNA+tRNA+peptide].[mtRF1] + [28S+39S+mRNA+tRNA+peptide+mtRF1]$
$\frac{d}{dt}[mtRF1] = -[28S+39S+mRNA+tRNA+peptide].[mtRF1]+[28S+39S+mRNA+tRNA+peptide+mtRF1] + [28S+39S+mRNA+tRNA+peptide+mtRF1]$
$\frac{d}{dt}[28S+39S+mRNA+tRNA+peptide+mtRF1] = -[28S+39S+mRNA+tRNA+peptide].[mtRF1] + [28S+39S+mRNA+tRNA+peptide+mtRF1]+[28S+39S+mRNA+tRNA+peptide+mtRF1]$
$\frac{d}{dt}[28S+39S+mRNA+tRNA] = [28S+39S+mRNA+tRNA+peptide+mtRF1]-[28S+39S+mRNA+tRNA] .[mtRRF1].[mtRRF2]+[28S+39S+mRNA+tRNA+mtRRF1+mtRRF2]$
$\frac{d}{dt}[peptide] = [28S+39S+mRNA+tRNA+peptide+mtRF1]$
$\frac{d}{dt}[mtRRF1] = -[28S+39S+mRNA+tRNA].[mtRRF1].[mtRRF2]+[28S+39S+mRNA+tRNA+mtRRF1+mtRRF2] + [28S+39S+mRNA+tRNA+mtRRF1+mtRRF2]$

$$\frac{d}{dt}[mtRRF2] = -[28S+39S+mRNA+tRNA].[mtRRF1].[mtRRF2]+[28S+39S+mRNA+tRNA+mtRRF1+mtRRF2] \\ +[28S+39S+mRNA+tRNA+mtRRF1+mtRRF2]$$

$$\frac{d}{dt}[28S+39S+mRNA+tRNA+mtRRF1+mtRRF2] = [28S+39S+mRNA+tRNA].[mtRRF1].[mtRRF2] \\ -[28S+39S+mRNA+tRNA+mtRRF1+mtRRF2]-[28S+39S+mRNA+tRNA+mtRRF1+mtRRF2]$$

$$\frac{d}{dt}[28S+39S] = [28S+39S+mRNA+tRNA+mtRRF1+mtRRF2]$$

$$\frac{d}{dt}[deacyl-tRNA] = [28S+39S+mRNA+tRNA+mtRRF1+mtRRF2]$$

$$\frac{d}{dt}[mRNA] = [28S+39S+mRNA+tRNA+mtRRF1+mtRRF2]$$

Script

The script used for simulation of mitochondrial translation termination is given in Table 5.9.

Table 5.9: Simulation script used for simulation of termination of mitochondrial translation.

```
1;
% solve the termination + ribosome recycling of mitochondrial
translation
function ds=mtfin(s)
% 1=28S+39S+mRNA+tRNA+peptide; 2=mtRF1;
3=28S+39S+mRNA+tRNA+peptide+mtRF1; 4=28S+39S+mRNA+tRNA; 5=peptide;
6=mtRRF1; 7=mtRRF2; 8=28S+39S+mRNA+tRNA+mtRRF1+mtRRF2; 9=28S+39S;
10=deacyl-tRNA; 11=mRNA;
% Equations for mitochondrial translation termination reactions
% the rate equations follow:
ds=zeros(11,1);

ds(1)= -s(1)*s(2)+s(3);
ds(2)= -s(1)*s(2)+s(3)+s(3);
ds(3)=  s(1)*s(2)-s(3)-s(3);
ds(4)=  s(3)-s(4)*s(6)*s(7)+s(8);
ds(5)=  s(3);
ds(6)= -s(4)*s(6)*s(7)+s(8)+s(8);
ds(7)= -s(4)*s(6)*s(7)+s(8)+s(8);
ds(8)=  s(4)*s(6)*s(7)-s(8)-s(8);
ds(9)=  s(8);
ds(10)= s(8);
ds(11)= s(8);
return
end
% use lsode to solve this set...
lsode_options("relative tolerance",1e-4);
lsode_options("absolute tolerance",1e-3);
t=0:0.2:200;
% supply the initial concentrations ...
s0=[1, 1, 0, 0, 0, 1, 1, 0, 0, 0, 0];
```

```
%   0   0   0   0   0   0   0   0   0   1   1
%   1   2   3   4   5   6   7   8   9   0   1
[s,T,MSG]=lsode(@mtfin,s0,t);
T
MSG
plot(t,s(:,1),"linewidth",5,t,s(:,2),"linewidth",5,t,s(:,3),"linewid
th",5,t,s(:,5),"linewidth",5,t,s(:,8),"linewidth",5,t,s(:,9),"linewi
dth",5);
grid on;
set (gca, 'FontName', 'Times');
set (gca,'FontSize',20);
axis([0,20,.001,1.01]);
xlabel ("Time/arbitrary units");
ylabel ("Concentration/arbitrary units");
set (gca,'FontSize', 20);
set( get(gcf,'children'), 'linewidth',4 );
legend("elo comp","mtRF1a", "U comp","peptide","Z comp", "55S ribo",
"location", "east");
```

The components, which are introduced in the system as input, have been given an initial concentration of 1. All the other components (intermediates and products) are kept at zero, as they are formed in the reaction system.

Result

Fig. 5.7 shows the simulation curves for selected components of mitochondrial translation termination phase. The elongation complex derived from the elongation phase and the auxiliary factors (mitochondrial release factor and two ribosome release factors) are the inputs required for this process. These components were fed into the system at an initial concentration of 1, all the other intermediates and products formed in this phase are kept at an initial concentration of 0. The script in Table 5.9 generates the graph shown in Fig. 5.7.

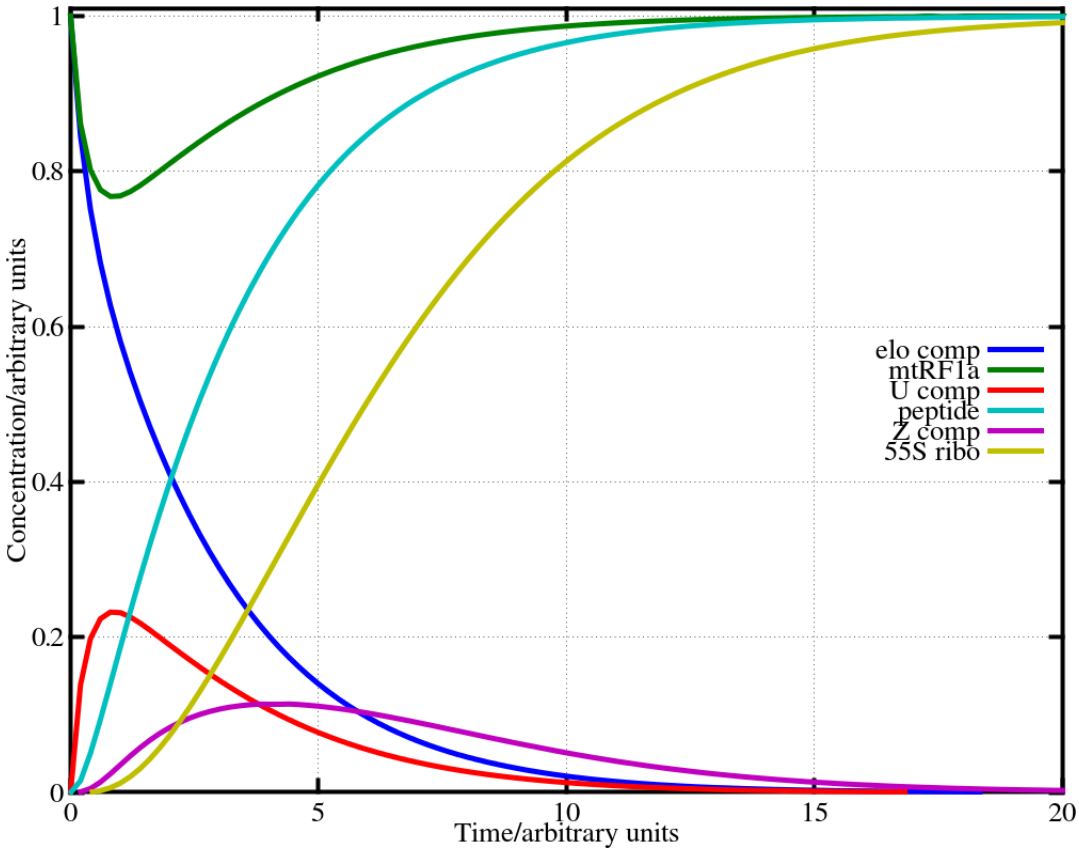

Figure 5.7: Simulation curves for mitochondrial translation termination. Elo comp: J complex, formed in elongation subset (Fig. 5.2), consists of 55S ribosome, peptidyl-tRNA linked with the full grown polypeptide chain at the P-site and stop codon of mRNA positioned at the A-site; mtRF1a: mitochondrial release factor 1a.

It is seen that the concentration of the elongation complex decreases as it is being used and is not generated in the due course of the reactions in this phase. The curve for mitochondrial release factor 1a (mtRF1a) goes down and then rises as it is used as a catalyst in this phase. It binds to the elongation complex to facilitate the release of peptide and is regenerated, once the peptide is released from the elongation complex. The curves for the two intermediate complexes (U and Z comp) first rise and then fall, indicating that these complexes were formed and were then used up in this phase. The curve for peptide rises, as is expected as the full-grown peptide is released from the elongation complex and is not used up in this phase. Also, intact mitoribosome is recycled in this phase, and 55S ribosome is released which is now ready for another round of translation.

References

Anderson, S., Bankier, A.T., Barrell, B.G., de Bruijn, M.H.L., & Coulson, A.R., Drouin, J., Eperon, I.C., Nierlich, D.P., Roe, B.A., Sanger, F., Schreier, P.H., Smith, A.J.H., Staden, R., & Young, I.G. (1981). Sequence and organization of the human mitochondrial genome. *Nature, 290*, 457-465.

Barrell, B.G., Bankier, A.T., & Drouin, J. (1979). A different genetic code in human mitochondria. *Nature, 282*, 189-194.

Bhargava, K., Templeton, P., & Spremulli, L.L. (2004). Expression and characterization of isoform 1 of human mitochondrial elongation factor G. *Protein expression and purification*, *37*, 368-376.

Cai, Y.C., Bullard, J.M., Thompson, N.L., & Spremulli, L.L. (2000). Interaction of mitochondrial elongation factor Tu with aminoacyl-tRNA and elongation factor Ts. *Journal of Biological Chemistry*, *275*, 20308-20314.

Cavalier-Smith, T. (1987). Eukaryotes with no mitochondria. *Nature 326*, 332-333.

Chu, D., Zabet, N., & von der Haar, T. (2012). A novel and versatile computational tool to model translation. *Bioinformatics*, *28*(2), 292-293.

Flach, E. H., & Schnell, S. (2006). Use and abuse of the quasi-steady-state approximation. *IEE Proceedings-Systems Biology*, *153*, 187-191.

Gaur, R., Grasso, D., Datta, P.P., Krishna, P.D., Das, G., Spencer, A., Agrawal, R.K., Spremulli, L., & Varshney, U. (2008). A single mammalian mitochondrial

translation initiation factor functionally replaces two bacterial factors. *Molecular Cell, 29,* 180-90.

Grasso, D.G., Christian, B.E., Spencer, A., & Spremulli, L.L. (2007). Overexpression and purification of mammalian mitochondrial translational initiation factor 2 and initiation factor 3. *Methods in Enzymology, 430,* 59-78.

Grohmann, K., Amalric, F., Crews, S., & Attardi, G. (1978). Failure to detect "cap" structures in mitochondrial DNA-coded poly(A)-containing RNA from HeLa cells. *Nucleic Acids Research, 5,* 637-651.

Jansen, R. P. (2000). Germline passage of mitochondria: quantitative considerations and possible embryological sequelae. *Human Reproduction*, *15*(suppl 2), 112-128.

Koc, E.C., & Spremulli, L.L. (2002). Identification of Mammalian Mitochondrial Translational Initiation Factor 3 and Examination of Its Role in Initiation Complex Formation with Natural mRNAs. *Journal of Biological Chemistry, 277,* 35541-35549.

Milanowska, K., Mikolajczak, K., Lukasik, A., Skorupski, M., Balcer, Z., Machnicka, M. A., Nowacka, M., Rother, K. M., & Bujnicki, J. M. (2013). RNApathwaysDB—a database of RNA maturation and decay pathways. *Nucleic acids research*, *41*(D1), D268-D272.

Miller, C., Saada, A., Shaul, N., Shabtai, N., Ben-Shalom, E., Shaag, A., Hershkovitz, E., & Elpeleg, O. (2004). Defective mitochondrial translation caused by a ribosomal protein (MRPS16) mutation. *Annals of neurology*, *56*(5), 734-738.

Muzumdar, R. H., Huffman, D. M., Atzmon, G., Buettner, C., Cobb, L. J., Fishman, S., Budagov, T., Cui, L., Einstein, F.H., Poduval, A., Hwang, D., Barzilai, N., & Cohen, P. (2009). Humanin: a novel central regulator of peripheral insulin action. *PloS one, 4*(7), e6334.

Nozaki, Y., Matsunaga, N., Ishizawa, T., Ueda, T., & Takeuchi, N. (2008). HMRF1L is a human mitochondrial translation release factor involved in the decoding of the termination codons UAA and UAG. *Genes to Cells, 13,* 429-438.

O'Brien, T.W. (2003). Properties of human mitochondrial ribosomes. *IUBMB Life, 55,* 505-513.

Pedersen, M. G., Bersani, A. M., & Bersani, E. (2008). Quasi steady-state approximations in complex intracellular signal transduction networks–a word of caution. *Journal of Mathematical Chemistry*, *43*, 1318-1344.

Pikó, L., & Matsumoto, L. (1976). Number of mitochondria and some properties of mitochondrial DNA in the mouse egg. *Developmental biology*, *49*, 1-10.

Polacek, N., & Mankin, A.S. (2005). The ribosomal peptidyl transferase center: structure, function, evolution, inhibition. *Critical reviews in biochemistry and molecular biology*, *40*, 285-311.

RajBhandary, U.L. (1994). Initiator transfer RNAs. *Journal of Bacteriology, 176,* 547-552.

Robin, E.D., & Wong, R. (1988). Mitochondrial DNA molecules and virtual number of mitochondria per cell in mammalian cells. *Journal of Cellular Physiology, 136,* 507-513.

Rorbach, J., Temperley, R., Bonnefoy, N., Tate, W., Lightowlers, R., & Chrzanowska-Lightowlers, Z. (2007). mtRF1a Is a Human Mitochondrial Translation Release Factor Decoding the Major Termination Codons UAA and UAG. *Molecular Cell*, *27*, 745-757.

Salinas, T., Duby, F., Larosa, V., Coosemans, N., Bonnefoy, N., Motte, P., chal-Drouard, L.M., & Remacle, C. (2012). Co-evolution of mitochondrial tRNA import and codon usage determines translational efficiency in the green alga Chlamydomonas. *PLoS Genetics*, *8*(9), e1002946.

Schwartzbach, C.J., & Spremulli, L.L. (1989). Bovine mitochondrial protein synthesis elongation factors. Identification and initial characterization of an elongation factor Tu-elongation factor Ts complex. *Journal of Biological Chemistry, 264,* 19125-19131.

Smith, A.C., Blackshaw, J.A., & Robinson, A.J. (2012). MitoMiner: a data warehouse for mitochondrial proteomics data. *Nucleic acids research*, *40*(D1), D1160-D1167.

Smits, P., Smeitink, J., & van den Heuvel, L. (2010). Mitochondrial Translation and Beyond: Processes Implicated in Combined Oxidative Phosphorylation Deficiencies. *Journal of Biomedicine and Biotechnology*, 737385, 1-24.

Spencer, A.C., & Spremulli, L.L. (2004). Interaction of mitochondrial initiation factor 2 with mitochondrial fMet-tRNA. *Nucleic Acids Research, 32,* 5464-5470.

Taanman, J. W. (1999). The mitochondrial genome: structure, transcription, translation and replication. *Biochimica et Biophysica Acta (BBA)-Bioenergetics*, *1410*(2), 103-123.

Temperley, R., Richter, R., Dennerlein, S., Lightowlers, R.N., & Chrzanowska-Lightowlers, Z.M. (2010). Hungry Codons Promote Frameshifting in Human Mitochondrial Ribosomes. *Science, 327,* 301.

Tsuboi, M., Morita, H., Nozaki, Y., Akama, K., Ueda, T., Ito, K., Nierhaus, K.H., & Takeuchi, N. (2009). EF-G2mt is an exclusive recycling factor in mammalian mitochondrial protein synthesis. *Molecular cell, 35,* 502-510.

Ward, B.L., Anderson, R.S., & Bendich, A.J. (1981). The mitochondrial genome is large and variable in a family of plants (Cucurbitaceae). *Cell, 25,* 793-803.

Wolfram: http://mathworld.wolfram.com/MonteCarloMethod.html

Summary

The metabolic pathways have been studied in great depth over years. The outcome of these detailed studies is a static metabolic pathway or a network. The molecules move along these pathways, get transformed and finally degraded. The biological system is highly dynamic with several combinations of reactions taking place simultaneously. The study of the dynamic behaviour is essential for valid interpretation of the physiological status of the cell at a given point in time. Further, in such a case whenever perturbations are experienced by the biological system, the impact can be studied if a dynamic model is available. Despite the realisation of the need for a dynamic model, only few studies have been reported in the literature. This can be attributed to several reasons listed below:

- Lack of experimental details as most of the experimental outcomes report the impact of a metabolite only on a selected set of reactions rather than the combined network. In such a case, the details required for the model are simply unavailable.
- Incorporating exact physiological conditions in a model is sometimes quite challenging. For example, multiple factors involved in transport system in intracellular and intercellular communications.
- Presence of a large number of components and connections between them makes it a difficult task to set up a dynamic model for the cellular system
- Moreover, such a model would vary from tissue to tissue and cell to cell

The present study is focused on the dynamic studies of selected pathways from the mitochondrial system. It can be considered as part of a bottom-up approach.

The broad objective of this report is the simulation, however crude, of the important biochemical functions in mitochondria. Mitochondrion being a semi-autonomous organelle with the potential to carry out replication, transcription and translation in addition to several essential metabolic pathways such as Krebs cycle, oxidative phosphorylation, etc. It consists of multiple copies of a genome which includes 13 protein-coding genes, 22 tRNAs and two rRNAs. These features bring it closer to be considered as a miniature model of cell in terms of functions. Modelling one organelle at a time shows a way for modelling the whole cell in parts and then combining these parts to form a grand model. Modelling of one organelle can be further done in parts, where individual pathways are simulated and then combined to form a network comprising all the pathways inside a given organelle. The approach can be simplified as, metabolic pathways → organelles → cells → tissues and so on.

On these lines, in the present study, generalised models were created for mitochondrial metabolic pathways Krebs cycle, oxidative phosphorylation, malate-aspartate shuttle, citrate-pyruvate shuttle and their interaction with ROS. These pathways were combined to form a single model. In addition, a molecular mechanism, mitochondrial translation, was also simulated.

The approach used in the present study includes (I) set up of the kinetic equations, (II) set up of the transporter equations, (III) mitochondrial translation, (IV) ETC and ROS; the effect of pH in simulation of the electron transport chain. Also transport across mitochondrial membrane using two shuttles, citrate-pyruvate and malate-aspartate, has been included. This approach may appear rather simplified and crude, when compared to the complicated nature of molecular mechanisms, but the results obtained from the simulation reasonably matches with our understanding of the biological system. The model can be further refined by including factors like membrane potential, kinetic parameters and physiological concentrations of the various components involved, intricate transport mechanisms, inhibitors, activators, modulators of the genes of the respective enzymes. The reason for not including these features is solely to keep the approach simple and versatile.

The present study indicates that steady-state concentrations form a basin, rather than a fixed point. This basin may comprise several combinations of multiple metabolites involved. Further, it is seen that the presence of multiple alternate pathways allow the system to attain steady-state even after multiple perturbations. However, a catastrophic change may lead to a different set of steady-state concentrations.

The present approach may have a broad range of potential applications:

- To study the ripple effects caused due to any perturbations in the system.
- To understand the dynamics and interdependency of the various pathways.
- To study the effect of enzyme dysfunctioning (caused by drug, inhibitor, etc.) on all the other components of the system.
- To design *in vitro* and *in vivo* experiments and to predict respective outcomes.

Several mitochondrial diseases are reported in the literature. There are 51 mitochondrial diseases reported in mitochondrial database (http://www.mitodb.com/). Mitochondrial defects lead to several degenerative diseases, cancer and ageing. For example, deficiency of any of the respiratory chain complexes may lead to Leigh syndrome. Now, the impact of the deficiency of one respiratory complex can be studied on all the other components of the system using the present model, even when all the kinetic parameters are not known. The deficiency can be subsumed in the

system by blocking the particular reaction partially or entirely, depending on the specific case. Similar approach can be applied to study various other pathological conditions.

The interplay between mitochondrial and nuclear genomes adds to the complexity of the mitochondrial system. Therefore, it is important to study the interrelationship of mitochondrial energy production, ROS generation, apoptotic pathways and corresponding nuclear intervention. These processes have been deliberately avoided for the sake of simplicity.

Several researchers have worked in the direction of kinetic simulation of metabolic pathways (Singh & Ghosh, 2006; Mogilevskaya, Demin & Goryanin, 2006). Most of these models are overly complicated, both structurally and computationally, and are difficult to be understood by biologists. Also, these models are made for a particular system and cannot be adapted easily to suit other related cases. On the contrary, the present approach is flexible for customisation.

This study can be considered as the first steps in integrating information derived from decades of experimental research. The study can be extended to form a more detailed model that can link metabolic pathways from the whole cell in a structured script. It will lead to a scenario where at any given point in time, one can interpret the effect of one or more perturbations on individual components and the system as a whole, with relative ease.

References

Mogilevskaya, E., Demin, O., & Goryanin, I. (2006). Kinetic model of mitochondrial Krebs cycle: unraveling the mechanism of salicylate hepatotoxic effects. *Journal of biological physics*, *32*(3-4), 245-271.

Singh, V. K., & Ghosh, I. (2006). Kinetic modeling of tricarboxylic acid cycle and glyoxylate bypass in Mycobacterium tuberculosis, and its application to assessment of drug targets. *Theoretical Biology and Medical Modelling*, *3*(1),27.

Publications

- ****Korla, K***., Vadlakonda, L., & Mitra, C. K. (2015). Kinetic Simulation of Malate-Aspartate and Citrate-Pyruvate Shuttles in Association with Krebs Cycle. *Journal of Biomolecular Structure and Dynamics*, (just-accepted), 1-31. doi**:** 10.1080/07391102.2014.1003603.
- ****Korla, K***., & Mitra, C. K. (2014). Kinetic modelling of coupled transport across biological membranes. *Indian Journal of Biochemistry and Biophysics*, *51*, 93-99.
- Mitra, C. K., & ***Korla, K***. (2014). Functional, Structural, and Sequence Studies of MicroRNA. In *miRNomics: MicroRNA Biology and Computational Analysis* (pp. 189-206). Humana Press.
- ****Korla, K***., & Mitra, C. K. (2013). Kinetic modelling of mitochondrial translation. *Journal of Biomolecular Structure and Dynamics*, (ahead-of-print), 1-17. doi**:** 10.1080/07391102.2013. 833135.
- ***Korla, K***., Arrigo, P., & Mitra, C. K. (2013). Promoters, toll like receptors and microRNAs: A strange association. *Indian Journal of Biochemistry and Biophysics*, *50*, 169-176.
- ****Korla, K***., & Mitra, C. K. (2014). Modelling the Krebs cycle and oxidative phosphorylation. *Journal of Biomolecular Structure and Dynamics*, *32*(2), 242-256.
- ***Korla, K***. and Mitra, C. K. "The quick and dirty way to explore the promoter regions of TLRs". Ralf Hofestädt, Nikolay Kolchanov (eds.) *German/Russian Network of Computational Systems Biology, Report 2012*. ISBN 978-3-8440-1573-7; ISSN 1432-4385.
- ****Korla, K***. and Mitra, C. K. "Kinetic simulation of the Krebs cycle". Ralf Hofestädt, Nikolay Kolchanov (eds.) *German/Russian Network of Computational Systems Biology, Report 2012*. ISBN 978-3-8440-1573-7; ISSN 1432-4385.
- ****Korla, K***. "Modelling mitochondrial network". Ralf Hofestädt, Nikolay Kolchanov (eds.) *German/Russian Network of Computational Systems Biology, Report 2012*. ISBN 978-3-8440-1573-7; ISSN 1432-4385.

*Work presented in these publications are included in the present text.